University of Southampton

Enhanced Design Performance Prediction Methods for Rudders Operating Downstream of a Propeller

Jason Smithwick, MEng

A thesis submitted for the degree of Doctor of Philosophy

Ship Science, School of Engineering Sciences

This thesis was submitted for examination in April 2000

UNIVERSITY OF SOUTHAMPTON

ABSTRACT

SCHOOL OF ENGINEERING SCIENCES
SHIP SCIENCE

Doctor of Philosophy

ENHANCED DESIGN PERFORMANCE PREDICTION METHODS FOR RUDDERS OPERATING DOWNSTREAM OF A PROPELLER

By Jason Edward Thomas Smithwick

Using a design spiral philosophy, methods have been developed and employed to predict rudder performance downstream of a propeller. The result of this work has been the development of a proven methodology that accounts for the physical basis of the interaction between the rudder and propeller of a ship.

The principal factors in rudder-propeller interaction have been assessed and a coherent presentation system for quantifying rudder and propeller performance has been discussed. Systematic experimental tests on a skeg-rudder and all-movable rudder downstream of a propeller have been carried out in a 3.5m by 2.5m low speed wind tunnel and an open laboratory. Results for the ship bollard pull condition and a further range of propeller thrust loading have been presented and discussed. The data created in experimental work has been harnessed with physical understanding through analytical interpretation to create an interpolation and correction method for predicting rudder performance with the upstream influence of a propeller in the form of a software program. A finding of the work has been a method for accurately predicting performance data at any propeller thrust loading from rudder free stream (2-D sectional lift coefficient) and bollard pull performance data. For detailed analysis of the flow regime of rudder propeller interaction computational fluid dynamics in the form of a surface panel method has been investigated as a tool to provide detailed design information on a skeg-rudder operating downstream of a propeller. By way of example several design investigations are presented using the aforementioned analysis methods.

ACKNOWLEDGMENTS

There are many people who have supported the development of this work and I would like to thank all of those who have been involved. Particular thanks go to Dr. Stephen Turnock for his supervision, enthusiasm and continued friendship. I would also like to thank Dr. Tony Molland who has been a mentor to whom I have looked up to during my undergraduate study and now in my professional work. I am also grateful to my colleagues at the Wolfson Unit M.T.I.A. for their forbearance during the writing up process. Lastly I would like to thank my family for their encouragement and Nicola for her patience and love.

Part of the work described in this thesis was carried out while the author was employed on a research contract for the Manoeuvrability of Ships and Estimations Schemes (MOSES) project funded by the E.P.S.R.C. and industrial partners; Harland and Wolff Shipbuilding and Heavy Industries Ltd., M.O.D., Vosper Thornycroft (UK), Yarrow Shipbuilders Ltd and VSEL through the Marine Technology Directorate Ltd. Under E.P.S.R.C. research grant Ref. No. GR/J73193. MTD No. SHP186

TABLE OF CONTENTS

APPENDICES

LIST OF FIGURES (within main body of document)

LIST OF TABLES

NOMENCLATURE

A	Rudder area (S.c)
AR	Aspect ratio
c	Rudder mean chord
C_d	Drag coefficient ($d/\frac{1}{2}\rho AU^2$)
C_d^*	Drag coefficient ($d/\frac{1}{2}\rho AK_T n^2 D^2$)
C_P	Pressure coefficient
CP_c	Centre of pressure chordwise, %c, measured from leading edge
CP_S	Centre of pressure spanwise, %S, measured from root
C_L	Lift coefficient ($L/\frac{1}{2}\rho AU^2$)
C_L^*	Lift coefficient ($L/\frac{1}{2}\rho AK_T n^2 D^2$)
C_N	Normal force coefficient
c_R	Rudder root chord
c_T	Rudder tip chord
d	Drag force
D	Propeller diameter
$dC_L/d\alpha$	Lift curve slope (the rate of change of lift with rudder angle at zero rudder incidence)
F	A generic force or moment
J	Propeller advance coefficient (U/nD)
K	Force Scaling Parameter
K_T	Thrust coefficient ($T/\rho n^2 D^4$)
K_Q	Torque coefficient ($Q/\rho n^2 D^5$)
L	Lift force
n	Propeller revolutions per second
M	Moment
N	Normal force
P/D	Propeller pitch ratio
Q	Propeller torque
Rn	Reynolds number ($\rho Vc/\mu$)
S	Rudder span
t	Section thickness

T	Propeller thrust
U	Speed
V	Distance to rudder steering gear or dynamometer centre from rudder root
w_T	Wake Fraction
W	Distance to rudder stock from rudder root leading edge
X	Longitudinal distance, propeller plane to rudder leading edge in line with propeller axis
Y	Lateral distance between propeller axis and rudder stock
Z	Vertical distance between rudder root and propeller axis
α	Net inflow angle
β	Inflow angle, drift angle or yaw angle
γ	Flow straightening factor
∂	Rudder angle relative to body (ship) axis
ξ	Coverage
η	Propeller efficiency (%)
Λ	Sweepback angle of rudder at quarter chord line
λ	Proportion of D impinging on rudder
μ	Dynamic Viscosity
ρ	Mass density
ψ	Propeller advance angle ($\tan^{-1}[J/0.7\pi]$)
ω	Propeller radians per second

Subscripts

0	At 0° or at a static value of 0
2-D	Two-dimensional
3-D	Three-dimensional
ACT	Actual
D	Dynamic
E	Effective
G	Geometric
i,j,k	An integer value associated with an array of values (i.e. i=1,2,3 etc.)
J=0	At an advance ratio of zero

P	Pressure or Propeller
R	Rudder
REQ	Required
FS	Free stream
x,y,z	In the direction or about the x,y,z axis respectively

Superscripts

n	Raised to the power of n
'	A transformed parameter

1 INTRODUCTION

1.1 Aims and Objectives

Manoeuvring devices be it for a yacht, ship or underwater vehicle, seldom operate in flow without the upstream influence of an object altering the fluid motion on to the device. When a manoeuvring device operates in this fluid motion its performance is altered to that when it is operating in the undisturbed free stream. Examples of objects that can influence the flow on to a manoeuvring device include a hull, a propeller, a keel or a duct. Each upstream influence can alter the fluid velocity and the fluid vorticity downstream and therefore the manoeuvring device coursekeeping performance.

A need for predicting coursekeeping at an early design stage in ship design is high. It is therefore necessary to predict the forces generated by a manoeuvring device not only for design of the device but also manoeuvring considerations.

By using the example of rudder design with an upstream influence of a propeller the work in this thesis aims to assess the principal factors in rudder-propeller interaction and examine methods by which one can systematically predict the performance of a manoeuvring device with the physical interaction of a propeller upstream. A method of predicting manoeuvring device forces can be implemented in a whole ship manoeuvring model [1],[2],[3],[4], it is also the aim of this work to establish a calculation method that can form this part of a manoeuvring model.

For a performance prediction method to be useful in design, it must be able to provide accurate and usable results. A further aim of the work is to present coherent methods for acquiring data for design.

To complete the aims and objectives the work is split into several distinct items, as follows:

i) Assess the principal factors in rudder propeller interaction and the sources of available data.

ii) Use experimental techniques to create further data and obtain a greater understanding of the mechanism of rudder-propeller interaction, particularly at zero ship speed.

iii) Investigate methods to harness experimental data, empirical evidence, and physical understanding to create a novel, widely applicable method for predicting rudder forces downstream of a propeller.

iv) Using computational fluid dynamics, investigate enhanced methods of predicting detailed rudder performance for design.

v) Demonstrate, by way of example, applications of the performance prediction methods to rudder design.

1.2 Background

1.2.1 Experimental Work

Experimental measurements and theoretical prediction of rudder forces provide a wide range of necessary data for use in analysing and predicting the manoeuvring performance of a ship.

The systematic parametric variation of experimental variables is obtained from the identified influential factors affecting performance. An in-depth knowledge of these factors can create efficient testing schedules as primary parameters are investigated in more detail. Identifying current sources of experimental data provides a knowledge base for further work. The scope of parametric variation and the experimental methods employed are useful in making decisions for future study. A review of the applicable experimental work in predicting rudder performance follows.

In 1972 Kerwin et al [5] tested a series of flapped rudders in a water tunnel and in 1977 Molland [7] carried out tests on a semi-balanced ship skeg-rudder in a wind tunnel. These tests were compared to previous results presented by Whicker and Fehlner [8]. This culmination of this work is summarised in [9]. The skeg-rudder work carried out by Molland concluded that 'the overall characteristics of the all-movable rudder.....compare

favourably with existing published data.....its characteristics form a very satisfactory basis with which to compare the skeg-rudder.' This work led to an extensive programme of experimental and theoretical research into the effect on manoeuvring of the stern arrangement of vessels and in particular the interaction between the ship hull, propeller and rudder.

English [6], in 1972, was carrying out tests on a jet-flapped rudder for use in ship manoeuvring at zero and low ship speed. A propeller and rudder were tested and the effect of the interaction was summarised with scaling effects also mentioned.

In 1989 Kracht [14] and Stierman [12] were carrying out tests on rudder-propeller combinations. Stierman's work was principally involved in the propulsive performance of a propeller with a rudder downstream, all tests were carried out at 0° rudder incidence and only rudder drag was measured. Kracht's work was principally involved in testing a rudder propeller combination in a cavitation tunnel.

In 1991 Molland and Turnock [13] conducted tests to ascertain the performance of several all-movable rudders with a propeller upstream and presented the principal parameters that affect rudder-propeller interaction. This work led on to a series of experimental programmes investigating a skeg-rudder behind a propeller [16] and investigations into four quadrant and low and zero speed performance with a propeller upstream [21] and [22].

With the increasing use of skeg-rudders in ships, sailing yachts and small motor vessels, further investigation of the performance of a skeg-rudder in the wake of a propeller and/or hull is considered necessary. The experimental work by Molland and Turnock led to a need for skeg-rudder performance to be investigated in more detail particularly for longitudinal separation, lateral separation and low and zero ship speed. The Author's principal experimental research area has been investigating the performance of the skeg-rudder downstream of a propeller.

1.2.2 Rudder Performance Prediction Methods

From vessel power prediction methods [19] to sailing yacht velocity prediction [20] many methods to date rely on a parametric series of test data to derive curve fits of performance. The prediction methods rely on physical understanding to derive the prediction formulae and calculate the effect of altering design parameters have on the performance. The performance prediction methods have a quoted range or envelope in which the results remain reliable, based on the extent of variation within the experimental tests.

In addition to extensive experimental tests, Whicker and Fehlner [8] presented theoretical and semi-empirical equations for estimating free-stream, low-aspect ratio, all-movable rudder performance. This work has been used extensively in estimating rudder performance on many craft. Molland [25] also presented several formulae for calculating the performance of all-movable rudders and skeg-rudders in the free stream. None of these calculation methods took into account the influence of a propeller upstream.

Manoeuvring simulations often have rudder performance prediction embedded within the methods, but tend to simplify the rudder-propeller interaction mechanism. The effect of the propeller on performance is often described as a mean inflow velocity proportional to propeller thrust loading [1], [2], [4]. Although this does account for the most significant influence on rudder performance, it does not allow for the balance of forces induced by the relative propeller coverage and rudder geometry. Although practical predictions of rudder-propeller performance can be achieved using these models the fundamental physical behaviour is not correctly simulated.

In 1992 Molland [26] presented a blade element-momentum theory and modified lifting line theory for calculating rudder forces downstream of a propeller. This was a complimentary theory to experimental work carried out previously and used the experimental data to correct, based on aspect ratio, the theoretical results from the lifting line calculation.

In 1993 the ITTC Manoeuvring Committee [24] recommended that 'More work is needed especially with regard to theoretical prediction methods at both concept and detailed design stages and standardisation of models' in the context of predicting rudder performance.

One of the results of the experimental work, described previously in this chapter, has been the development of a large database. This relates the changes in propeller operating condition and the geometric description of the rudder-propeller system to the resultant performance of the rudder in terms of developed rudder forces and moments. Experimentation is invaluable in this type of work for the process of validation and also in general interpolation and extrapolation of data.

By making use of the experimental work, a combination of experimental data and physical understanding of rudder-propeller interaction can be used to create a suitable method to determine rudder performance with the upstream influence of a thrusting propeller. In 1996 Molland et al [3] produced an enhanced rudder performance prediction model using a combination of physically based curve fitting and look-up tables based on experimental work. The results from this work produced a more physically correct model of the effect of the propeller upstream in a ship simulator. Using actual rudder test data and physically based corrections is an accurate method of predicting rudder performance and is therefore suitable for a rudder performance prediction method.

For practical purposes a preliminary rudder design tool that uses lower order geometric definition to predict performance is advantageous. In interpreting experimental results the physical modelling is limited by the availability of good experimental data and physical knowledge.

1.2.3 Computational Fluid Dynamics (CFD)

For detailed analysis of rudder performance a CFD approach needs to be employed such that it can produce meaningful results with a higher resolution than, for example, simply total rudder forces and moments. In designing rudder scantlings it is useful to have an understanding of the distribution of load over the rudder so local reinforcement can be positioned where only necessary thus producing a more efficient design.

Although pressures and therefore local load distributions can be measured experimentally, to apply a method that calculates local pressure in the same manner as the rudder performance prediction methods described previously holds little physical basis as a detailed analysis of the flow regime is required. Therefore a prediction method is needed

that can predict the rudder performance in detail. A surface or domain based CFD method has the capacity to predict local rudder pressure [27] and [31]. By correct validation the CFD method can be used to obtain detailed local information of the flow for detailed design.

CFD has been used extensively in acquiring appendage design data, particularly for yacht keels [29] and [30]. The author has also used CFD to analyse the performance of sailing yacht keel and rudder [36 and Appendix D]. The work has generally concluded that CFD is a useful tool in measuring the performance of an appendage design.

The application of CFD on rudders and manoeuvring devices has employed several types of numerical methods. Willis et al [34] used a vortex lattice theory for calculating the hydrodynamic forces developed by a rudder with a non uniform flow. This theory represents the flow by a distribution of vorticity over the rudder boundaries. With this method the rudder is assumed to have zero thickness and is principally used to obtain total forces rather than pressure distributions and hence distribution of loading.

Wright [31] has modelled a rudder using a Reynolds averaged Navier Stokes (RANS) method to model a rudder downstream of a propeller. The results with the propeller upstream have proved to be unreliable and this is echoed by Turnock in [32]. Panel methods have also been used to model rudder-propeller interaction. Turnock [27] used a surface panel method to model the performance of a rudder downstream of a propeller. The surface panel method supplies results of pressure distribution and integration of these results can give total forces and moments. The results from this method were very close to experimental results although caution is advised as the potential flow model can over predict lift and under predict total drag [32] as there are no viscous effects.

In general CFD has been used for assessing the performance of a particular pre-defined design but CFD has also been employed as a designing tool for optimisation, Su et al [35] used a surface panel method for hydrofoil design. By adjusting the foil shape using the CFD data a resultant shape with a specified pressure distribution was calculated. This effectively reverses the use of CFD whereby a performance is defined and a suitable geometry is given as a result rather than the geometry being defined and the performance given as the result.

In selecting a suitable method for modelling manoeuvring device performance it is necessary to identify the most useful and applicable method. As geometric and fluid domain definition is often one of the most time consuming processes in any numerical flow model, the CFD method must be intuitive to use in defining the rudder geometry and subsequent calculations should also be relatively fast to allow for large parametric variations. The trade off of computational work and production of results should therefore be considered in selecting a CFD method for a particular application.

In 1999 the ITTC Manoeuvring Committee [28] recommended that 'Work should be pursued on CFD approaches to reduce the required amount of experiments'. CFD has been investigated, in this work, for the purpose of predicting the rudder performance to assess the viability of using such a method to extend the experimental database.

1.3 Ship-Rudder-Propeller Flow

A propeller upstream of a ship rudder accelerates and rotates the inflow into the rudder. To investigate the advantages and disadvantages of having the upstream influence of a propeller, the interdependence of the rudder and propeller must be determined.

In examining rudder-propeller interaction problem it is necessary to identify the various independent parameters which affect rudder performance. The influence of fluid flow, geometry and relative positions of the rudder and propeller all need to be considered. The rudder performance needs to be quantified and also related to other results for comparison. A suitable presentation must be adhered to for meaningful analysis of the effect of the aforementioned variables.

Once the variables that influence rudder manoeuvring performance have been identified the method of data collection and scope of parametric studies can be defined. Presentation and analysis of all the factors that affect rudder performance will help determine the important variables used in a performance prediction method.

1.4 Design Philosophy

In any type of design process the principal factors that strongly affect the performance of the design need to be identified. These factors are governed by the scope of the design and its operating conditions. At any design inception these parameters are generally coarse in their detail and as the design progresses the level of detail will increase. The refinement of a design is termed as a design spiral, a set of simple parameters are analysed and refined until a final solution is obtained, each design iteration getting smaller in the scope of variation but progressively improving and expanding the detail of the design.

Within a design spiral fusion of the available data through a coherent presentation system is required. To analyse a design, systematic variation of parameters are required to arrive to a solution. Existing data can supply an envelope or scope in which to work. This can then be used to create further data by interpolation and to a certain extent extrapolation. Other methods employing direct calculation and experimentation are also used. Within a design spiral the analysis method of the design often increases in accuracy and complexity until the final results are quite specific to a set of requirements.

The choice of rudder shape, size, type and position will influence the manoeuvring performance of a rudder. This thesis employs the design spiral method to analyse manoeuvring device performance. By identifying existing data and creating a further envelope of data, the coarse design parameters can be used to create an initial set of results. The design can then be optimised using a more in-depth analysis tools that require a higher definition of the design parameters.

1.5 Geometric Definition

Any method of analysis that predicts the performance of manoeuvring devices requires definition of their geometry. Any geometric definition will require a certain amount of discretisation. The method of predicting performance largely defines the level of detail needed for geometric definition.

The geometry definition of say a rudder can range from principal dimensions such as span, chord and thickness ratio to a full surface definition for use with CFD analysis. The complexity of the geometric definition can range from elementary properties, such as span

and chord up to detailed three-dimensional surface definition. In the case of some higher order computational fluid dynamics codes, even the domain of the fluid the device is operating in has to be defined. For example, an application of the equations produced by Whicker and Fehlner in [8] indicate how the rudder lift and drag varies with rudder angle. This method uses a small amount of information about the rudder, whereas a surface panel flow analysis with full rudder surface definition can give pressure distributions and information on the wake downstream produced by the rudder.

Where manoeuvring and propulsion devices interact with each other and alter their flow, the relative position or locality is another important factor. In the case of a rudder-propeller system the flow impinging on the rudder from the propeller can greatly alter the rudder performance. This coverage has to be quantified by defining their relative positions in space referred to a particular co-ordinate system. The choice of co-ordinate system is always important and the particular system used in this work has been described in Chapter 2. When a designer is planning a stern arrangement it is also convenient to refer to a ship's axis system by defining a local co-ordinate system for the rudder-propeller arrangement this can then be referred back to the ship's axis system at any time by a base point. The rudder stock position is a common reference point and is even used in defining the length of a ship.

In the current work, geometric definition is to be limited up to and including the three-dimensional surface definition, as the methods used do not require any more detail than this. The level of geometric definition is described individually in each relevant Chapter and in the context of the method used to predict rudder performance.

1.6 Summary and Thesis Layout

Previous relevant published work has been discussed as a background to reaching the aims set out in the introduction. The philosophy behind the work presented in this thesis follows the design spiral approach. Levels of geometric definition have been identified and are referred to throughout the work.

Ship rudder propeller flow has been discussed briefly and the importance of developing a logical system of presentation and analysis of rudder performance. Chapter 2 presents a

coherent outline of the fundamental mechanism of rudder propeller interaction and the philosophy behind the methods employed in the work. The philosophy is derived from work to date, as described previously in this chapter, and the continued work presented in this thesis.

By identifying the previous experimental work and the scope of the parametric variation, the need for further experimental work on a skeg rudder downstream of a propeller has been identified. The need for more experimental work at low ship speed has also been recognised. Chapter 3 describes a series of wind tunnel tests and an innovative laboratory approach to rudder propeller testing to obtain all-movable and skeg-rudder performance data downstream of a propeller and hull.

Current and previous methods of predicting the performance of a rudder downstream of a propeller have been discussed and the need for a consistent method of predicting rudder-propeller performance at design stage has been highlighted. The large amount of experimental work carried out to date and the work described in this thesis has been identified as an extensive source of design data.

The experimental work, parametric database and underlying physical understanding have been coupled together in the form of a new computer program [23] which allows the designer easy access to practical rudder design information. This allows, for instance, the manoeuvring performance of a specific rudder-propeller system to be assessed and at the same time generate the resultant rudder stock torque (e.g. for steering gear sizing or rudder scantlings). The software allows a complete stern arrangement, including multiple rudder-propeller systems, to be investigated. Chapter 4 harnesses the experimental data, physical understanding and the ability to incorporate data from other prediction methods to create a method for rudder performance prediction downstream of a propeller and describes the software implementation of this method.

Practical design studies show, by example, the application of a design method and demonstrate the extent of applicability. Design studies can also reinforce the mechanism of rudder-propeller interaction for a higher understanding. Chapter 5 describes practical design studies of several types of rudder-propeller systems using the method described in Chapter 4.

CFD has been identified as a way of obtaining further parametric variation of data for design and methods for tightening the design spiral for detailed rudder performance data. A surface panel method has been applied to model the rudder-propeller interaction mechanism. This method has been chosen due to its proven performance [27] in modelling this type of interaction and the compromise between the level of the numerical model definition and the level of detail of the results is suitable for this application. Chapter 6 describes the theoretical framework of a surface panel method and the implementation of the method to numerically model the process of rudder-propeller interaction.

Chapter 7 demonstrates the use of the surface panel method detailed in Chapter 6, to investigate the numerical modelling of the flow around a skeg-rudder and propeller and provide detailed information on the distribution of loading for design. The results are compared against experimental results produced in Chapter 3 for validation.

The principal conclusions and findings are presented in Chapter 8 with reference to the established aims and objectives of the work. Recommendations for future work are detailed with the main conclusions.

References used in the work are presented in Chapter 0. Most figures and tables are presented in the main text with the plots of experimental results presented in Appendix A and Appendix B.

2 SHIP-RUDDER-PROPELLER FLOW

2.1 Introduction

A ship designer is required to devise an overall stern arrangement which satisfies the requirements of the owner as regards speed and overall fuel consumption while ensuring the vessel is able to maintain its course and satisfy manoeuvring requirements at low and service speed. Prediction of rudder forces and moments has its use in detailed rudder design. In particular their use is important in establishing rudder scantlings, stock diameter and likely torque for the steering gear.

The performance of a rudder operating behind a propeller can differ significantly from the free stream performance. When a ship is moving ahead the flow passing through the propeller is accelerated and rotated. The swirl and acceleration induced in the flow by the propeller alters the speed and incidence of the flow arriving at a rudder aft of the propeller. This controls the forces and moments developed by the rudder. In addressing the rudder-propeller interaction problem it is necessary to identify the various independent parameters on which the rudder forces depend.

The aim of this chapter is to identify and discuss the significant variables that affect rudder performance with the influence of a propeller upstream. In doing so the objective is to establish a coherent system of presentation for subsequent investigation and analysis of rudder-propeller performance.

2.2 Axis Definition

In defining the rudder and propeller it is necessary to define an axis system in which they operate. The axis definition used in the rudder-propeller system is shown in Figure 2.1 and uses a right-handed Cartesian system with the origin located at the centre of the rudder stock level with the rudder root.

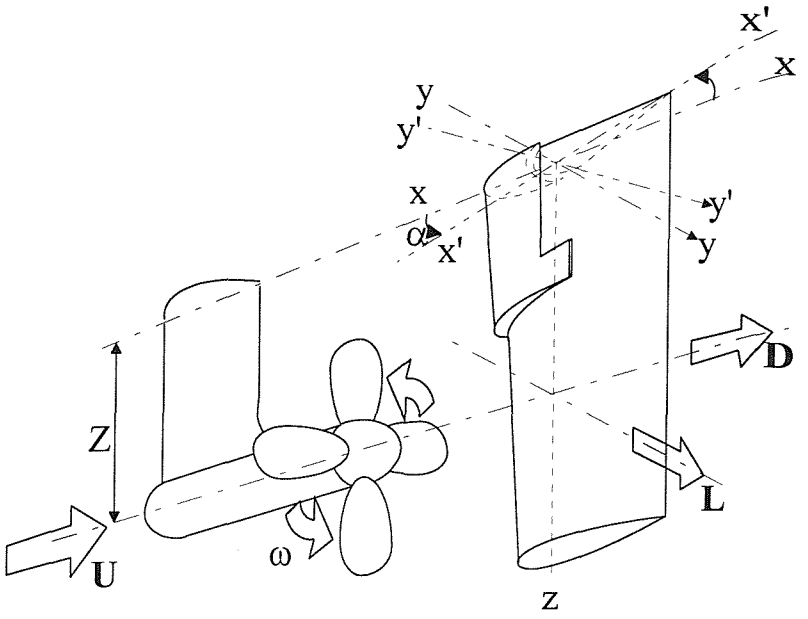

Figure 2.1 Rudder-Propeller Axis Definition

Lift or side force is perpendicular to the inflow direction and is positive to the starboard of the ship.

Drag is parallel to the inflow direction and is positive to the aft of the ship.

M_X is the moment about the x-axis (or ship axis).

M_Y is the moment about the y-axis.

M_Z is the moment about the z-axis (or rudder stock).

Moments are positive around the axis according to normal convention (i.e. anti-clockwise looking down on to the axis).

In wind tunnel tests and CFD analysis the rudder is presented inverted, with the tip at the top and the root at the bottom as this was the orientation for the particular experimental investigation. The axis system described above still applies to these configurations.

2.3 Governing Physical Parameters

Molland and Turnock [13] summarised the various independent parameters which govern rudder-propeller interaction. It is convenient to group them into four categories that can then be used to assess their affect on rudder performance.

The four groups of parameters are defined as follows.

i) Flow variables which control the magnitude of the forces developed. These include the time dependent quantities U (free stream velocity) and n (propeller rate of revolution) and the properties of the fluid, density (ρ) and dynamic viscosity (μ). Also included is the drift angle β_R between the ship and the free-stream.

ii) Rudder geometric variables which determine how the flow passes over the rudder and hence the force developed. This is controlled by the rudder incidence (α) span (S), mean chord (c), stock position (V), thickness (t), section shape, sweep and twist.

iii) Propeller geometric variables which control how the propeller imparts energy into the flow and generates thrust. For a given rudder type this is determined by its diameter (D), mean pitch (P), boss diameter, sweep, pitch and thickness distributions, number of blades and blade area ratio.

iv) Relative position and size of the rudder and propeller. The two units can be separated longitudinally (X), laterally (Y) and vertically (Z). The relative size is defined as the coverage (ξ) and is equal to the proportion of the rudder span in way of the propeller race.

These four groups may be represented in terms of non-dimensional parameters as in Equation [2.1].

$$\begin{pmatrix} L, \\ d, \\ M_X, \\ M_Y, \\ M_Z \end{pmatrix} = f\left\{\begin{matrix} \left[J, Rn, \beta\right], \\ \left[\alpha, AR, \frac{t}{c}\right], \\ \left[\frac{P}{D}\right], \\ \left[\frac{X}{D}\right], \left[\frac{Y}{D}\right], \left[\frac{Z}{D}\right], \left[\frac{\lambda D}{S}\right] \end{matrix}\right\} \quad [2.1]$$

2.4 Propeller Thrust Loading

The effect of increasing thrust loading, as reported in [13], is to:

i) increase the lift-curve slope above that of free-stream.

ii) significantly delay stall, even for low thrust loading (high J).

iii) stall is no longer the same for positive and negative incidence.

iv) drag component due to lift increases.

v) CP_c moves forward from free stream position.

vi) CP_S increases for positive incidence and decreases for negative incidence.

It is the propeller thrust loading (K_T/J^2) which principally controls the manoeuvring performance of the rudder as described in Chapter 3 and shown in experimental results Figure A-1.

2.5 Coverage and Rudder Angle Balance

Coverage defines the proportion of the area of the rudder that is within the propeller race. The magnitude of the thrust loading imparted to the fluid in the propeller race will control the value of side-force generated for a given rudder incidence for that area if the rudder is within the propeller's race. The coverage, therefore, is a measure of the proportions of the rudder where the force is dictated primarily by the propeller and that due to the free stream. A rudder with a larger coverage will be more strongly influenced by changes in propeller thrust loading.

The average flow generated by the propeller has an axial and a swirl component. The net effect of the swirl is an effective shift in local rudder flow incidence in one direction above the propeller axis and in the opposite direction below the axis. For a rudder with the same area above and below the propeller axis the angular offset effect will cancel. However, for example, tapered rudders or a rudder for which the propeller tip protrudes below the rudder tip, the effect of the rudder angle balance is an angular offset in the rudder performance. Similar effects arise from variation in lateral and longitudinal rudder-propeller separation.

2.6 Geometrical Properties of Rudder-Propeller Interaction

The principal geometrical properties that affect rudder-propeller interaction relate to the relative positions of the rudder and propeller and may be summarised as the longitudinal separation (X/D), lateral separation (Y/D) and vertical separation (Z/D).

X/D: A wide variation exists in the choice of X/D, a survey of recent new buildings indicates a range of X/D from 0.25 up to about 0.50 [13], some local variations occurring due to the amount of rake on the propeller, the use of controllable pitch propellers and the amount of taper on the rudder. It is not generally clear if the X/D value has been chosen on

the grounds of manoeuvring (rudder forces), propulsion (thrust deduction), or whether these aspects have been considered.

Y/D: A lateral offset of the rudder from the propeller shaft centreline is often the practice with twin screw vessels. This enables the propeller tailshaft to be removed without removing the rudder. Such a lateral offset may also be used on smaller higher speed craft to avoid the propeller hub core vortex impinging on the rudder, leading to rudder cavitation. Typical values of Y/D used in practice vary from 0.0 to about 0.25.

Z/D: On larger vessels Z/D tends to a value of around S/D-0.5 with the rudder tip approximately coincident with the propeller tip. On smaller vessels the necessity of propeller shaft inclination can lead to Z/D values of down to about 0.5. Limitations on all-movable rudder root bending moments and stock diameters will normally preclude extending the span of the rudder fully into the propeller race.

2.7 Low Speed and Four Quadrant Operation

When a ship is manoeuvring at very low or zero speed the rudder relies on the propeller to create an induced velocity to produce a manoeuvring sideforce. In this mode of operation the flow is completely controlled by the propeller and therefore is of particular interest in determining the effect of a propeller upstream of a propeller.

Although most requirements for ship manoeuvring capabilities are defined at service speed it is crucial that a ship manoeuvres well at low speed and has known performance in all four quadrants of operation e.g.:

i) Ship ahead, propeller ahead.
ii) Ship ahead, propeller astern.
iii) Ship astern, propeller astern.
iv) Ship astern, propeller ahead.

2.8 Data Definition

In the coming Chapters various coefficients and symbols will be used to quantify rudder and propeller performance, it is therefore necessary to define these symbols and in some cases why they are used and also their significance.

Using the relevant speed U (m/s) and revolutions n (revs/sec) the advance ratio J is calculated as:

$$J = \frac{U}{nD} \qquad [2.2]$$

where D is propeller diameter. The non-dimensional thrust coefficient (K_T) and torque coefficient (K_Q) are given by:

$$K_T = \frac{T}{\rho n^2 D^4} \qquad [2.3]$$

$$K_Q = \frac{Q}{\rho n^2 D^5} \qquad [2.4]$$

where ρ is the density.

The propeller efficiency η is given by:

$$\eta = \left(\frac{J}{2\pi}\right) \times \left(\frac{K_T}{K_Q}\right) \qquad [2.5]$$

The non-dimensional coefficient form of the rudder forces are obtained as follows:

$$C_L = \frac{L}{\frac{1}{2}\rho U^2 A} \qquad [2.6]$$

$$C_d = \frac{d}{\frac{1}{2}\rho U^2 A} \qquad [2.7]$$

The non-dimensional coefficient form of the rudder moments are obtained as follows:

$$C_{Mz} = \frac{Mz}{\frac{1}{2}\rho U^2 Ac} \qquad [2.8]$$

$$C_{Mx} = \frac{Mx}{\frac{1}{2}\rho U^2 AS} \qquad [2.9]$$

$$C_{My} = \frac{My}{\frac{1}{2}\rho U^2 AS} \qquad [2.10]$$

Where U is the free stream velocity (m/s), S the rudder span, c the mean rudder chord, and A the total rudder area (A=S.c).

For the nominal bollard pull case the force and moment coefficients are non-dimensionalised using $K_T n^2 D^2$ which represents the square of the propeller induced velocity at J=0. These non-dimensionalised coefficients are designated by C_L^* and C_d^* etc. and are defined as follows:

$$C_L^* = \frac{L}{\frac{1}{2}\rho A K_T n^2 D^2} \qquad [2.11]$$

$$C_d^* = \frac{d}{\frac{1}{2}\rho A K_T n^2 D^2} \qquad [2.12]$$

$$C_{Mz}^* = \frac{Mz}{\frac{1}{2}\rho A c K_T n^2 D^2} \qquad [2.13]$$

$$C_{Mx}^* = \frac{Mx}{\frac{1}{2}\rho A S K_T n^2 D^2} \qquad [2.14]$$

$$C_{My}^* = \frac{My}{\frac{1}{2}\rho A S K_T n^2 D^2} \qquad [2.15]$$

The propeller theoretical velocity is used because the free stream velocity U tends to zero, thus any non-dimensionalisation with respect to U becomes void and the inclusion of K_T allows the influence of propeller pitch ratio (P/D) to be represented. Investigation of the results indicate that the two representations Equations 2.6 to 2.10 and Equations 2.11 to 2.15 converge satisfactorily at low J values. An examination of the use of these non-dimensional coefficients can be seen in the written discussion of [62].

The position of the centre of pressure on the rudder in the spanwise and chordwise directions is obtained as follows:

$$CP_c = \left(\frac{M_z}{N} + W\right) \times \frac{100}{c} \qquad [2.16]$$

$$CP_S = \left(\frac{M_N}{L} - V\right) \times \frac{100}{S} \qquad [2.17]$$

where W is the distance of the rudder stock from the leading edge and V represents the distance from the dynamometer measurement centre to the rudder root. M_N is

$\sqrt{M_x^2 + M_Y^2}$. CP_c is the percentage of rudder chord from the root leading edge, CP_S the percentage of span from the rudder root.

In comparing the overall propulsive effect of the rudder-propeller system, two effective propeller thrust coefficients are defined. The net thrust of the propeller and rudder combination $K_{T(R+P)}$ is defined as:

$$K_{T(R+P)} = K_T - K_D \qquad [2.18]$$

and the net thrust excluding the free-stream drag of the rudder $K_{T(st)}$ defined as:

$$K_{T(st)} = K_T - (K_D - K_{D0}) \qquad [2.19]$$

where K_D is the drag coefficient of the rudder and K_{D0} the free-stream drag coefficient of the rudder. K_D can be expressed in terms of C_D:

$$K_D = \frac{d}{\rho n^2 D^4} = \frac{1}{2}\frac{A}{D^2} J^2 C_D \qquad [2.20]$$

Useful measures of the performance of rudders are lift curve slope at zero incidence $dC_L/d\alpha$ and the corresponding drag at zero incidence C_{d0}. These values are obtained directly from the rudder performance data or by theoretical or numerical methods.

The influence of upstream body and/or propeller slipstream on the effective angle of drift seen by the rudder is defined as a flow straightening factor γ:

$$\gamma = \frac{\alpha_0}{\beta_R} \qquad [2.21]$$

where β_R is the geometric yaw (or drift) angle at the rudder and α_0 the angle of rudder incidence for zero sideforce at that drift angle.

The actual incidence that the rudder encounters or the effective rudder angle α_E is defined as:

$$\alpha_E = \partial - \gamma \beta_R \qquad [2.22]$$

where ∂ is the rudder angle relative to the ship's axis.

2.9 Summary

The principle variables that control rudder performance in undisturbed free-stream and the interdependence of the rudder and propeller and their respective operating conditions has been identified. The influences of fluid flow, geometry and relative positions of the rudder and propeller have been discussed. A suitable presentation system has been identified for analysis of the effect of the categorised parameters.

Non-dimensional rudder performance has been defined as a function of free-stream speed and propeller induced velocity for lower advance ratios. The assertion that rudder performance can be defined as a function of the propeller operating condition suggests that rudder performance could be investigated using the propeller velocity only and no free stream speed applied. This has the advantage that modelling the ship speed is not required in the bollard pull condition and therefore testing in a wind tunnel or water tunnel to induce a ship speed is not necessary and can reduce the cost of experimentation.

The identification of the individual factors that affect rudder performance downstream of a propeller can be used to establish the extent of parametric variation in experimentation. Rudder geometry, propeller performance and the operating condition are required to be studied and accounted for. When studying the effect of relative position of the rudder and propeller it is more effective to have a large variation of longitudinal separation (X/D) as this is the largest variation on ships. The effect of lateral separation (Y/D) is high and should also be studied to a greater degree with vertical separation (Z/D) varied to investigate coverage and balance effects. The influence of the important dominating variables in rudder-propeller interaction have been identified and can be considered when creating a method for rudder performance prediction.

3 EXPERIMENTAL WORK

3.1 Introduction

With the increasing use of skeg-type rudders in ships due to structural considerations and general overall performance, it is necessary to investigate the skeg-rudder performance downstream of a propeller in more detail. Although tests have been carried out on skeg-rudders [16] more variation is required on lateral separation (Y/D) and longitudinal separation (X/D). There is little published data on the performance of the skeg-rudder and all-movable rudder operating in the true bollard pull condition and this is another area that needs consideration in the testing programme.

The aim of this chapter is to describe testing methods and present results from an experimental programme designed to satisfy the need for examining the less investigated parameters in skeg-rudder or all-movable rudder and propeller interaction. The individual testing programmes are summarised in more detail in the description of the tests. The three principle objectives to satisfy the aims of the experimental work are as follows:

i) Determine skeg-rudder and propeller performance plus the effect of a hull form upstream on performance.

ii) Develop cost effective experimental techniques for determining rudder and propeller interaction.

iii) Determine the rudder and propeller interactions at low and zero advance ratio (J=0).

3.2 Review of Previous Experimental Work

Over a significant period of time an extensive programme of experimental and theoretical research into the effect on manoeuvring of the stern arrangement of vessels and in particular the interaction between the ship hull, propeller and rudder has been on going at the University of Southampton. The result of this work has been the development of a proven methodology [13], which accounts for the physical basis of the interaction between the various stern components.

One of the results of the research has been the development of a large experimental database. This relates the changes in propeller operating condition and the geometric description of the rudder-propeller system to the resultant performance of the rudder in terms of developed rudder forces and moments. The experimental database includes tests at low speed and in all four quadrants.

The extensive experimental measurements and theoretical prediction of rudder forces provide a wide range of necessary data for use in predicting the manoeuvring performance. The extent of the rudder models tested are detailed in Table 3.1 and the overall propeller details are summarised in Table 3.2. Details of the experimental method are also given in [13].

Table 3.1 Rudder Model Particulars

Designation	Type	Span (m)	Tip Chord (m)	Root Chord (m)	Tip Offset (m)	Aspect Ratio
Rudder 0	Skeg	1.0	0.593	0.741	0.148	1.5
Rudder 1	All-movable	1.0	0.593	0.741	0.148	1.5
Rudder 2	All-movable	1.0	0.667	0.667	0.0	1.5
Rudder 3	All-movable	1.2	0.667	0.667	0.0	1.8
Rudder 4	All-movable	1.3	0.667	0.667	0.0	1.95
Rudder 5	All-movable	1.0	0.800	0.800	0.0	1.25
Rudder 6	All-movable	1.0	0.556	0.556	0.0	1.8

All rudders have a NACA 0020 constant section with square tips.

Table 3.2 Propeller Model Particulars

Designation	Modified Wageningen B.4.40 Series
Range of revolutions (rpm)	0 to 3000
Number of blades	4
Diameter (m)	0.8
Boss Diameter (max)	0.2
Mean Pitch Ratio	0.95
Blade Area Ratio	0.4
Rake (degrees)	0
Blade thickness ratio t/D	0.050
Section shape	Based on Wageningen B series
Blade outline shape	Based on Wageningen but with reduced skew

3.3 The Investigations

The following Chapter presents the results from a detailed wind tunnel and laboratory investigation into the performance of a skeg-rudder and all-movable rudder downstream of a propeller and hull combination. The experiments were carried out in the University of Southampton 3.5m x 2.5m low-speed wind tunnel in March 1995 and the Sir George Edwards Laboratory in January 1996.

The two sets of test schedules were designed to obtain rudder performance data for a range of ship operating conditions including free stream, varying propeller advance ratios and at a bollard pull condition. The free stream and higher advance ratios were tested in the wind tunnel to use wind speed as a simulated ship speed. The bollard pull (J=0) tests were conducted in an open laboratory to simulate a ship with no speed.

The use of an open laboratory in rudder testing is a novel and innovative approach, there are several advantages associated with this method. The wind tunnel used in previous tests is a closed circuit tunnel and therefore the propeller will circulate the air just as a wind tunnel fan would. The result is a small inflow velocity into the propeller, this is only a nominal bollard pull (J=0.17) case which does not represent the true bollard pull of zero inflow speed into the propeller and hence zero ship speed. Another important advantage of

this method is the open laboratory approach negates the need for a wind tunnel in the bollard pull case and hence cost is reduced and more parametric tests can be conducted.

3.4 Description of Models

3.4.1 Rudder

For the experimental investigations two rudders were used; designated rudder No. 2 and skeg-rudder No. 0 (using the same designations as [13]). A detailed description of the method of manufacture of the rudder models is given in [38]. Table 3.1 presents the particulars of the rudders used in the current investigation and Figure 3.1 their overall dimensions. The rudders had pressure tappings to give complete coverage of the rudder surface, also detailed in Figure 3.1. The manufacturing technique for the pressure tappings is outlined in [17].

For the tests the rudders had a roughness strip attached 5.7% of the chord from the rudder leading edge on both sides for turbulence stimulation. The roughness strips were manufactured from 12mm wide double-sided tape densely covered with 100 grade carborundum grit (0.15mm diameter).

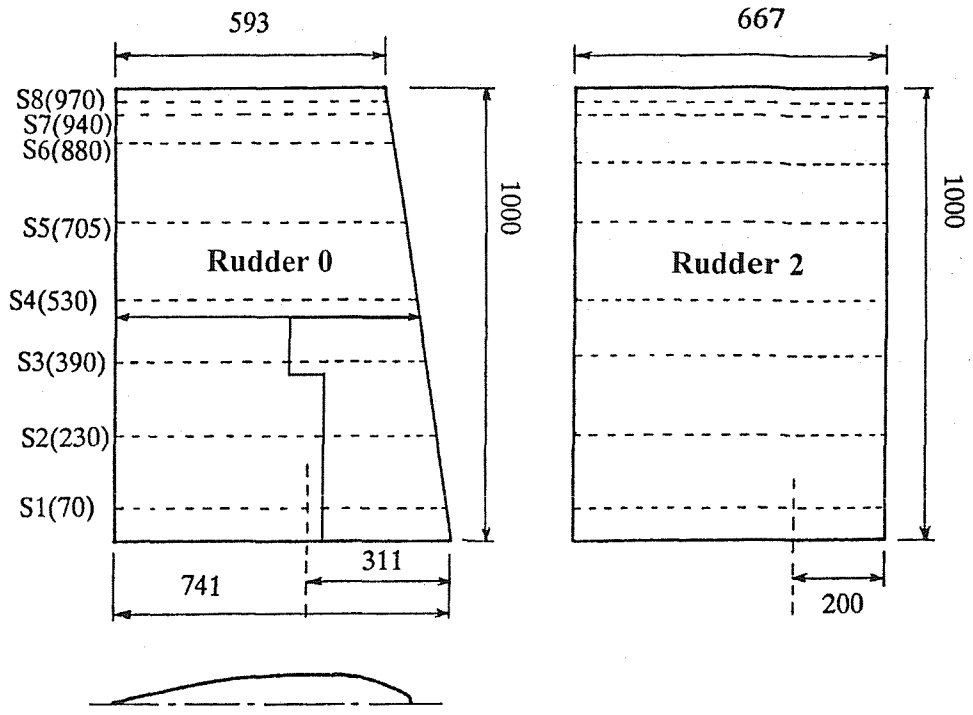

Figure 3.1 Dimensions of Two Rudder Models

3.4.2 Propeller

A representative propeller design, based on the Wageningen B4.40 was used. Modifications made to the basic Wageningen design are detailed in [39] and consisted of altering the blade root shape to allow an adjustable pitch design with four separate blades and a split hub. Other changes involved removing rake and decreasing blade sweep to reduce centripetal loading moments at the root and also increasing the hub/diameter ratio from 0.167 to 0.25. Overall propeller details are summarised in [39] and a comparison of the basis and modified Wageningen B4.40 can be seen in Figure 3.2.

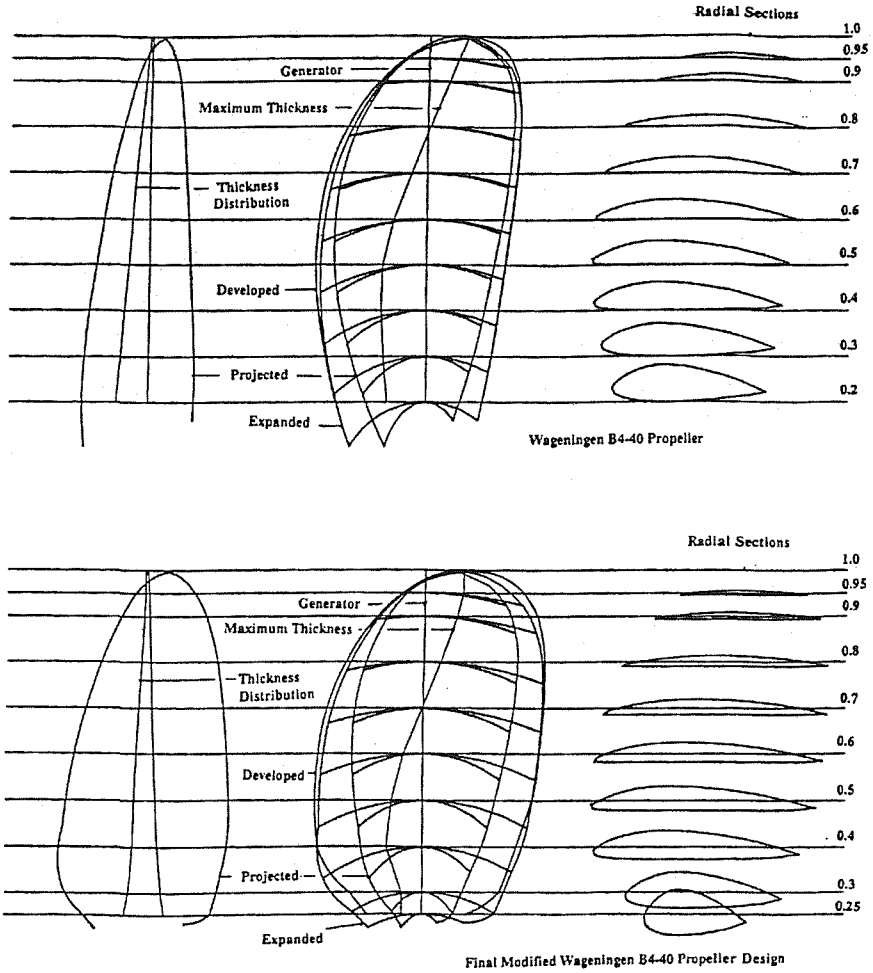

Figure 3.2 Comparison of Basis and Modified Wageningen B4.40 Propeller

The split hub was manufactured from aluminium alloy and a positive clamping action allows the four blades to be rotated and clamped to the desired pitch ratio setting. The four blades were manufactured using hybrid carbon/glass fibre laid up in the same split female mould to produce identical blades. The production of the composite blades is detailed in [40] and the machining of the female mould in [39]. In appearance the hub/blade root region is similar to that of a typical controllable pitch propeller.

3.4.3 Mariner Stern Form Hull

The Mariner form [44] was used as the representative ship stern thus allowing the results to be used in conjunction with those from the rest of the MOSES managed research programme. A scale factor of 8.4 matches the existing rudder-propeller rig to that of the Mariner stern geometry. If the whole Mariner form were represented this would give an

impractical model length of 19m for the inverted hull form. Vertically, the floor of the working section is aligned with the design waterline.

Of primary importance with regard to rudder-propeller-hull interaction, is the direction imparted to the flow by the stern and the velocity profile within the hull wake. A physically representative stern flow can be achieved through the use of an exact stern shape upstream of the propeller for a proportion of the ship length and correct thickening of the model wake through the use of boundary layer stimulation.

The stern extends from the propeller plane to section 17. A total model length of 2.69m from propeller plane to model leading edge allows drift angles of up to ±15° to be achieved without undue tunnel blockage effects. The final stern design uses the exact Mariner form to section 18 and then fairs using elliptical section to the front of the model. The shape of the resulting model waterlines is similar to that of an airfoil and should not cause undue problems with flow separation for drift angles up to 15°. Calculations based on the typical wind tunnel speed of 10m/s, showed that the thickness of the boundary layer on the Mariner stern model needed to be doubled to achieve approximate similitude with full-scale. This was achieved through the use of surface mounted studs. Construction of the model is detailed in [43] which includes a table of offsets and pressure tapping positions.

3.5 Apparatus

3.5.1 General

The overall rig for testing the interaction of ship rudders and propellers is shown in Figure 3.3. The rig consists of two independent units, which allow free-stream (open-water) tests to be carried out independently on rudders and propellers as well as the investigation of their interaction. This configuration is designed to fit under the working section of the University of Southampton's 2m by 1.5m and 3.5m by 2.5m wind tunnel.

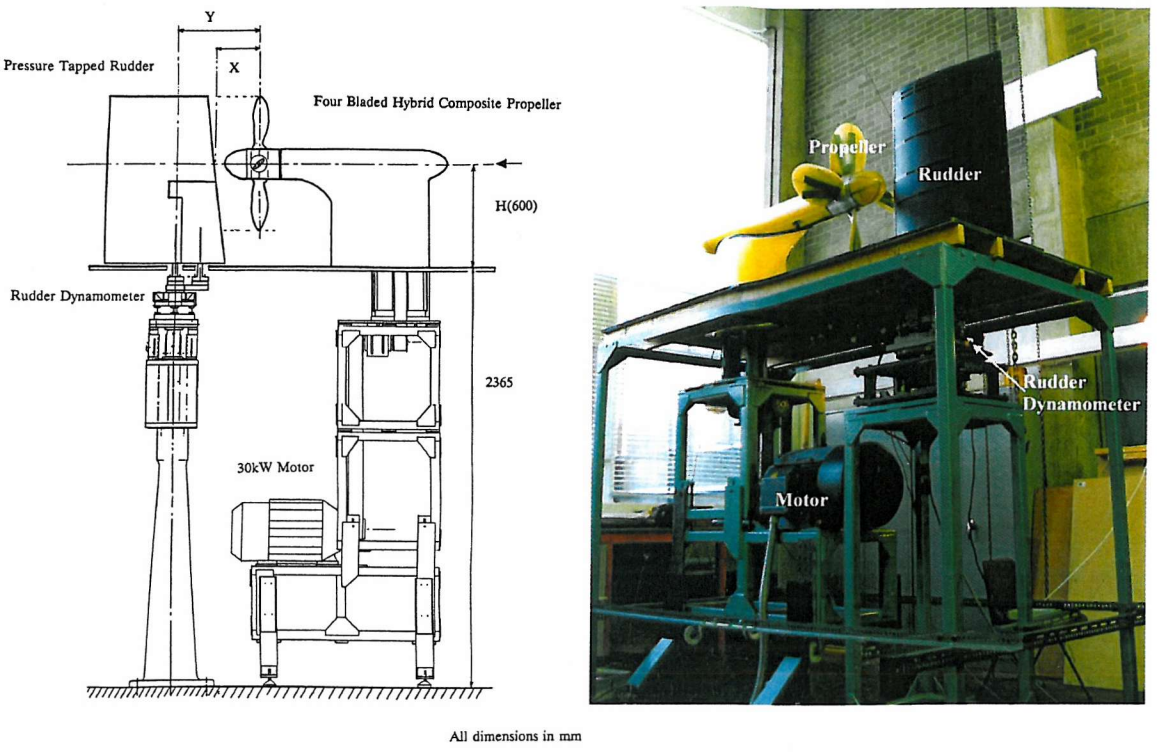

Figure 3.3 Views of Overall Test Rig for Investigation of Rudder and Propeller Interaction.

For the bollard pull open laboratory tests it was necessary to create a raised floor framework in the Sir George Edwards Laboratory of the University of Southampton. The rig is designed to be portable and can be used in any working space of sufficient volume and with a 3-phase 30 kilowatt power supply. This is detailed in Figure 3.3 with engineering drawings shown in Figure 3.4. The relative positions of the skeg-rudder, propeller and mariner stern form in the 2.5m by 3.0m wind tunnel can be seen in Figure 3.5.

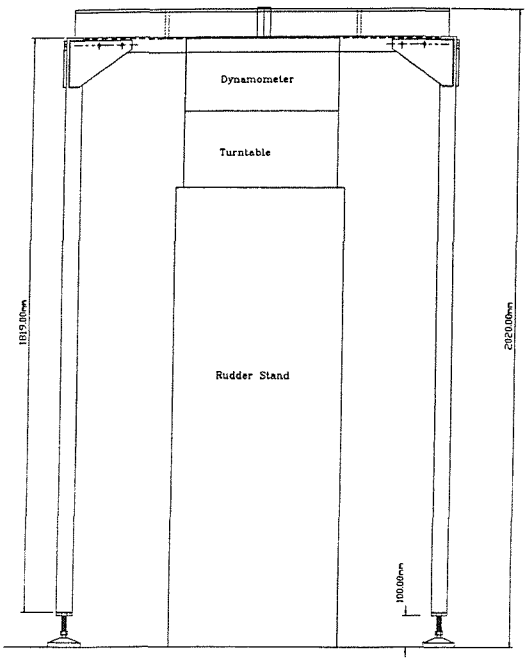

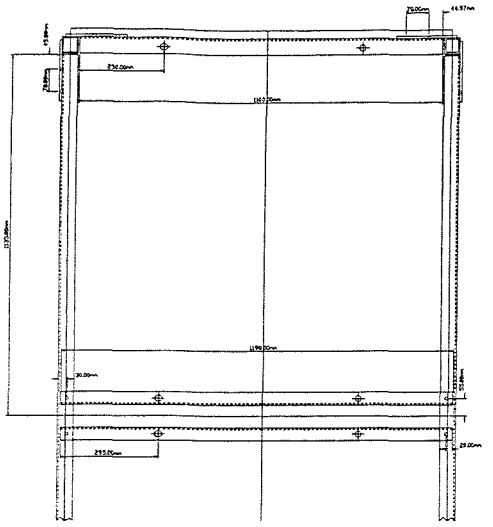

SPECIFICATIONS	CONTRACT NO. C60 R47	COMPANY University of Southampton Department of Ship Science
Information Only	DRAWN BY: Jason Smithwick Room 1015, Building 22 Extension 3584	TITLE Rudder and Propeller Zero J Test Rig
FOR: Workshop	DESIGNED BY: Jason Smithwick	End View of Assembly
All dimensions in mm. Do not scale from drawing	SIZE A4 / FSCM NO. / DWG NO. / FILE NAME END.SKD	
	SCALE 1mm =10mm / DATE 26/10/95 / SHEET 1 of 1	

SPECIFICATIONS	CONTRACT NO. C60 R47	COMPANY University of Southampton Department of Ship Science
Information Only	DRAWN BY: Jason Smithwick Room 1015, Building 22 Extension 3584	TITLE Rudder and Propeller Zero J Test Rig
FOR: Workshop	DESIGNED BY: Jason Smithwick	Plan View of Assembly
All dimensions in mm. Do not scale from drawing	SIZE A4 / FSCM NO. / DWG NO. / FILE NAME PLAN.SKD	
	SCALE 1mm =10mm / DATE 25/10/95 / SHEET 1 of 1	

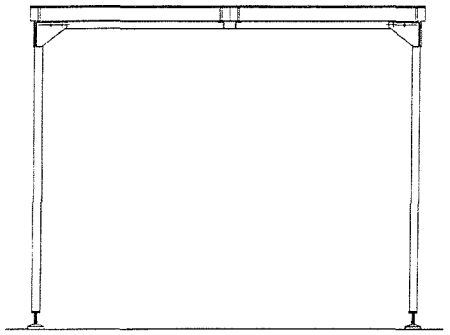

SPECIFICATIONS	CONTRACT NO. C60 R47	COMPANY University of Southampton Department of Ship Science
Information Only	DRAWN BY: Jason Smithwick Room 1015, Building 22 Extension 3584	TITLE Rudder and Propeller Zero J Test Rig
FOR: Workshop	DESIGNED BY: Jason Smithwick	Profile Assembly Drawing
All dimensions in mm. Do not scale from drawing	SIZE A4 / FSCM NO. / DWG NO. / FILE NAME PROFILE.SKD	
	SCALE 1mm= 20mm / DATE 26/10/95 / SHEET 1 of 1	

Figure 3.4 Assembly views of rudder and propeller zero J test rig.

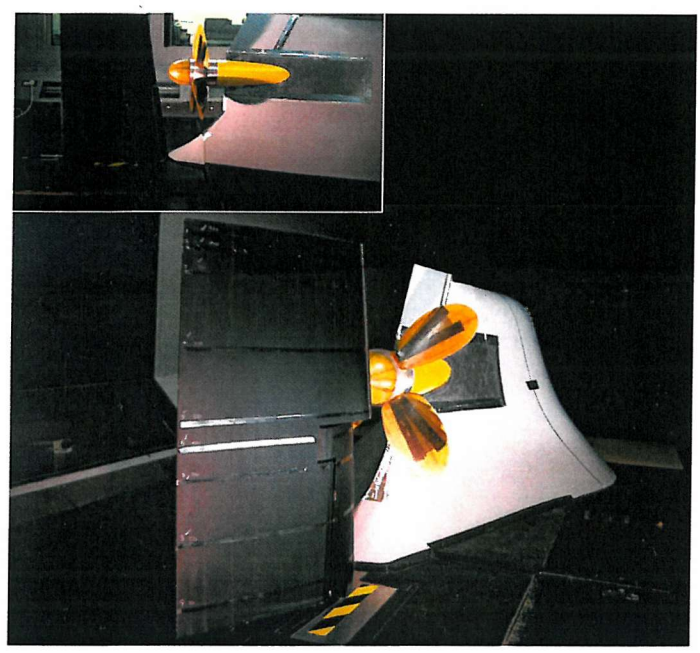

Figure 3.5 Views of Skeg-Rudder, Propeller and Hull Relative Positions

3.5.2 Rudder Rig/Dynamometer

The rig consists of a steel structure attached to the floor, which supports a five-component strain gauge dynamometer below the tunnel working section. A description of the design and calibration of the dynamometer is given in [41]. The rudder is bolted to a turntable which is in turn bolted directly to the dynamometer. The dynamometer is levelled and adjusted vertically so that there is a small gap of approximately 2.5mm (0.004c) between the rudder root and the floor of the wind tunnel working section. The rudder dynamometer and turntable can be seen in Figure 3.6.

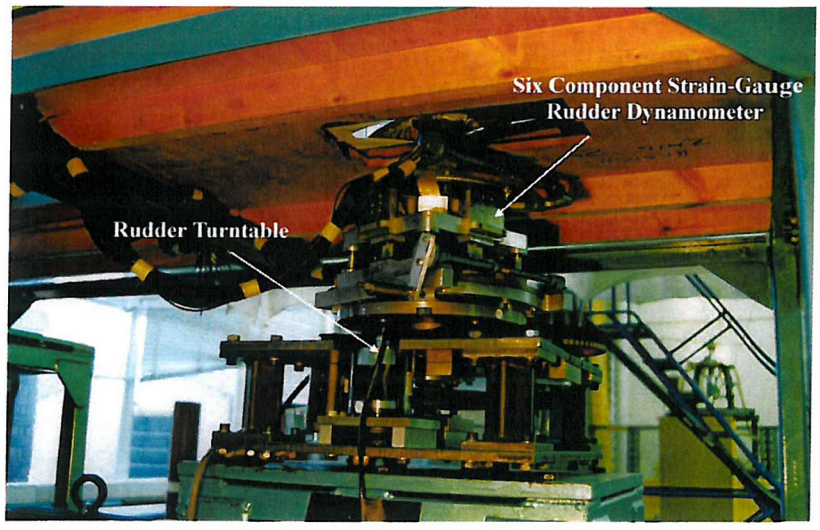

Figure 3.6 Rudder Dynamometer and Turntable

3.5.3 Propeller Rig

Full details of the propeller rig are given in [38]. The rig is designed in such a way that the propeller can be adjusted vertically, longitudinally and at an angle of attack to the flow if required. The base position of the tests reported on were carried out with the propeller's axis of rotation 600mm above the wind tunnel floor. The propeller rotates anti-clockwise when viewed from aft (looking upstream).

An in-line strain gauge dynamometer mounted close to the propeller measures the delivered thrust and torque. The design and static calibration of this dynamometer is detailed in [42]. The two measurement components of the dynamometer are connected via a slip-ring assembly to Fylde Bridge balance units with a built in stabilised power supply. The bridge balance output voltage is measured directly (without amplification) using a Schlumberger Minate digital voltmeter.

A variable frequency inverter is used to control the 30kw electric drive motor and the propeller rate of revolutions can be continuously varied in small discrete steps between 0 and 3000 rpm. An optical shaft encoder was used to measure propeller revolutions and gives a voltage proportional to shaft rpm.

3.5.4 Data Acquisition System

The large number of individual data readings required the use of a new automated system for data acquisition. An enhanced acquisition system has been developed, by the author, for these particular sets of tests, involving a PC and necessary interface cards. The total system has the same function as the system detailed in [13] but the software has been enhanced and changed to suit the new acquisition cards together with several added facilities for more automated acquisition. A diagrammatic representation of the acquisition system can be seen in Figure 3.7 showing the software functions.

Bridge output signals from the five-component rudder dynamometer, the rudder pressure transducers, and the propeller thrust/torque dynamometer are measured using a digital voltmeter connected to the data acquisition PC via an IEEE interface. Voltages for the dynamometers are supplied by Fylde Bridge-Voltage Units and are measured using an analogue to digital acquisition card inside the PC and control of the scanivalve unit is

executed via a parallel interface also located on the card. Both the parallel and analogue ports are connected via an interface box to allow versatile connection and more than one control function. All acquisition is controlled by software running on a personal computer and the results stored on hard disk for subsequent analysis. A control system schematic can be seen in Figure 3.8 with the control and acquisition system layout shown in Figure 3.9.

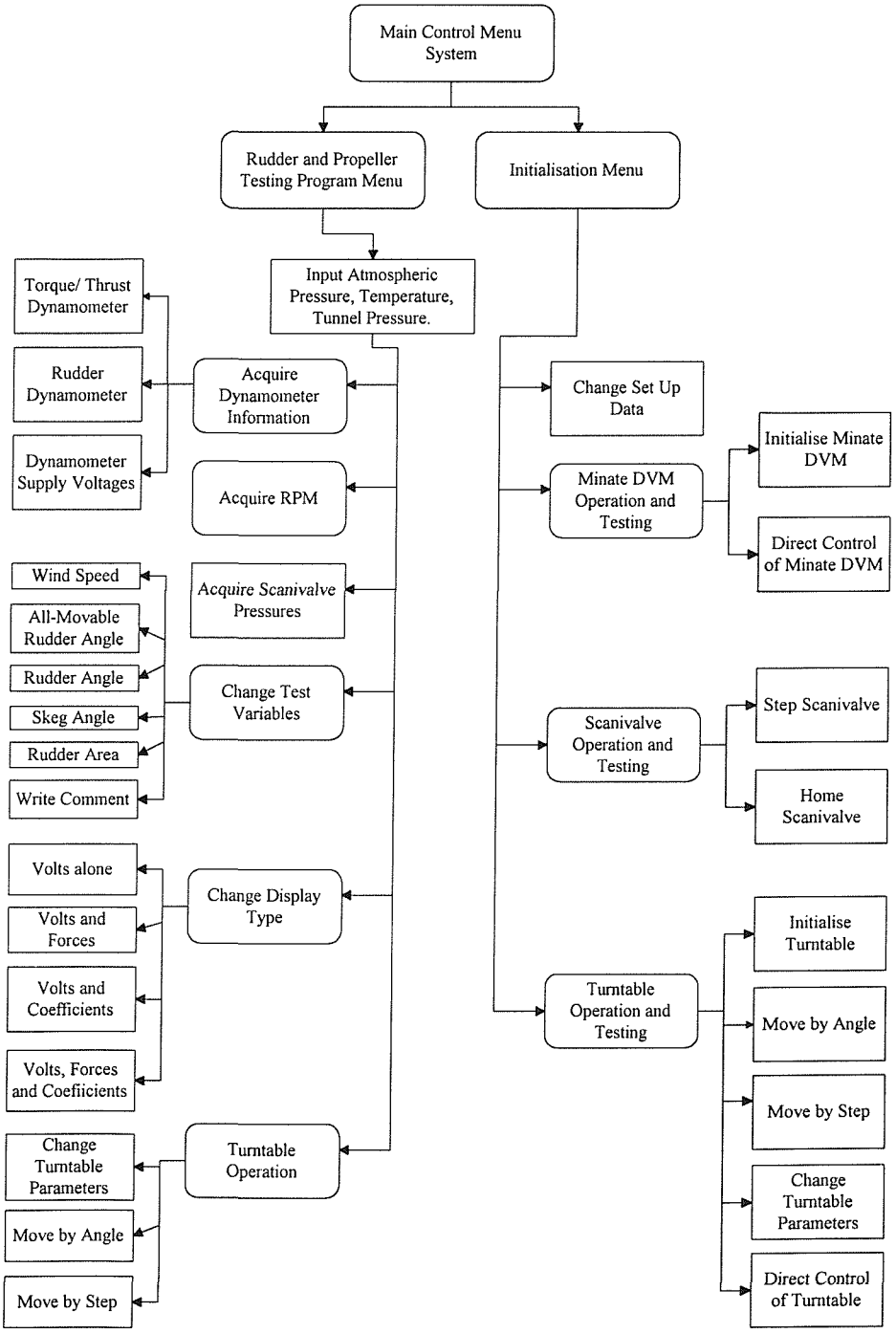

Figure 3.7 Rudder-Propeller Acquisition Program Schematic

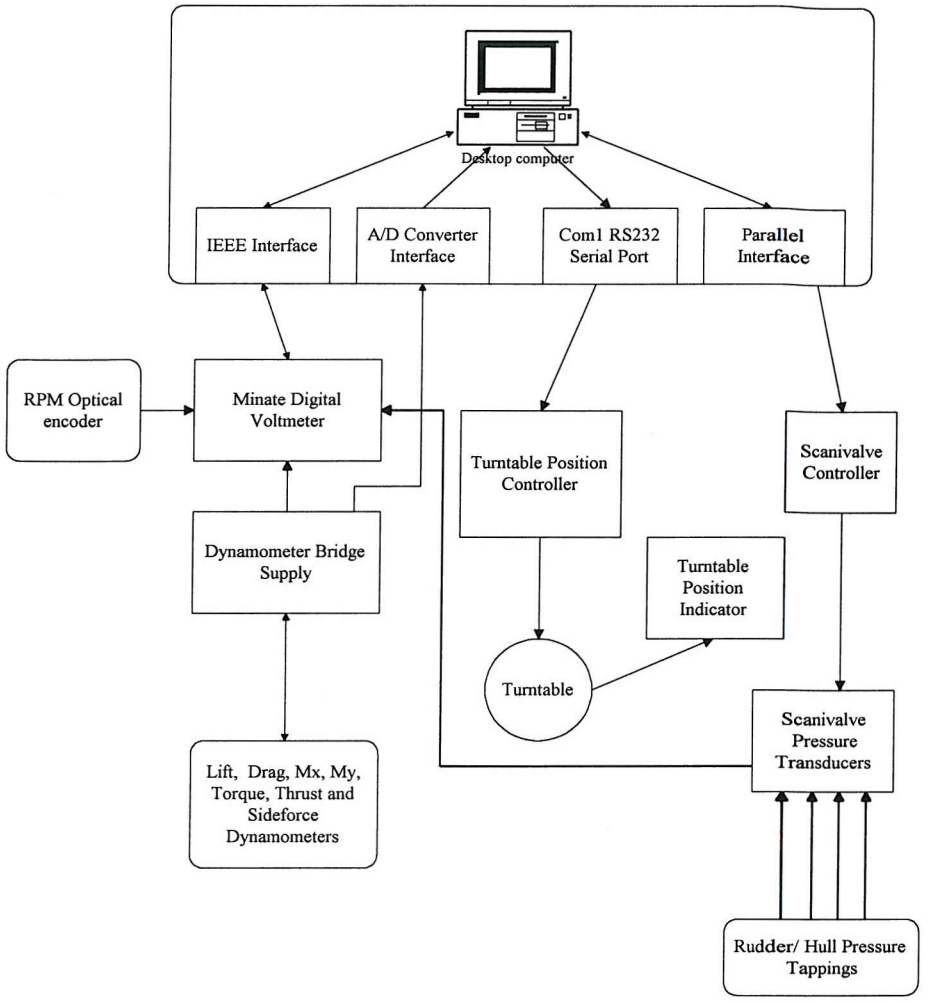

Figure 3.8 Rudder-Propeller Experimental Setup Schematic

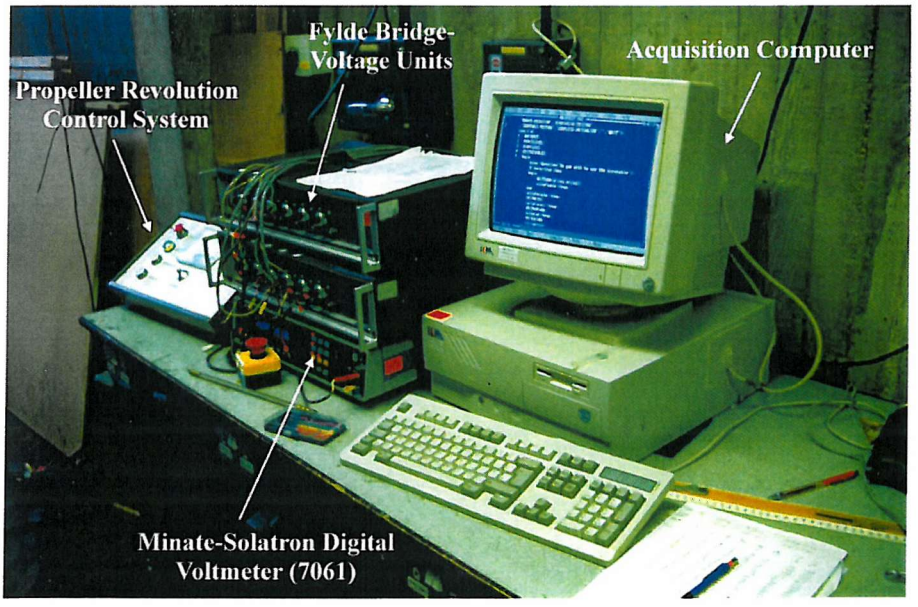

Figure 3.9 Control and Acquisition System Layout

3.6 Data Reduction and Corrections

A computer program, described in [15], was used to provide the data in coefficient form as described in Chapter 2. The program incorporates the rudder dynamometer five-component interaction matrix and correction formulae and the resolution of forces and moments from instrument axes to stream axis as necessary. A cross plot of raw rudder data yielded the angular misalignment of the rudder rig and this correction was applied to all measured angles before insertion in the program.

The analysis program incorporates the propeller dynamometer calibrations hence allowing direct calculation of the propeller coefficients. The static calibration carried out on the Torque-Thrust dynamometer gave a linear response to loading of both thrust and torque with negligible interactions [42].

Tunnel boundary corrections were investigated but found to be unnecessary, as effects such as tunnel blockage for the 3.5m x 2.5m working section were found to have a negligible effect for the rudder size and propeller diameter tested.

The acquisition of rudder and hull surface pressures, together with reference static and dynamic pressures from the tunnel, allowed direct calculation of the local static pressure coefficient C_P. To obtain surface pressures, four differential pressure transducers used in conjunction with the rotary scanivalve give a maximum of 144 individual pressure measurements for any test. The no-wind pressure transducer output voltage V_{P0} was measured at the beginning of each test. The reference pressure connected to all four transducers was the static line of the main wind tunnel pitot-static probe. This line was also connected to one input port for each transducer to give a 'real' zero pressure difference value V_{P0}. The pitot line was connected to another input port to give a voltage V_{DP} proportional to the total tunnel dynamic pressure.

For each pressure port measurement V_P, the non-dimensionalised pressure coefficient C_P is obtained directly as:

$$C_P = \frac{V_P - V_{P0}}{V_{DP}} \qquad [3.1]$$

This expression does not require an explicit value for the calibration constant of the particular pressure transducer, since the transducer has a linear response.

As the location of each pressure measurement on the rudder surface is known, integration of C_P around the chord of the rudder for a constant span allows the local non-dimensional Normal Coefficient C_N to be calculated. The integration was carried out using a quadratic numerical procedure similar to Simpson's rule but with variable spacing.

3.7 Wind Tunnel Testing Programmes (J>0)

Results are reported from two 10 working day sessions of testing in the 3.5m x 2.5m low speed wind tunnel. The basic propeller-rudder tests were carried out at a nominal Reynolds number of 0.4×10^6, based on a free stream velocity of 10m/s.

Velocities induced by the propeller on to the rudder at the higher thrust loadings led to effective Reynolds numbers of up to 1.0×10^6 over much of the rudder based on rudder chord. English [18] indicated that a satisfactory Reynolds number, based on propeller diameter and rpm, to avoid scaling problems would be greater than 1.4×10^6. The lowest rpm used on these tests was 800rpm which for an 800mm diameter propeller gives a Reynolds number, based on propeller diameter and rpm, of 1.53×10^6.

Rudder No. 2 was tested in the base position with the propeller axis 600mm above the wind tunnel floor, zero lateral separation, and a longitudinal separation of X/D=0.39. A four-bladed propeller configuration with a pitch ratio setting of P/D=0.95 was used. This arrangement corresponded to the mid-longitudinal position used in previous tests reported in [13]. Figure A-1 shows Rudder No. 2 results compared to tests conducted in [15] in 1991. Correspondence of results between test sessions was good and demonstrated the repeatability of the test methodology. The flow alignment was found to be +0.8° for the all-movable rudder No. 2 and +0.2°for the skeg-rudder No. 0. "Open-water" tests were also carried out with four blades at a pitch ratio of P/D=0.95 at a range of positive revolutions for wind speeds of 10m/s and 15m/s.

3.7.1 Rudder-Propeller Interaction

The skeg-rudder No. 0 performance was the main point of interest in this part of the investigation with rudder No.2 being used principally for verification. Correspondence of results between test sessions was good and demonstrated the repeatability of the test methodology.

In the base position the skeg-rudder No. 0 was tested at advance ratios, J=0.94, J=0.51 and J=0.35 which corresponds to a freestream velocity of 10m/s at a rate of revolution of the propeller of 800rpm, 1460rpm and 2100rpm respectively. Measurement of the propeller and rudder force dynamometers were made at incidence increments of 5° between -35° and +35°. For the investigation of rudder torque the rudder dynamometer measurements were taken for the movable rudder part only (excluding skeg) and for the investigation of manoeuvring forces the total rudder plus skeg forces were taken. Surface pressure surveys were carried out at 10° increments between -30° and +30°. Measurements were taken for the rudder-propeller combination with a lateral separation Y/D=±0.25 and Y/D=±0.125. These positions were all tested for manoeuvring forces with the position of Y/D=+0.25 tested for torque forces also. With a position of Y/D=-0.25, at one single advance ratio of J=0.35, the skeg angle was also changed to ±5° with rudder angles of -5°,0° and 5°

The rudder was tested with the wind tunnel fan stationary to simulate a nominal bollard pull condition. The flow induced by the propeller drove the tunnel flow at a slow but measurable speed thus giving an effective advance ratio of J=0.17. The steady-state wind speed imparted by the propeller to the air in the tunnel was measured using a Betz manometer connected to the tunnel pitot-static tube upstream of the rudder-propeller rig. It should be noted that velocities induced by the propeller at the higher revs. led to effective Reynolds Numbers of up to 0.75×10^6 over much of the rudder. Results presented in [18] indicate that tests at these conditions should preclude any significant scale effect. The test procedure and results obtained from an earlier preliminary study are described in [21].

3.7.2 Rudder-Propeller and Hull Interaction

The Mariner stern form was initially installed at a drift angle of 0°. In the base position the skeg-rudder No. 0 was tested for the 'freestream' (propeller stationary) case in way of the rudder and hull combination and in the bollard pull (J=0) condition. A pressure survey over

the hull model surface and dynamometer forces were measured at 10° increments between -30° and 30°.

For the three advance ratios, J=0.94, J=0.51 and J=0.35 dynamometer forces were measured at 5° increments between -35° and 35°. A pressure survey over the hull was conducted at 10° increments between -30° and 30°. The rudder was tested for two other longitudinal positions of X/D=0.52 and X/D=0.64 as well as the base position of X/D=0.39. In all cases, measured forces and pressures were taken in the same manner as for the base position.

3.8 Open Laboratory Testing Programme (J=0)

Results are reported from a 10 day working session of testing in the Sir George Edwards Laboratory. Both the performance of skeg-rudder No. 0 and the all-movable rudder No. 2 were investigated in the bollard pull condition (J=0). In the base position both rudders were tested at a rate of revolution of the propeller of 1160rpm and 1460rpm. Measurement of the propeller and rudder forces were made at incidence increments of 5° between -45° and 45° for the all-movable rudder No.2 and -35° to 35° for the skeg-rudder No. 0. Measurements were taken for the skeg-rudder-propeller combination with a lateral separation Y/D=±0.375, Y/D=±0.25 and Y/D±0.125. Also measurements were taken at longitudinal separations of X/D=0.46 and X/D=0.52.

For the all-movable rudder No. 2 additional longitudinal separations were tested at X/D=0.30 and X/D=0.34. Also two extra lateral separations were tested at Y/D=±0.375. An additional investigation of the effect of lateral separation on rudder No. 2 was carried out at a longitudinal separation of X/D=0.52 for four lateral positions at Y/D=±0.25 and Y/D=±0.125.

3.9 Presentation of Data

The notation of rudder incidence and coefficients used in the presentation is as described in Chapter 2. The propeller rotates in an anti-clockwise direction when viewed from aft.

The main types of graphical presentation used in this report are:

Rudder performance — Rudder sideforce, drag, CP_c and CP_S are plotted against rudder incidence. Lift and drag are always perpendicular and parallel to the ship axis even for cases where a drift angle is imposed on the bodies. CP_c and CP_S are derived from moments and forces and for low rudder incidence only a small moment and force is produced and can lead to erroneous results. The resultant plots of CP_c and CP_S are plotted to the minimum rudder angle possible and for small angles can be deceptively large or small.

Propeller performance — Propeller thrust and thrust augment (the difference between actual and open-water propeller thrust) are plotted against advance ratio J.

Sectional rudder performance — Integration of rudder surface pressure measurement allows the spanwise variation in rudder sideforce to be obtained. The sectional force coefficient C_N is presented to a base of rudder span for different rudder incidence.

Hull forces — Integration of the hull surface pressure coefficients allows hull forces to be obtained. The forces are non-dimensionalised with respect to rudder area for direct comparison between hull and rudder forces.

Additional forms of presentation are described within the discussion.

3.10 Discussion of Results for Wind Tunnel Tests (J>0)

3.10.1 Influence of Propeller on Rudder Performance

Figures A-1 to A-5 show the effect of varying propeller thrust loading on rudder performance for the rudder-propeller geometries tested in the base position. The overall shape of the rudder lift drag curves varied little for the rudders tested. The effect of increasing thrust loading, also reported in [13], is to:

i) increase the lift-curve slope above that of free-stream.

ii) significantly delay stall, even for low thrust loading (high J).

iii) stall is no longer the same for positive and negative incidence.

iv) drag component due to lift increases.

v) The chordwise centre of pressure moves forward from free stream position.

vi) The spanwise centre of pressure increases for positive incidence and decreases for negative incidence.

It is the propeller thrust loading (K_T/J^2) which controls the manoeuvring performance of the rudder and this is clearly demonstrated in Figures A-1 to A-5

3.10.2 Rudder Plus Skeg Forces

Figures A-2 and A-3 show the influence of propeller thrust loading on the forces developed on the skeg and all-movable part of the semi-balanced skeg-rudder No. 0. The lift curve slope of the skeg-rudder shows a drop for all J values at an incidence of -5°. This is due to the gap flow between the skeg and the movable part of the rudder thus causing a pressure drop that decreases the lift. This phenomenon has been described in detail by Molland in [7]. The lift drop only occurs at about -5° due to the additive effect of the influence of the propeller on the pressure difference at that incidence. At +5° the pressure difference will be less due to the influence of the propeller flow on that side. This will limit or halt the gap flow and thus no drop in lift is experienced. A similar, associated change is seen in the drag characteristics. The chordwise and spanwise centre of pressure behave in a similar manner to the all-movable rudder No. 2.

3.10.3 Rudder Alone Forces (Rudder Torque Considerations)

Figures A-4 and A-5 show measured forces solely for the movable part of the skeg-rudder (excluding skeg) of skeg-rudder No. 0. The main result is a lift force offset such that zero lift force does not occur at a rudder incidence of 0°. This is due to the asymmetric flow of the propeller on the tapered rudder geometry and the flow straightening of the propeller flow induced by the skeg onto the movable part. At higher propeller thrust loading (lower J values) the effect becomes more apparent and the offset increases. This is also seen in the spanwise centre of pressure with CP_S moving towards the rudder tip for positive incidence.

The rudder lift and drag are, in general, lower for the rudder alone compared to rudder plus skeg forces due to skeg producing sideforce from the downstream influence of the movable part. This phenomenon is the same as that experienced by the trailing edge flaps of an aeroplane wing.

3.10.4 Influence of Lateral Separation on Rudder Performance

Figure A-6 to Figure A-9 show the effect of lateral separation of the rudder and propeller. The general result of separating the rudder laterally from the propeller is to cause an offset in the lift curve slope so that zero lift no longer occurs at a rudder incidence of 0°. A negative shift of incidence for zero rudder force is experienced for positive separation and conversely a positive shift of incidence is experienced for negative lateral separation. Rudder drag is generally larger for all values of lateral separation compared to Y/D=0.

Figure A-10 shows the effect of one lateral position on rudder alone forces. The effect is the same as the rudder plus skeg result but the magnitudes of the forces are less.

3.10.5 Influence of Hull and Propeller on Rudder Performance

Figures A-11 to A-13 show rudder force characteristic for rudder No. 2 with the model hull upstream of the rudder-propeller combination for various propeller thrust loadings.

Figure A-11 shows for all values of J, lift on rudder No. 2 has decreased and drag has increased with the presence of the hull. Chordwise centre of pressure has moved backwards towards the trailing edge and spanwise centre of pressure has moved down towards the root due to the presence of the hull.

Figures A-12 and A-13 show for all values of J, lift and drag on the skeg-rudder No.0 have followed the same pattern as for rudder No. 2. The change is not so marked as for rudder No. 2 with the lift drop being less and the drag increase being only a small percentage larger than that without the hull upstream. It is interesting to note the change in slope at -5° is still present.

Figure A-14 shows the freestream results with the propeller stationary. Results are as expected with the lift and drag being considerably less than that of the propeller in operation especially at high thrust loading (low J value). The decrease in the lift-curve slope is 53% which, based on a lift identity, corresponds to an equivalent Taylor wake fraction [10] of 0.27.

3.10.6 Influence of longitudinal Separation on Rudder Performance for Hull and Rudder-Propeller Combination

Figures A-15 to A-17 show the effect of longitudinal separation of the rudder and propeller-hull combination for various propeller thrust loadings.

The change in lift with increased longitudinal rudder-propeller separation is small with a slight decrease for rudder No.2 and skeg-rudder No. 0. Longitudinal separation does alter the drag on the rudder and increased separation appears to reduce drag, particularly at lower advance ratios. The centre of pressure chordwise and spanwise does not alter significantly with increased separation.

3.10.7 Influence of Yaw Angle on Rudder Performance for Hull and Rudder-Propeller Combination

Figure A-18 shows forces for the skeg-rudder, propeller and hull combination at a yaw angle of -7.5° for various propeller thrust loadings. The forces shown are for the ship axis with lift being perpendicular to the hull centreline and drag parallel to the hull centreline.

The main result of introducing a yaw angle on the combination is to produce an offset such that some lift is experienced at zero rudder incidence. Another effect of yaw angle is that zero force is not experienced at the same angles for varying J. This phenomenon is due to the straightening effect of the propeller. For higher propeller thrust loading (lower J value) the offset will be greater and tend towards -7.5° as the flow is curved towards the ship axis due to the action of the propeller.

Figure A-19 shows forces for only the all-movable part of the skeg-rudder. The effect is similar to that of the total skeg and rudder forces but the influence of the propeller is

greater when accounting for torque. The offset at higher J values tends to an angle greater than -7.5° and this is due to the cumulative effect of the flow straightening and the twisting of the flow shown in Figure A-4.

3.10.8 Influence of Rudder on Propeller Thrust Loading

The propeller force results presented are for three values of advance ratio J. These advance ratios, for a given pitch ratio, have a known open-water thrust coefficient K_T, shown in Figure A-20. However, Figures A-21 to A-30 show the influence of the rudder type, the hull, the longitudinal and lateral separation, and the yaw angle on the measured propeller thrust coefficient at zero incidence, These are to be compared with the propeller open-water characteristics, given in Figure A-20.

Figures A-21 and A-22 show the thrust and thrust augment experienced with rudder No. 2 and skeg-rudder No. 0 respectively. These indicate that the general influence of a rudder, in way of the propeller race, on the propeller performance is to lead to a positive thrust augment to the open water characteristics. The thrust augment is due to the blockage of the flow by the rudder causing an effective reduction in speed of inflow into the propeller.

With increasing thrust loading (lower J) the thrust augment, due to the rudder blockage, generally increases.

3.10.9 Influence of Lateral Separation on Propeller Performance

Figure A-23 shows the influence of lateral separation of the skeg-rudder propeller combination on thrust and thrust augment. As the rudder is moved away from the centreline. The thrust augment experienced is not linear this is more clearly shown in Figure A-24. Depending on the advance ratio, maxima and minima are experienced at various lateral positions. For the higher thrust loading (J=0.51) the asymmetry of the flow is apparent with maxima experienced at +0.125 and -0.25 and minima experienced at +0.25 and -0.125 for the limited lateral separation tested. The non-linearity is due to the non-uniform flow induced by the rudder through the propeller and therefore these positions experience different thrust augments when the lateral position of the rudder is varied.

3.10.10Influence of Hull and Rudder on Propeller Performance

Figures A-25 and A-26 show the propeller thrust and thrust augment with the hull present for skeg-rudder No. 2 and skeg-rudder No. 0 respectively. The thrust augment experienced is greater than that of just the rudder and propeller. This is again due to the fact that there is an effective speed reduction of inflow due to the presence of the hull.

3.10.11Influence of Longitudinal Separation on Propeller Performance

Figures A-27 and A-28 show the propeller thrust and thrust augment for varying rudder-propeller longitudinal separation for the hull and rudder No.2 and the hull and skeg-rudder No. 0 respectively. Thrust augment is non-linear with separation. As the rudder moves aft the thrust increment decreases and then starts to increase again and this is more clearly shown in Figure A-29. For all three advance ratios there is a minimum experienced around a longitudinal separation of X/D=0.52. It is thought likely that this effect is propeller pitch dependent.

3.10.12Influence of Yaw Angle on Propeller Performance

Figure A-30 shows the thrust and thrust increment for a Yaw angle of -7.5° for the skeg-rudder No.0 and Hull. The thrust augment experienced over all the J values was larger than that of zero yaw angle. This is due to the angle of flow entering the propeller obliquely and altering the propeller performance from that in a uniform flow.

3.10.13Spanwise Distribution of Local Normal Force Coefficient (C_N)

Figures A-31 to A-33 show the spanwise distribution of local normal force for all-movable rudder No. 2 and Figures A-34 to A-36 for skeg-rudder No. 0 for three J values of 0.94, 0.51 and 0.35 respectively. The increase in rudder lift caused by the tip vortex is apparent at the higher values of rudder incidence.

The influence on the force distribution of the increase in thrust loading can clearly be seen. At high J values the force coefficient outside the impinging propeller slipstream is of the same order as that within the slipstream whereas at low J values the slipstream local force coefficients dominate the loading on the rudder.

The lift distribution of the skeg-rudder in the region of the skeg is lower than that for the all-movable region. This is due to zero skeg incidence and therefore the lift induced by the split portion of the rudder is less. There is a noticeable discontinuity at 500mm span corresponding to the tip of the skeg part.

3.10.14Hull Forces

Figures A-37 to A-40 show the force data from integrating the pressures over the hull. The forces are presented for varying rudder angles and thrust loading. It can be seen that the general trend is similar to that on the rudder. A negative force is experienced on the hull for negative rudder incidence and similarly a positive force is experienced for a positive incidence. This is evident for all cases including the freestream case (Figure A-37). It can be seen that for the free stream case the linear regression shows an offset at 0° of incidence this may be due to a slight asymmetry to the model and also a slight misalignment to the wind tunnel axis.

For increasing thrust loading (lower J) the force magnitude on the hull is greater. When the hull is yawed an offset on the force is experienced.

3.11 Discussion of Results for Bollard Pull Tests (J=0)

3.11.1 Influence of Propeller Revolutions on Rudder Performance

Figures B-1 and B-2 show the changes in sideforce, drag and centres of pressure at zero J, for the all-movable rudder No. 2 and skeg-rudder No. 0 respectively. The results are presented for two rates of propeller revolutions. Increasing the propeller rpm between 1160 and 1460 does not have any significant effect on rudder lift and drag coefficients or centres of pressures. A small stall angle difference is experienced between the two propeller rates of revolution on all-movable rudder No. 2 at higher angles of incidence (Figure B-1). This effect is likely to do with the higher propeller rpm of 1460 causing slightly more unsteady flow which, in general, tends to keep the flow attached to the rudder thus preventing stall. All subsequent results are presented for 1460rpm only as the non-dimensional results show the same performance.

3.11.2 Influence of Rudder Types on Performance

Figures B-1 and B-2 show that lift and drag for the all-movable rudder No. 2 is generally higher than the skeg-rudder No. 0. Chordwise centre of pressure is further forward towards the leading edge on the all-movable rudder and spanwise centre of pressure is higher. This is due to the rudder taper on the skeg-rudder No. 0 and also the fact that the skeg-rudder is a split configuration where the root section of the leading edge of the rudder does not have an angle of attack with respect to the flow.

3.11.3 Influence of Longitudinal Separation on Rudder Performance

Figures B-3 to B-7 show for 1460rpm the effect of longitudinal separation on all-movable rudder No. 2 and Figures B-8 to B-10 show the effect for skeg-rudder No. 0. There is very little change in lift curve slope with separation. Drag is reduced with increasing separation and for an X/D greater than 0.34 a thrust is generated at zero incidence. This phenomenon can be seen in Figure B-7 and Figure B-10 for the all-movable and skeg-rudder respectively. A thrust at an X/D greater than 0.39 is exhibited by both rudder types and is consistent with previously reported results [21].

3.11.4 Influence of Lateral Separation on Rudder Performance

Figures B-11 to B-16 show the influence of Y/D on all-movable rudder No. 2 in the base longitudinal position of X/D=0.39. Lateral positions of Y/D=±0.375 show a marked reduction in lift curve slope once the position of the rudder is greater than a Y/D of ±0.25. In general drag is higher for values of lateral positions outside of Y/D=0.

Figure B-17 shows lift and drag at zero incidence for varying lateral position Y/D. The lift offset produced at zero incidence is due to the propeller race rotating. This causes a shift of the zero lift position with respect to rudder incidence. It should be noted that once the lateral position of the rudder is greater then ±0.25 of the diameter of the propeller the lift offset begins to level off. This is due to the rudder being pulled outside the main governing part of the propeller race. Drag shows similar trends to that of lift with increasing drag up to a Y/D=±0.25 and it decreases once the rudder is outside the main proportion of the propeller race. An interesting feature to note is; if the rudder is in the mid-lateral position

there is thrust experienced on the rudder although the magnitude of this thrust is relatively small.

Figures B-18 to B-22 show the influence of Y/D on the all-movable rudder No. 2 at a longitudinal position of X/D=0.52. The same trends are indicated by this case as for the base longitudinal position X/D=0.39. This concludes that a similar tendency for lift and drag on the rudder due to the influence of lateral position is shown for varying longitudinal position.

Figures B-23 to B-29 show the influence of lateral position Y/D on skeg-rudder No. 0. The results obtained indicate the same trends as that for the all-movable rudder No. 2 and therefore the trends are not rudder specific.

3.11.5 Influence of Rudder on Propeller Thrust Loading.

Figures B-30 and B-31 show effect of the all-movable rudder No. 2 and skeg-rudder No. 0 on propeller performance at zero advance ratio (J=0) respectively. Propeller thrust (K_T) and Torque (K_Q) remain reasonably constant over the range of rudder angles. There is a thrust and torque augment on the propeller compared to the open water performance presented in Figure A-20. Values for K_T and K_Q are greater than the zero advance ratio open water propeller performance which are 0.37 and 0.053 respectively.

Figure B-31 shows the propeller thrust and torque for two varying rates of propeller revolutions (1460 and 1160 rpm) in general K_T and K_Q are independent of propeller speed for this case.

3.12 Summary of Wind Tunnel Tests (J>0)

The overall shape of the rudder lift and drag curves varied little for the parameters tested including rudder geometry.

In considering the torque effects of a skeg-rudder, measuring the movable part forces only reveal a zero offset in the lift and drag curves at 0° of rudder incidence due to the propeller flow.

In general the effect of having a skeg-rudder as opposed to an all-movable rudder shifts the spanwise centre of pressure towards the tip and a drop in the lift and drag curve is experienced at a round -5° due to skeg gap flow and asymmetric propeller race.

Lateral separation of the rudder stock from the propeller axis causes a shift in rudder incidence for zero lift. This shift in incidence for zero lift increases with thrust loading. In other respects the rudder lift and drag characteristics are unchanged.

Longitudinal and lateral separation of the rudder stock from the propeller axis influence the thrust augment experienced by the propeller due to the rudder in a non-linear manner.

Hull sideforce is produced due to the downstream influence of the rudder-propeller combination. The main influence is near the propeller plane. Rudder incidence and propeller advance ratio have an effect and an increase in lift was found to be of the order of 10% of actual rudder lift for a given rudder incidence.

The experimental work enables a better understanding of skeg-rudder performance behind a hull and propeller combination. It also gives an indication of the influence of the propeller on the rudder.

3.13 Summary of Open Laboratory Tests (J=0)

At zero ship speed the accelerating effect of the propeller is clearly demonstrated.

Skeg-rudder and all-movable rudder performance are similar at zero J with slight variations in centres of pressure.

Propeller force data is similar for the two types of rudder with a thrust and torque increase due to the rudder.

The large amount of presented data will provide more resource for low speed ship operation in cases, for example, of restricted seaway operation and manoeuvring in port.

In general the behaviour of the rudder performance at zero J over the range of parametric variations (X/D, Y/D etc.) is similar to that experienced at higher advance ratios. The indication that these results provide is that, the novel approach of rudder performance at laboratory zero J test procedure could be used to provide rudder design information at a greatly reduced cost compared with higher advance ratio wind tunnel tests.

3.14 General Summary

A large parametric experimental study into the effect of a propeller operating upstream of a rudder has been presented and the results discussed. The extent of parameters tested for the work presented in this thesis can be seen in Appendix E, which details the total test database used in the method presented in Chapter 4.

An enhanced data acquisition system has been created and proved successful in acquiring rudder and propeller data. Tests have been carried out in a wind tunnel and in an open laboratory. The data collected from wind tunnel tests continues and extends an extensive series of tests carried out by Molland and Turnock [13].

The experimental work provides further insight into the rudder-propeller interaction mechanism. The presented data supplies essential information for development of a rudder performance prediction method and validation of theoretical methods.

4 RUDDER PERFORMANCE PREDICTION METHOD

4.1 Introduction

When a ship designer is detailing a ship's stern arrangement with a rudder downstream of a propeller a performance prediction method is required that accounts for the effect of propeller thrust loading and relative rudder-propeller position. It is necessary to have a method that produces results for sideforce and drag for manoeuvring consideration plus centre of pressure and moments for the derivation of steering gear torque and rudder scantlings.

The aim of this chapter is to demonstrate the development and use of a performance prediction method for a rudder operating downstream of a propeller. The rudder performance prediction method allows the effect of design changes and trade-off studies to be carried out in a rapid and robust manner. Rudder performance is quantified for zero speed through to normal service speed and for rudder angles up to ±70°. The software allows a complete stern arrangement including multiple rudder-propeller systems to be investigated.

4.2 Rudder Performance Prediction Method Philosophy

The rudder performance prediction method employs an interpolation mechanism which uses appropriate data from a physical database and harnesses this with correction algorithms based on physical understanding to arrive at a solution for a required rudder-propeller operating condition. The method uses free stream rudder performance, open water propeller performance and rudder-propeller interaction data to provide predictions of rudder performance operating downstream of a propeller. By using a known data set, parameters such as rudder geometry, propeller operating conditions and relative rudder-propeller separations can be adjusted to provide interpolated and corrected results, from the physical database, to a required stern arrangement and operating condition.

The data sources used by the method is not limited to just experimental or standard series data but can have rudder performance data from theoretical methods such as CFD or even

actual ship trials data. Data sources can be mixed to obtain a controlled fusion of experimental, theoretical and numerical performance data.

Experimental data can be very useful in deriving a performance prediction method but it must be presented in an accessible form for inspection of the database at a particular set of design parameters. Parametric studies of experimental work such as those described in [19] and [20] present the data in the forms of statistical curve fits to experimental data. The performance prediction is based on a set of formulae using design parameters to derive a result. The design parameters originate from an understanding of the principle variables that affect the performance.

Using the data from experimental work described in Chapter 3 and previous experimental work by Molland and Turnock [13], the test data and understanding of the mechanism of rudder-propeller interaction have been coupled together in the form of a computer program which gives results of rudder performance downstream of a propeller.

The rudder performance prediction method is a way of deriving rudder performance from rudder performance data, as with the statistical curve fits, but the prediction method is not bound by any particular set of data. This is a novel and flexible approach to performance prediction from empirical data. The interpolation mechanism of the database, based on a tree search algorithm, automatically uses both the closest data set and, where necessary, correction algorithms formulated from parametric relationships based on underlying physics. Therefore any rudder-propeller performance data can be input into the method and providing the required result is within the scope of the available data, interpolation and extrapolation can take place to derive a result.

The scope of the database the method uses is not limited in any way. Any type of rudder and propeller performance can be incorporated. With a large database the way in which the data is exercised needs to be highly accessible. The method has been implemented in the form of a software program to supply a transparent interface to the interpolation and correction algorithm. A user is only required to consider the geometry, the operating conditions of the rudder-propeller system and the most appropriate test database set for the required configuration to obtain results. The program dynamically interpolates and corrects the database to give results of performance for the required operating condition.

The software program can be used to perform reliable parametric studies of the influential variables in defining rudder performance downstream of a propeller. This can be applied to manual optimisation of the principle dimensions of a rudder and the relative separations of the rudder and propeller to obtained a desired performance.

4.3 Software Data Structure

The rudder performance prediction software was developed using the object orientated C^{++} programming language [64] to provide a graphical user interface under a Windows based operating system.

The implementation of suitable data structures or objects based on the individual components of the rudder-propeller system has been fundamental in creating consistent and efficient software code. Object orientation has allowed properties of each component to be stored and used in a highly accessible form.

Object orientated programming has an inward approach to programming that relies on a hierarchical structure of an object that has a set of procedures and functions embedded within them. The object orientated programming technique has the advantage that the software is structured in self contained elements. Functions and procedures can be found in the software code alongside the variables that they manipulate, thus creating a logical organisation of programming code for efficient and accurate software development.

An example of an object orientated data structure within the program is the rudder. The rudder object has a series of properties associated with it (e.g. root chord, span etc.) described in Section 4.6 of this Chapter. These properties can be used in functions and methods of the object to calculate further properties or derive other information about the object. A simple example is rudder area, it is not necessary to store rudder area as a variable as it can derived geometrically from the root chord, tip chord and span. This therefore becomes a function of the rudder rather than a property and is at all times consistent with the current rudder geometrical properties. The area function is embedded within the rudder object and therefore is always accessible when using the rudder object in software code.

The extent of the rudder object data can be as comprehensive as required, rudder free stream data can be stored together with its operational conditions also functions using other objects can be implemented. As an example, parts of the code used to create the rudder and propeller object records can be seen with comments in Appendix C.

4.4 Software Implementation

The rudder design program consists of 10,000 lines of compiled programming code from 39 linked C^{++} source files. The total development time was over a period of 1 year including implementing the techniques involved in object orientated programming.

The rudder performance database created for this work consists of 6 different rudder geometries. The program includes a total of 85 sets of rudder performance data each with rudder forces and moments for an average of 17 rudder angles. The program therefore manages a database of around 8000 individual data items. The extent of the database with each data set test condition can be seen in Appendix E.

The rudder design program concept is based on a series of objects namely; a ship, its associated rudders and its associated propellers. By linking rudders and propellers an interaction set can be described. A set of operation conditions for all the components such as rudder angles, propeller rate of revolutions and ship speed can be defined to derive forces and moments for a specific condition or set of conditions.

A typical screen capture of the rudder-propeller program can be seen in Figure 4.1 showing the application windows and an example of the calculated results.

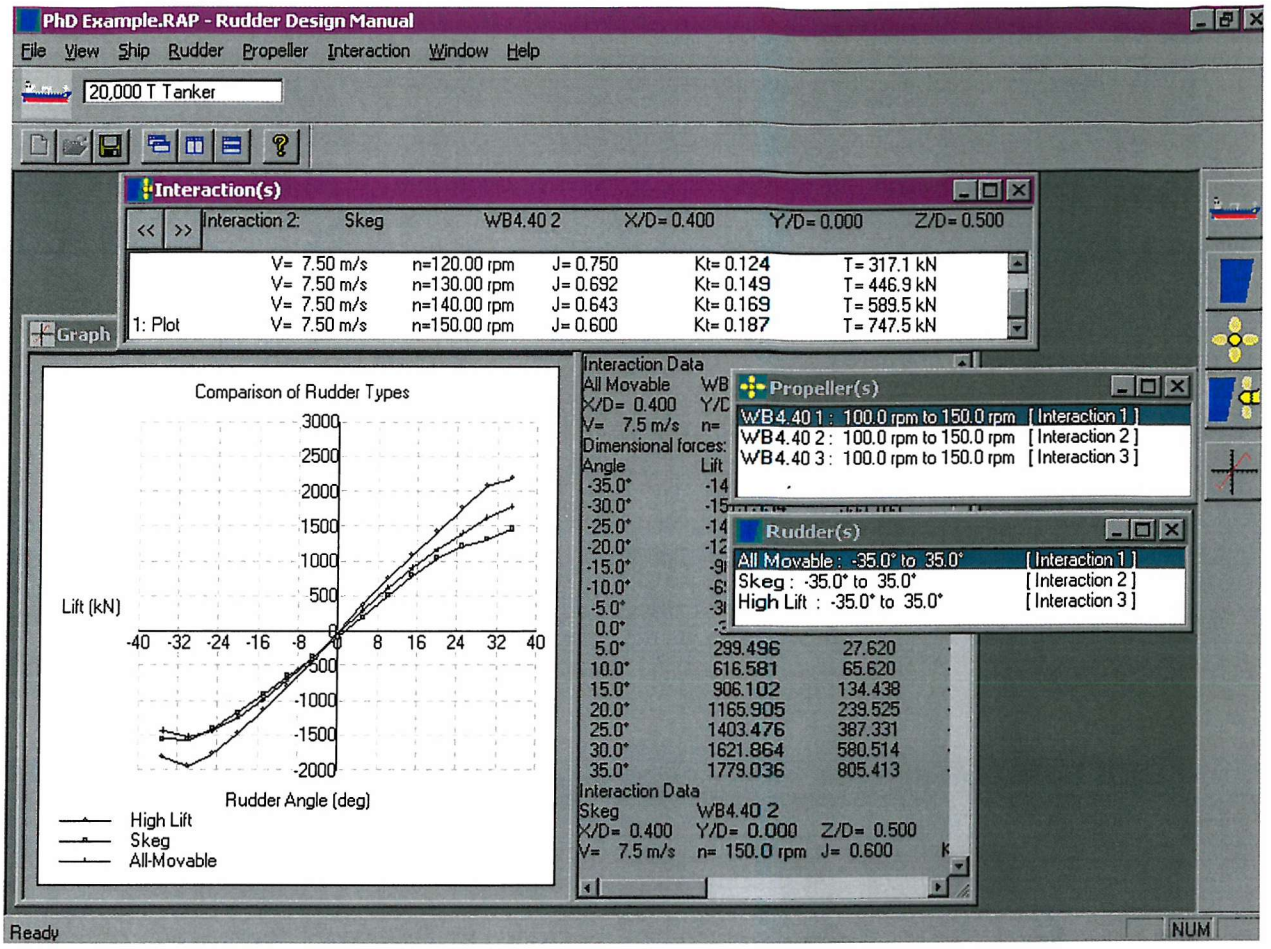

Figure 4.1 Typical Screen Capture of Rudder Design Software

The software harnesses the experimental data with physical and empirical formulae to obtain forces and moments on a rudder operating downstream of a propeller. The software has a specific data flow throughout. Data resources are from text input file and user input. The general data flow is indicated in Figure 4.2.

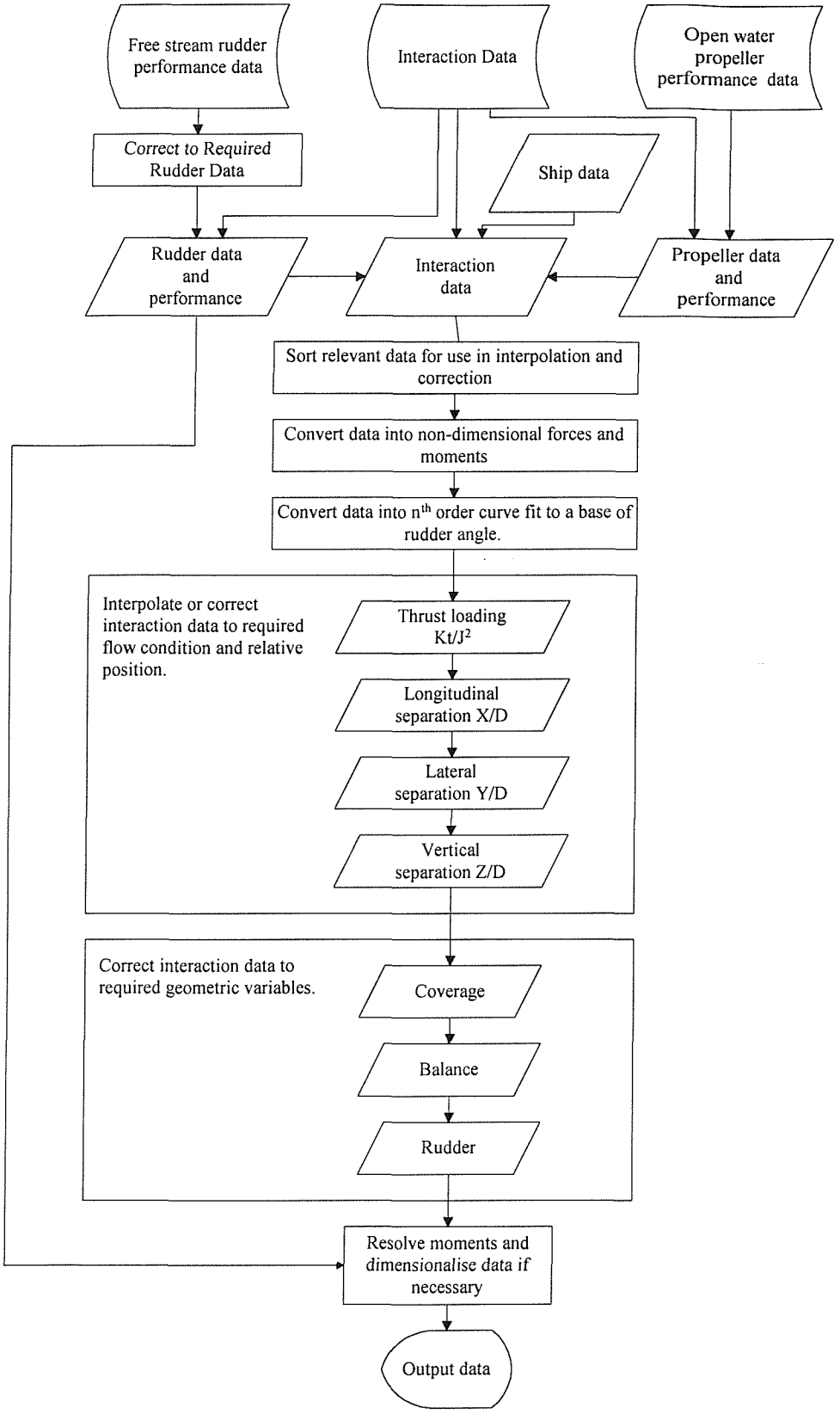

Figure 4.2 Program Flow Diagram

The basic data sources are as follows:

i) Free stream rudder data (forces and moments, L, d, M_X, M_Y, M_Z)

ii) Open water propeller data (K_T against J for given P/D)

iii) Rudder and propeller interaction data, which consists of forces and moments for a particular set of interaction parameters such as separation and propeller thrust loading.

From the knowledge of rudder free stream performance, propeller open water performance and the mechanism of rudder-propeller interaction, the performance for the required operating condition is derived by correcting the closest interpolated base data. Data correction is based on theoretical predictions of performance formulated from the underlying physics described in Chapter 2.

The first step in obtaining performance for a rudder operating downstream of a propeller is defining the ship's stern arrangement and the respective performance of the rudder and propeller in the undisturbed free stream.

4.5 Ship Definition

Ship definition in the context of the rudder performance prediction program is denoted by the ship speed. The influence of ship form etc. is principally governed by the speed that enters the propeller to define the advance ratio. Results for rudder performance are supplied at the discrete ship speeds for a particular advance ratio based on propeller rate of revolutions.

4.6 Rudder Definition

A rudder in the context of the prediction method is defined by its particulars, position, free stream performance and a range of operating conditions (i.e. angles). Figure 4.3 shows the rudder input form from the program with a series of pages to define the rudder context.

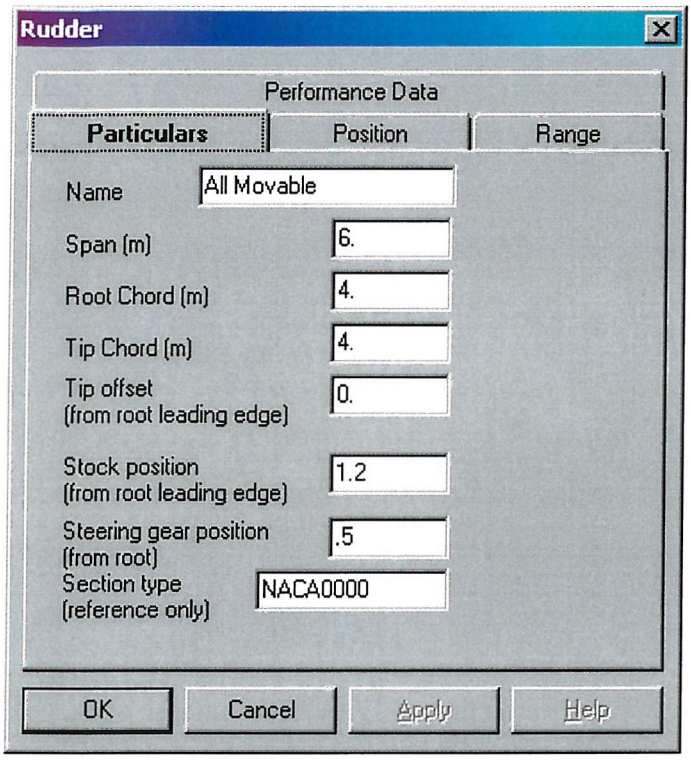

Figure 4.3. Rudder Input Form

Figure 4.4 indicates the various rudder particulars used to describe a rudder geometry on the particulars page.

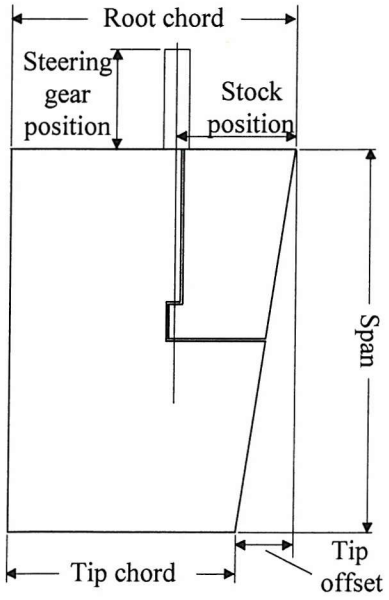

Figure 4.4. Rudder Geometry Definition

As the rudder position is only used to define the rudder-propeller separation the position can be relative to any point on the ship providing that the interacting propeller position is defined relative to the same point.

The range of rudder operating conditions consists of a series of rudder angles. Results for rudder performance are then supplied at these discrete angles.

The free stream rudder performance describes rudder lift, drag and moments as a function of rudder angle. The performance is defined in a variety of ways:

i) 2D lift curve slope ($dC_L/d\alpha$) : This is the lift curve slope of the rudder section and can be obtained from sources such as [49] or a CFD method.

ii) 3D lift curve slope ($dC_L/d\alpha$) : This is the lift curve slope of the actual rudder.

iii) data table : actual performance data at discrete rudder angles.

The definition of the rudder free stream performance can include data at discrete rudder angles and therefore it is extremely flexible. Data from any type of rudder including skeg, high lift and flat plate rudders can be input into the program for subsequent analysis of the rudder downstream of the propeller.

If the geometrical properties of the rudder in the free stream data file do not match the input values, the program will correct the performance on a basis of aspect ratio. In this way a rudder with similar performance to the required rudder can be corrected. For example, if skeg-rudder performance is known for a rudder aspect ratio of 2.7, but the required skeg-rudder performance is at an aspect ratio of 3, the program will correct the experimental data to the required data and use results for free stream performance. The free stream rudder correction method is described later in section 4.10.

4.7 Propeller Definition

A propeller in the context of the application is defined by its particulars, position, open water performance and a range of operating conditions (i.e. rate of revolutions). Figure 4.5 shows the propeller input form with a series of pages to define the propeller context.

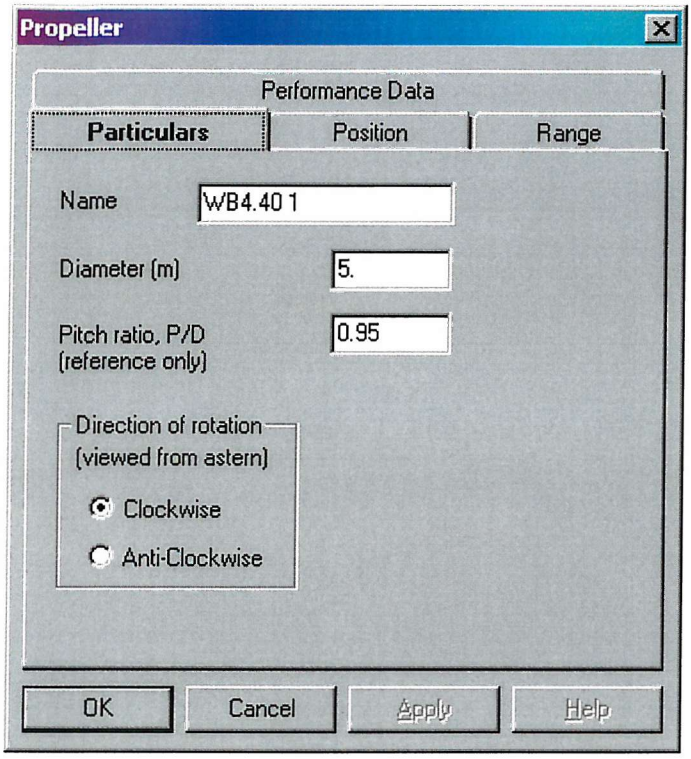

Figure 4.5. Propeller Input Form

The propeller geometry is defined by a diameter and a direction of rotation. Pitch ratio can be input but only as a reference as the open water propeller performance is defined for a particular propeller pitch ratio.

As the propeller position is only used to define the rudder-propeller separation the position can be relative to any point providing that the rudder position is defined relative to the same point.

The range of propeller operating conditions consists of a series of propeller rates of revolutions (rpm). Results for rudder performance are then supplied at discrete values of propeller advance ratio based on the ship speed.

The propeller open water performance characteristics describe the variation of propeller thrust with advance ratio. The performance can an be defined in three forms:

i) Fixed thrust value of the delivered thrust of the propeller for the specified operating rate of revolutions and ship speed.

ii) A power curve fit of the form in Equation [4.1].

$$K_T = K_{TJ=0} - \left(\frac{K_{TJ=0}}{J^n_{K_T=0}} \right) \times J^n \qquad [4.1]$$

where K_T at J=0, J at K_T=0 and the power n are user defined to match propeller data.

iii) data table of actual performance at discrete advance ratios.

Figure 4.6 shows the shape of the propeller performance curve for the propeller tested in Chapter 3 and the curve fit to the experimental data with three values of the power n. The propeller performance is representative of most standard ship propellers and it shows that a typical value for the power n is 1.35 to match experimentally measured performance.

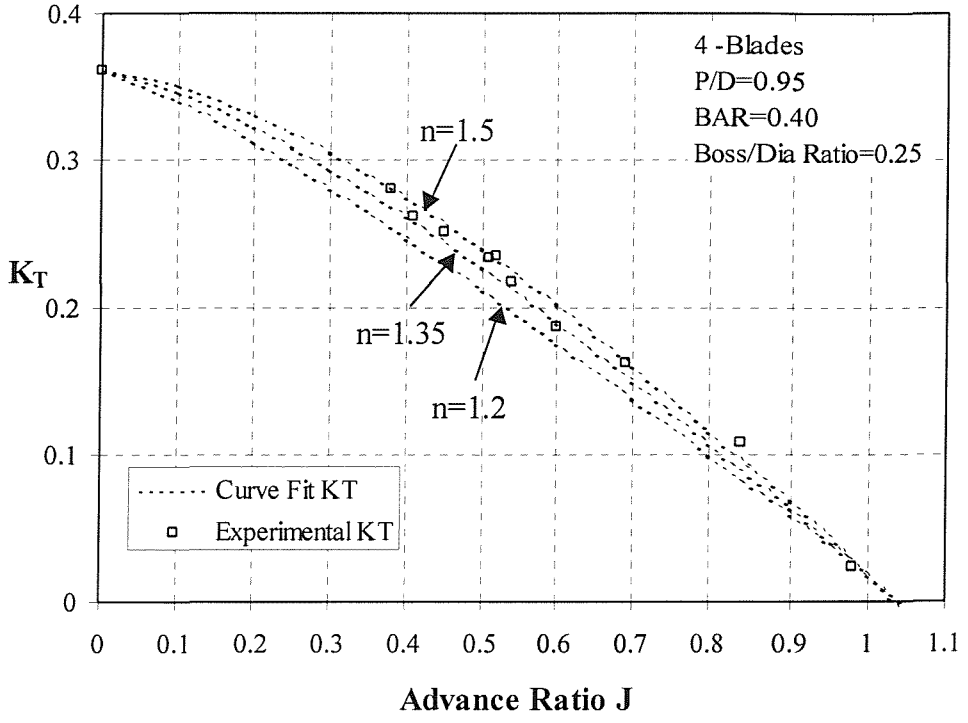

Figure 4.6. Comparison of Experimental Propeller Performance with Curve Fit.

Propeller open water performance can be described at discrete thrust loadings in a similar way to the rudder's performance. To be able to have any type of propeller operating upstream of a rudder provides great flexibility in assessing rudder-propeller performance as the influence of many types of propellers from ducted units to contra-rotating propellers can be input into the program.

4.8 Rudder-Propeller Interaction Definition

Once the respective geometry and free stream performance of the rudder and propeller are defined they can be linked to form a rudder-propeller interaction and the locality of the rudder and propeller can be calculated to define the relative separations.

The interacting rudder and propeller has a defined interaction data set. The interaction data set consists of a list of rudder performance data files at particular vertical separation, lateral separation, longitudinal separation, ship speed and propeller rate of revolutions. The interaction data is used for interpolation, extrapolation and correction to derive rudder forces and moments for the defined condition of the input rudder and propeller. The data consists of a list of rudder forces and/or moments at discrete rudder angles.

The most appropriate data set must be used to minimise the level of interpolated data correction. For example, if two rudders were tested with respective aspect ratios of 2.5 and 3.7 and the required input rudder has an aspect ratio of 3, it is more appropriate to use the test data at an aspect ratio of 2.5 as this is the physically closest data set.

A full stern arrangement can be defined in the program by having multiple propellers interacting with multiple rudders. By defining an overall stern arrangement the total manoeuvring forces can be calculated as a summation as well as individual manoeuvring and design forces and moments.

Once the user has defined the required rudder and propeller geometry, performance, operating conditions and the most appropriate interaction data set, the program dynamically interpolates and corrects the data to obtain rudder performance results for the required condition.

4.9 Interpolation Tree Mechanism

The interpolation tree is the fundamental method used in the software. A tree search is used to obtain results at the required geometrical and flow properties from a given rudder database by interpolation and, where necessary, correction. The interpolation tree method maximises the use of actual experimental data and thereby reduces the amount of correction required for each result.

Figure 4.7 describes the interpolation tree for a full database. Subscript U indicates a value above the required and L a value below.

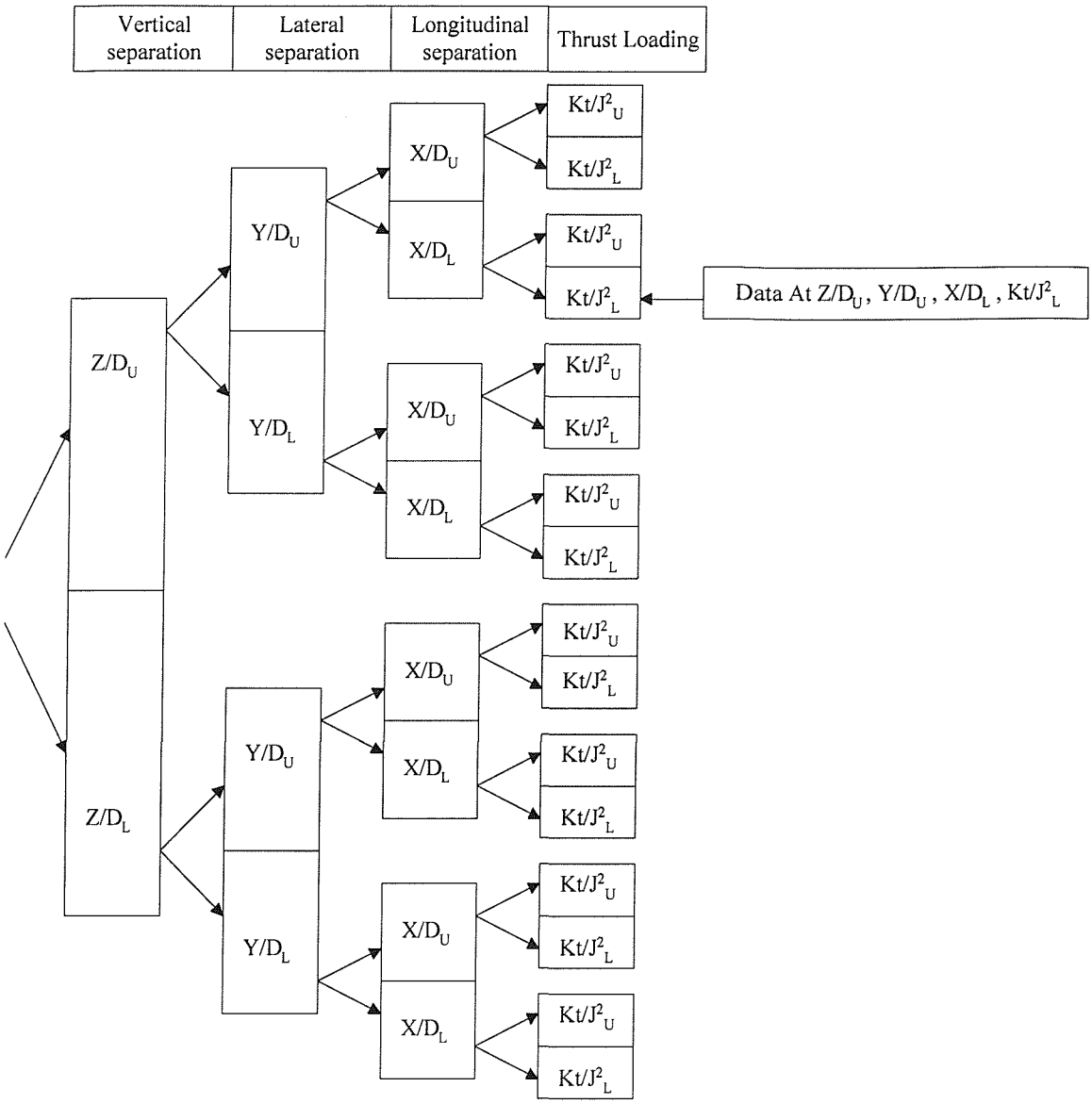

Figure 4.7 Interpolation Tree Flow Diagram

The algorithm starts by searching the database and first selecting the closest sets of available force and moment data to the required conditions. By moving from left to right in Figure 4.7 the method finds two subsets of data above and below the required Z/D, thus forming the first branch of the tree. For each branch the method then searches these data subsets and finds the closest data above and below the required Y/D, this continues for X/D until a data subset is found at the closest Kt/J^2 for each branch of the tree. The data bracketing the required condition can then be used for interpolation or if a data set is not

found above or below the required parameters the side of that branch terminates and this data will be corrected to the required condition rather than interpolated. If a data set is found with a parameter at the required condition the method will use the data directly.

The corrections or interpolations are carried out by moving backwards through the tree (right to left in Figure 4.7) interpolating rudder forces and moments for the bracketed data and correcting rudder forces and moment for the branches of the tree that are missing a data set above or below the required parameter. The allocated order of the parameters has been chosen according to the degree of variation of the parameters in ships and also experimentation.

Consider the required conditions:
K_T/J^2=0.8, X/D=0.40, Y/D=0.10, Z/D=0.90

Figure 4.8 shows the tree for an example sparse database for the required conditions. For the top branch of the tree tests have only been carried out for Z/D of 1.25 at a Y/D of 0.0, an X/D of 0.39 and at a thrust loading of 2.17. This data at these required conditions is adjusted to the required condition first by correcting the forces and moment to the required thrust loading of 0.8 then to the correct X/D of 0.4 and finally to the correct Y/D of 0.1. The data table is therefore at a condition of K_T/J^2=0.8, X/D=0.40, Y/D=0.10, Z/D=1.25. This process is repeated for the bottom part of the tree at a Z/D of 0.75 where the tree is more densely populated. Where data sets exist above and below the required condition these can be interpolated rather than corrected. This is the case where the final two data sets at the left hand of the tree are at a Z/D of 1.25 and a Z/D of 0.75. These data tables are at the required K_T/J^2, X/D and Y/D and can be interpolated to obtain data at the required condition of Z/D=0.9.

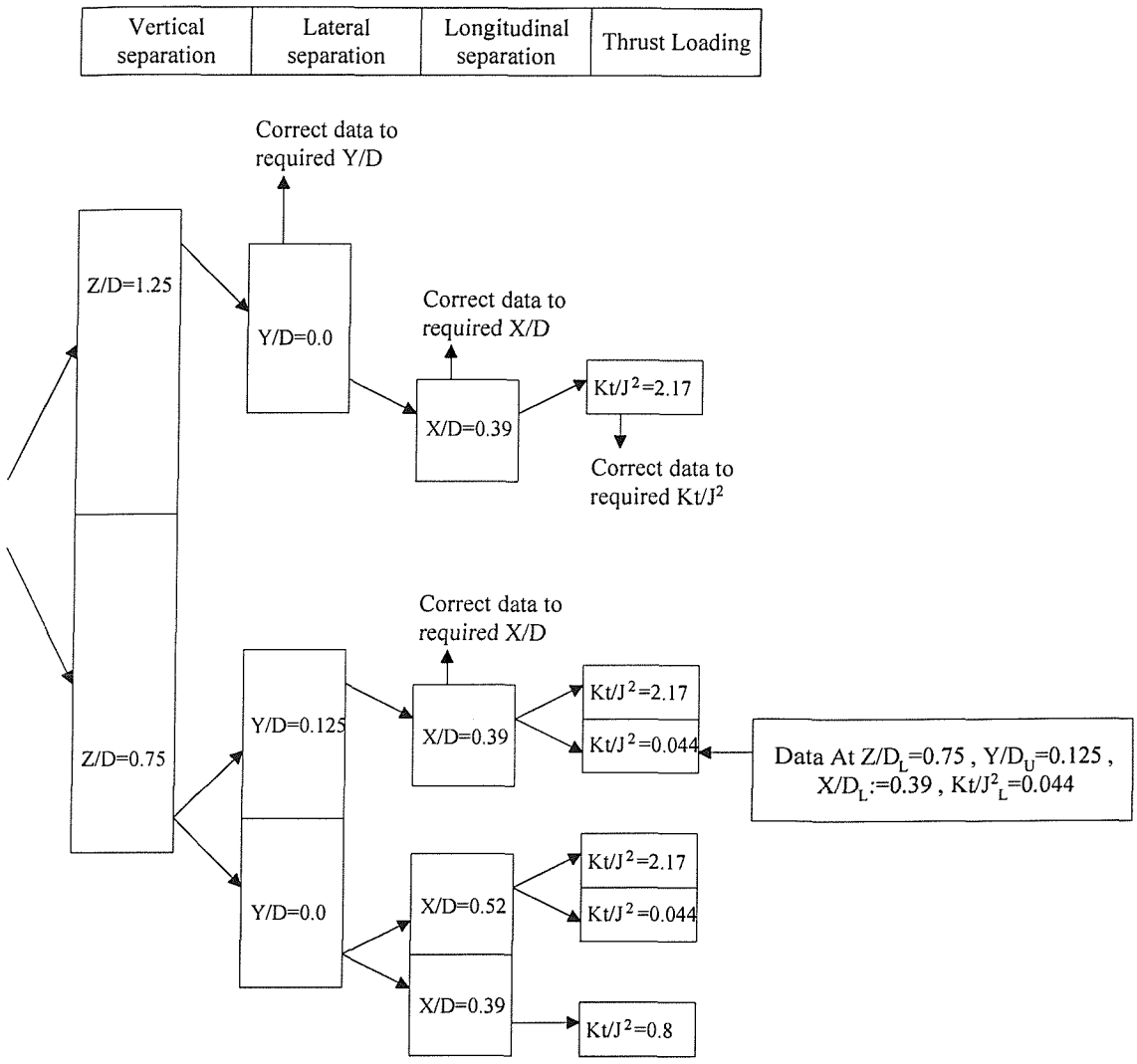

Figure 4.8 Sparse Interpolation Tree

Corrections and interpolations are made to derive a correct set of forces and moments on the rudder from a user defined database. The choice of the database is left to the user and it is important to apply the most valid and effective database to obtain accurate results. Corrections are made for rudder geometry and the interaction parameters such as rudder-propeller separation and propeller thrust loading

4.10 Rudder Data Correction

To correct rudder data from a base rudder, the data is scaled using a parameter f based on aspect ratio and sweepback. This coefficient is based on work on low aspect ratio rudders presented in [8].

$$f = 1.8 + \cos(\Lambda) \times \sqrt{\frac{4 \times AR_E^2}{\cos^4(\Lambda)}} \qquad [4.2]$$

If for example only the 2-D lift curve slope was specified 3-D rudder performance can be calculated using:

$$\frac{dC_L}{d\alpha}_{3-D} = \frac{dC_L}{d\alpha}_{2-D} \times \left(\frac{2 \times AR_E}{f} \right) \qquad [4.3]$$

To obtain lift, drag and torque from free stream data the following formulae can be applied.

A polynomial curve is a suitable curve fit for modelling rudder lift, drag and torque curves with rudder angle. Consider the cubic curve fit to a force or moment as a function of rudder angle:

$$F = A + B\alpha + C\alpha^2 + D\alpha^3 \qquad [4.4]$$

Lift:

$$A = 0, \quad B = \frac{dC_L}{d\alpha}_{3-D}, \quad C = 0, \quad D = \frac{-\frac{dC_L}{d\alpha}_{3-D}}{3 \times \alpha_{STALL}} \qquad [4.5]$$

Drag:

$$A = 0.015, \quad B = 0, \quad C = \frac{0.37 \times \left(\frac{dC_L}{d\alpha}_{3-D} \right)^2}{2 \times AR_E}, \quad D = 0 \qquad [4.6]$$

Moment about Z:

$$C_M = \frac{0.25}{\left(1 + \frac{1}{AR_E}\right)}$$

$$A = 0.0$$

$$B = (0.25c - W) \times \frac{dC_L}{d\alpha}_{3-D} + \left(\frac{0.37 \times \frac{dC_L}{d\alpha}_{3-D}}{AR_E} \right) - (C_M - 0.25) \times c \times \frac{dC_L}{d\alpha}_{3-D} \qquad [4.7]$$

$$C = 0$$

$$D = (0.25c - W) \times \left(\frac{\frac{dC_L}{d\alpha}_{3-D}}{3 \times \alpha^2_{STALL}} \right) - (C_M - 0.25) \times c \times \left(\frac{\frac{dCL}{d\alpha}_{3-D}}{3 \times \alpha^2_{STALL}} \right)$$

4.11 Propeller Data Correction

For a particular input propeller the non-dimensional thrust is obtained for a specific advance ratio and this is used to determine the propeller thrust loading K_T/J^2 used in the interpolation and correction method.

No corrections are made to the propeller performance data as corrections to the propeller thrust characteristics cannot be applied simply to a base propeller for variations in propeller geometry and pitch. A particular propeller's performance upstream of a rudder is therefore described explicitly in the software and the thrust loading is derived from the propeller thrust at the required operating advance ratio.

4.12 Interaction Data Correction

Rather than relying solely on curve fitting, the correction algorithm applies a change to the force on the rudder to the nearest known set of data. This ensures that the software experimental database is utilised fully. Moments are also corrected from an actual rudder to a required rudder.

The applied principle of the data correction is that the rudder can be split into an area controlled by the free stream flow and an area in way of the propeller in which the

performance is controlled by the propeller thrust loading but related to the free stream rudder performance [22].

In order to derive the change in force or moment a correction is applied to the free stream properties of the rudder. The force or moment is calculated at the actual value of the parameter and then at the required value by scaling and/or applying an offset to the free stream rudder performance. The scaling value is derived from a quadratic curve fit of rudder force data downstream of a propeller, presented by Molland and Turnock in [13], and is proportional to the thrust loading and is calculated as follows:

$$K_0 = 1.0 + 0.96\frac{K_T}{J^2} - 0.042\left(\frac{K_T}{J^2}\right)^2 \qquad [4.8]$$

The curve fit is valid up to a thrust loading of 8.0. A quadratic fit is used for the scaling value K_0 in the region $0< K_T/J^2 <=8.0$ and represents a decaying increase with thrust loading as found with the experimental data in [13].

For low J (i.e. $K_T/J^2>8.0$) a different parameter must be used as the thrust loading K_T/J^2 tends to infinity. A parameter based on the difference between the operational thrust coefficient K_T and the thrust coefficient at an advance ratio of J=0 (K_{T0}).

$$K_P = \frac{(K_{T0} - K_T)}{K_{T0}} \qquad [4.9]$$

The angular offset at zero lift due to the propeller is proportional to the balance which is defined as:

$$balance = 2\left(\frac{Y}{D}\right)\sqrt{0.25 - \left(\frac{Y}{D}\right)^2} + \left(\frac{A_1 - A_2}{D \times c}\right) \qquad [4.10]$$

where A_1 is the area above the propeller axis and A_2 the area below the propeller axis all within the propeller race.

The angular offset can be calculated by an exponential curve fit of the angular offset at zero lift from data presented in [13] using the following parameters:

$$a = 375 \times \left(1 + e^{\left(-0.555\frac{K_T}{J^2}\right)} - e^{\left(-0.105\frac{K_T}{J^2}\right)} - e^{\left(-0.123\frac{K_T}{J^2}\right)} \right) \quad [4.11]$$

$$b = 25 \times \left(1 - e^{\left(-0.534\frac{K_T}{J^2}\right)} \right) \quad [4.12]$$

$$\alpha_{OFFSET} = a \times balance^3 + b \times balance \quad [4.13]$$

An exponential curve fit is used as the increase in angular offset with thrust loading tends to decay with thrust loading.

So the force at a particular thrust loading and balance can be calculated from the free stream force or moment:

$$F(\alpha_0) = K_0 \times F(\alpha_0 - \alpha_{OFFSET})_{FS} \quad [4.14]$$

Where the parameter applied implies no change in coverage (i.e. K_T/J^2, X/D) the equation is:

$$F_i = F_{iACT} + \xi \times (F_{REQ} - F_{ACT}) \quad [4.15]$$

where ξ is the ratio of the rudder area within the propeller race divided by the area out of the propeller race.

Where the parameter applied does imply a change in coverage (i.e. Y/D, Z/D and Coverage) the equation is:

$$F_i = \left(\frac{\xi_{REQ}}{\xi_{ACT}} \right) \times (F_{iACT} - (1 - \xi_{ACT}) \times F_{FS}) + (1 - \xi_{REQ}) \times F_{FS} + \xi_{REQ} \times (F_{REQ} - F_{ACT})$$

[4.16]

Where there is the final correction for the rudder type the correction equation is:

$$F_i = \left(\frac{\xi_{REQ}}{\xi_{ACT}} \right) \times (F_{iACT} - (1 - \xi_{ACT}) \times F_{FS\,ACT}) + (1 - \xi_{REQ}) \times F_{FS\,REQ} + \xi_{REQ} \times (F_{REQ} - F_{ACT})$$

[4.17]

There is also a correction applied for the direction of the propeller rotation. The correction involves a complete reversal of the y-axis. This is represented by calculating forces or moments at the negative values of the required rudder angles. By applying a reversal to the signs of the forces and angles the forces are resolved back to the correct axis system and required angles.

When calculating the rudder performance by splitting the rudder into an area controlled by the free stream and an area controlled by the propeller race a significant function of the program arises. If this is taken to an extreme, the addition of free stream data and bollard pull data can be used to obtain rudder performance data for a range of propeller advance ratios using the scaling parameter K_P derived in equation [4.9]. The force at a particular thrust loading can be calculated from the free stream result (F_{FS}) and bollard pull ($F_{J=0}$) result as follows:

$$F_i = (1-\xi)\times F_{FS} + \xi \times K_P \times F_{J=0} \qquad [4.18]$$

4.13 Moment Correction

Moments are also corrected from an actual rudder to a required rudder using the following formulae:

$$M_{Z\,REQ} = M_{Z\,ACT} + C_N \times (W_{REQ} - W_{ACT}) \qquad [4.19]$$

$$M_{X\,REQ} = M_{X\,ACT} + C_N \times (V_{REQ} - V_{ACT}) \qquad [4.20]$$

$$M_{Y\,REQ} = M_{Y\,ACT} + C_N \times (V_{REQ} - V_{ACT}) \qquad [4.21]$$

4.14 Output and Results

When creating a rudder propeller interaction a schematic of their relative positions can be plotted for validation and to ensure the correct stern arrangement has been entered into the program. An example of the schematic can be seen in Figure 4.9.

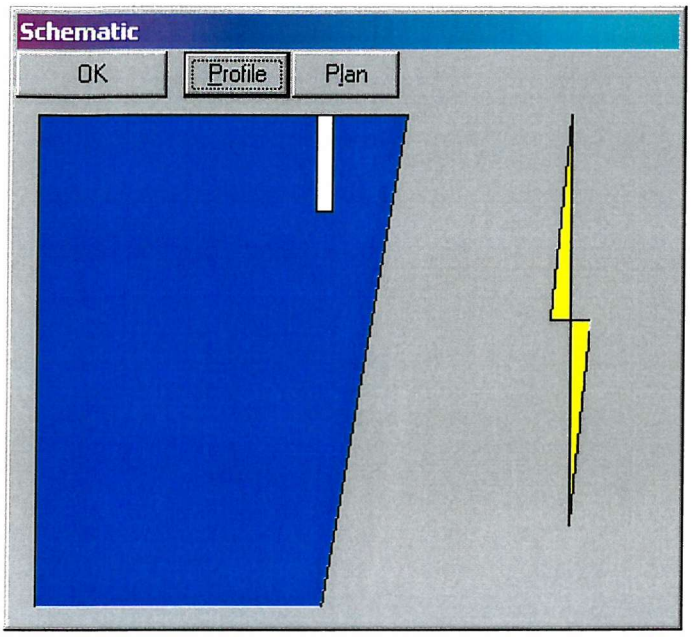

Figure 4.9 Screen Capture of Rudder and Propeller Schematic

The output of the program is rudder lift, drag, moments and derived spanwise and chordwise centre of pressure. Data output of the program is in the form of text and a graphical display. Figure 4.1 shows an example output from the program. The results can be output as coefficients in non-dimensional format or absolute values of force or moment. The results can be saved as computer data files or printed for incorporation into other programs.

The program can provide simultaneous plots of multiple rudder-propeller combinations for comparison purposes and cumulative results of rudder performance for stern arrangements with more than one rudder and propeller.

4.15 Summary and Recommendations

The ability to adjust relatively coarse rudder-propeller geometric and flow variables at an early design stage and get reliable results of rudder performance is a powerful tool. The rudder performance prediction method can be used at a conceptual design stage or as an applied design evaluation to measure the effect on developed rudder forces for changes of the steering gear arrangement. The user-base can therefore range from a naval architect conceiving a new ship design to a shipyard altering an existing ship.

The calculation process uses a specific database to interpolate and fit results by correcting experimental rudder and propeller data to the required rudder and propeller geometry and flow parameters. Results can be incorporated into the program from many sources. Specific experimental tests and physical understanding have formed the basis of the source data but results from trials or CFD analysis could easily be incorporated through the use of data files for further interpolation and extrapolation.

The range of validity of the rudder performance prediction method relies on the available data. The range is substantial with the experimental data described previously. For example the effect of lateral separation (Y/D) has been tested to ±0.375. The interpolation mechanism increases its range of validity with the larger the variation of the available interpolation parameters and the denser the database. The database size can be large and the software is only limited by the range of parameters defined within the method.

The implementation of the rudder performance prediction method provides a versatile development framework for which additional influences and parametric relationships can be built in. Hull form effects, effect of leeway, shallow water and propulsive consequences could all be built into the current framework by expanding the interpolation scope. The same method of interpolation and correction could, for example, be used to measure the effects of a yacht keel upstream of a rudder to examine appendage interaction effects. By a series of experimental studies effects such as appendage longitudinal separation, leeway angle and heel angle could all be accounted for using the interpolation tree method.

A manoeuvring simulator could use the output of rudder performance for several propeller thrust loadings as look up tables to estimate the rudder manoeuvring force at varying ship speed or propeller rate of revolutions. Several parametric studies of rudder geometry can be carried out and the performance data from these incorporated into a manoeuvring simulator to assess the effect of the changes on ship manoeuvring performance.

The prediction of rudder performance at higher advance ratios from bollard pull data and free stream data becomes very powerful combined with the fact that testing a rudder-propeller combination in the bollard pull condition in an open laboratory is a very efficient testing method as described in Chapter 3. This is a new and innovative approach to predicting rudder performance. No wind tunnel tests are needed to study the effect of

rudder-propeller interaction if the free stream performance can be predicted reliably and combined with only open laboratory tests. The validity of this assumption is tested in the design investigations in Chapter 5.

The rudder performance prediction method forms an integral process in the design spiral. By allowing variation of relatively coarse geometric and flow variables, rudder-propeller manoeuvring forces can be predicted reliably at an early design stage. The methodology allows parametric studies to be carried out and comparisons to be made between varying rudder and propeller types, and the development of rudder design and manoeuvring forces for a wide range of stern arrangements. Other design studies such as twin screw arrangements are easily implemented within the current framework. Effects such as lateral offset of rudders from the centreline of propellers can also be investigated providing useful design information.

5 RUDDER DESIGN INVESTIGATIONS

5.1 Introduction

Worked design investigations demonstrate the flexibility of the rudder performance prediction method and the ways in which a design approach can be used to investigate design choices. The investigations examine the applicability of the method by analysing test cases and testing at the edge of the working envelope. Quality assurance is very important to any designer and valid worked examples can give confidence and assurance by demonstrating how the available design parameters can be varied to give reliable results.

There are many factors and design choices that need to be made when detailing the stern arrangement of a ship. The aim of this Chapter is to demonstrate the use of and validate the rudder performance prediction method, described in Chapter 4. In particular assessing how practical the analysis tool is through a series of relevant studies related to ship design. Five design investigations are included to validate and demonstrate the use of the approach:

i) A validation case for the prediction of rudder forces for a lateral offset.
ii) An investigation into the choice between a skeg-rudder, an all-movable rudder and a high performance rudder.
iii) The prediction of rudder torque for off-design conditions.
iv) The influence of rudder shape related to the vertical position of the propeller.
v) The prediction of rudder data for higher advance ratios ($J>0$) solely from free stream and bollard pull ($J=0$) data.

The geometry, relative position and operating conditions for each rudder-propeller combination are described with the calculated data and discussion of the implications of the results. The rudder performance database used in the following design investigations is from experimental work presented in Chapter 3 and previous experimental work by Molland and Turnock [13]. Refer to Chapter 3 for the designated rudder particulars, test conditions and parametric variations.

The process of defining a rudder, propeller and the interaction in the rudder design program is described in Chapter 4 together with the calculation method. Results are used directly from the program and are presented in either non-dimensional or dimensional form as appropriate.

5.2 Case 1 – Lateral Offset Validation Case

The aim of this particular study is to show a validation case where rudder forces are predicted for a tested lateral offset position from a database where that particular set of data has been removed. The method calculates the results by interpolation and correction and these can be compared against the test results.

The calculation of skeg-rudder performance uses experimental data for designated skeg-rudder No. 0 for its free stream data and interaction data set. The designated skeg-rudder 0 database used for the validation case can be seen in Appendix E. The database used has all results at Y/D=±0.125 removed.

To compare against experimental data the dimensions of the rudder and propeller are to scale of designated skeg-rudder No. 0, shown in and Table 5.1 and Table 5.2 respectively. Non-dimensional lift coefficients are presented for comparison purposes. The relative position of the rudder and propeller are at a longitudinal separation of X/D=0.39, lateral separations of Y/D=±0.125 and a vertical separation of Z/D=0.75.

The operating conditions of the rudder-propeller system at an advance ratio of J=0.51 corresponding to a ship speed of 19.4 knots at a propeller speed of 245 revolutions per minute.

Table 5.1 Case 1, Rudder Particulars

Type	Span (m)	Tip Chord (m)	Root Chord (m)	Tip Offset (m)	Aspect Ratio	Stock Position (m)
Skeg	6.0	3.6	4.5	0.89	1.5	1.0

Rudder has a NACA 0020 constant section with square tips.

Table 5.2 Case 1, Propeller Particulars

Designation	Modified Wageningen B.4.40 Series
Range of revolutions (rpm)	133, 245 & 350 rpm
Number of blades	4
Diameter (m)	4.8
Boss Diameter (max)	1.25
Mean Pitch Ratio P/D	0.95
Blade Area Ratio	0.4
Rake (degrees)	0
Blade thickness ratio t/D	0.050
Section shape	Based on Wageningen B series
Blade outline shape	Based on Wageningen but with reduced skew

5.2.1 Case 1, Results and Discussion

Figure 5.1 shows the predicted and experimental rudder lift curves for the defined operating conditions.

It can be seen that the predicted results of rudder lift and drag coefficients compare well with the experimental results for both lateral offset positions. The predicted angular offset due to the propeller wake is close to the experimental data and the lift and drag curves are very similar in magnitude and shape. The validation case has shown that by removing a set of data from the database, rudder performance can still be derived accurately using the interpolation and correction method.

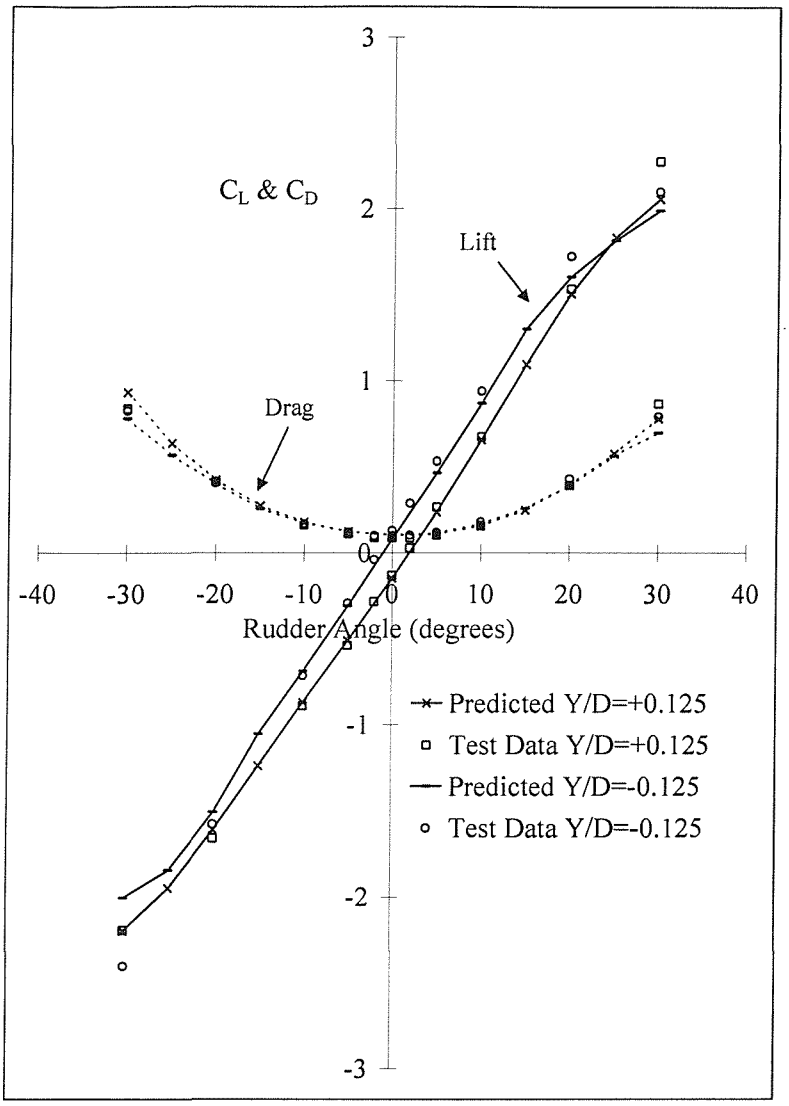

Figure 5.1 Case 1, Comparison of Predicted and Experimental Lift and Drag Coefficients

5.3 Case 2 – Effect of Rudder Type

The aim of this particular study is to investigate the selection of rudder type and how the operation of the ship affects the installed rudder option. The performance of a skeg-rudder, all-movable rudder and a high performance rudder are examined to investigate the trade-off between reduced rudder area and increased manoeuvring side-force.

Three different rudder options have been used for the investigation of the effect of rudder type and these are detailed in Table 5.3. Operation and geometric particulars of the propeller upstream of each of the rudders are given in Table 5.4.

Table 5.3 Case 2, Rudder Particulars

Type	Span (m)	Tip Chord (m)	Root Chord (m)	Tip Offset (m)	Aspect Ratio	Stock Position (m)
All-movable	6.0	4.0	4.0	0.0	1.5	1.0
Skeg	6.0	3.5	4.5	1.0	1.5	1.0
High Lift	6.0	4.0	4.0	0.0	1.5	1.0

Table 5.4 Case 2, Propeller Particulars

Designation	Modified Wageningen B.4.40 Series
Range of revolutions (rpm)	100-200 rpm
Number of blades	4
Diameter (m)	5.0
Boss Diameter (max)	1.25
Mean Pitch Ratio P/D	0.95
Blade Area Ratio	0.4
Rake (degrees)	0
Blade thickness ratio t/D	0.050
Section shape	Based on Wageningen B series
Blade outline shape	Based on Wageningen but with reduced skew

The all-movable and skeg-rudder performance is defined using experimental free-stream data from tests on designated rudders No. 2 and 0 respectively, these are detailed in Chapter 3. The high lift rudder performance is defined as a 3-D lift curve slope of 0.065 and a stall angle of 25°. Both the all-movable and high lift rudder use the designated rudder No. 2 experimental rudder-propeller interaction data with the skeg-rudder using the designated rudder No. 0 data as the base interaction database.

The operating condition of the rudder-propeller system uses a typical ship operating at a speed of 14 knots and a propeller rate of revolutions of 120 rpm. This condition corresponds to an advance ratio of J= 0.497 using a Taylor wake fraction [10], w_T of 0.32.

The relative positions of the rudders and propeller are at a longitudinal separation of X/D=0.4, a lateral separation of Y/D=0.0 and a vertical separation of Z/D=0.5. The

operating condition and relative separation of the rudder and propeller does not correspond to any particular test data set and is therefore testing the interpolation and correction procedure of the rudder performance prediction method.

5.3.1 Case 2, Results and Discussion

Lift and drag forces are calculated for each rudder at the defined operating condition. Figure 5.2 shows the rudder lift and drag curves.

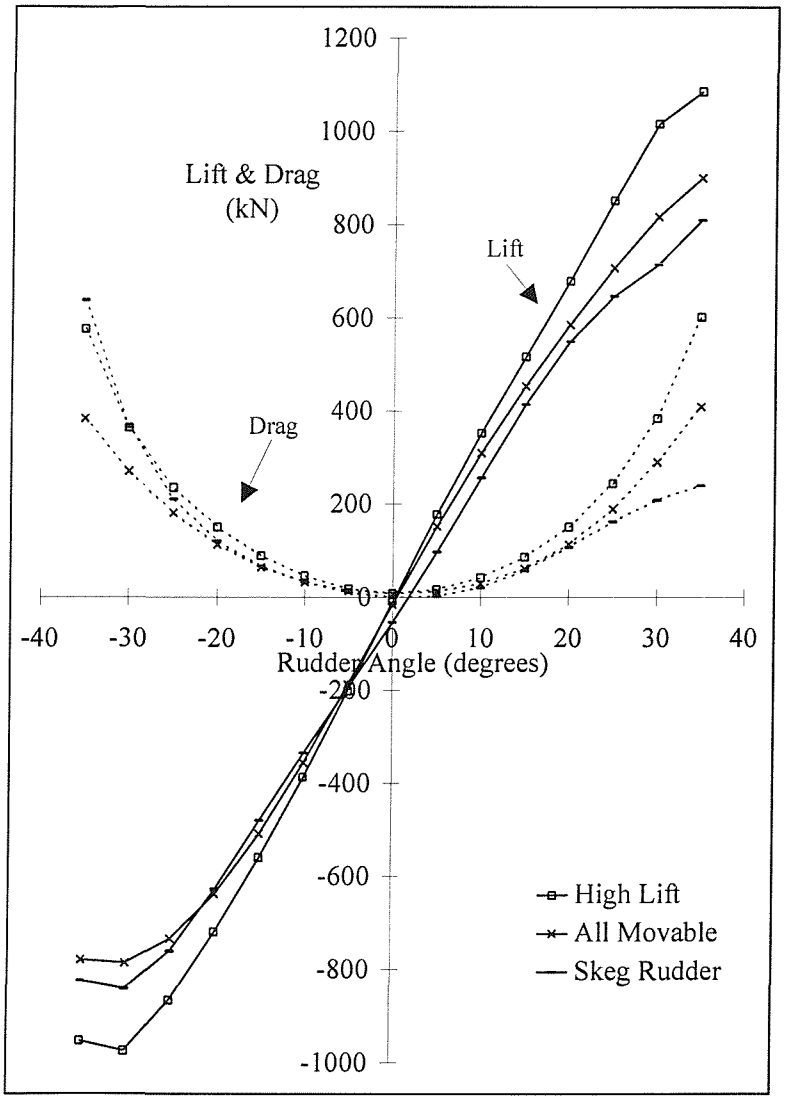

Figure 5.2 Case 2, Lift and Drag Results for Rudder Types

The relative performance of the rudder types are similar and as expected with the high-lift rudder exhibiting a higher lift curve slope ($dC_L/d\alpha$) and a corresponding increase in drag over the all-movable rudder and skeg-rudder downstream of a propeller.

There is a small offset in the zero lift angle of the skeg-rudder and this is due to the sweepback and taper of the skeg-rudder. The rudder taper causes an increased area at the top of the rudder in the propeller flow compared with the lower part in the propeller flow causing an asymmetry of rudder loading at zero rudder incidence.

The design implication of this particular study is that the high-lift rudder area could be reduced somewhat to match the lift produced to that say of the all-movable rudder, with a consequent reduction in rudder drag, this could be attractive in terms of rudder layout and cost. The reduction would result in a high lift rudder area of 20.7m^2 compared to an all-movable rudder area of 24.0m^2. The reduction in rudder area could be achieved, for example, by reducing the chord to 3.45m. The results of this change are shown in Figure 5.3.

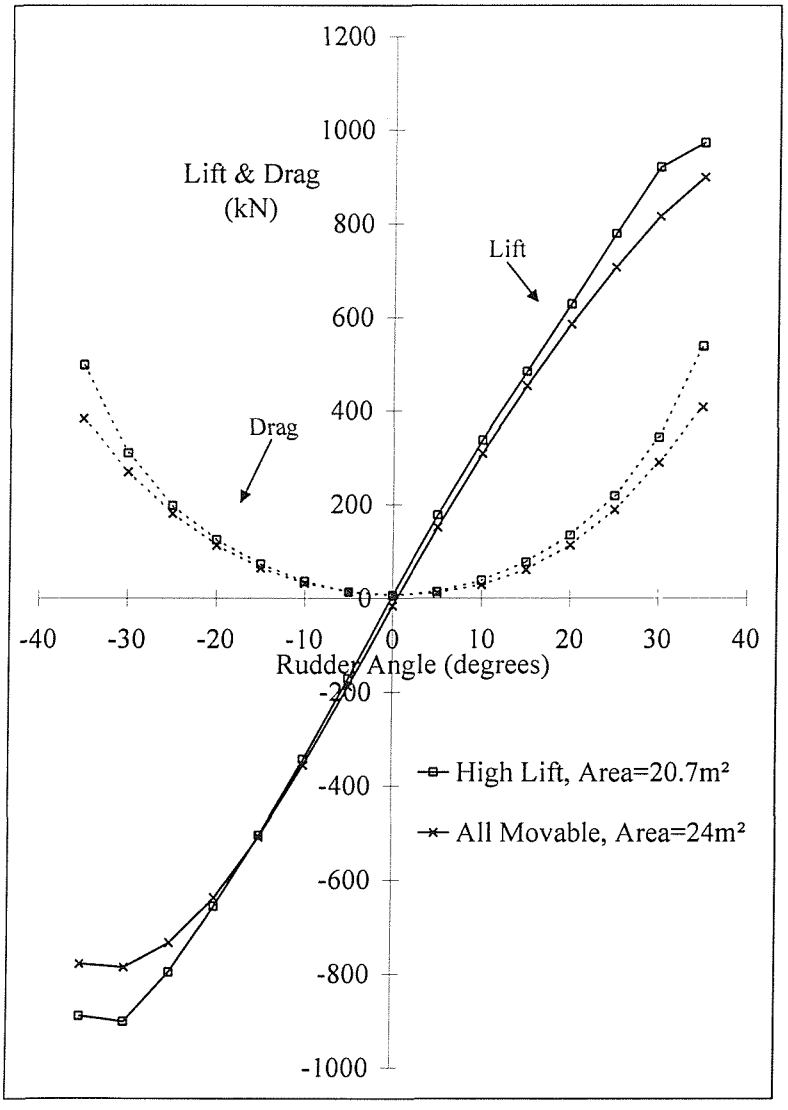

Figure 5.3 Case 2, Lift and Drag Results for Two Rudder Areas

For any rudder on a ship it desirable to maximise lift to drag ratio particularly in a vessel that requires a substantial amount of manoeuvring in its operation. The high-lift rudder is most suitable for this application.

In a vessel that does not require a large amount of manoeuvring a small drag coefficient at zero incidence (C_{d0}) is desirable for powering considerations as the rudder is in this position much of the time. The all-movable rudder is most suited to this application. Where a rudder is large it may experience high structural loads. A skeg is often desirable in this case as it gives extra support for the bending moment experienced at the rudder root through the use of a stock bearing at the tip of the skeg part.

5.4 Case 3 – Effect of Off-Design Conditions

This design investigation is aimed at examining rudder steering gear torque moments for structural considerations in ship design and off design conditions. Appropriate sizing of the steering gear can have profound implications for manoeuvring. It is essential that available and required rudder torque matches across the whole range of possible rudder incidence and ship advance speed.

For this particular study the all-movable rudder, with particulars detailed in Table 5.3, is used with the propeller detailed in Table 5.4. The relative positions of the rudder and propeller are the same as Case 2. The all-movable rudder uses free stream and interaction test data from designated rudder No. 2. The predictions of rudder torque are at several operating conditions, detailed in Table 5.5.

Table 5.5 Case 3, Operating Conditions

V (knots)	w_T	Rpm	J	K_T
0.0	---	120.0	0.0	0.365
7.0	0.32	120.0	0.245	0.311
14.0	0.32	120.0	0.497	0.229
14.0	0.32		Free stream	

5.4.1 Case 2, Results and Discussion

Figure 5.4 shows the rudder torque at the rudder stock against rudder helm angle for the defined set of operating conditions.

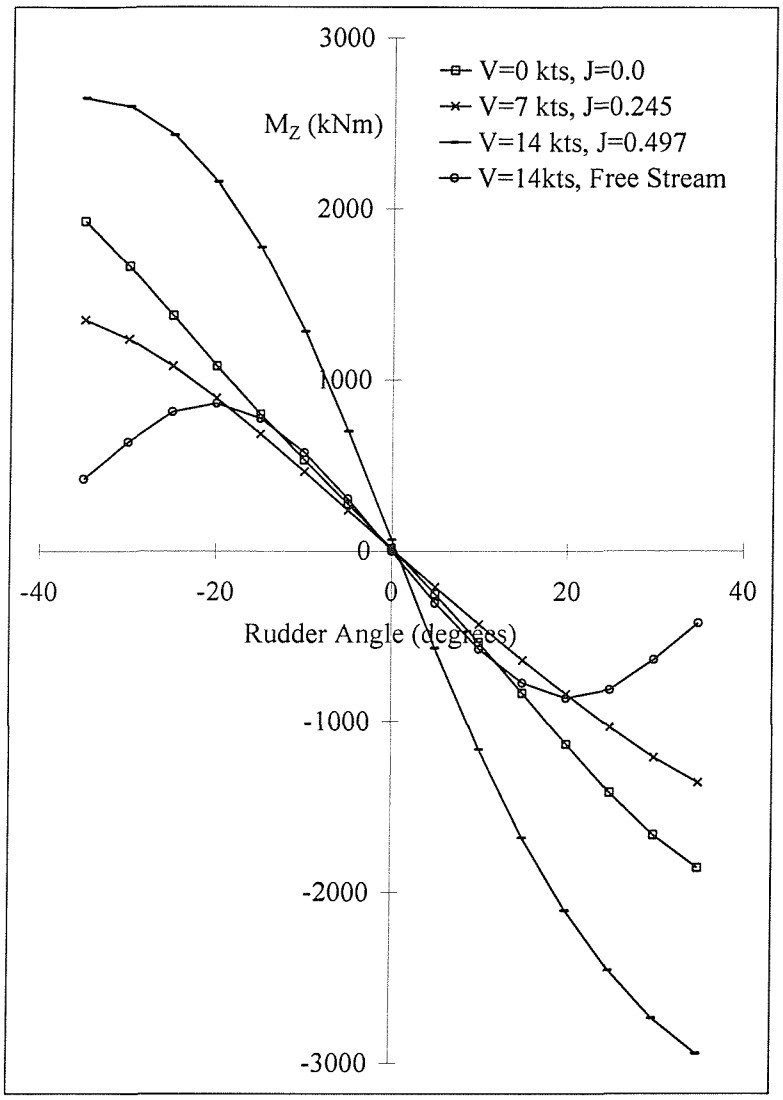

Figure 5.4 Case 3, Torque Moment Results for Ship Operating Conditions

The torque curves for all operating condition are of similar shape with the highest result in the design condition for all rudder angles. The results indicate a higher torque in the bollard pull condition (J=0) than that of an advance ratio of J=0.245. This is due to the thrust loading being higher for the bollard pull condition and the propeller flow is more dominant than the free stream flow. The free stream torque result is the same magnitude as the bollard pull condition up to 20° incidence and then it reduces. The reduction is due to

the rudder stalling at an earlier angle in the free stream as the propeller has the effect of increasing the stall angle as found in the experimental work discussed in Chapter 3.

The design implications of this study are such that the highest torque is experienced at the design condition at 35° rudder incidence, but at this condition a large helm angle may not often be applied as the ship is in an open seaway. When a ship is moving in a restricted seaway at low speed, high rudder angles may be used and therefore the designer should still be wary of the high torque exhibited in the bollard pull condition as this could be the most severe case.

The stock moment can be altered by changing the position of the stock. In this case for a movement of the stock from 25% to 20% of rudder chord would reduce the peak torque values but increase the range of incidence for which the rudder does not weather vane. This can be achieved simply by changing the rudder stock position in the program from 1.0m to 0.8m and the results from this calculation are presented in Figure 5.5.

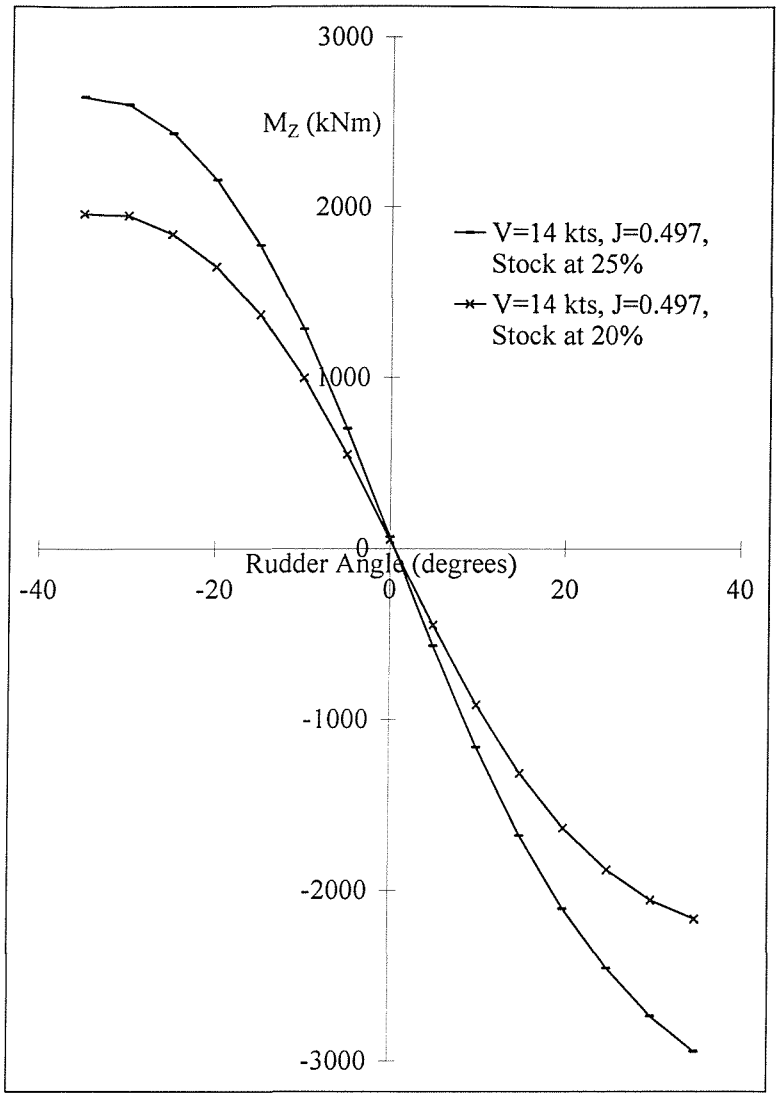

Figure 5.5 Case 3, Torque Moment Results for Two Stock Positions

5.5 Case 4, Effect of Relative Propeller Position and Rudder Particulars

This design investigation is aimed at investigating the influence of rudder shape, in particular aspect ratio, and the effect the relative vertical position of the propeller has on the balance and coverage of the rudder. Rudders whose tip does not extend to the full depth of propeller are often found on naval vessels or high speed motor vessels.

Two different rudder types were used for the investigation detailed in Table 5.6. The particulars of the propeller are the same as Case 2 and are detailed in Table 5.4.

The relative positions of the rudder and propeller are detailed in Table 5.7 and Figure 5.6 indicates the relative propeller coverage on all-movable rudders A and B.

Table 5.6 Case 4, Rudder Particulars

Type	Span (m)	Tip Chord (m)	Root Chord (m)	Tip Offset (m)	Aspect Ratio	Stock Position (m)
All-movable A	6.0	4.0	4.0	0.0	1.5	1.0
All-movable B	5.0	4.0	4.0	0.0	1.25	1.0

All rudders have a NACA 0020 constant section with square tips.

Table 5.7 Case 4, Rudder-Propeller Relative Positions

Type	X/D	Y/D	Z/D
All-movable A	0.4	0.0	0.7
All-movable B	0.4	0.0	0.7

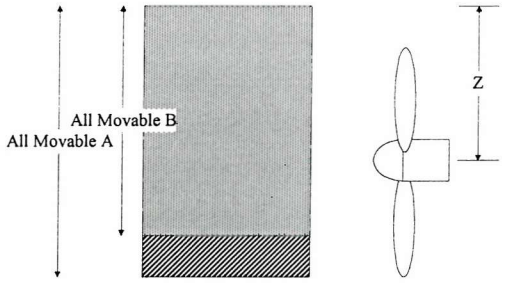

Figure 5.6 Case 4, Rudder-Propeller Schematic

The operating condition of the rudder-propeller system uses a typical ship operating at a speed of 14 knots and a propeller rate of revolutions of 120 rpm. This condition corresponds to an advance ratio ,J, of 0.497 using a wake fraction, w_T. of 0.32.

5.5.1 Case 4, Results and Discussion

Figure 5.7 shows the rudder lift and drag curves for the defined operating condition.

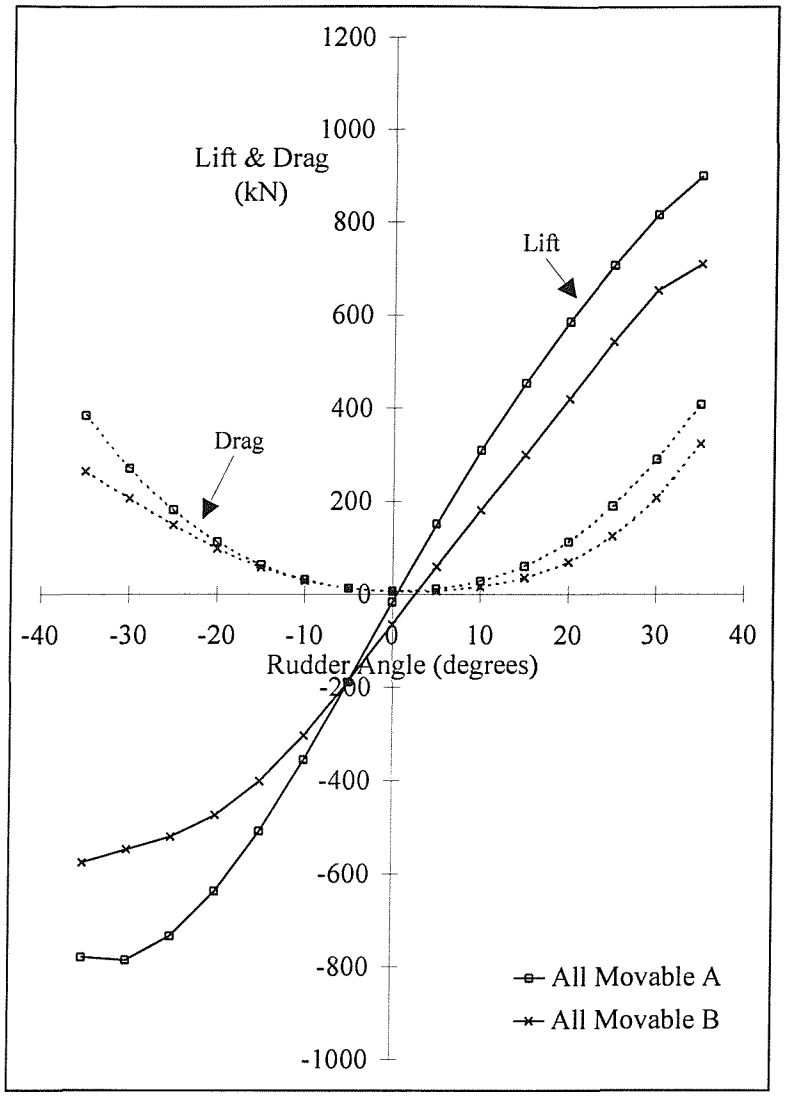

Figure 5.7 Case 4, Lift and Drag Results for Two Rudder Geometries

The lift and drag curves for both rudders are similar. The effect of having partial coverage from the propeller is to offset the lift curve slope such that the angle of attack at zero lift is not at 0°. This effect is due to the asymmetry of the propeller race on to the rudder.

The implication of choosing the all-movable rudder B arrangement in preference to rudder A for this particular study are such that there would have to be a constant incidence offset or toe-in on the rudder for zero rudder sideforce when not manoeuvring. The offset will change for varying propeller advance ratios. For the design condition the design speed and matching propeller thrust would have to be used to calculate a suitable constant offset. For the example presented in Figure 5.7 the toe-in on all-movable rudder B for zero lift would

be 2°. The direction of the propeller rotation is also critical since if the propeller were rotating in the opposite direction the incidence offset would have to be reversed.

5.6 Case 5 – Performance Prediction from Free Stream and Bollard Pull Data

The aim of this particular study is to investigate the scope of the rudder performance prediction method by limiting the rudder force data used in the rudder design program to free stream and bollard pull (J=0) results only. By calculating results for advance ratios greater than zero (J>0) the program extrapolates this test data for rudder performance prediction. The process of predicting rudder performance has been described in more detail in Chapter 4 and is testing the method at the edge of the working range due to the extrapolation of the bollard pull data to higher advance ratios being the most testing case.

The calculation of skeg-rudder performance uses experimental data for designated skeg-rudder No. 0 for its free stream data and interaction data set. The interaction data set is limited to bollard pull tests (J=0) only.

To compare against experimental data the dimensions of the rudder and propeller are the same as Case 1 and are to scale of designated skeg-rudder No. 0 shown in Table 5.1 and Table 5.2 respectively. Non-dimensional lift coefficients are presented for comparison purposes. The relative position of the rudder and propeller are at a longitudinal separation of X/D=0.39, a lateral separation of Y/D=0.0 and a vertical separation of Z/D=0.75.

The operating conditions of the rudder-propeller system at an advance ratio of J=0.35, 0.51 and 0.94 corresponding to a ship speed of 19.4 knots at a propeller speed of 350, 245 and 133 revolutions per minute respectively.

5.6.1 Case 5, Results and Discussion

Figure 5.8 shows the predicted and experimental rudder lift curves for the defined operating conditions.

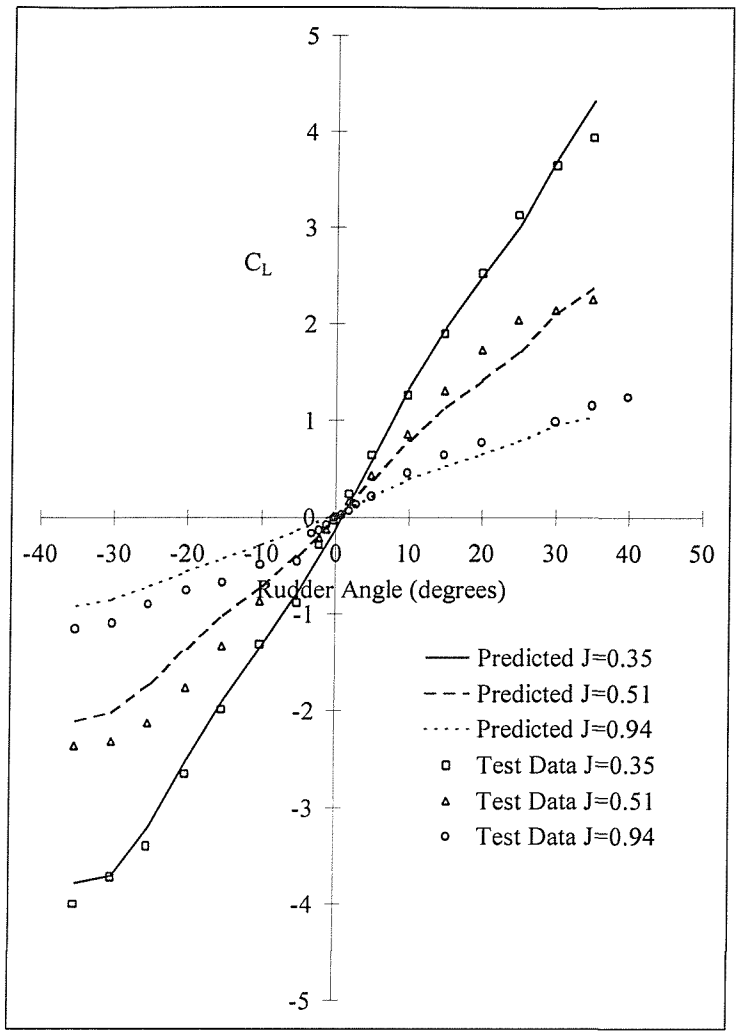

Figure 5.8 Case 5, Comparison of Predicted and Experimental Lift Coefficients

It can be seen that the predicted results compare well with the experimental results. As the advance ratio increases and hence thrust loading drops the results become less accurate. The results at J=0.35 are within 2% of the experimental results up to 20 degrees, whereas the results for J=0.51 are within 10% and J=0.94 are 20%. This shows the further the deviation from the bollard pull condition the results become less reliable. The results are more reliable for smaller rudder angles.

The skeg-rudder has a complex lift curve slope associated with the skeg gap flow as described in Chapter 3 and shown in Figure A-2. It is therefore an arduous test for the rudder performance prediction method and has given reliable results particularly at higher thrust loading.

The principle reason for divergence from the experimental results at higher advance ratios are due to the calculation of the scaling parameter K_P (Equation [4.9]) based on thrust loading in the bollard pull condition (K_{T0}) and the required thrust loading. The assumption is the rudder force generated by the propeller decreases linearly with propeller thrust loading, this is true with small deviations from the bollard pull condition but at higher advance ratios the rudder performance behind a propeller is not this simplistic.

The design implications of this particular case study are related more to design inception. This particular study demonstrates the accurate prediction of skeg-rudder manoeuvring performance behind a propeller at higher advance ratios from the bollard pull condition data.

5.7 Summary and Recommendations

A primary decision in designing a ship's stern arrangement is rudder type. The effect of using various rudder types has been demonstrated for a typical operating condition and the consequences of each design discussed. The type of rudder installation depends on the specific ship's operation. The requirements are defined by manoeuvring considerations and structural considerations.

The prediction of off design conditions has been shown, this is a powerful tool as it allows the designer to comprehensively investigate the suitability of a rudder design in many operation situations. The effect of adjusting the relative rudder-propeller position has been shown and this allows the designer to investigate the performance of many different types of rudder-propeller arrangements.

The prediction of rudder performance at higher advance ratios from purely rudder free stream and bollard pull data has been shown. This provides confirmation of the coverage method described in Chapter 4 and shows that the laboratory tests detailed in Chapter 3 are a valid and novel way of obtaining rudder performance data downstream of a propeller. The advantages of this have been discussed in Chapter 3 and 4 and the design investigation reinforces this conclusion.

The validity of the method has been shown and further investigation of the calculation of the scaling parameter K_P away from the bollard pull condition is necessary to accurately predict rudder performance at high propeller advance ratios purely from bollard pull data and 2-D sectional lift coefficient.

The presented design investigations show, by way of example, the validation of the rudder performance prediction method for a wide range of rudder types, operating conditions and investigated parameters. The investigations have shown the rudder performance prediction methodology and software to be a practical design tool for ship manoeuvring considerations and for structural steering gear considerations.

6 SURFACE PANEL ANALYSIS METHOD

6.1 Introduction

Experimental analysis of rudder-propeller interaction can often be cumbersome and expensive, particularly for large parametric variations. If a computational tool can be implemented to accurately predict the rudder-propeller interaction mechanism the burden on experimental work could be reduced. For the computational method to be an effective analysis tool it must supply results such as detailed load distribution at the same or at a higher resolution as experimental work. A systematic parametric variation of design parameters using a CFD study should conceptually be the same as an experimental study. Design parameters should be varied on the same understanding of the physical basis to obtain detailed information on the influence on performance.

The principle purpose for using a computational tool is to investigate the feasibility of modelling a skeg-rudder downstream of a propeller. The necessity of further parametric variation has been identified. This is a difficult test case due to the complexity for skeg-type rudders. The skeg-rudder has many geometric intricacies and the method must not only be able to predict the flow around this detail but also provide a sufficiently flexible method of geometric definition.

A reasonable compromise between computational effort and physical accuracy in modelling the flow interaction is achieved by the use of a lifting surface panel method. A surface panel method named PALISUPAN written by Dr. Stephen Turnock of the Department of Ship Science at the University of Southampton has been used and its theoretical methods and operation are described in [27] and [59] respectively. The same panel method is capable of modelling in isolation the individual rudder and propeller with the interaction between the two bodies accounted for by the modification of their respective inflow velocity fields.

The surface panel method has been developed and applied to the numerical modelling of an all-movable rudder downstream of a propeller by Turnock [27] and by the author to model yacht hull-keel-rudder interaction [36 and Appendix D], [37]. The aim of this chapter is to detail the theoretical framework of this CFD method with the objective of

predicting the performance of a skeg-rudder downstream of a propeller and supply detailed information on the distribution of loading.

6.2 Development of Computational Geometry Models

The surface panel method requires a three-dimensional geometry definition of the actual body surface. Geometric definition within the code is carried out by a series of parametric cubic splines fitted around an initial set of definition points located on the body surface. By interpolating the cubic splines, varying panel distributions can be set over the body to concentrate panels in areas of intense curvature and regions of particular interest. The body is discretised into quadrilateral panels to create a grid over the surface of the body and on a wake sheet. For further information on the process of geometry definition within the panel code see [59].

An effective geometric definition of the individual bodies of the rudder-propeller system is required to give a discretisation of suitable quality such that the numerical method will converge. Care must be taken over the number of panels used in the chordwise and spanwise directions. Panel size distributions and wake definition should also be considered when creating the computational geometry.

Many geometric parameters can affect the solution or indeed whether the model will converge to a solution at all. Several numerical tests are conducted varying the available panelling parameters. By validation, examination of convergence histories and inspecting particular areas of interests such as high pressure gradients, the geometric definition of the surface of the bodies and the wake can be adjusted such that the solution is as stable and as numerically correct as possible.

Wake adaptation by means of aligning the wake to the flow has not been implemented with this particular model as the computational time and effort increases quite considerably using this method [27]. In general the wake is defined behind and parallel to the body and is rotated with the body if necessary.

6.3 Surface Panel Analysis

The method used to predict the performance of the rudder-propeller system is based on theoretical foundation of a lifting surface model. The following is a summary description of the theory described by Turnock in [27] to present the theoretical basis and methods used.

In a lifting surface panel formulation the approximation of the full Navier-Stokes equation assumes that the flow is inviscid, incompressible and irrotational and satisfies Laplace's potential equation:

$$\nabla^2 \phi = 0 \qquad [6.1]$$

A body is described in the formulation by dividing the surface into discrete quadrilateral panels. Each panel is represented numerically as a known distribution of constant strength sources and dipoles of unknown strength. The flow is then resolved by solving a matrix of source and dipole influences upon the fluid. A further condition is required in order that the difference in pressure on the trailing edge of the body is zero, (Kutta-Joukowski condition). This is carried out by defining the wake sheet downstream of the body and iterating the solution by adjusting the wake strength until the pressure difference is as near to zero as required for an accurate solution.

A detailed description of the method and a review of its historical development is given by Hess [50]. Lamb [51] showed that a quantity satisfying Laplace's equation can be written as an integral over the bounding surface S of a source distribution per unit area s and a normal dipole distribution per unit area m distributed over the S. If v represents the disturbance velocity field due to the bounding surface (or body) and is defined as the difference between the local velocity at a point and that due to the free-stream velocity then.

$$\underline{v} = \nabla \phi \qquad [6.2]$$

where ϕ is defined as the disturbance potential. This can be expressed in terms of a surface integral as:

$$\phi = \iint_{S_B}\left[\frac{1}{r}\sigma + \frac{\partial}{\partial n}\left(\frac{1}{r}\right)\mu\right]dS + \iint_{S_W}\frac{\partial}{\partial n}\left(\frac{1}{r}\right)\mu dS \qquad [6.3]$$

where S_B is the surface of the body and S_W a trailing wake sheet. In the expression [6.3] r is the distance from the point for which the potential is being determined to the integration point on the surface. $\partial/\partial n$ is a partial derivative in the direction normal to the local surface. A dipole distribution is used to represent the wake sheet. Hess [49] showed that this can be directly related to the vorticity distribution used in vortex lattice methods. For a steady-state solution the wake dipole strength distribution is uniquely determined by the application of the Kutta condition at the body trailing edge. Based on Morino's method, [54], on the body surface the source strength per unit area is prescribed by satisfying the condition for zero normal velocity at the panel centroid.

$$\sigma_S = U \cdot n \qquad [6.4]$$

where n is the unit normal outward from the panel surface and U the specified inflow velocity at the panel centroid. Numerical discretisation of [6.3] is achieved by representing the actual body surface as N quadrilateral panels. This gives the dipole potential at the centroid of panel i as:

$$\phi_i = \frac{1}{2\pi}\sum_{j=i}^{N}\left(\left(U \cdot n_j\right)S_{ij} - \phi_j D_{ij}\right) + \sum_{k=1}^{M}\Delta\phi_k W_{ik} \qquad [6.5]$$

where for panel j:

S_{ij} is the source influence coefficient of a unit strength panel.

D_{ij} is the dipole influence coefficient of a unit strength panel and

W_{ik} the influence of the constant strength wake strip extending to infinity.

As there are N independent equations corresponding to the N body surface panel centroids, [6.5] is closed and can be evaluated. Expressed in matrix form it becomes:

$$\left[D_{ij} + W_{ik}\right]\phi = \left[S_{ij}\right]U \cdot n_j - \left[W_{ik}\right]\left(\frac{d\Delta\phi}{d\Delta p}\Delta p\right)^t \qquad [6.6]$$

Equation [6.6] can then be iteratively solved by progressive adjustment of the wake strength until the pressure loading at the trailing edge has been removed to any significant degree. Solution of the linear system of equations gives the vector of dipole potentials ϕ. Numerical differentiation of this potential along the body surface allows the surface velocity, hence pressures on the surface to be evaluated.

The process primarily involves calculation of the interaction matrix and then solving a dense set of linear equations in the form of the dipole matrix. Solving the dipole matrix is accomplished using a Jacobian block iterative solver. With this solver the memory requirement is proportional to the square of the number of panels in a block and computational work can be greatly reduced in comparison to direct inversion. The flow chart of the overall scheme of the panel method can be seen in Figure 6.1.

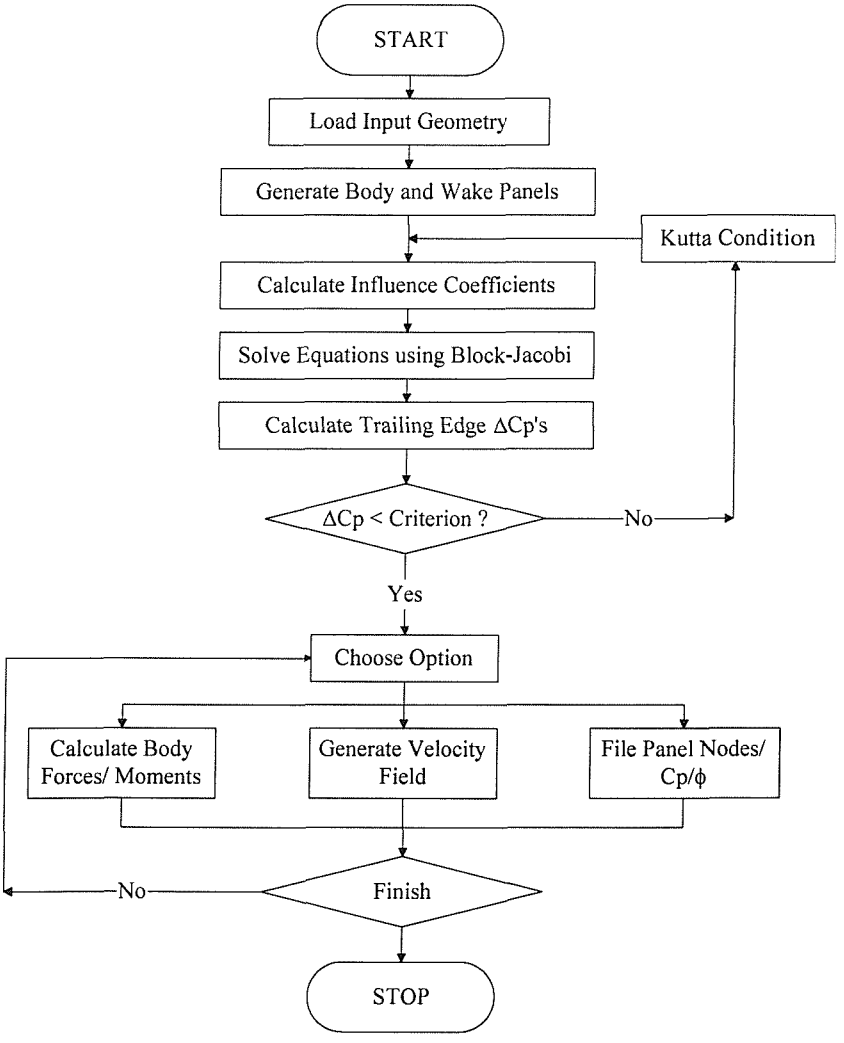

Figure 6.1 Flow Chart of Overall lifting Surface Algorithm.

6.4 Calculation of local Pressures, Forces and Velocities

The numerical solution determines the final dipole strength at the centre of each panel and hence potential on the surface of the body. To obtain practical information from this result a numerical differentiation is carried out. The differentiation of dipole potential is used to find the disturbance velocity tangential to the panel surface. The disturbance velocity can then be used to calculate the total surface velocity on the body and from this the velocity in the overall co-ordinate system. This velocity is used to calculate the local non-dimensional pressure coefficient C_P for each panel.

$$C_P = 1 - \frac{U_t^2}{U_\infty^2} \quad [6.7]$$

To obtain the total forces the distribution of pressure is integrated over the surface of the body for all panels and from the forces non-dimensional lift and drag coefficients are derived. The use of potential flow theory allows the circulation and hence lift (side force) and lift induced drag to be determined. However, as the local velocity is known for each panel the local panel skin friction coefficient can be empirically estimated and summed to give a total frictional force.

6.5 Interaction Velocity Field Method

The PALISUPAN software was developed as a series of procedures corresponding to the various stages in solving the perturbation potential method. This allows a specific program to solve body flow interaction by splitting the flow solution into multiple parts and accounting for the interaction by means of a modified inflow velocity field.

Using the interaction method the bodies are not all modelled in one numerical pass thus creating a further iteration loop around the solution method described earlier. Take the example of rudder-propeller interaction, first the propeller flow model is solved to get a velocity influence upon the rudder. The rudder flow is then solved with the modified inflow velocity field to get a subsequent field on the propeller. This process is repeated with the starting point on the propeller being the velocity influence solved in the previous numerical pass. The procedure repeats until the difference in the results of body forces have iterated down to a minimum required value. Figure 6.2 is a flow chart of the overall velocity interaction process.

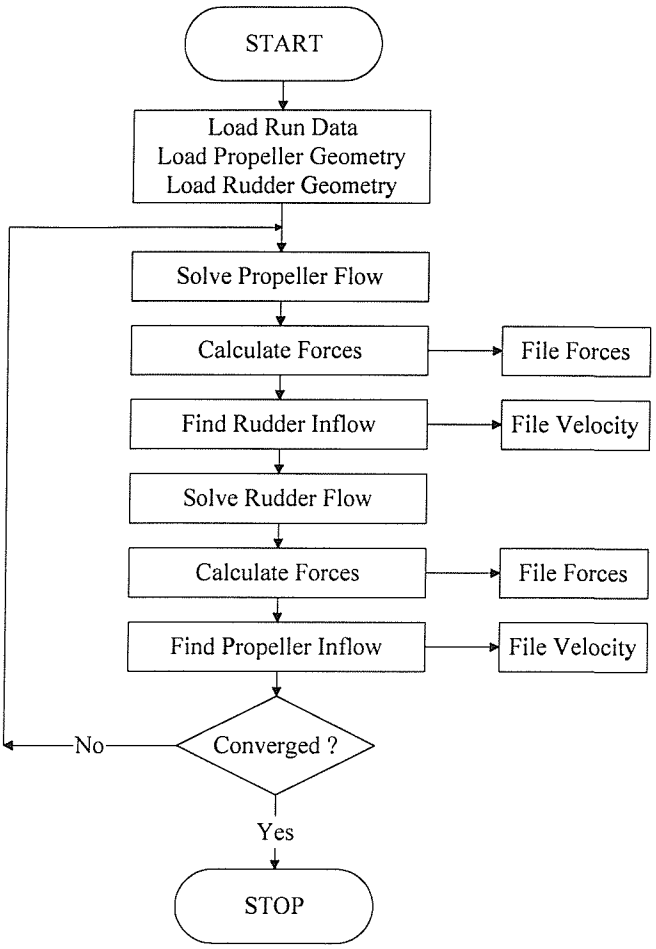

Figure 6.2 Flow Chart of Interaction Velocity Field Method Algorithm

The interaction velocity field approach allows the available number of panels for a given body to be maximised to the computer memory available and hence allow higher quality grids to be created on individual bodies. It can also be used to lower the memory requirement for each numerical pass.

The interaction velocity method effectively creates a matrix conditioner for the solution of the dipole strengths on the surface of the bodies. As the solution is separated into single parts, individual flow solutions can be calculated thus reducing the complexity of the influence coefficient matrix $[S_{ij}]$. The matrix conditioner is particularly useful when there is a concentrated interaction between two bodies. This allows the matrix to be solved at a faster rate and to a better quality by the iterative solution algorithm. Without this matrix conditioning a direct inversion matrix solver may have to be used which greatly increases the memory requirements and the number of operations the code has to execute and thus increasing the amount of time to obtain a converged solution to the problem.

6.6 Visualisation and Validation

Visualisation is an important part of understanding the way the geometry has been produced and the results that are obtained from the computational fluids calculations. Vast amounts of information can be analysed qualitatively using effective visualisation. The program in its form prior to the work undertaken in this thesis was a console application where no integral visualisation tool was available making validation cumbersome and time consuming.

By incorporating ANSI C code to visual C^{++} the PALISUPAN program has been refined to include input forms and enhanced visualisation tools using data structures within the existing program. The visualisation tools were written using open graphics libraries [65] under the Windows operating system for rendering of discretised geometries and also plotting of pressure results using red, green, blue intensity plots. Other additional visualisation tools have been created in the program to analyse the source influence coefficient matrix ($[S_{ij}]$) quality as this is a good indication of the reliability of the solution or indeed if the solution will converge. High values of the influence coefficient matrix outside the blocks of the Jacobian iterative solver are undesirable [27], this information can be visualised and further diagnostics can be carried out.

A screen capture of the program is shown in Figure 6.3 showing a panelled racing yacht rudder from the analysis presented in [36 and Appendix D]. An intensity plot representation of the influence coefficient matrix can also be seen to the right of the figure. The order of the panels in the influence coefficient matrix are chordwise around the rudder and then from the root to the tip. The brighter values represent higher values in the influence coefficient matrix and it can be seen that the highest values are the self influence down the leading diagonal of the matrix.

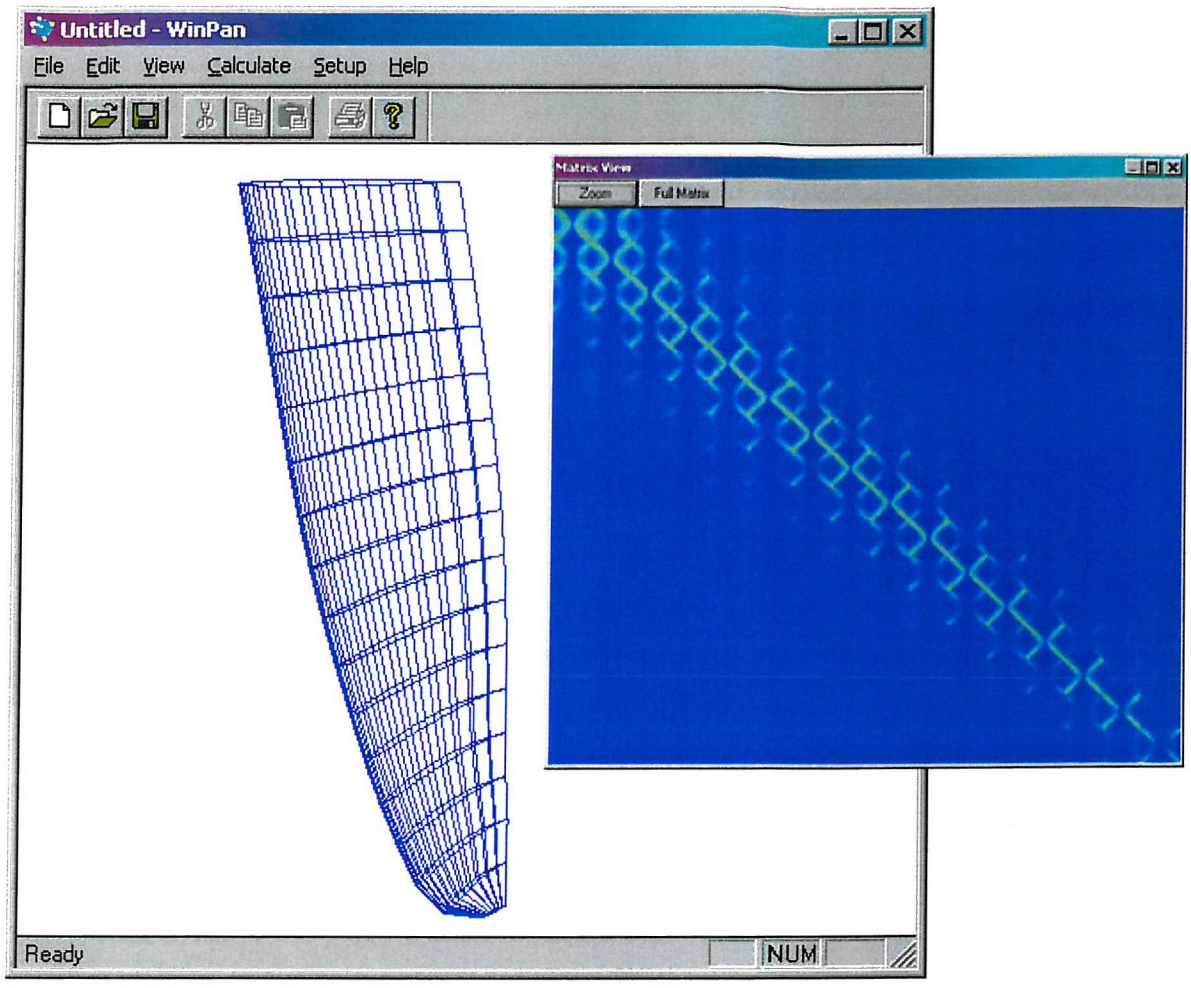

Figure 6.3 Screen Capture of Enhanced Surface Panel Program

Solution examples from the CFD method were also rendered using version 1.0 of the Virtual Reality Modelling Language (VRML) [63] based on an unstructured grid system. This format can be used by world wide web based browser applications and is becoming a new standard in representing three-dimensional worlds. An example of this is shown in Figure 6.4 showing the results from the surface panel analysis of the skeg-rudder investigated in Chapter 6 in an internet browser. The skeg can be seen in the bottom of the figure aligned to the flow and the movable part has an incidence of 10° with the rudder leading edge moving away from the viewing point. The intensity plot corresponds to the pressure distribution where the red represents a maximum pressure coefficient, C_P of 0.99 and the blue a minimum of –6.51.

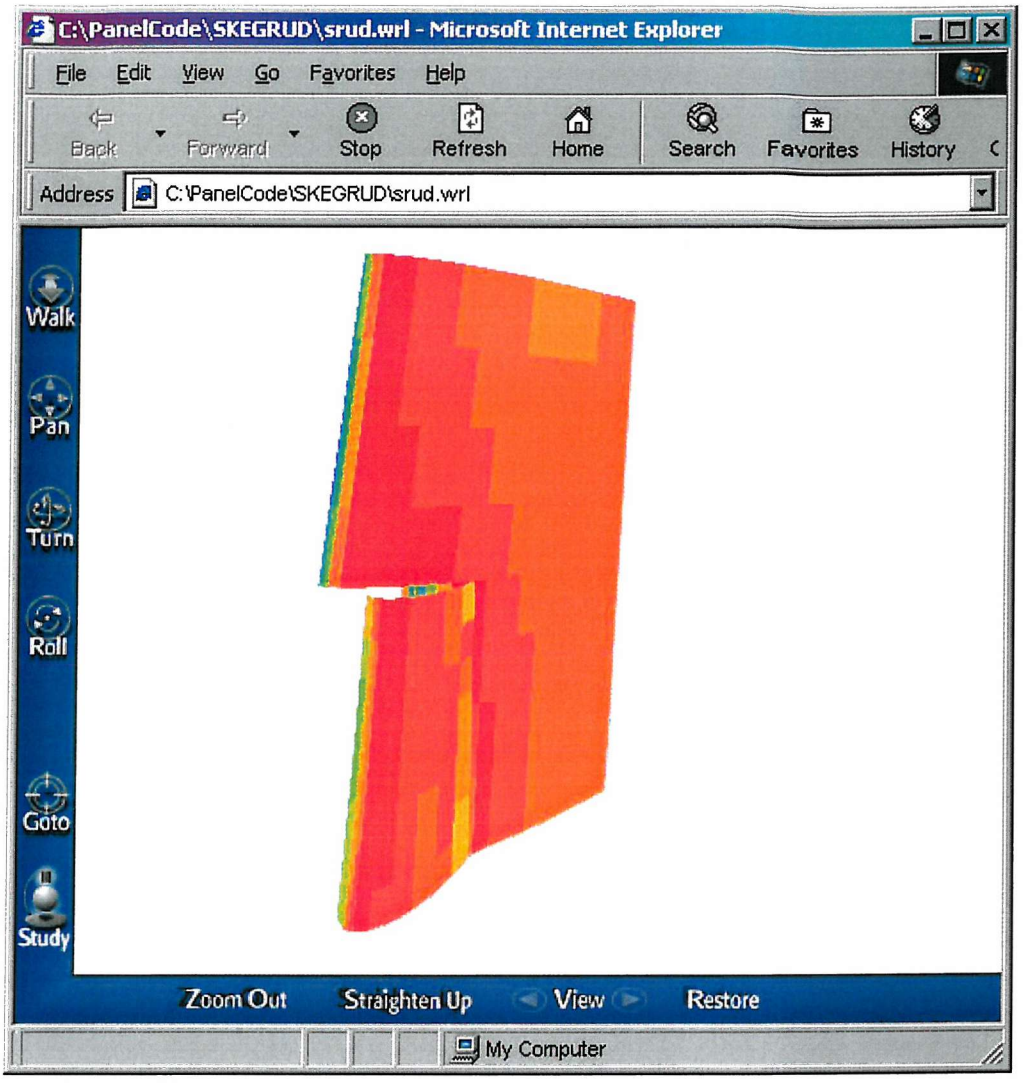

Figure 6.4 Screen Capture of VRML Visualisation Using an Internet Browser

6.7 Summary and Recommendations

Geometry creation with the surface panel method is flexible enough to define a skeg-rudder surface with the intricacies of the skeg gap. The enhanced visualisation tools aids CFD geometry development and validation of results.

The surface panel method can calculate surface pressure and hence supply detailed information of the distribution of loading on a rudder as well as total forces and moments. The results can be presented in a form that experimental results can be compared directly for validation.

The interaction velocity method is a powerful tool particularly in modelling rudder-propeller interaction. The method allows the rudder and propeller influence coefficient matrix solution to be separated and their influence accounted for by an adjustment of the inflow velocity field.

Enhanced visualisation tools have been produced to aid the geometry creation and solution diagnostic phase. The calculated panelled geometry can be viewed prior to surface panel analysis and this is a great advantage as this can often be the most time consuming part. The source influence coefficient matrix can be viewed qualitatively to identify numerical errors and solution robustness again before the solution phase. Detailed results can be viewed as colour intensity plots to analyse the solution and with further work on the current framework other information such as pressure contours and velocity vectors on and around the body can be visualised.

The results of a CFD code can be used to tighten the design spiral by supplying a greater depth of understanding of a rudder design and its performance. Data from the CFD results can be implemented back into the rudder performance prediction method described in Chapter 4 to extend the database.

The described CFD method has been successful in modelling an all-movable rudder downstream of a propeller [27] and therefore it is feasible that it has an application on the more complex flow regimes involved with a skeg-rudder. The application of the method to skeg-rudder performance prediction is described in the following Chapter 7.

7 SKEG-RUDDER PERFORMANCE ANALYSIS

7.1 Introduction

The aim of this Chapter is to demonstrate the use of computational fluid dynamics to model skeg-rudder performance to provide in-depth design data in greater detail than that supplied by the rudder performance prediction method described in Chapter 4. The exercise is designed to investigate the validity of using the surface panel method such that the comprehensive results can provide data for detailed rudder scantling design and understanding of rudder flow for enhanced performance.

Before reliably using any results from a CFD method for design, validation must occur to prove the method and investigate its scope. Experimental data is very useful in validating a CFD method. The results presented in this case study are compared against experimental results obtained in the tests described previously in Chapter 3.

The modelling of a skeg-rudder downstream of a propeller using a surface panel method is a novel approach. The intricacies involved in the geometry definition and obtaining a numerical solution is much higher than an all-movable rudder due to the presence of multiple elements in the total rudder geometry.

Once a computational method has been validated its scope can be tested. Parameters can be varied out of the scope of variation of experimental data to provide additional design data. The aim of the work is to obtain information determining the level of validity of the method and its application to predicting skeg-rudder and propeller interaction performance.

7.2 Skeg-Rudder Definition

Turnock [27] has successfully modelled an all-movable rudder downstream of a propeller using the surface panel method and it is the same implementation of this method that is being used to model the skeg-rudder downstream of a propeller.

The skeg-rudder presented in this particular study has the same geometrical properties as designated skeg-rudder No. 0 detailed in Chapter 3 and shown in Figure 7.1. The principle

difference between the actual skeg rudder tested and the numerical skeg model is the skeg part has no protrusion into the movable part for the rudder stock bearing, indicated by the dotted line in Figure 7.1. This simplification was introduced due to the problems involved in geometry definition of this particular region. The effect this part has on the flow is minimal compared to the general effect of having a skeg part to a rudder and in general this is the effect to be modelled and investigated.

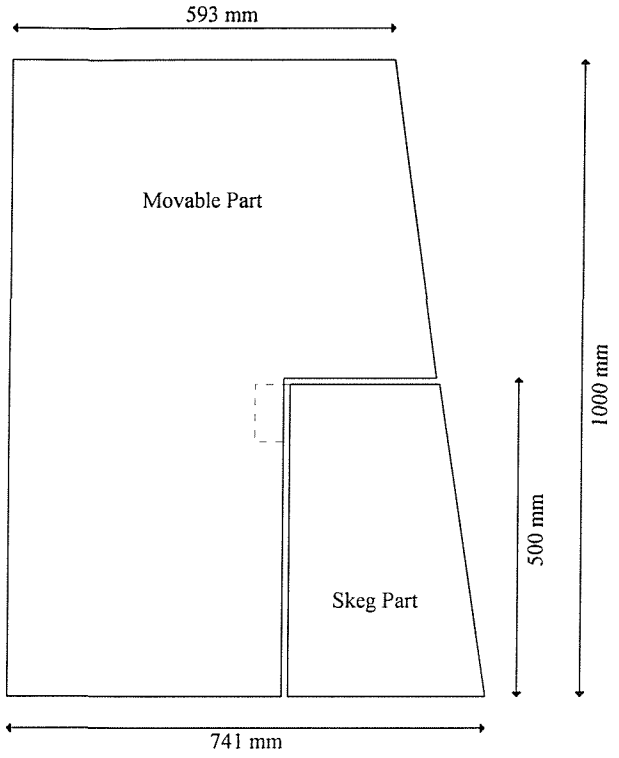

Figure 7.1 Representation of Skeg-rudder Geometry used in CFD Approach

Numerical definition of skeg-rudder geometry is problematic. The geometry is such that there are relatively small gaps between the skeg and the movable part of the rudder. This not only presents a problem in geometrical definition but also in the numerical modelling of the flow regime within and around the gap.

In general the definition of a rudder in the surface panel method developed by Turnock [27] requires rudder waterlines to be defined at various heights. This method is flexible enough to define a CFD rudder geometry from an initial set of coarse design parameters derived from the rudder performance prediction method detailed in Chapter 4. Once the tip chord, root chord, tip offset and respective thickness ratios are known a rudder can be

defined by scaling airfoil section offsets and placing them at the correct height and longitudinal offset. In this same way the skeg rudder geometry can be defined by three waterlines, namely at the root, the mid-span position and the tip.

The skeg part and movable part are not sealed on the top. This simplification is present to reduce the complication in geometry creation and the numerical solution. The direction of the flow is principally longitudinal so this has little effect on the forces, moments and pressure developed on the movable part.

Definition of a wake sheet to satisfy the Kutta condition detailed in Chapter 6 is also necessary to model the rudder performance correctly. The wake sheet is defined as a set of lines leading downstream from the trailing edge of the rudder at the surface definition waterlines.

Several different types of skeg-rudder geometrical definitions are used within the panel method to test the necessary complexity of the rudder geometry to obtain reliable results. The least complicated of the definitions do not include the gap between the skeg part and the all-movable part of the rudder. For full physical representation the most intricate models include the gap. A plan view of a section of the various rudder geometries (i) to (iv) can be seen in Figure 7.2 to 7.5 with a descriptions of the models to follow:

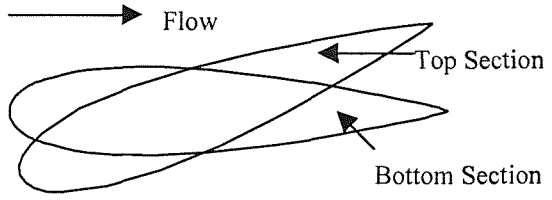

Figure 7.2 Plan View of Split Skeg-rudder Model

i) Split rudder: The rudder is split in two parts, top and bottom. The top part with no skeg in front is movable and the other part is completely fixed thus splitting the skeg horizontally. The movable part of the rudder not in way of the skeg is defined by a mid-span section and a tip section. The movable part of the rudder in way of the skeg is defined by a root and the mid-span section encompassing the skeg section as a continuous surface and not deflecting with rudder angle.

Figure 7.3 Plan View of Sealed Skeg-rudder Model

ii) Sealed rudder: Effectively a model with no gap between the skeg and the movable part. Thus representing no gap flow. All the bodies are lifting bodies and are represented with a wake sheet at the trailing edge. The movable part of the rudder not in way of the skeg is defined by a mid-span section and a tip section. The movable part of the rudder in way of the skeg is defined by a root and the mid-span section encompassing the skeg section as a continuous surface and the aft of the section, where the movable part is located, deflecting with rudder angle.

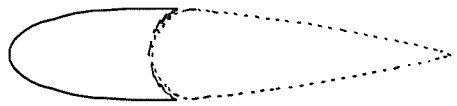

Figure 7.4 Plan View of Non-Lifting Skeg Model

iii) A non-lifting skeg: The gap is modelled in the geometry but there is no Kutta condition and thus no circulation represented on the skeg part of the rudder. The movable part of the rudder is a lifting body with a wake sheet off the trailing edge. The movable part of the rudder not in way of the skeg is defined by a mid-span section and a tip section. The movable part of the rudder in way of the skeg is defined by a root and the mid-span section. The skeg is defined by a root and mid-span section forward of the movable part.

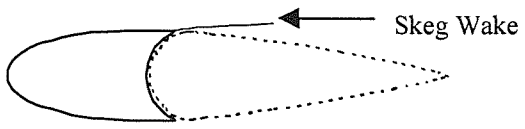

Figure 7.5 Plan View of Lifting Skeg Model

iv) A lifting skeg: Essentially the same geometry as the non-lifting skeg. The lifting skeg and lifting rudder are defined as two individual bodies. The skeg is one body with a wake sheet off the suction (separation) side of the skeg and the movable part of the skeg-rudder has a wake sheet extending downstream from the trailing edge.

The generation of these models included varying panel distributions in the chordwise and spanwise directions to obtain satisfactory definition for geometry and a flow solution. The most suitable for the movable part of the rudder is a sinusoidal distribution with a concentration of panels at the leading edge as found for the all-movable rudder [27]. The skeg-rudder panel distribution has varying panel division over the front and back sections.

In the skeg-rudder definitions (iii) and (iv), where the skeg part of the rudder is defined as an individual body, the geometry is defined by splitting the surface using two separate chordwise panel distributions. The front section has a sinusoidal distribution with a concentration at the leading edge as per the movable part. The back section of the skeg has a sinusoidal distribution with a concentration of panels at the two trailing edge corners of the skeg. This particular panel distribution was used due to the need for a higher panel density at the trailing edge as this is a region of high curvature and these panels are at an acute angle to the adjacent panels on the front section.

A representation of the panelled skeg-rudder geometry (iv) can be seen in perspective view in Figure 7.6. The figure is from the output of the Windows based surface panel method described in Chapter 6, with the rudder and skeg wakes highlighted and a view of the skeg part in isolation.

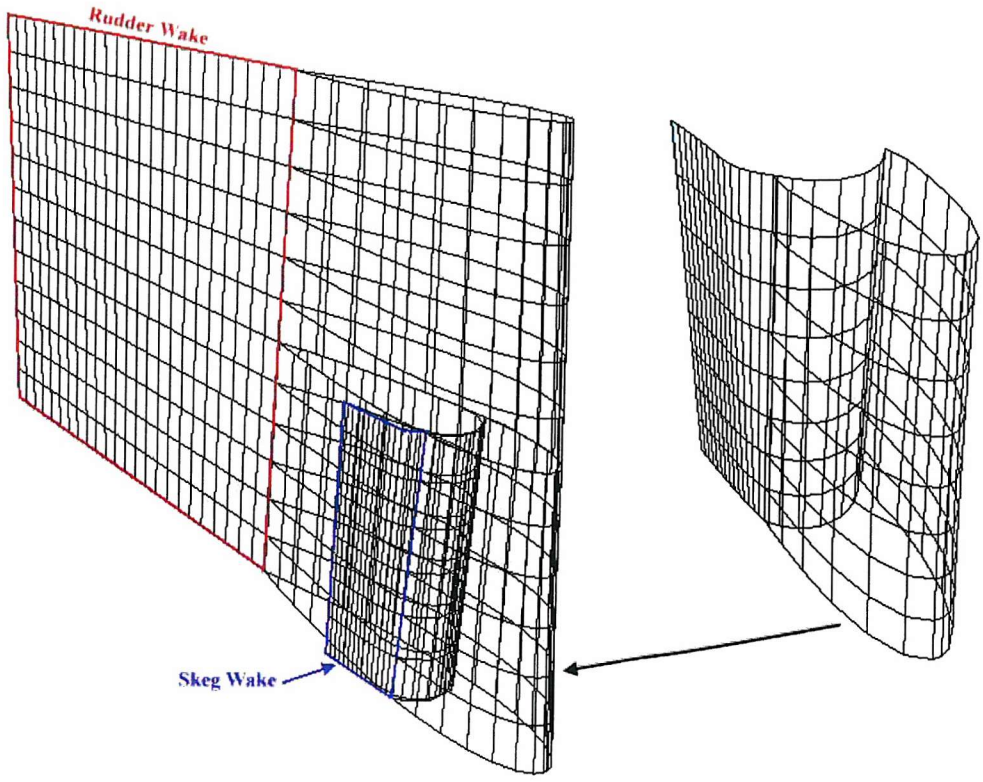

Figure 7.6 Panelled Skeg-rudder Geometry

7.3 Propeller Definition

The implementation of the propeller model is the same as described in Turnock [27] as this has proven successful in modelling the propeller flow onto an all-movable rudder. The propeller presented in this particular study has the same geometrical properties as the modified Wageningen B4.40 detailed in Chapter 3.

The whole four-blade propeller and boss geometry is rotationally symmetric. Therefore, only one blade and a quarter segment of the boss need be modelled. The overall geometry is split into two components, a non-lifting body (cylindrical boss) and lifting-surface (blade).

Definition of the modified Wageningen B4.40 blade used to NC machine the wind tunnel model propeller blade was also used to generate sections at different radii out along the propeller blade. These sections were then used to create the surface panel data. The use of the same base propeller data ensures an identical geometry between lifting-surface model and experiment. The trailing wake sheet is specified as lying on a helical surface following a given

pitch for each section. The panelled propeller geometry with the trailing wake sheet can be seen in perspective view in Figure 7.7.

The assumptions and methods used in creating the numerical propeller model, including wake adaption issues and free stream validation are presented in [27].

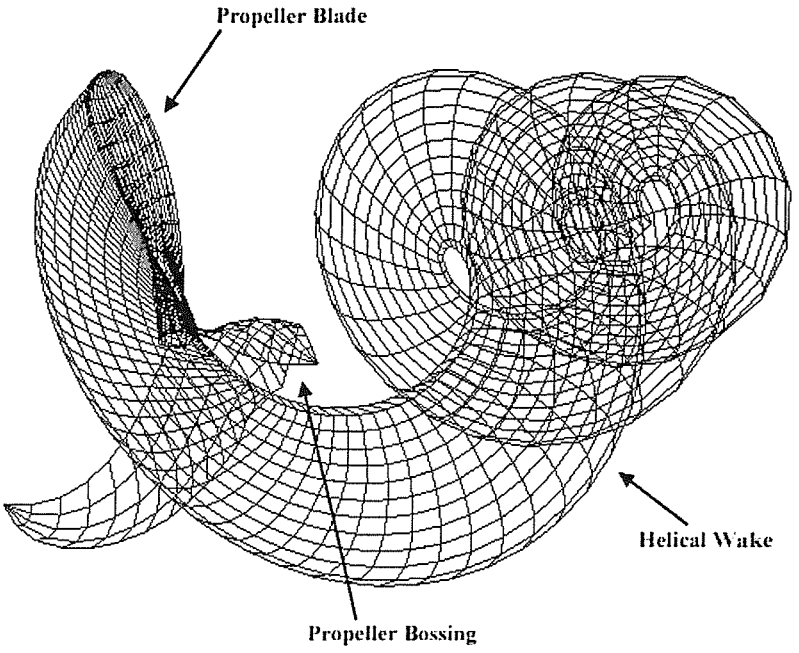

Figure 7.7 Panelled Propeller Geometry

7.4 Skeg-Rudder and Propeller Interaction

The method chosen to model the interaction is to separate the rudder and propeller and account for the interaction between them through the use of a modified inflow. This has been described in more detail in Chapter 6 and [27].

First the propeller geometry is loaded into the program and the panels generated. The propeller is solved first due to the stronger influence of the propeller on the rudder. The circumferential averaged velocity field at the rudder stock position is found and the rudder inflow velocity field modified accordingly. The rudder geometry is then loaded, panels generated, and the flow about it solved. A circumferentially averaged propeller inflow velocity field at the propeller plane is found and the whole cycle repeated until convergence, based on rudder forces, is deemed to have occurred. Relevant information is filed after each

flow solution and velocity field generation. This process is also described in Figure 6.2, Chapter 6. The program structure allows the flow to be solved for a series of rudder incidences.

The format of the geometry input file allowed the information defining both the rudder and propeller to be held in computer memory without the need to re-load from file for each iteration cycle.

7.5 Rudder Interaction Velocity Field

In cylindrical co-ordinates, the fluid velocity induced by the propeller has three components. A component due to the axial acceleration, a radial component, and a circumferential or swirl component. The magnitude of each of these components is dependent on the distance from the propeller plane of revolution, radial position and the angular position relative to the blade generator.

The wake sheet downstream of the propeller determines the local structure of the velocity field. The discontinuity of potential across the wake sheet gives rise to large differences in the magnitude of velocity tangential to the panel surface. Also, the presence of the wake edge can lead to large local velocities. The determination of the velocity field downstream of the propeller is carried out on a regularly spaced grid of points. These points are evenly spaced in the axial, radial, and circumferential directions. The spatial averaging of velocity at a given radius generates the time-averaged velocity for use as a rudder inflow velocity field. If an axially varying inflow field is to be used, this process is repeated at a regular axial spacing to give a series of time averaged velocities. At each axial station the rudder inflow velocity is the vector sum of the free-stream velocity and that due to the propeller interaction. The inflow velocity field uses this information to specify the cartesian components of velocity for a given spatial location.

The data defining the initial velocity field is included in the geometry input file. At subsequent iterations the velocity field calculation process modifies these. An inflow velocity defined at 20 radial stations with averaging over 30 points per radius was found to be acceptable [27].

7.6 Propeller Inflow Velocity Field

A spatially averaged velocity field at points in a cylindrical tube upstream of the rudder is obtained. This allows the average reduction in axial velocity passing through the propeller due to the rudder to be found. Also, spatially averaged swirl, and radial components can be found. The velocity field including the inflow velocity is generated on a cylindrical disk for inclusion in the geometry input file in an identical manner to that for the rudder. The velocity field at 10 radial points averaged over 20 points at 18^{o} increments was found to adequately define the propeller inflow [27].

7.7 Iteration and Convergence

The downstream position of the rudder means the propeller has a far greater influence on the rudder than the rudder has on the propeller. Therefore, the first stage in determining the interaction is to solve the flow around a free-stream propeller. The downstream velocity field of the propeller is then generated and applied to the rudder. On solution of the rudder flow the rudder upstream velocity field is obtained. This field is then applied to the propeller and the process is repeated until convergence has occurred.

A number of convergence criteria are possible. One of the principal applications of the work is for manoeuvring characteristics in which of prime interest is the rudder sideforce. Therefore, the convergence of total rudder lift was chosen. It was found that after three complete cycles the change in rudder sideforce was less than 0.1% and after 8 cycles less than 0.01%.

7.8 Free Stream Skeg-Rudder Results

Validation was first carried out with the skeg-rudder operating in the free stream. Once a satisfactory free stream model has been validated using the panel method it can then be modelled downstream of the propeller. The results for the free stream tests are presented in Figure 7.8.

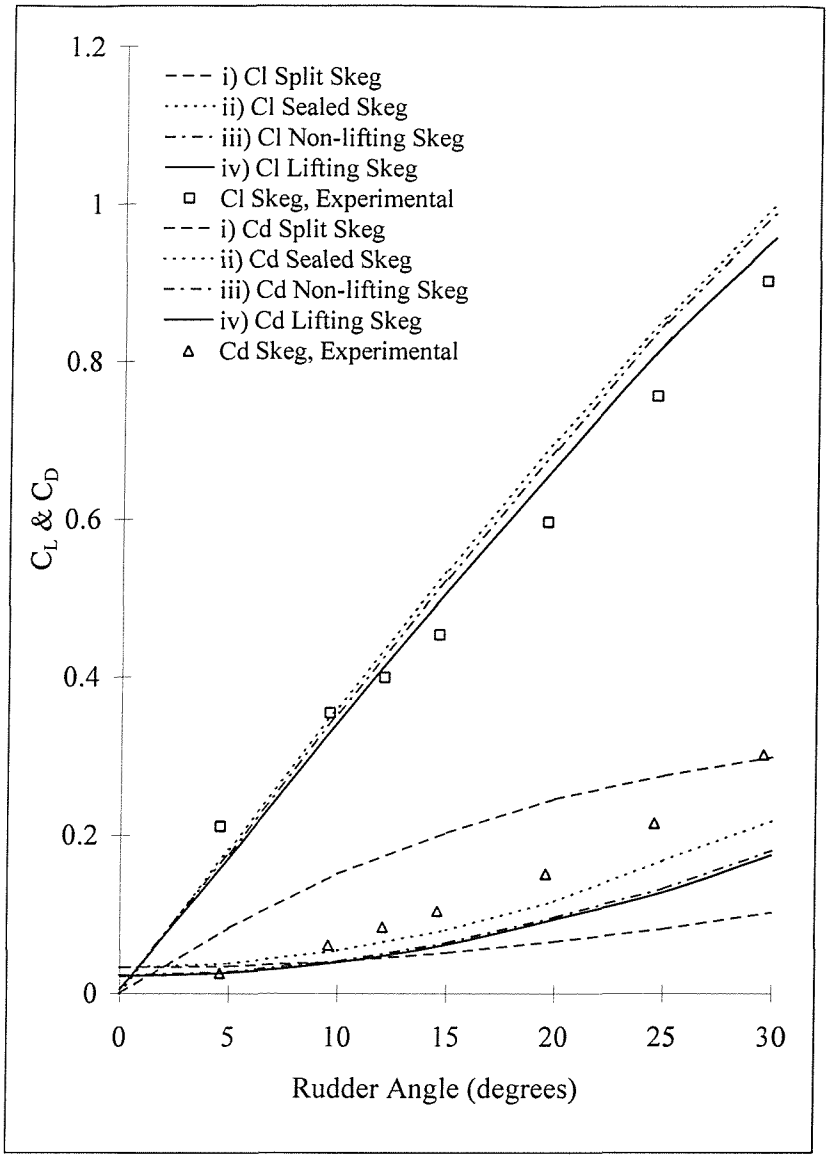

Figure 7.8 Comparison of Experimental and Theoretical Results for Free Stream Skeg-Rudder

The model that most represents the physics of the flow is the lifting skeg model. This is due to the fact that the sealed gap model does not represent any of the effects associated with the gap flow and the non-lifting skeg model cannot model any circulation around the skeg which is again necessary in modelling the nature of the gap flow. The split-skeg model is least successful and the forces are significantly lower than other models as the lower movable part is fixed at 0° incidence and is therefore producing no lift or induced drag. The lifting skeg model is to be used in modelling the skeg-rudder downstream of the propeller as the manoeuvring force or lift force results represents the closest match to free-stream experimental data.

The free stream lift results correlate well with experimental results. A panel method has a tendency to over predict lift [33] because of the neglect of modelling the boundary layer, this is evident in the results. The drop in lift at a rudder incidence of 10° associated with the gap flow and found in experimental work in [7] is not apparent with the any of the skeg-rudder CFD results. The effect is primarily due to separation of the flow induced be the initiation of significant flow through the gap and as the surface panel method does not predict separation it does not model this effect. The free stream drag results correlate well with experimental results. The composition of the drag results, base drag and induced drag, also correspond with experimental results.

7.9 Skeg-Rudder in Propeller Race

The test case considered in this calculation had no lateral separation (Y/D=0) The longitudinal separation (X/D) was 0.39 and the experimental test advance ratio (J) is 0.35 corresponding to a propeller speed of 2100 revolutions per minute and a free stream speed of 10m/s.

Figure 7.9 presents the force results for the rudder-propeller combination and Figure 7.10 presents the integration of chordwise pressure along the rudder span

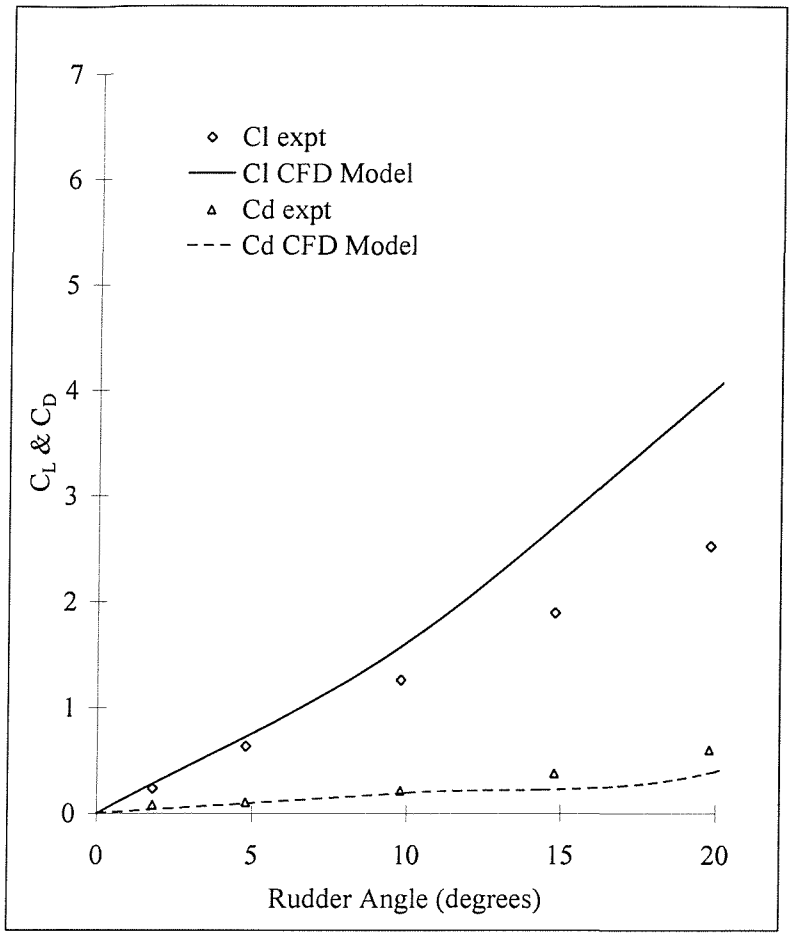

Figure 7.9 Experimental and Theoretical Forces for Skeg-Rudder and Propeller Combination.

The results with the propeller influence are higher than the free stream rudder as demonstrated in experiments. The results compared with the experimental results are generally good up to a rudder incidence of 10° and again showed the same trends in the prediction of lift and drag due to the panel method.

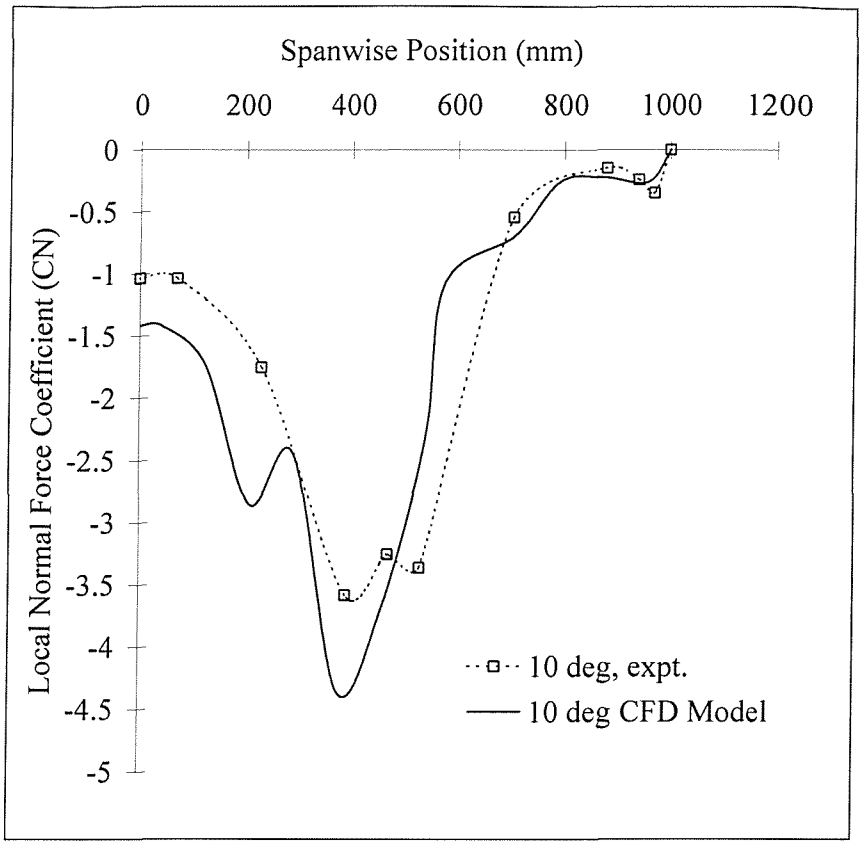

Figure 7.10 Experimental and Theoretical Distribution of Normal Force Coefficient for Skeg-Rudder and Propeller Combination.

Figure 7.10 shows that the general trend of calculated spanwise C_N is very similar to the experimental results with peaks occurring at similar spanwise positions. The CFD model has a higher total pressure at the root or at 0mm spanwise position. This is due to the boundary condition set at the reflection plane. The CFD method assumes a perfect reflection plane whereas the tests in the wind tunnel had a slight gap between the flow and rudder causing a loss of pressure due to cross-flow from the high pressure side to the low pressure side. In reality the reflection plane is not perfect and is often distorted as it is either the ships hull or the water surface.

The surface panel method tends to smooth out the effect of the skeg at a spanwise position of around 500mm. The load of pressure seen in the CFD results is more prominent than the experimental results, this shows the CFD method is not predicting the drop in lift across the gap fully. The presence of the protrusion of the skeg into the movable part has been removed from the numerical geometry and this is also at 500mm spanwise position, this will have an effect on the experimental results at that spanwise position.

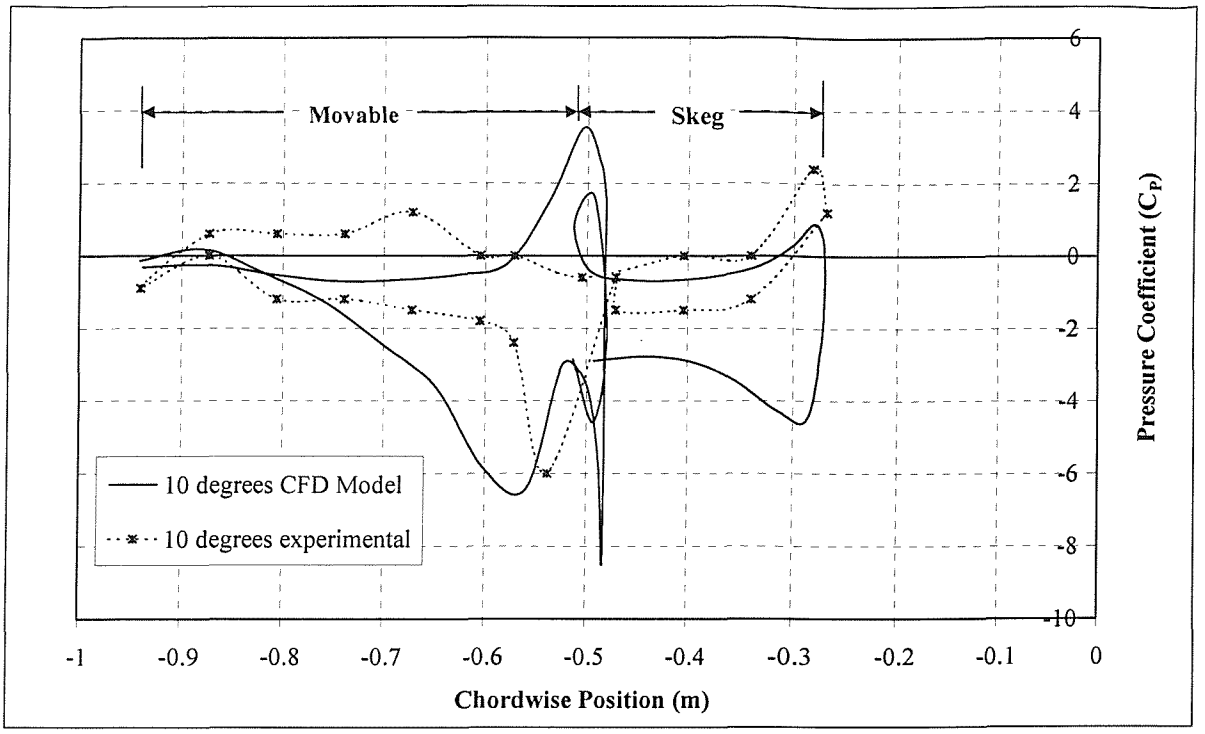

Figure 7.11 Experimental and Theoretical Chordwise Pressure Distribution for Skeg-Rudder and Propeller Combination at a Spanwise position of 0.3m from Rudder Root

Figure 7.11 shows the experimental and theoretical results of local pressure coefficient along the chord at a spanwise of position of 0.3m. The results are presented for a rudder angle of 10°. It can be seen that the CFD pressure results show the same trends as the experimental results but are generally larger in magnitude. The spanwise position is in way of the skeg part where there is a high influence from the close locality of the skeg and movable parts of the rudder, this influence has been over-predicted using the surface panel analysis and this is reflected in the results.

The limitations of the surface panel method in conjunction with the block Jacobian matrix solver are shown in this result where extremely high influences such as tight gap flows cannot be modelled completely as the velocities and hence pressures are too high with the absence of viscous effects.

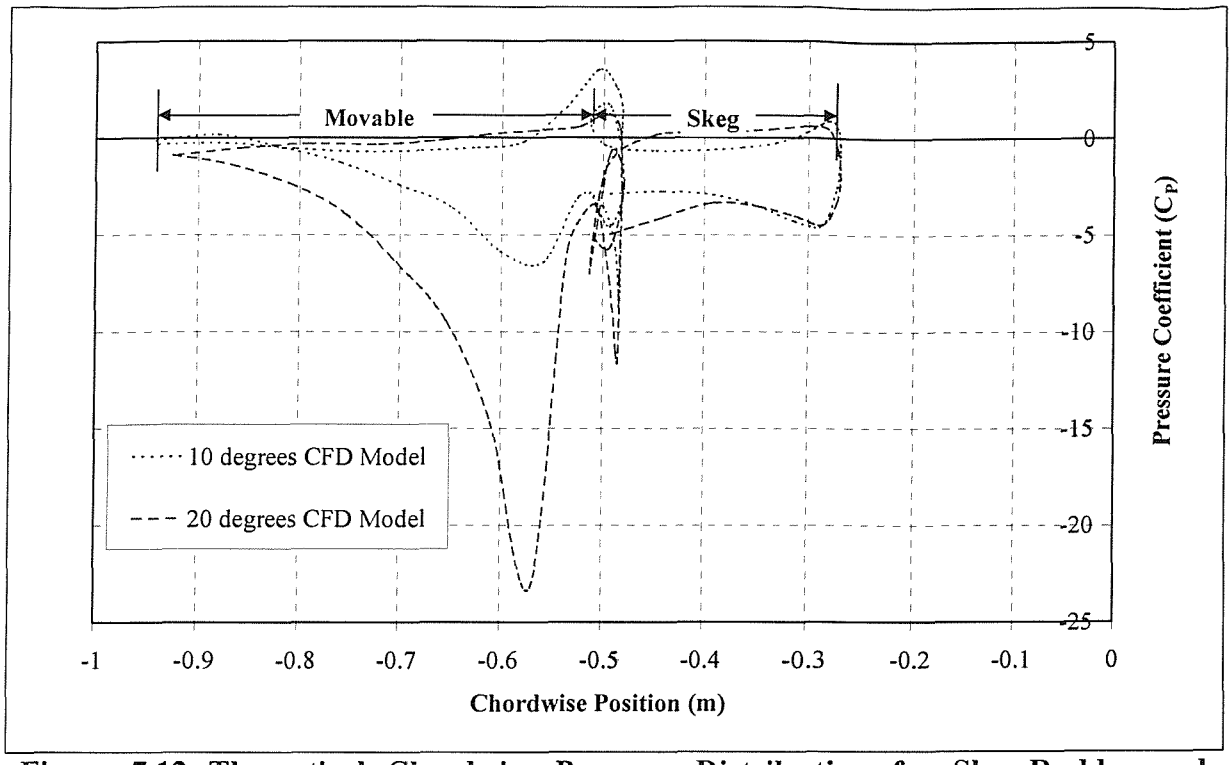

Figure 7.12 Theoretical Chordwise Pressure Distribution for Skeg-Rudder and Propeller Combination at a Spanwise position of 0.3m from Rudder Root

Figure 7.12 shows the predicted pressure distribution for 10° and 20°. The large peak of pressure at around –0.575m chordwise position for 20° is much higher than the 10° result and this is reflected in the lift results presented in Figure 7.9. As can be seen from Figure 7.10 at the same spanwise position of 390mm the results from the CFD method are higher, this suggests that the pressure is being over predicted in this region.

7.10 Summary and Recommendations

The skeg rudder in general has a more complex flow regime than an equivalent all-movable rudder and therefore presents a new problem to rudder performance prediction. The prediction of skeg-rudder forces and spanwise loading are comparable to experimental results but are not as accurate as the free stream results. The interaction method can be used to predict the performance of a skeg-rudder downstream of a propeller with relatively reliable accuracy up to 10°.

The free stream lift and drag results show good correlation with experimental results but the drop in lift curve slope at 10° is not apparent in the CFD results. To model the gap flow

effect a higher order CFD method to correctly account for viscous effects and separation is required. Wright in [31] has attempted to model an all-movable rudder downstream of a propeller using a higher order Reynolds Averaged Navier Stokes (RANS) method with limited success and the complications introduced by the introduction of a more complex skeg-rudder geometry into the model could further reduce the validity of results.

The lift, drag, spanwise C_N, and pressure results at a rudder incidence of 10° and downstream of the propeller show a reasonable correlation to the experimental results. The results at a higher rudder incidence tend to diverge from the experimental results. The difference in pressure from the CFD and experimental results around the skeg gap is causing the results to be higher especially at higher angles of attack. At over 10° of rudder incidence the lift curve detaches from the experimental results, this is due to the potential surface panel method not predicting the separation of the flow around the skeg gap and the method tends to accelerate the flow through the gap without viscous effects. The numerical solution of the flow showing peaks of pressure around the skeg gap area are also due to the close proximity of the skeg and rudder panels at higher angles of attack.

The investigation of skeg-rudder performance prediction using a surface panel method has been an exploratory exercise into the validity of using such a method. Various methods of modelling the skeg rudder geometry have been investigated. The model could be enhanced by several other additions to the geometry. The protrusion of the skeg into the movable part is problematic to model as a lifting body due to there being no clear trailing edge but the protrusion could be modelled using a non-lifting body with no wake and hence no kutta condition to satisfy. Figure 7.6 shows the top and bottom of the skeg part are not sealed this can be sealed by defining a non-lifting surface on the top and could enhance the modelling of the effect on the complex flow regime within the gap between the movable part and the skeg. The wake downstream of the propeller is defined for an open water propeller but in reality the wake will be deflected by the presence of the rudder particularly at higher angles of attack. The consideration of this effect could be implemented by having a diverting wake, although this could prove problematic in predicting the diverted shape of the wake and in obtaining a numerical solution.

There are several ways in which the numerical solution and hence the accuracy of the CFD results could be enhanced for the skeg-rudder-performance prediction. The Jacobian block

iterative matrix solver described in [27] and implemented in the surface panel method relies on a leading diagonal of matrix values to solve a set of linear equations for the flow solution. These matrix values are related to the influence coefficient described in Chapter 6. Because of the high influence of panels in the skeg gap area there are higher values outside the leading diagonal. The Jacobian matrix solver is not as robust with values outside this area and it may therefore be necessary to find a more suitable matrix solver or a method of conditioning the matrix for a particular solver.

The CFD method used in modelling the skeg-rudder performance can provide results for total forces and moments. The generated data can be incorporated into the rudder performance prediction method for extending the range of available data for further interpolation and extrapolation. In this way the design spiral can be continuous until a suitable solution for a rudder design has been found.

The distribution of the load is indicated along the span for a rudder with a thrusting propeller upstream, this provides important detailed information for designing rudder scantlings. Once a particular geometry has been modelled and validated, further investigation into lateral, longitudinal and vertical separation can be implemented with ease as can the introduction of a hull into the model to complete the interaction group. These type of parametric variations can be expensive and cumbersome using tests but can easily and economically be implemented using the surface panel method. This type of calculation is a natural progression in the design spiral from the rudder performance prediction method. Total rudder-propeller manoeuvring forces can be calculated using the rudder performance prediction method and once a suitable set of coarse design parameters have been decided upon, detailed information can be calculated for structural considerations.

8 CONCLUSIONS

8.1 Introduction

The principal factors in rudder-propeller interaction have been assessed and using a design spiral philosophy, methods have been developed and employed to predict rudder performance downstream of a propeller. The result of this work has been the development of a proven methodology which accounts for the physical basis of the interaction between the rudder and propeller of a ship. By way of example, applications of the performance prediction methods have been demonstrated.

Individual conclusions and recommendations from the work are presented with overall conclusions presented at the end of this chapter.

8.2 Rudder-Propeller Interaction Mechanism

The rudder-propeller interaction mechanism and the principal factors that affect rudder performance downstream of a propeller have been identified. The geometric definition of the rudder and propeller, their operating condition and their relative positions has a significant influence on the performance of the rudder.

To predict the performance of manoeuvring devices there must be a coherent harnessing of all the available methods. The methods must therefore be coherent in their form of presentation and have some cross validation such that, for example, the experimental results match a CFD method and these both are consistent with other fundamental theoretical methods. A coherent presentation system has been described and used throughout the work to present, examine and compare rudder performance.

In identifying the main geometric and flow variables that affect rudder performance and the current experimental work to date, the parametric variation in experimentation can be established. The skeg rudder has been identified as a more widely used rudder type and requires more information to establish its performance downstream of a propeller. The bollard pull condition data has been identified as a potential way of obtaining information on rudder performance downstream of a propeller.

8.3 Experimental Tests of Rudder-Propeller Interaction

Parametric studies supply data and understanding of the rudder-propeller interaction mechanism. By investigating rudder and propeller interaction with the particular case of a skeg-rudder, the physical influences of the interaction with the propeller have been examined and discussed.

Skeg-rudder performance has been presented at a range of propeller thrust loading for J=0, 0.17, 0.35, 0.51, 0.94 and at free-stream. A range of relative rudder-propeller separation has been investigated; X/D from 0.39 to 0.52 and Y/D from –0.375 to 0.375. The influence of the wide range of parametric variations has been discussed.

Open laboratory tests in the bollard pull condition (J=0) have been used as a novel and innovative approach to rudder testing. The experimental results from the parametric variations exhibited the same trends as those at higher ship speeds and therefore these types of tests can be used to determine the rudder-propeller interaction mechanism for many geometric configurations. Experimental cost can be greatly reduced using the open laboratory method and as open laboratory space is generally more available than a wind tunnel, this method can allow for future in-depth parametric studies of rudder-propeller interaction.

8.4 Rudder Performance Prediction Method and Design Investigations

The systematic variation in the experimental work has produced validation data and a database for interpolation and extrapolation. From an understanding of the behaviour of a rudder in a free stream, the influence of a propeller and its associated thrust loading has been quantified in a method that can be used to predict rudder forces and moments for varying rudder shape and position. These forces and moments are critical in the rudder design itself and also in predicting the likely effect on the manoeuvring performance and the consequential steering gear torque for a particular stern arrangement of a ship. The use of the approach provides ship designers with a much clearer and an interactive understanding of the implications of rudder-propeller design choices.

The rudder performance prediction method in the form of a software program provides a transparent interface to the theoretical formulation and computational database. The use of

object orientated programming techniques have allowed efficient implementation of the defined parametric variables and processes.

The rudder performance prediction method is flexible in the way computational data can be incorporated into the program. Data from experimental work, CFD, trials and any other theoretical predictions or measurements can be incorporated easily into the program thus producing a seamless fusion of data for the process of calculating the effect of an upstream propeller on rudder performance.

Results from the rudder performance prediction method can be incorporated into a manoeuvring simulation for accurate prediction of ship rudder-propeller interaction effects. Specific rudder data for a wide range of conditions can be used for interpolation of the rudder performance at a particular operating point of a ship. The accurate prediction of rudder manoeuvring force through the use of data derived from experimental tests and physically based corrections gives the designer confidence.

The use of the rudder performance prediction method has been enhanced by its ability to predict rudder forces with a propeller upstream at a particular ship speed and propeller thrust loading from solely free stream performance (e.g. 2D sectional lift curve slope) and bollard pull data. This is an important assumption, by splitting the rudder into two distinct parts, one controlled by the propeller, the other by the free stream, the rudder forces downstream of a propeller at any advance ratio can be predicted. Using purely bollard pull data and free stream data takes this assumption to the extreme and the method still provides accurate workable results up to an advance ratio of J=0.51. The calculation of the propeller scaling parameter K_P could be enhanced for more accurate results at higher advance ratios and it is recommended that this can be investigated in greater detail.

The methods presented in this thesis are strengthened by example. Worked design investigations provide completeness and confidence in the processes used. The consequences of design choices have been quantified and suggestions of further design options discussed and shown. The ability to analyse and predict the effect of rudder types, off design conditions and rudder-propeller relative positions are crucial in the design of the stern arrangement of a ship. To be able to vary geometry and the locality of a rudder-propeller system and predict the combined performance is an important capability.

Everyday questions asked by rudder designers can be answered quickly by using the rudder performance prediction method.

8.5 Surface Panel Analysis of Skeg-Rudder Performance

Computational fluid dynamics in the form of a surface panel method has been used as a tool to enhance the rudder design analysis. The use of CFD has not only provided a mechanism for analysis but also an understanding of the numerical methods used and their possibilities and limitations.

The surface panel method has been identified as a suitable computational tool for obtaining detailed information on the distribution of pressure and hence loading on a rudder operating downstream of a propeller. The interaction velocity field method has also been recognised to have a powerful application in this type of complex flow analysis. The joint application of these methods has been successful in modelling an all-movable rudder downstream and the work presented in this thesis has applied the process to calculate the flow over a skeg-rudder downstream of a propeller.

Visualisation tools allow interactive understanding and validation when creating a CFD model and analysing the results. Large amounts of information can be inspected qualitatively and quantitatively. The visualisation tools created for use with the surface panel method allow grid quality and solution quality to be assessed prior to calculation and have proved to be valuable during geometric definition and solution analysis.

Computational flow analysis of the skeg-rudder in the free-stream has provided comparable results of lift and drag with experimental work using a lifting skeg model up to a rudder incidence of 30°. The prediction downstream of a propeller has provided comparable results for lift, drag and spanwise loading up to a rudder incidence of 10° and has shown that there are uncertainties creating a numerical model of this complexity using the surface panel method for rudder angles greater than 10°. The complex flow regime between the skeg-part and the movable part of the rudder has not been predicted accurately. It is a recommendation that this phenomenon can be investigated further using computational fluid dynamics and if necessary a higher order method be used to account for viscous effects and flow separation.

The spanwise loading and pressure distributions from the computational fluid dynamics has given comparable results up to 10° of rudder incidence and this information can be used to conduct in-depth analysis for designing rudder scantlings and in optimising the performance of the rudder for manoeuvring. The data obtained from the computational skeg-rudder analysis can be used in the rudder-design method to give further sets of parametric data.

8.6 General Summary and Recommendations

The rudder performance prediction method has proved that meaningful data can be obtained from a reduced set of systematic parametric variation. When a designer generates a requirement for a rudder-propeller system and identifies a coarse set of design parameters that may satisfy the requirement they need an analysis tool that can predict performance from the initial set of parameters. Data from detailed parametric studies can be used to satisfy this need, but there must be an accessible way of managing and using the data with methods available to allow for variance in the geometry and flow condition from the base parametric data. The rudder performance prediction method provides an analysis tool with the flexibility to allow the designer to adjust rapidly the design parameters and get information on the performance of a rudder downstream of a propeller from any set of parametric rudder performance data.

Once a general analysis of rudder-propeller performance has been complete and the performance satisfies the initial set of designers requirements a method is needed that can accept specific detailed design parameters. The method must assess the performance in higher resolution to give information on the distribution of loading for in-depth design specification. The CFD method has been identified and used as an enhanced method to obtain these results.

If the initial requirements or specification set out by the designer change due to the results from the detailed analysis the designer can repeat the process with ease and iterate to a satisfactory solution. This iterative process is based on a design spiral principle and the work presented in this thesis adopts that philosophy. The designer can use the information obtained from the more detailed surface panel analysis and incorporate it into the rudder

performance prediction method, this can tighten the design spiral and reduce the number of iterations needed to obtain a satisfactory solution.

An important finding of the work presented in this thesis has been the prediction of the performance of a rudder downstream of a propeller at advance ratios greater than zero can be produced from the combination of just free stream and bollard pull data. This is a new and innovative method and has a large consequence on rudder-propeller testing. It is a recommendation that this method can be investigated further as it can be of considerable economic benefit.

The use of the data and methods described in this thesis can supply a designer with enhanced analysis techniques to create a more efficient stern arrangement for a ship. The methodical route taken from experimental work, analytical interpretation of experimental data and theoretical investigation has supplied a better understanding of the rudder-propeller interaction mechanism and has provided enhanced design performance prediction methods for rudders operating downstream of a propeller.

REFERENCES

[1] Inoue, S., Hirano, M., Kajima, K. and Takashina, J. 'A practical calculation method of ship manoeuvring motion', International Shipbuilding Progress, Vol. 25, No. 325, Sept 1981.

[2] Ogawa, A. and Kasai, H., 'On the mathematical model of manoeuvring motion of ships', International Shipbuilding Progress, Vol. 25, No. 292, 1978.

[3] Molland,. A.F., Turnock, S.R. and Wilson, P.A. 'Performance of an enhanced rudder force prediction model in a ship manoeuvring simulator' International Conference on Marine Simulation and Ship Manoeuvrability (MARSIM), Copenhagen, Denmark, September 1996, pp. 425-434.

[4] Kajima, K. and Yoshitaka, F. 'Effect of roll motion on manoeuvrability of ship' International Symposium and Workshop on Force Acting on a Manoeuvring Vessel, Val de Reuil, France, September 1998.

[5] Kerwin, J.E., Mandel, P, and Lewis, S. 'An experimental study of a series of flapped rudders', Journal of Ship Research, December 1972, pp. 221-239.

[6] English, J.W. and Bain, D.C., 'Some manoeuvring devices for use at zero and low ship speed', Transactions NECEIS, Vol. 88 1971/1972, pp. 31-50.

[7] Molland A.F. 'The free stream characteristics of a semi-balanced ship skeg-rudder', Ship Science Report No. 3/77, University of Southampton, 1977.

[8] Whicker L.F. and Fehlner L.F. 'Free stream characteristics of a family of low aspect ratio control surfaces for application to ship design'. D.T.M.B. Report 933, December 1958.

[9] 'Hydrodynamics of control surfaces', Section 14, Principles of Naval Architecture, second revision, Volume III, 'Motions in Waves and Controllability' edited by Lewis, E.V, The Society of Naval Architects and Marine Engineers, 1989, pp. 291-316.

[10] 'Interaction between hull and propeller', Section 4, Principles of Naval Architecture, second revision, Volume II, 'Resistance, Propulsion and Vibration' edited by Lewis, E.V, The Society of Naval Architects and Marine Engineers, 1988, pp. 145-153.

[11] Stierman, E.J. 'The Influence of the Rudder on the Propulsive Performance of Ships Part I', International Shipbuilding Progress, Vol. 36, No 407, 1989, pp. 303-334.

[12] Stierman, E.J. ' The Influence of the Rudder on the Propulsive Performance of Ships Part II', International Shipbuilding Progress, Vol. 36, No 408, 1989, pp. 405-435.

[13] Molland A.F., & Turnock, S.R., 'The prediction of ship rudder performance characteristics in the presence of a propeller' International Symposium on Manoeuvring and Control of Marine Craft (MCMC), University of Southampton, 1992

[14] Kracht, A.M. 'Rudder in the slipstream of a propeller', ISRP International Symposium on Ship Resistance, Shanghai, China, April 1989, pp. 66-71.

[15] Molland, A.F. and Turnock, S.R. 'Wind tunnel investigation of the influence of propeller loading on ship rudder performance', Ship Science Report No. 46, University of Southampton, 1991.

[16] Molland, A.F. and Turnock, S.R., 'Wind tunnel investigation of the influence of propeller loading on a semi-balanced skeg-rudder', Ship Science Report No. 48, University of Southampton, 1993.

[17] Molland, A.F. and Turnock, S.R. 'Further wind tunnel tests on the influence of propeller loading on ship rudder performance', Ship Science Report No. 52, University of Southampton, 1992

[18] English, J.W., and Bain, D.C., 'Some manoeuvring devices for use at zero and low ship speed', Trans. NECEIS, Vol. 88, 1971/72.

[19] Robinson J., 'Performance prediction of chine and round bilge hull forms.'. International Conference on the Hydrodynamics of High Speed Craft, Royal Institution of Naval Architects (RINA), London, November 1999.

[20] Keuning, J.A. and Sonnenberg U.B. 'Developments in the velocity prediction based on the Delft systematic yacht hull series', International Conference on the Modern Yacht, Royal Institution of Naval Architects, Portsmouth, March 1998.

[21] Molland, A.F. and Turnock, S.R. 'Preliminary wind tunnel investigation of the influence of propeller loading on a ship rudder in the bollard (J=0) condition', Ship Science Report No. 49, University of Southampton, 1993.

[22] Molland, A.F. and Turnock, S.R., 'Prediction of ship rudder-propeller interaction at low speeds and in four quadrants of operation', International Symposium on Manoeuvring and Control of Marine Craft (MCMC), 1994.

[23] Smithwick, J.E.T., Molland, A.F. and Turnock, S.R. ,'Design studies of the manoeuvring performance of rudder-propeller systems', Seventh International Symposium on Practical Design of Ships and Mobile Units, (PRADS), The Hague, September, 1998

[24] 'Final report and recommendations of The Manoeuvrability Committee' The 20th ITTC International Towing Tank Conference, Proceedings Volume 1, San Francisco, California September, 1993, pp.309-1361.

[25] Molland A.F., ' Rudder Design Data for Small Craft', Ship Science Report No. 1/78, University of Southampton, 1978

[26] Molland A.F., 'The prediction of rudder-propeller interactions using blade element momentum and modified lifting line theory', Ship Science Report No. 54, University of Southampton, 1992.

[27] Turnock, S.R., 'Prediction of ship rudder-propeller interaction using parallel computations and wind tunnel measurements', PhD. Thesis, Department of Ship Science, University of Southampton, 1993.

[28] 'Final report and recommendations of The Manoeuvrability Committee' The 22nd ITTC International Towing Tank Conference, Proceedings Volume 1, Seoul, Korea & Shaghai, China, September 1999, pp71-118.

[29] Rosen, B.S. and Laiosa, J.P. 'SPLASH, non-linear and unsteady free-surface analysis code for grand prix yacht design' The Thirteenth Chesapeake Sailing Yacht Symposium, Society of Naval Architects and Marine Engineers (SNAME), January 1997. pp. 211-225.

[30] Caponnetto, M., Casstelli, A., Dupont, P., Bonjour, B., Mathey, P., Sanchi, S.,and Sawley, M.L. 'Sailing yacht design using advanced numerical flow techniques', the Fourteenth Chesapeake Sailing Yacht Symposium, SNAME, January 1999, pp. 97-104.

[31] Wright, A., 'Integrated computational fluid-structural modelling of a rudder', M.Sc. Thesis, Department of Ship Science, University of Southampton, 1996.

[32] Turnock, S.R. 'Interpretation of CFD results for use in ship hydrodynamic design', The International CFD Conference, Ulsteinvik, Norway, June 1999.

[33] Katz, J and Plotkin, A. 'Low-speed aerodynamics – from wing theory to panel methods', McGraw-Hill, Inc. 1991.

[34] Willis, C.J., Crapper, G.D. and Millward, A. 'A numerical study of the hydrodynamic forces developed by a marine rudder.' Journal of Ship Research, Vol 38. No. 3, September 1994, pp. 182-192.

[35] Su, Y, Ikehata, M and Kai, H 'Design of three-dimensional hydrofoils by surface panel method', Proceedings of the Third Osaka Colloquium on Advanced CFD Application to Ship Flow and Hull Form Design, Osaka Prefecture University, May 1998, pp. 275-295.

[36] Smithwick, J.E.T and Turnock, S.R., 'Practical analysis of the hydrodynamic performance of the Reflex 28 keel and rudder', International Conference on the Modern Yacht, Royal Institution of Naval Architects (RINA), Portsmouth, March 1998.

[37] Smithwick, J.E.T, 'An investigation into the hydrodynamic forces and interaction of the hull and keel of a yacht using a parallel lifting surface panel method.', Part III Honours Report, Department of Ship Science, University of Southampton, May 1993.

[38] Turnock, S.R. 'A test rig for the investigation of propeller/rudder interactions', Ship Science Report No. 45, University of Southampton, 1990.

[39] Turnock S.R. 'Computer aided design and numerically controlled manufacture of a split mould for a composite model ship propeller', Ship Science Report No. 42, University of Southampton, , 1990.

[40] Molland, A.F. and Turnock S.R. 'The design and construction of propeller blades in composite materials for a wind tunnel model', Ship Science Report No. 41, University of Southampton, 1990.

[41] Molland, A.F. 'The design, construction and calibration of a five-component strain gauge wind tunnel dynamometer', Ship Science Report 1/77, University of Southampton, 1976.

[42] Molland, A.F. and Turnock, S.R. 'The design, construction and calibration of a thrust and torque dynamometer for a wind tunnel propeller model', Ship Science Report No. 44, University of Southampton, 1990.

[43] Molland, A.F. and Turnock, S.R. 'Wind tunnel tests on the effect of a ship hull on rudder performance at different angles of drift', Ship Science Report No. 76, University of Southampton, 1995.

[44] Russo, V.L. and Sullivan E.K., 'Design of the mariner-type ship' Society of Naval Architects and Marine Engineers (SNAME) Transactions, Vol. 61 1953.

[45] Molland, A.F. and Turnock, S.R. 'Wind tunnel tests on the influence of propeller loading on ship rudder performance: Four quadrant, low and zero speed operation.' Ship Science Report No. 64, University of Southampton, 1993

[46] Smithwick J.E.T, Molland, A.F. and Turnock, S.R., 'Wind tunnel tests on the influence of propeller loading and the effect of a ship hull on skeg-rudder performance', Ship Science Report No. 90, University of Southampton, July 1995.

[47] Smithwick J.E.T, Molland, A.F. and Turnock, S.R., 'Investigations of the influence of propeller loading on a ship in the bollard (J=0) condition', Ship Science Report No. 94, University of Southampton, February 1994.

[48] Molland A.F., Wellicome J.F., and Turnock S.R., 'Interaction velocity field method for predicting ship rudder-propeller interaction', Society of Naval Architects and Marine Engineers (SNAME) Propellers/Shafting Symposium, No. 18, September 1994.

[49] Abbot, I.H. and Von Doenhoff, A.E. 'Theory of Wing Sections', Dover Publications Inc, 1958.

[50] Hess. J.L., 'Panel methods in computational fluid dynamics', Annual Review of Fluid Mechanics, Vol 22, 1990, pp. 225-274.

[51] Lamb, H, 'Hydrodynamics', Cambridge University Press, sixth edition, 1932.

[52] Hess, J.L. 'The problem of three-dimensional lifting flow and its solution by means of a surface singularity distribution', Computational Methods Applied Mechanical Engineering, 4:283-319 also Rep MDC-J5679, McDonnell Douglas Aircraft Co. Long Beach, California, 1972.

[53] Lee, J-T, 'A potential based method for the analysis of marine propellers in steady flow', Ph.D. thesis, M.I.T. Dept of Ocean Engineering, August 1987.

[54] Morino, L., and Kuo, C-C, 'Subsonic potential aerodynamics for complex configurations: A general theory', A.I.A.A. Journal, Vol 12. No. 2 February 1974.

[55] Kerwin, J.E., Kinnas, S.A., Lee, J-T, Shih, W-Z, ' A surface panel method for the hydrodynamic analysis of ducted propellers', Society of Naval Architects and Marine Engineers (SNAME) Transactions, Vol. 95, 1987.

[56] Newman, J.N., 'Distribution of sources and normal dipoles over a quadrilateral panel', Journal of Engineering Mathematics, Vol 20, pp. 113-126, 1986.

[57] Hess, J.L. and Smith, A.M.O., 'Calculation of non-lifting potential flow around arbitrary three dimensional bodies', Journal of Ship Research, Vol. 8, No. 2, Sept. 1964,.

[58] Maitre, T.A., and Rowe, A.R., 'Modelling of flow around a propeller using a potential based method', Journal of Ship Research, Vol 35., No. 2, June 1991, pp.114-126.

[59] Turnock, S.R., 'Technical manual and user guide for the surface panel code: PALISUPAN', Ship Science Report No. 100, University of Southampton, October 1997.

[60] Molland, A.F. and Turnock, S.R., 'Developments in modelling ship rudder-propeller interaction', CADMO 1994.

[61] Molland, A.F. and Turnock, S.R., 'Some effects of rudder-propeller-hull arrangements on manoeuvring and propulsion', The Sixth International Symposium on Practical Design of Ships and Mobile Units (PRADS), 17-22 September 1995.

[62] Molland, A.F. and Turnock, S.R., 'Wind tunnel investigation of the influence of propeller loading on ship rudder performance', Transactions of The Royal Institution of Naval Architects (RINA), Vol 135, 1993.

[63] Bell, G., Parisi, A. and Pesce, M. 'The virtual reality modelling language version 1.0 specification', World Wide Web Address: www.virtpark.com/theme/vrml/, (first visited February 98)

[64] Brain, M., Lovette, L., 'Visual C++ 2, Developing professional applications in Windows 95 and NT using MFC', Prentice-Hall P.T.R., 1995

[65] Silicon Graphics, 'OpenGL.org' World Wide Web Address: www.opengl.org, (first visited December 1997).

APPENDIX A - PLOTS OF RESULTS FROM WIND TUNNEL TESTS

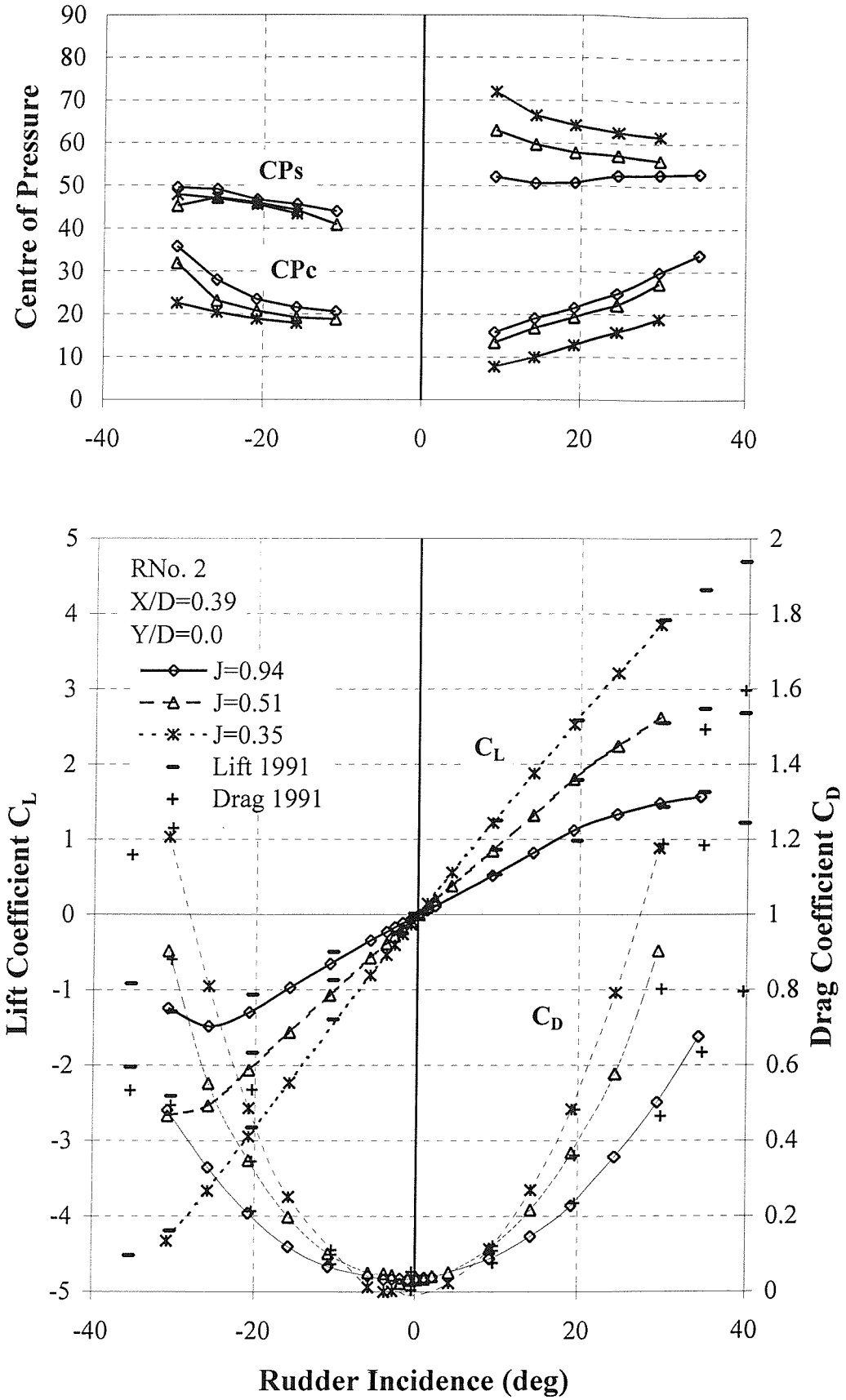

Figure A-1 Influence of Propeller Thrust Loading on the Performance of Rudder No. 2

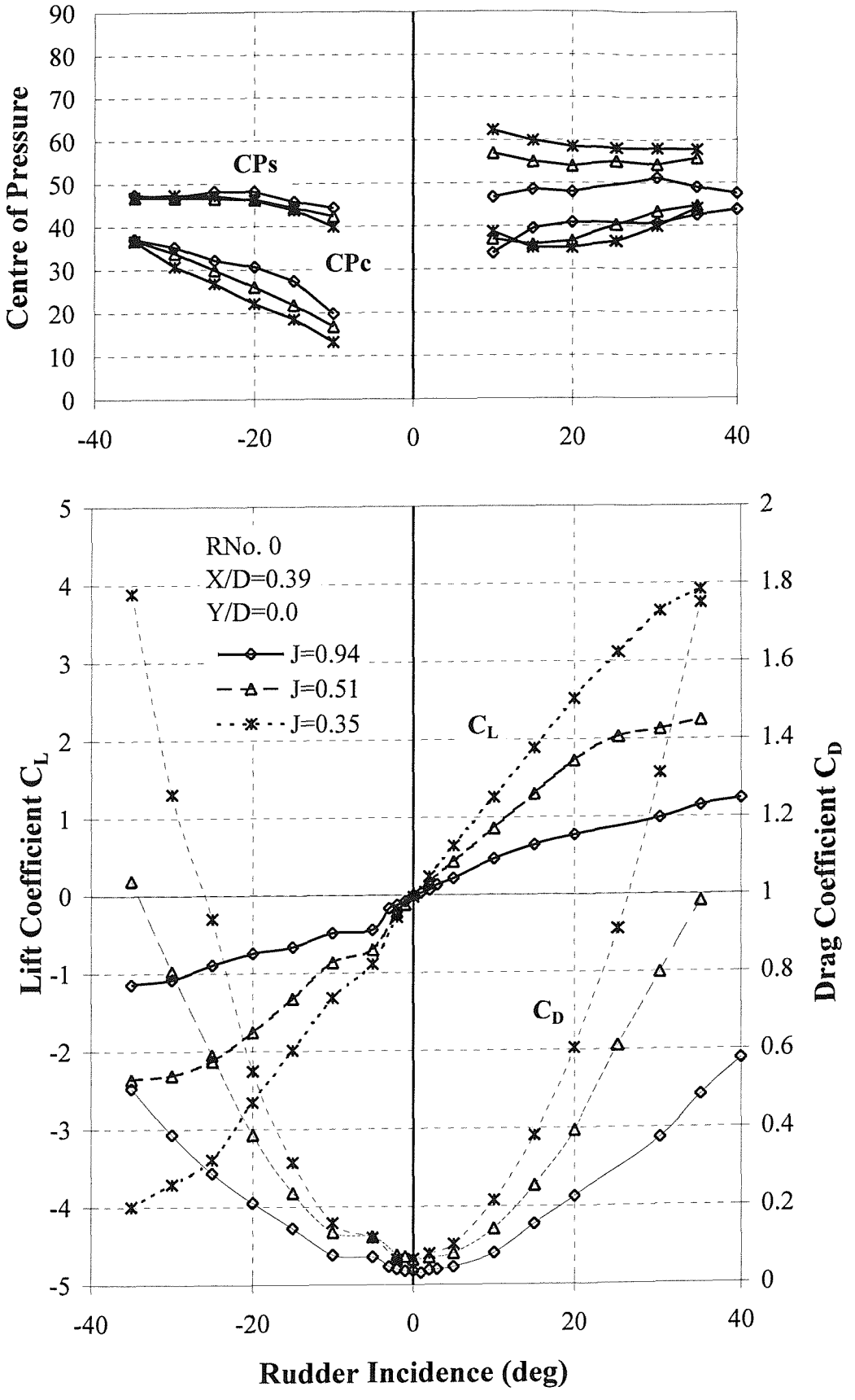

Figure A-2 **Influence of Propeller Thrust Loading on the Performance of Skeg-Rudder No. 0 (rudder plus skeg forces)**

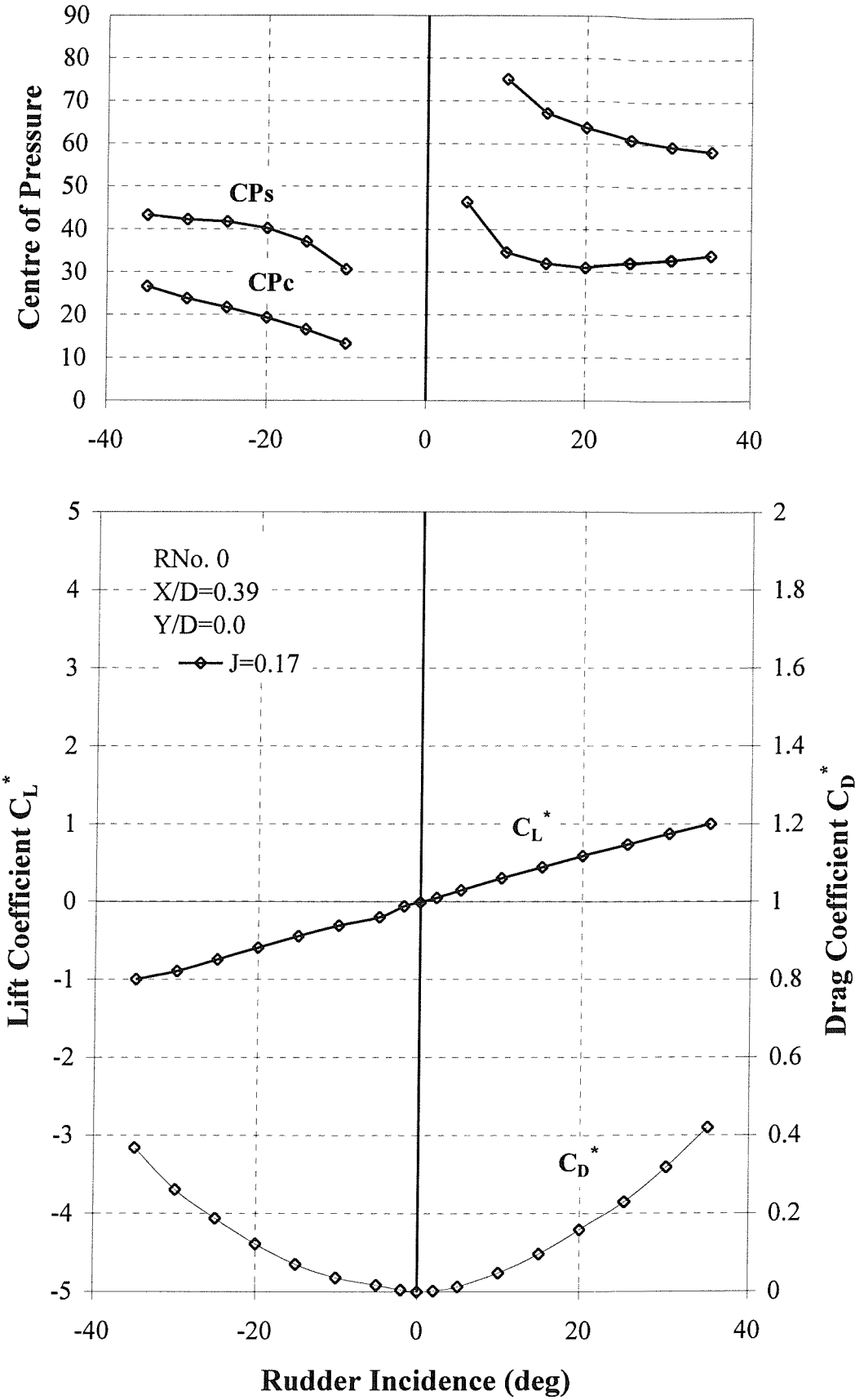

Fig. A-3 **Skeg-Rudder No. 0 Performance at a Propeller Advance Ratio of J=0.17 (rudder plus skeg forces)**

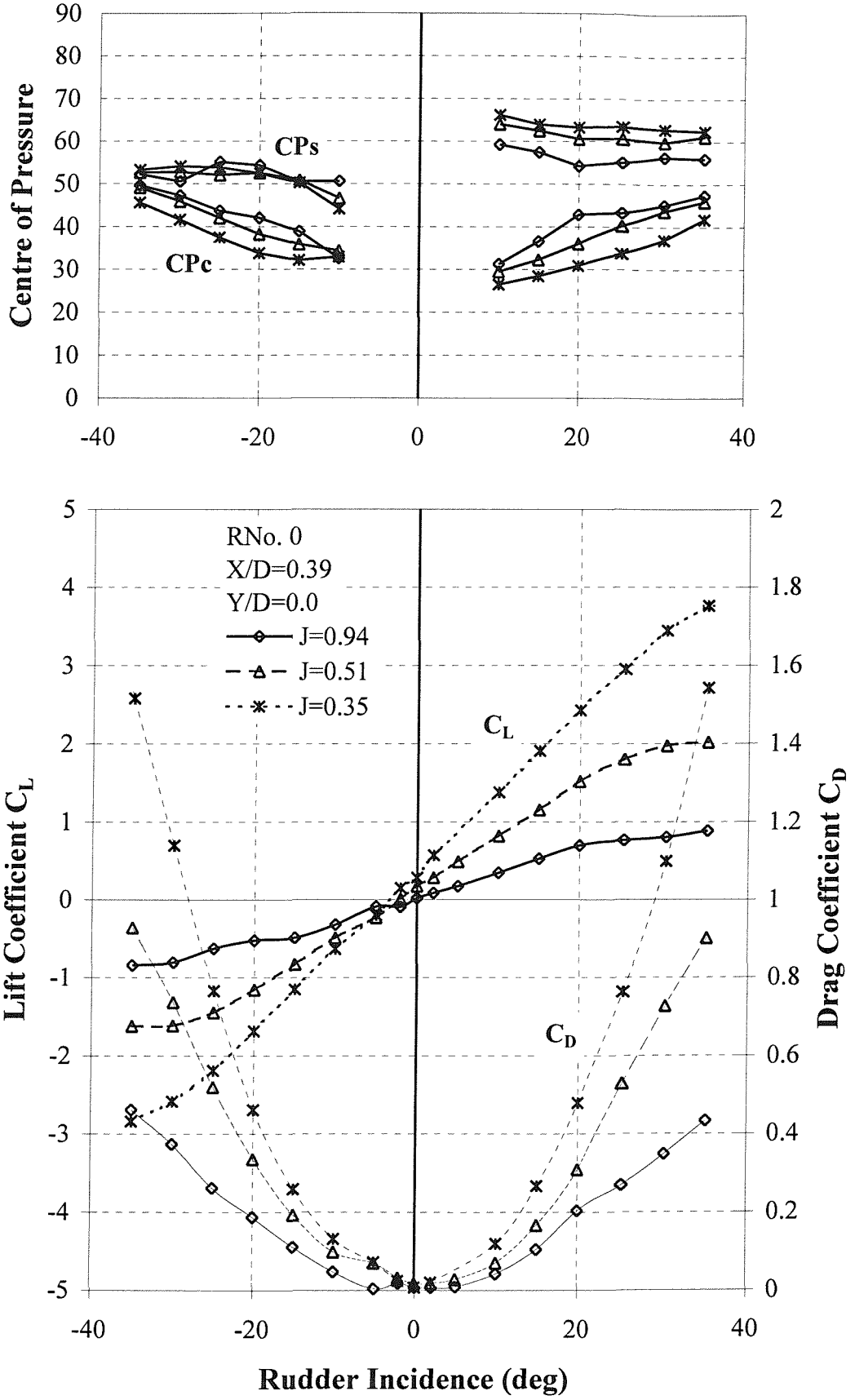

Figure A-4 **Influence of Propeller Thrust Loading on the Performance of Skeg-Rudder No. 0 (rudder alone forces)**

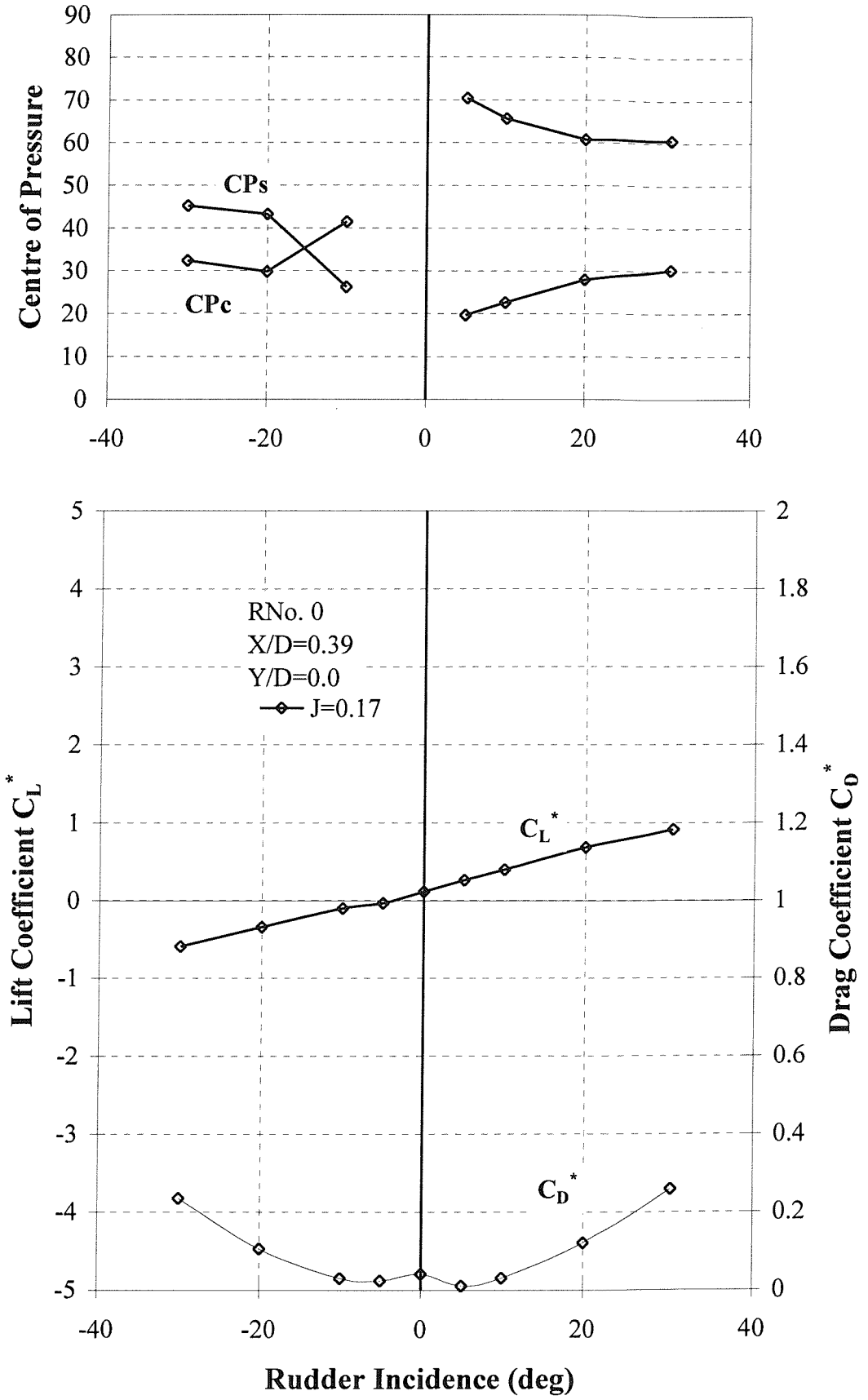

Figure A-5 **Skeg-Rudder No. 0 Performance at a Propeller Advance Ratio of J=0.17 (rudder alone forces)**

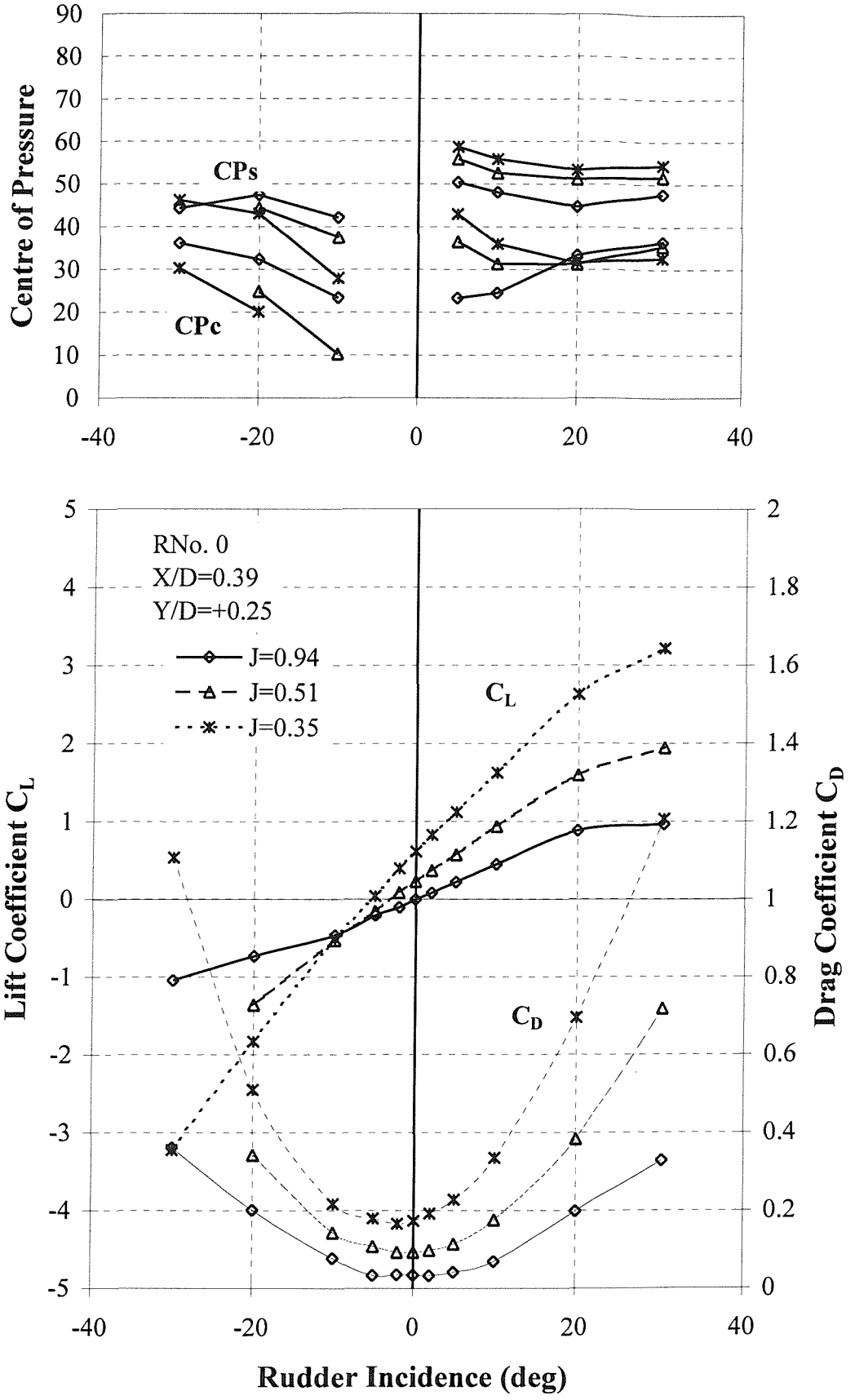

Figure A-6 **Influence of Propeller Thrust Loading on the Performance of Skeg-Rudder No. 0 at a Lateral Separation of Y/D=+0.25 (rudder plus skeg forces)**

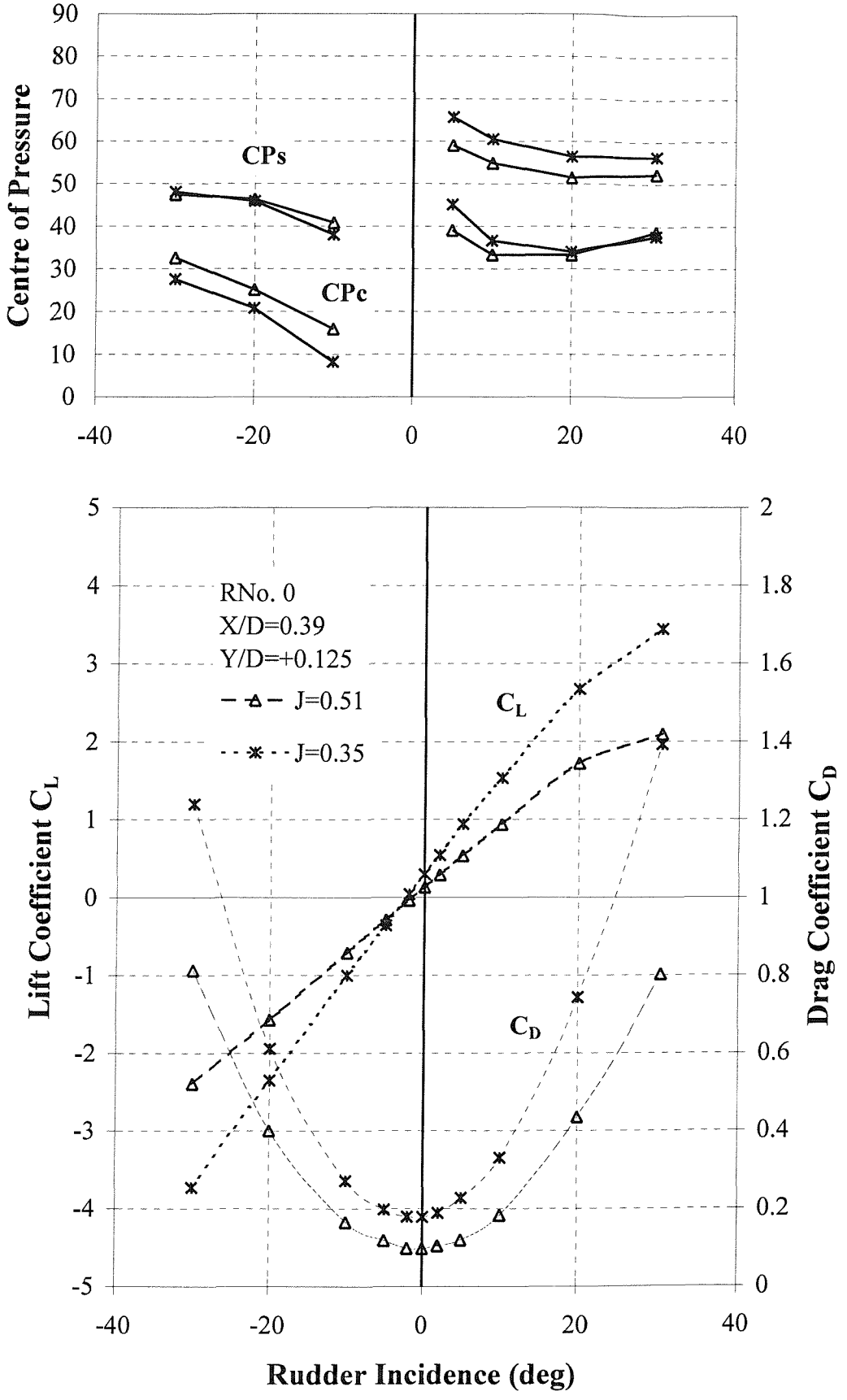

Figure A-7 **Influence of Propeller Thrust Loading on the Performance of Skeg-Rudder No. 0 at a Lateral Separation of Y/D=+0.125 (rudder plus skeg forces)**

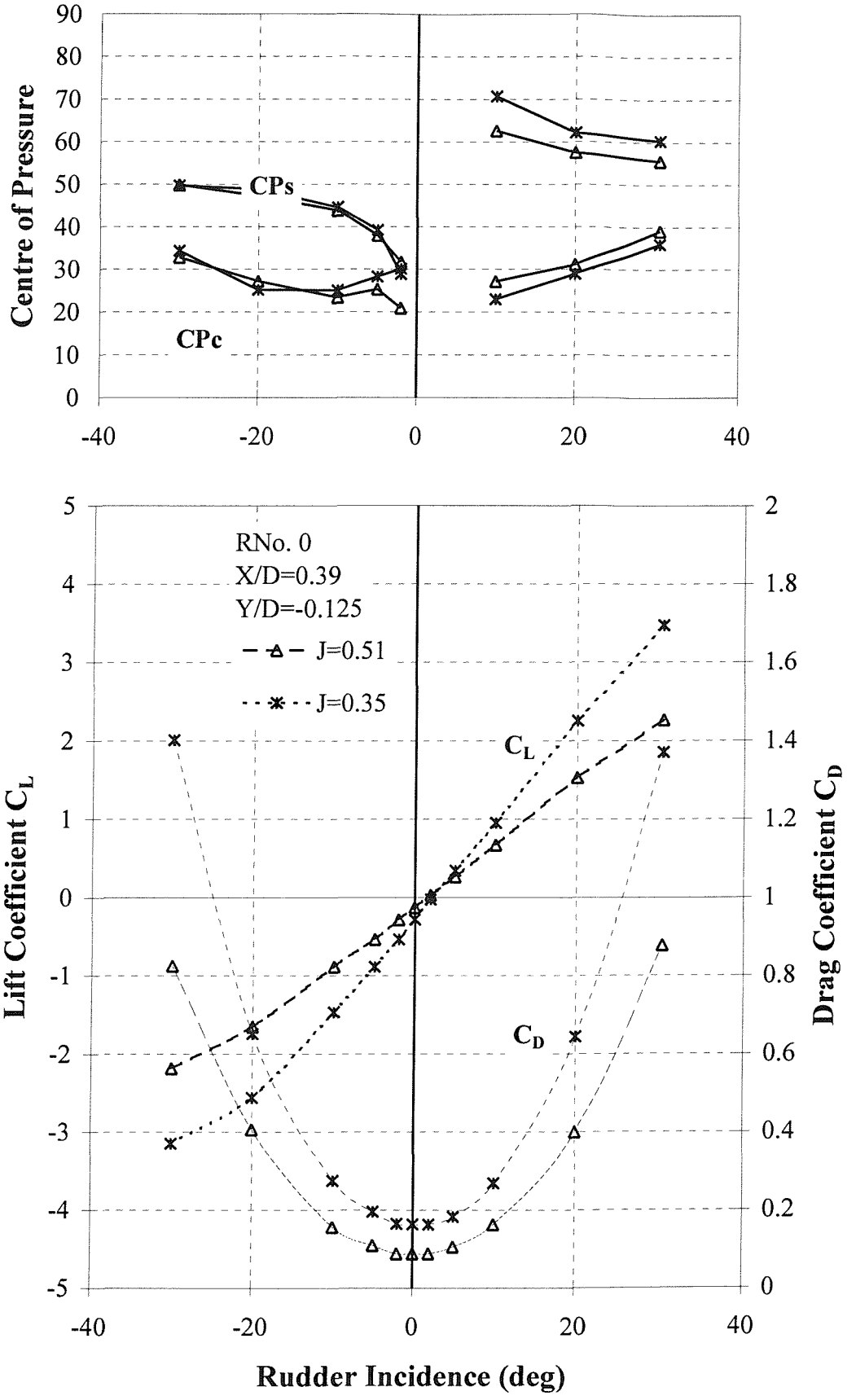

Figure A-8 **Influence of Propeller Thrust Loading on the Performance of Skeg-Rudder No. 0 at a Lateral Separation of Y/D=-0.125 (rudder plus skeg forces)**

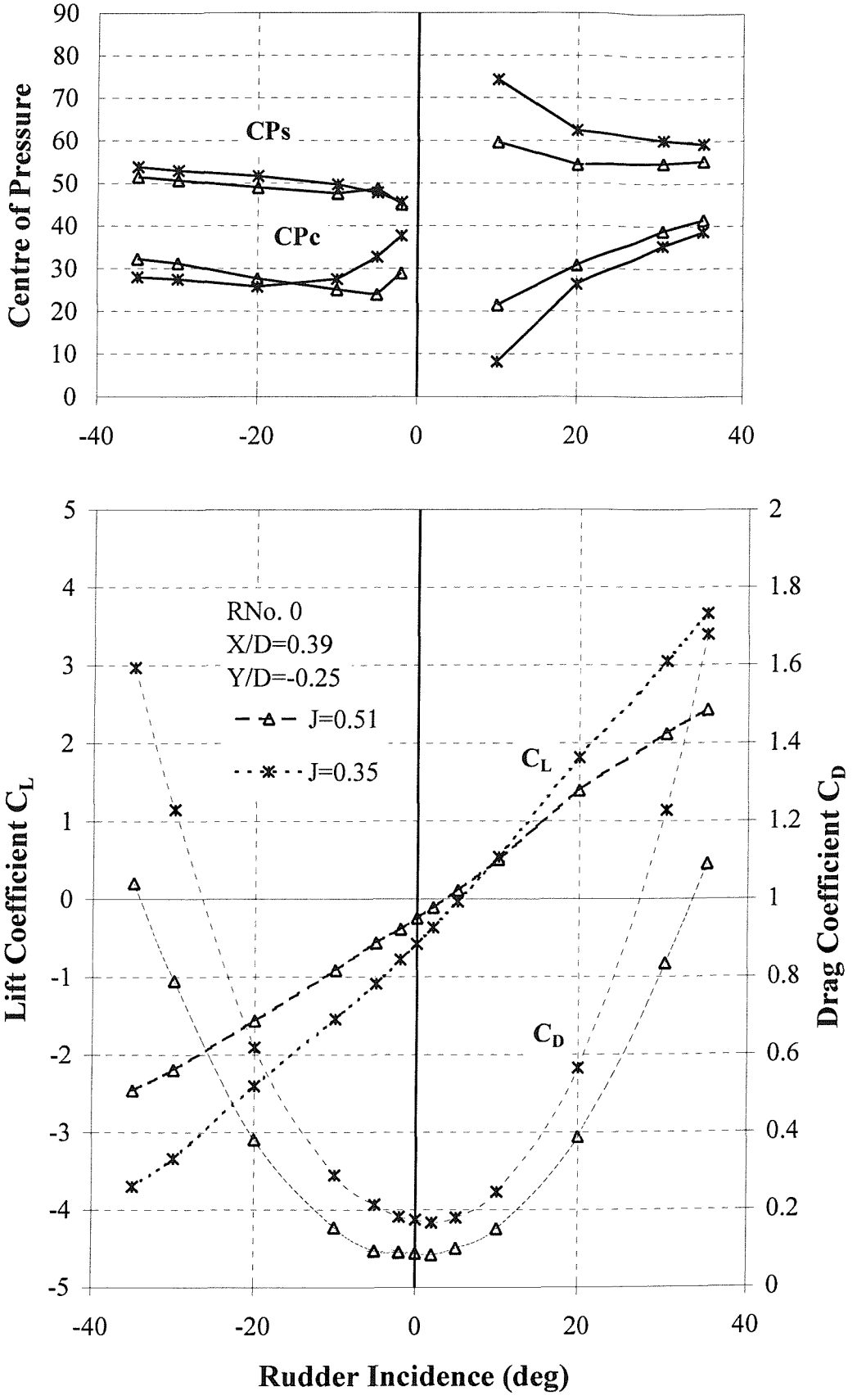

Figure A-9 **Influence of Propeller Thrust Loading on the Performance of Skeg-Rudder No. 0 at a Lateral Separation of Y/D=-0.25 (rudder plus skeg forces)**

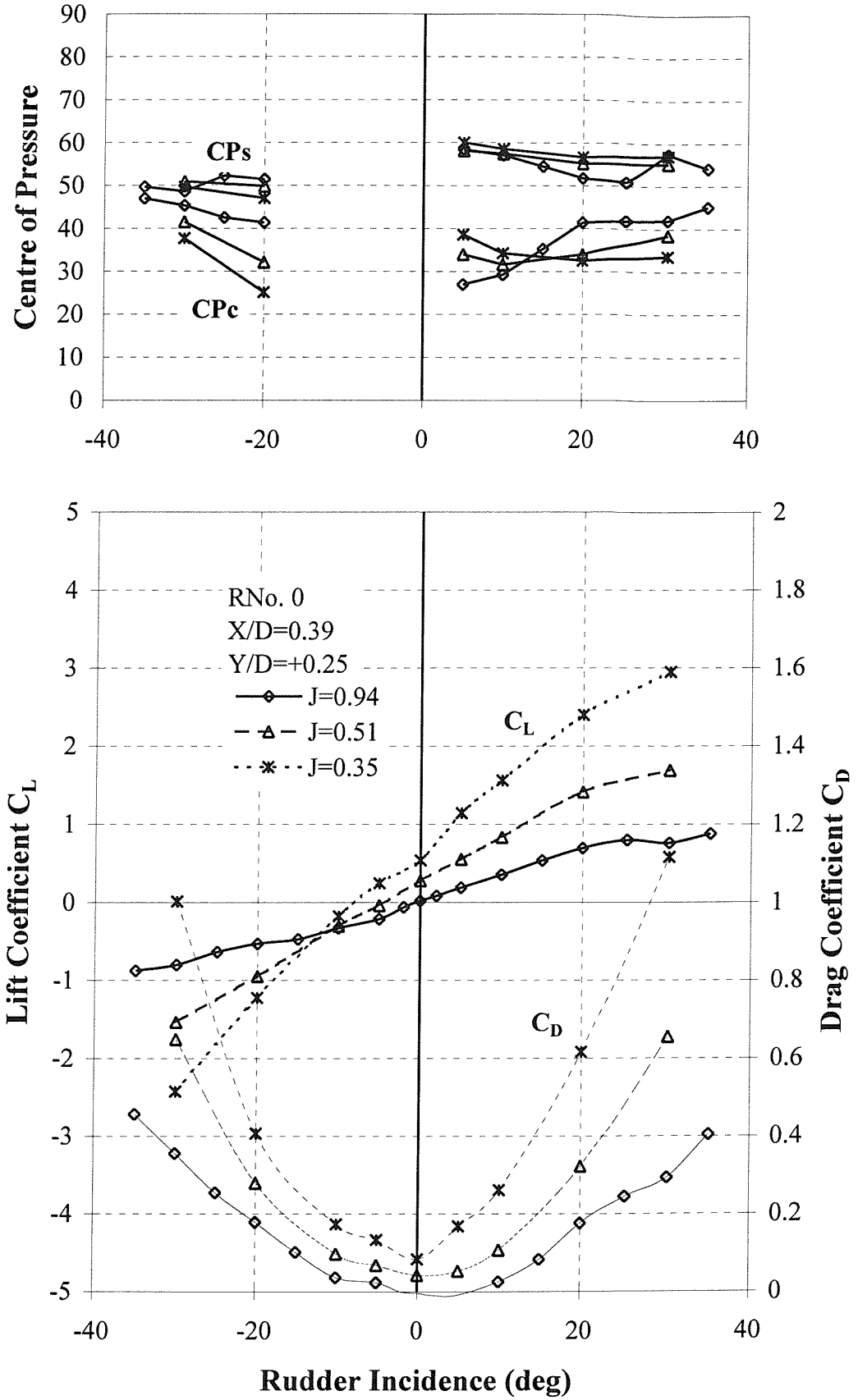

Figure A-10 Influence of Propeller Thrust Loading on the Performance of Skeg-Rudder No. 0 at a Lateral Separation of Y/D=+0.25 (rudder alone forces)

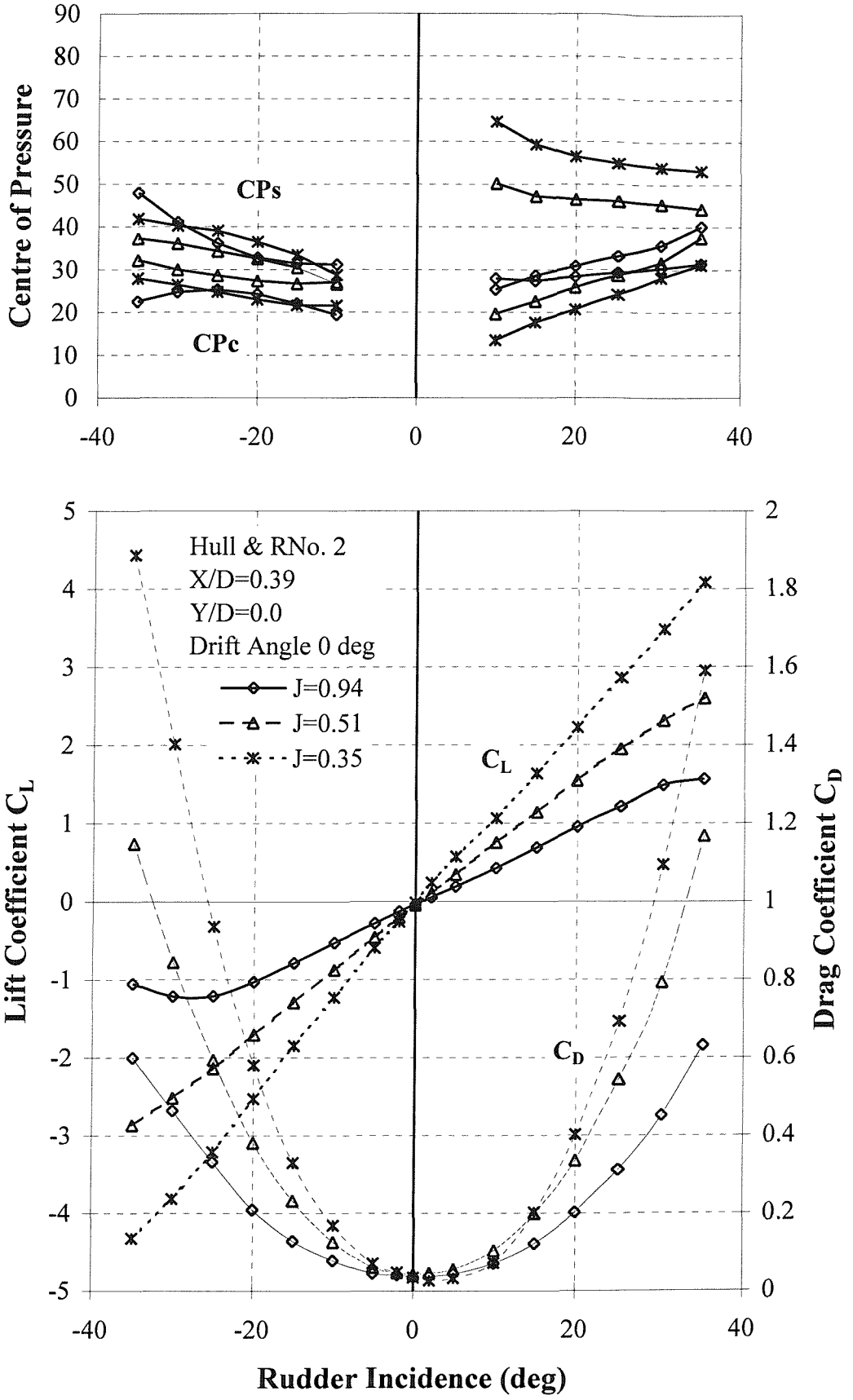

Figure A-11 Influence of Propeller Thrust Loading on the Performance of Rudder No. 2 Behind the Hull.

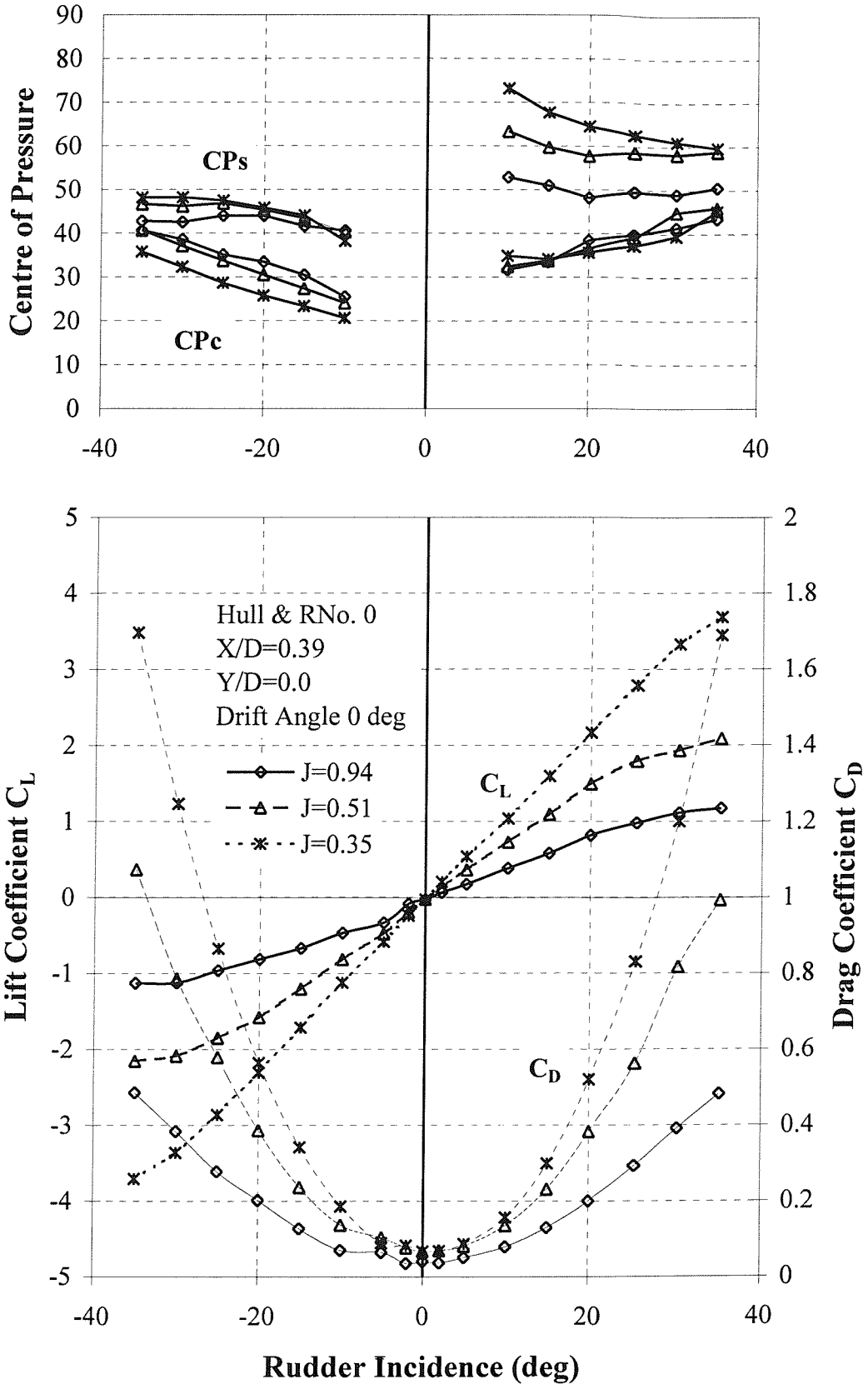

Figure A-12 Influence of Propeller Thrust Loading on the Performance of Skeg-Rudder No. 0 Behind the Hull (rudder plus skeg forces

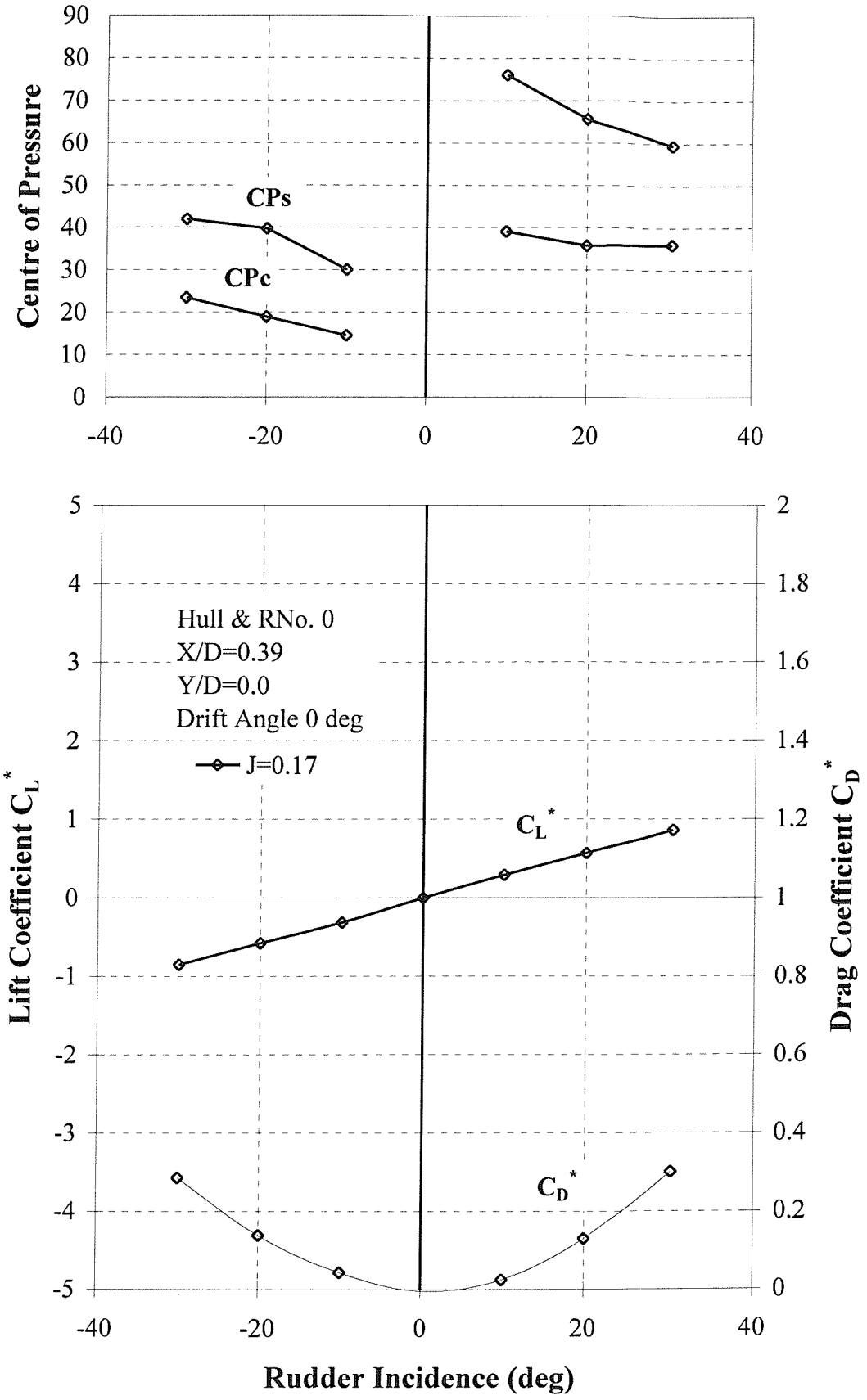

Figure A-13 Skeg-Rudder No. 0 Performance at a Propeller Advance Ratio of J=0.17 and Behind the Hull (rudder plus skeg forces)

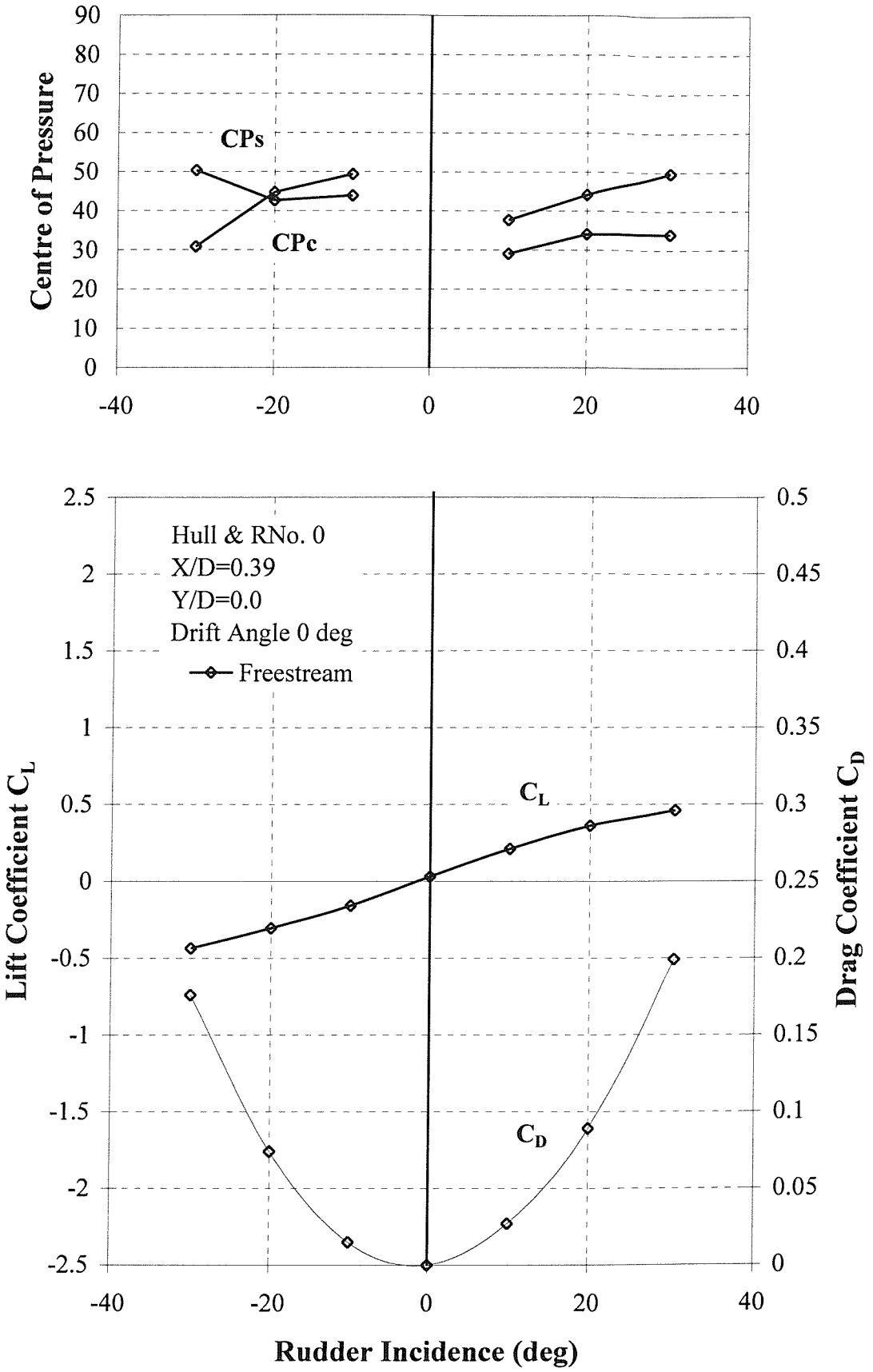

Figure A-14 Skeg-Rudder No. 0 Performance in Freestream Behind the Hull and Stationary Propeller (rudder plus skeg forces)

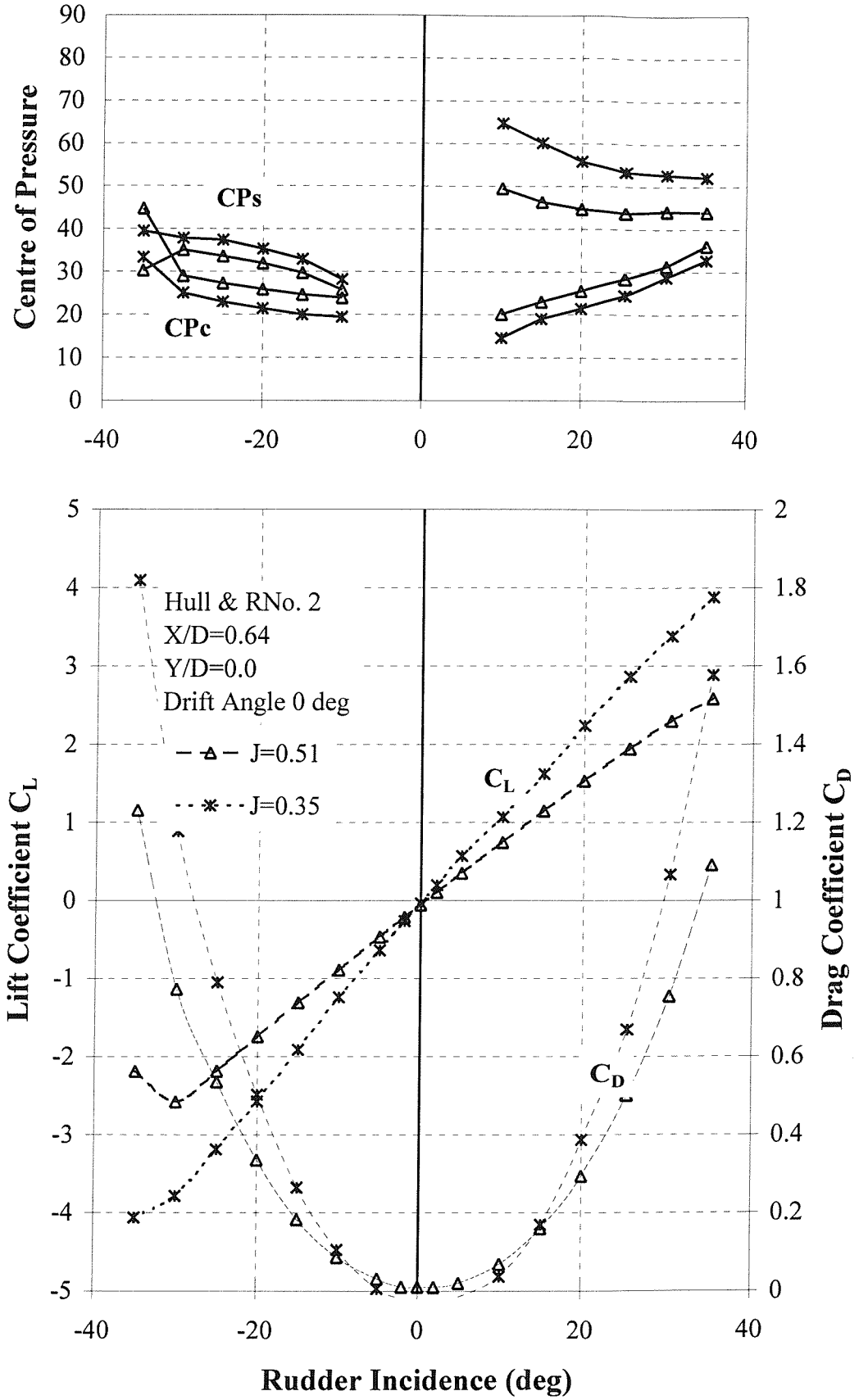

Figure A-15 Influence of Propeller Thrust Loading on the Performance of Rudder No. 2 Behind the Hull and at a longitudinal Separation of X/D=0.64.

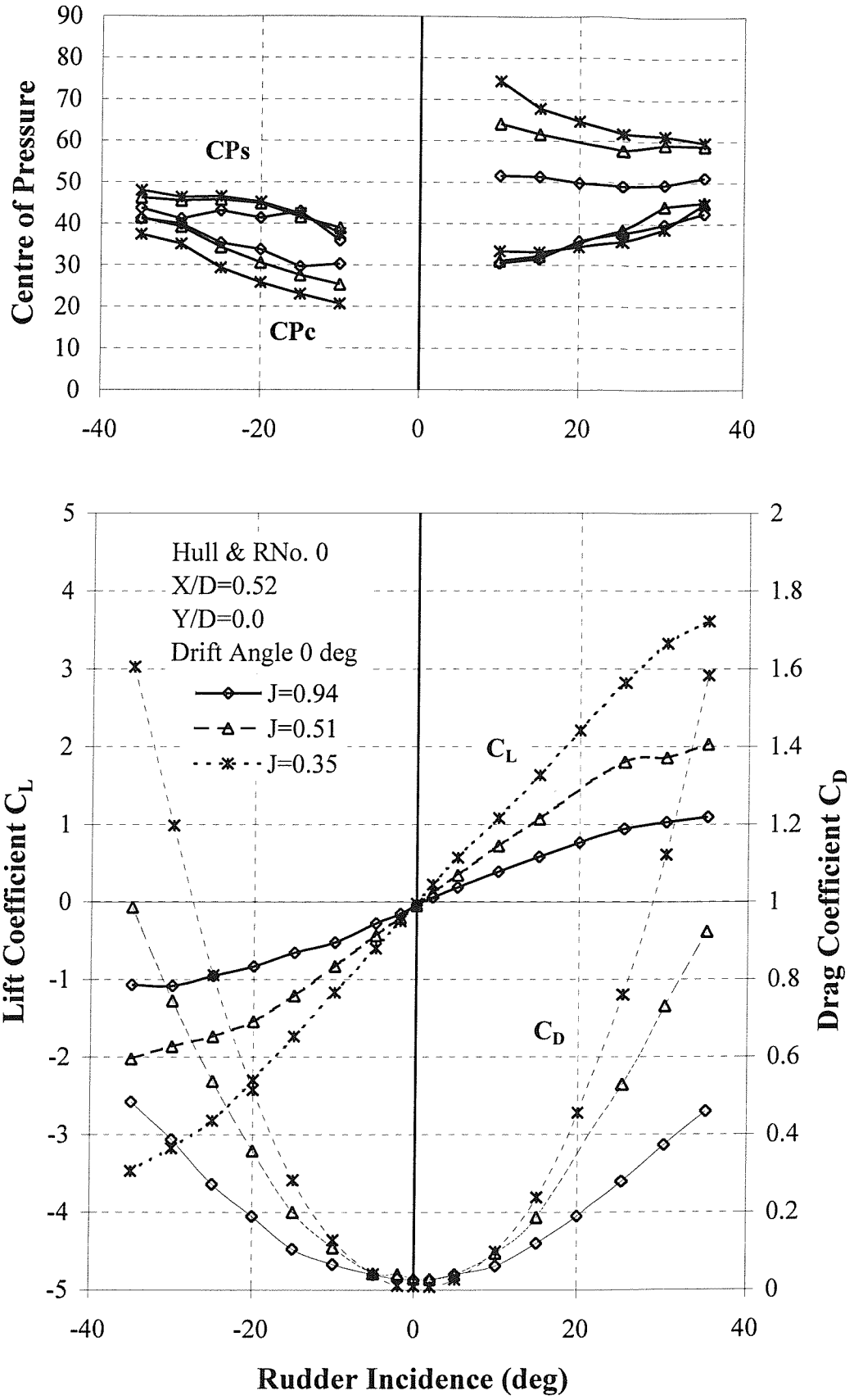

Figure A-16 **Influence of Propeller Thrust Loading on the Performance of Skeg-Rudder No. 0 Behind the Hull and at a Longitudinal Separation of X/D=0.52 (rudder plus Skeg forces)**

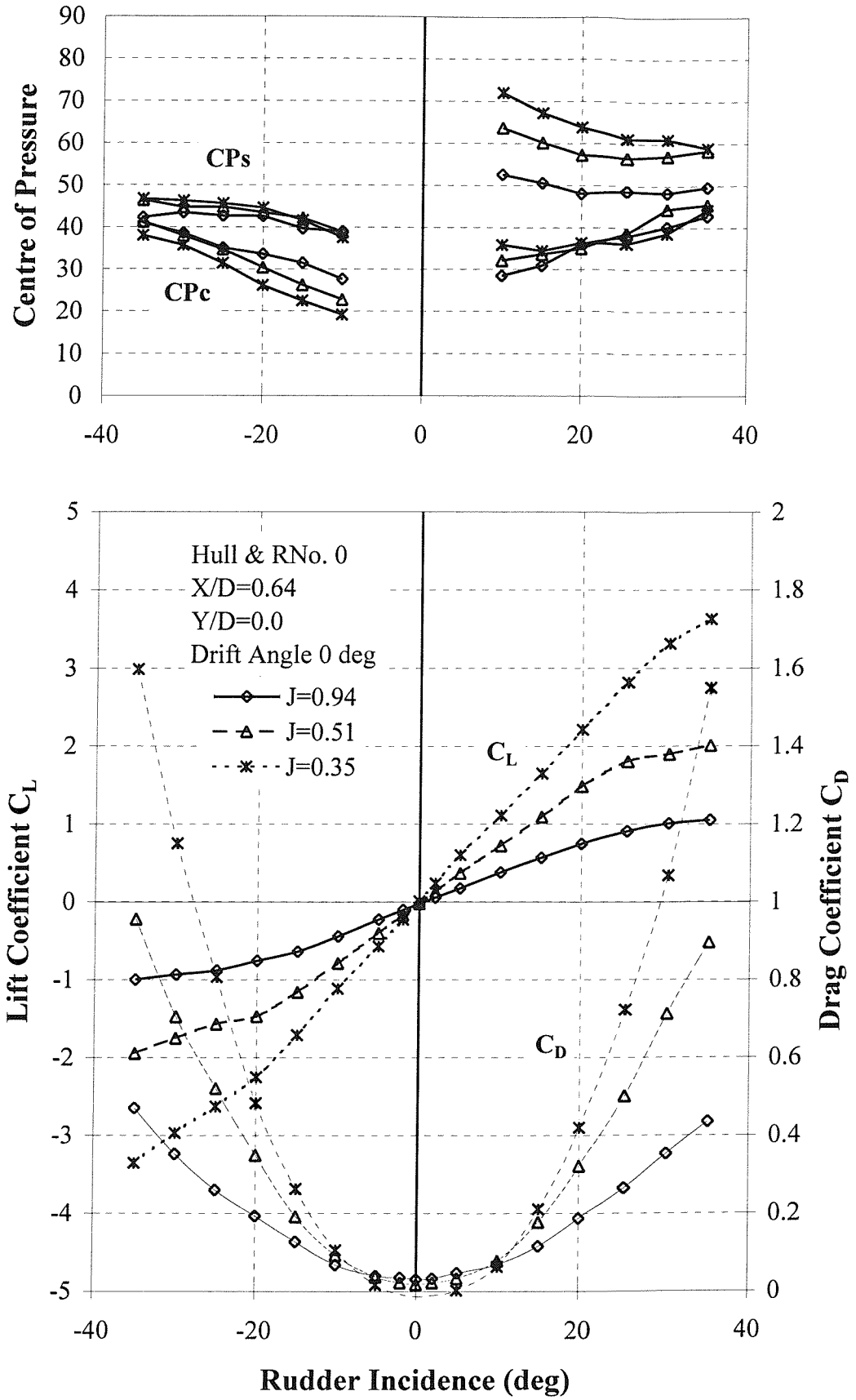

Figure A-17 Influence of Propeller Thrust Loading on the Performance of Skeg-Rudder No. 0 Behind the Hull and at a Longitudinal Separation of X/D=0.64 (rudder plus Skeg forces)

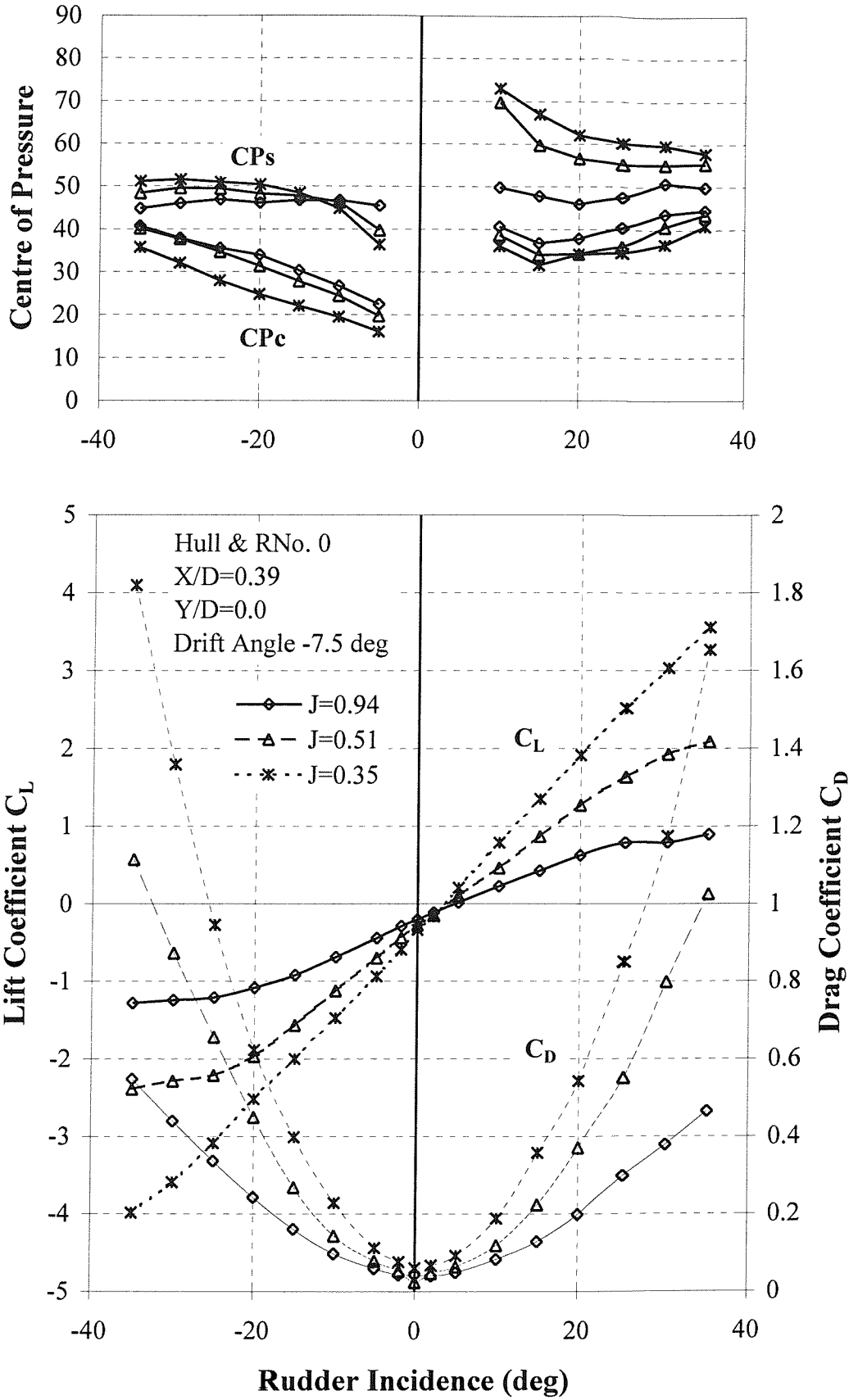

Figure A-18 **Influence of Thrust Loading on the Performance of Skeg-Rudder No. 0 Behind the Hull and at a Yaw Angle of -7.5 degrees (rudder plus skeg forces), skeg angle -7.5 degrees**

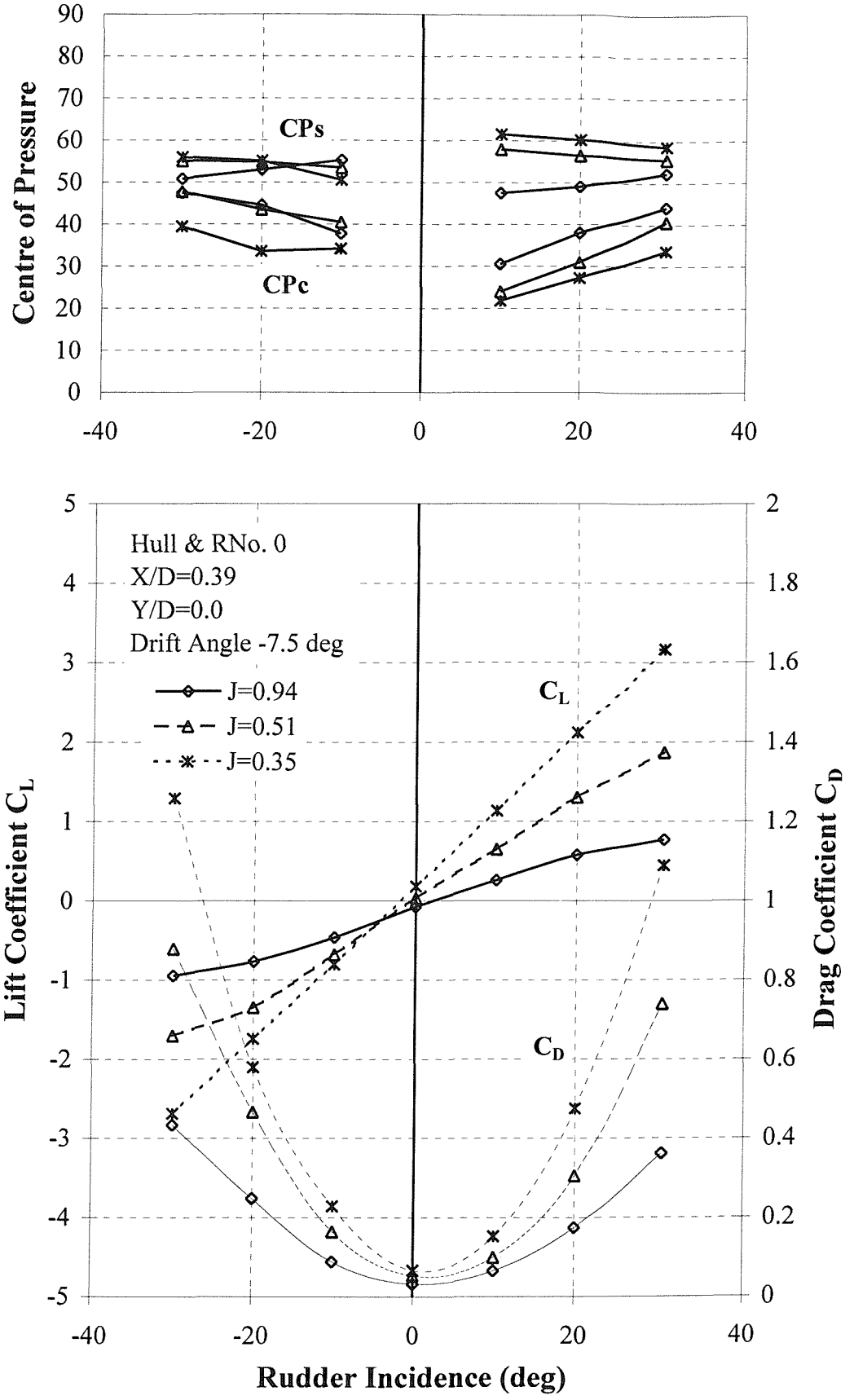

Figure A-19 Influence of Thrust Loading on the Performance of Skeg-Rudder No. 0 Behind the Hull and at a Yaw Angle of -7.5 degrees (rudder alone forces), skeg angle -7.5 degrees.

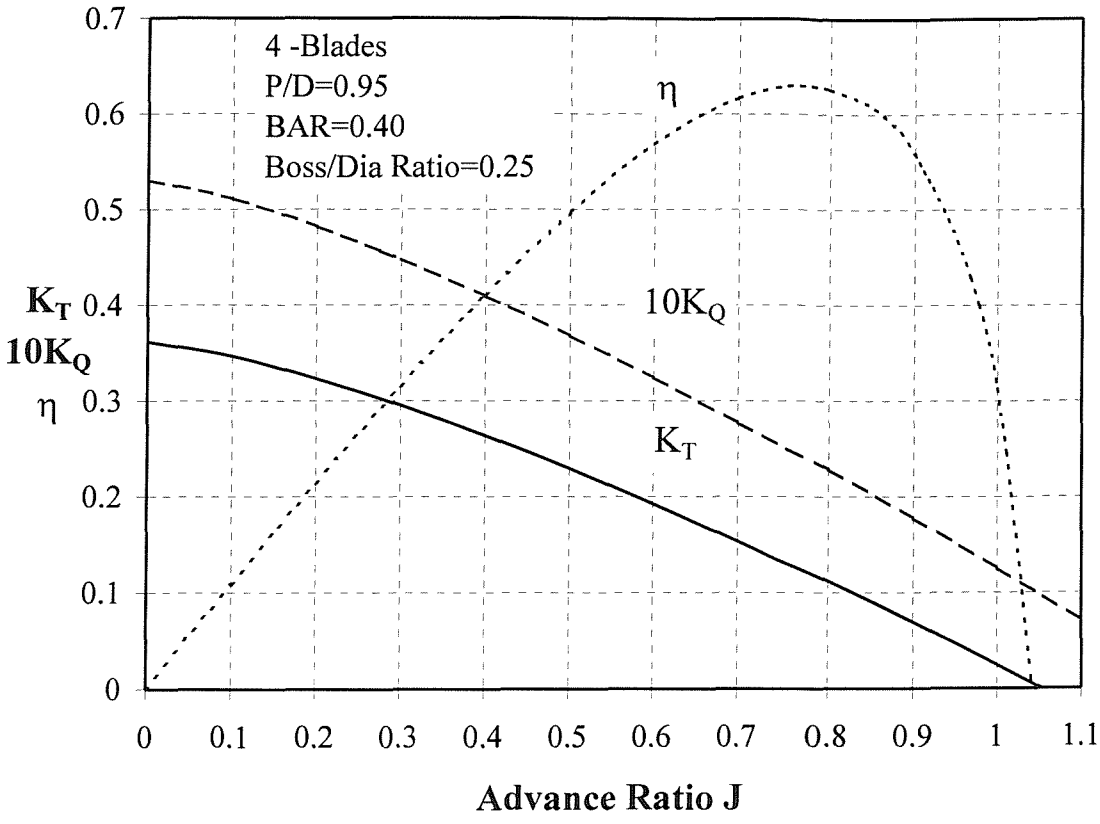

Figure A-20 Freestream (Open Water) Propeller Characteristics of Modified Wageningen B.4.40 at a mean Pitch Ratio of 0.95.

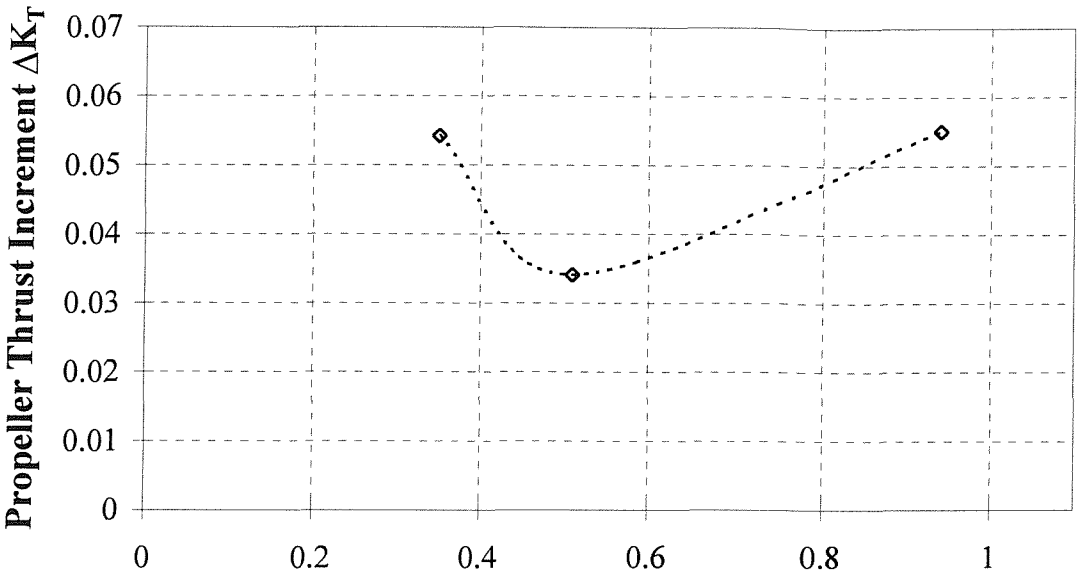

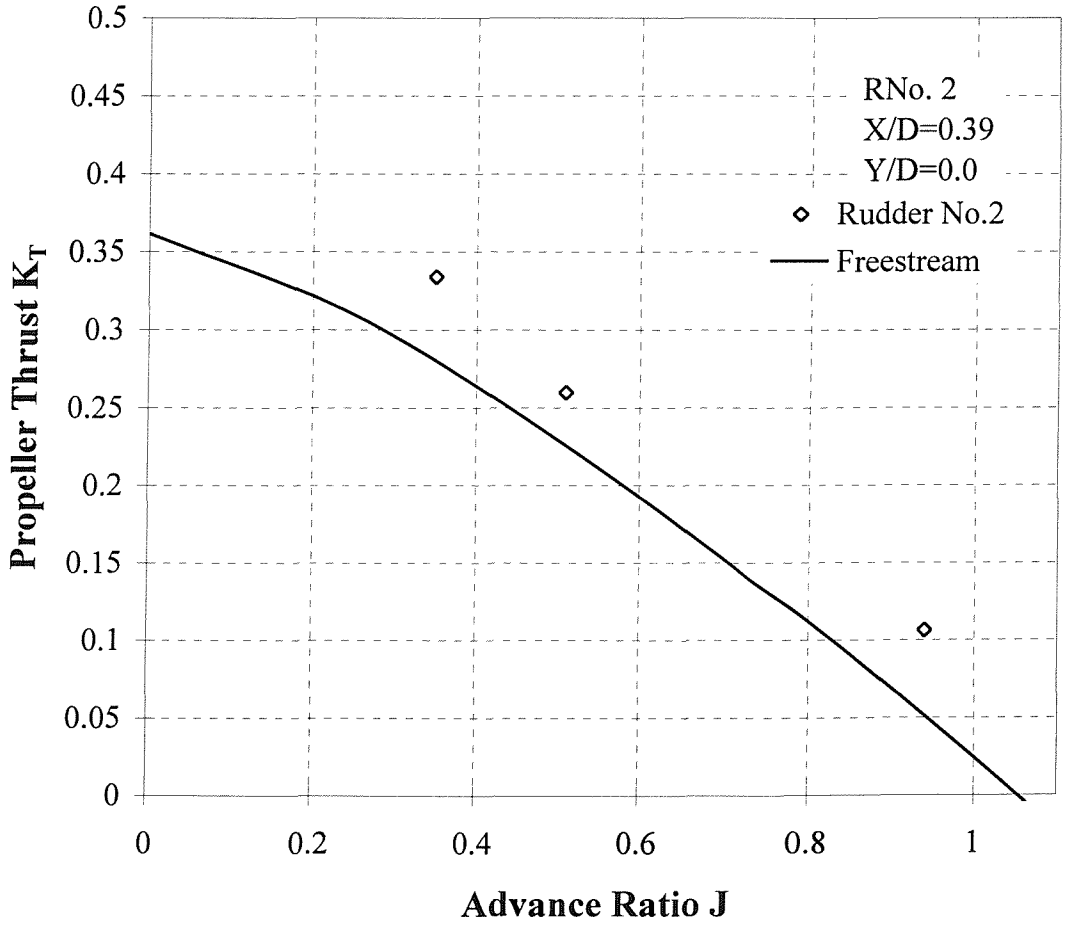

Figure A-21 Propeller Thrust and Thrust Increment Against Advance Ratio for Rudder No. 2

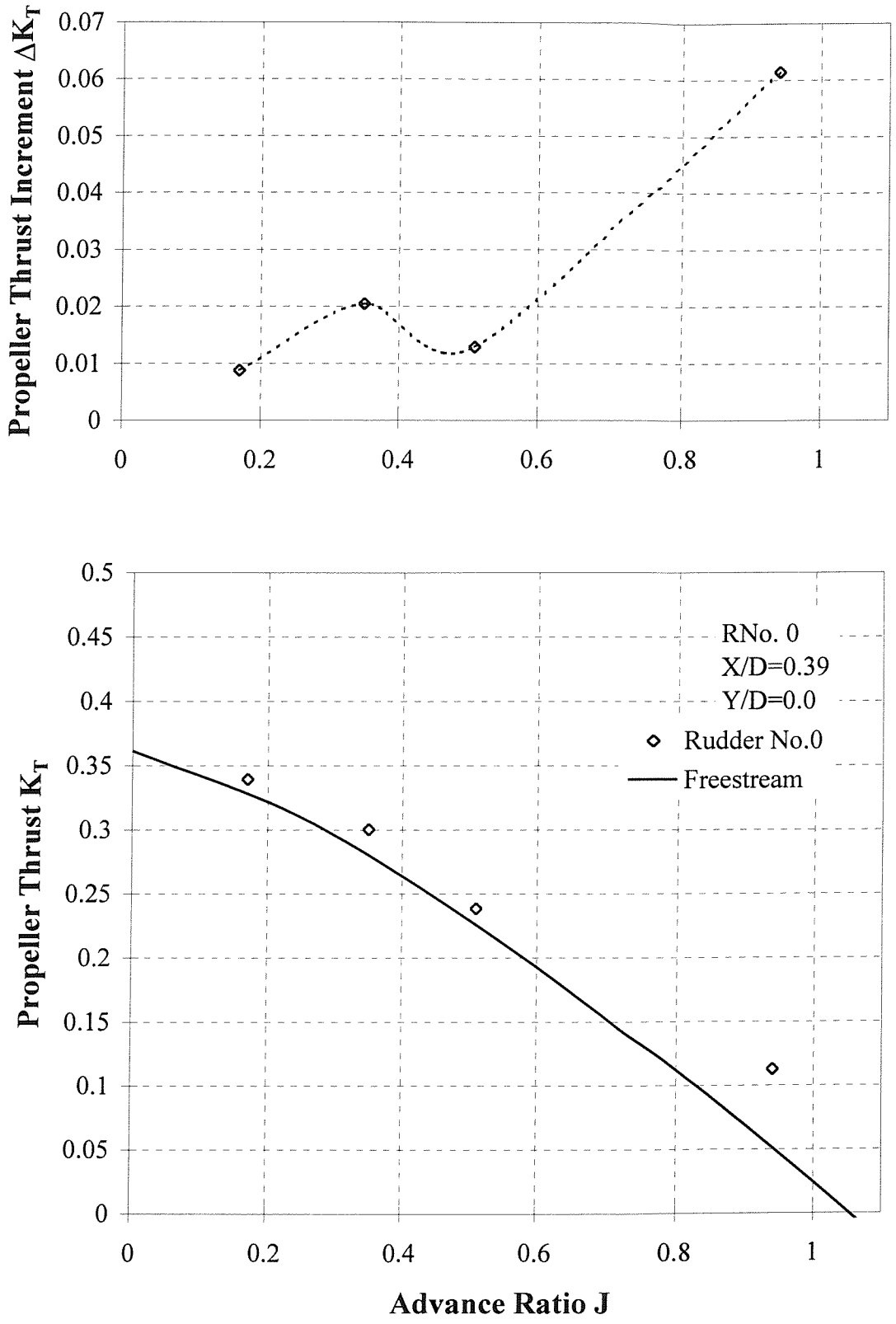

Figure A-22 Propeller Thrust and Thrust Increment Against Advance Ratio for Skeg-Rudder No. 0

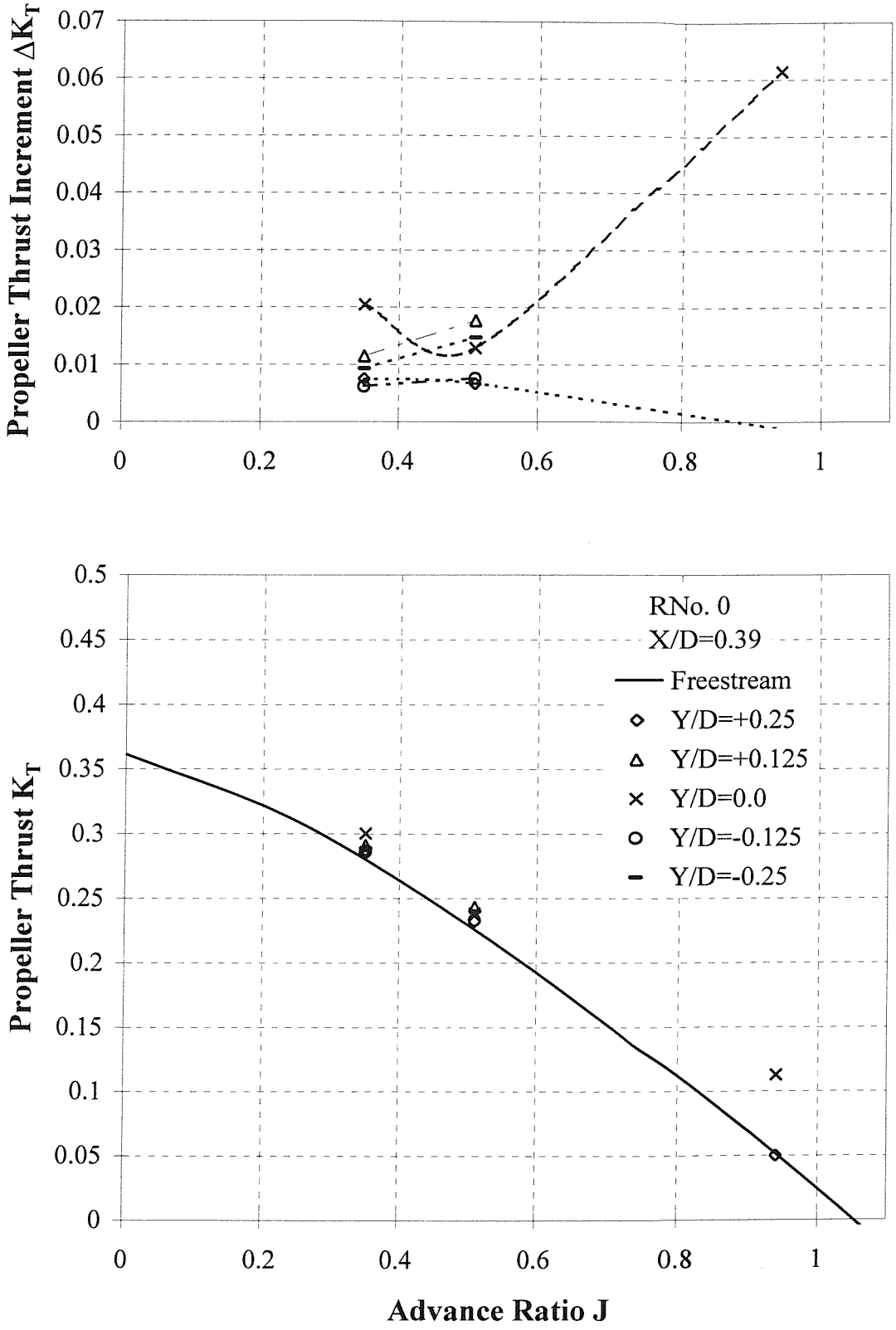

Figure A-23 Comparison of Propeller Thrust and Thrust and Thrust Increment Against Advance Ratio for a Lateral Separation of Skeg-Rudder No. 0 and Propeller of Y/D=+0.25, +0.125, 0.0,-0.125, -0.25.

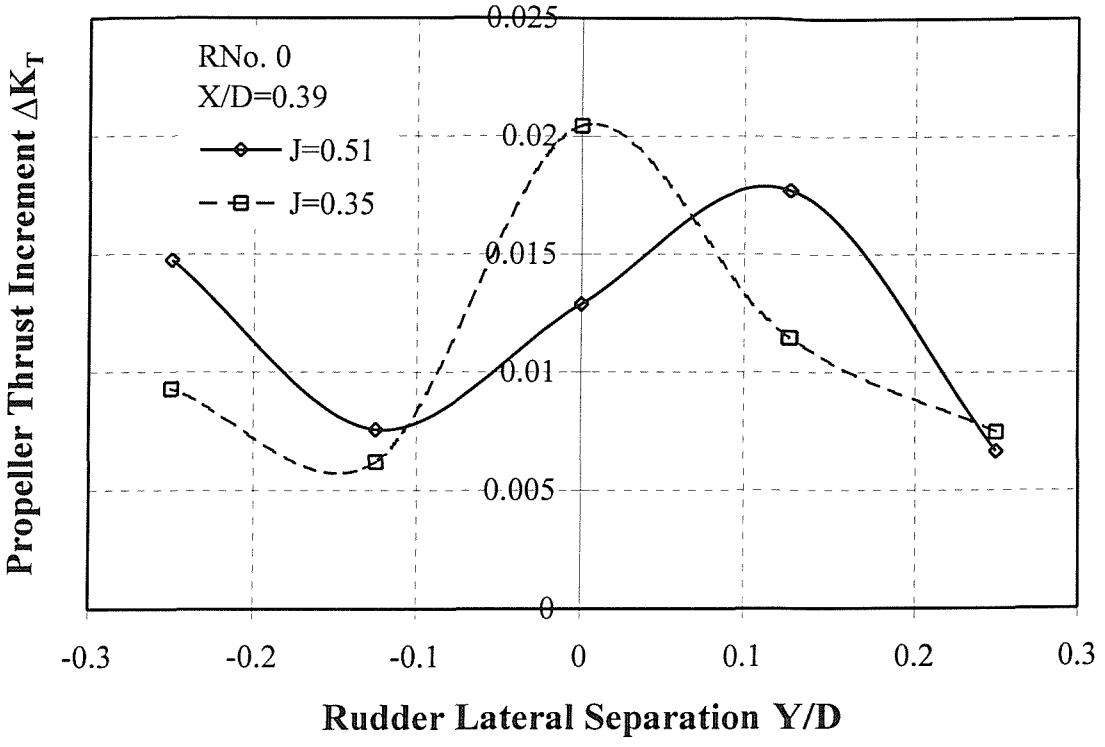

Figure A-24 Thrust Increment Against Rudder/Propeller Lateral Separation Y/D of Skeg-Rudder No. 0 for Two Advance Ratios of J=0.51 and 0.35.

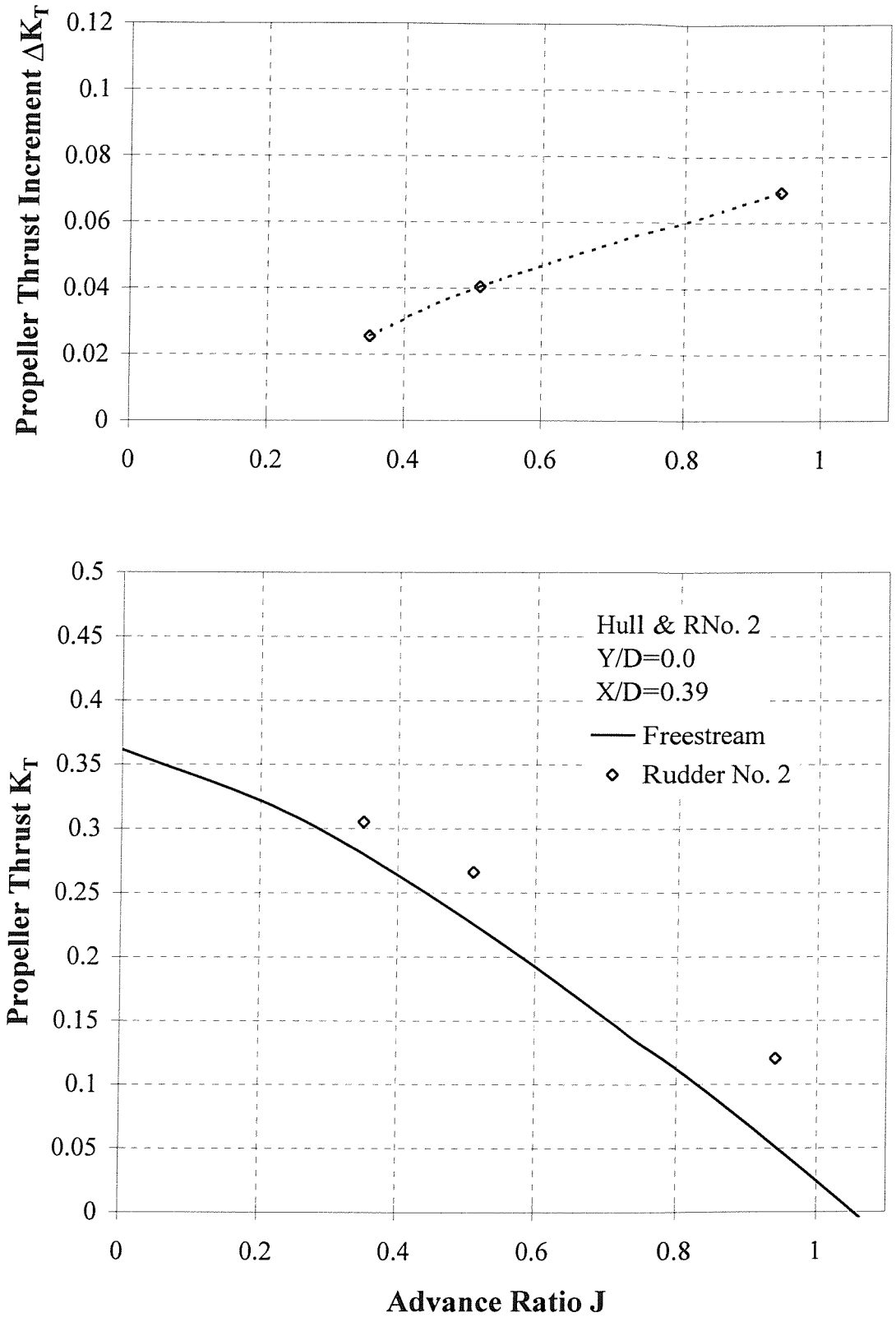

Figure A-25 Propeller Thrust and Thrust Increment Against Advance Ratio for Rudder No. 2 and Hull

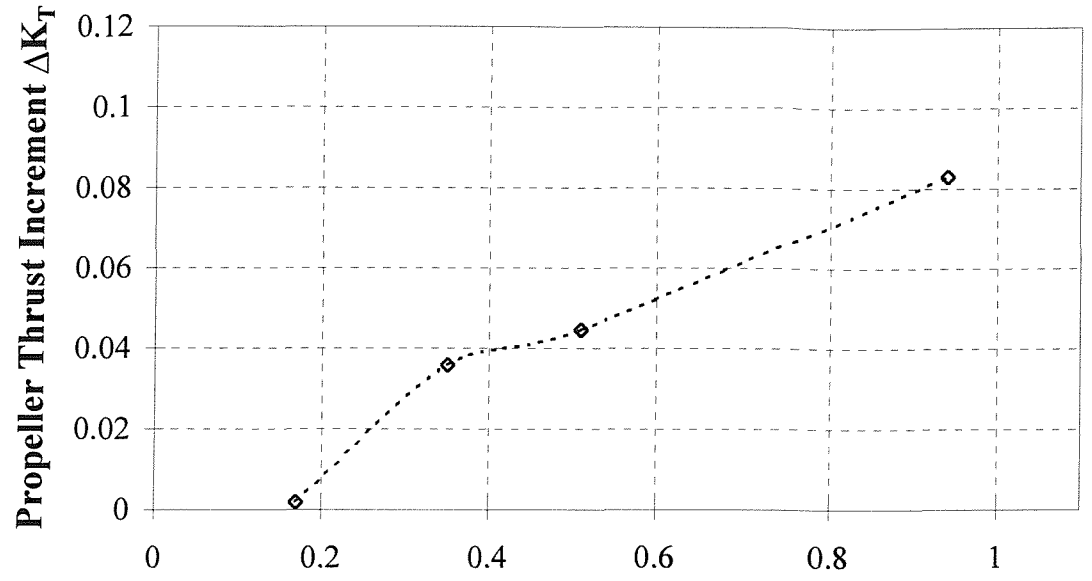

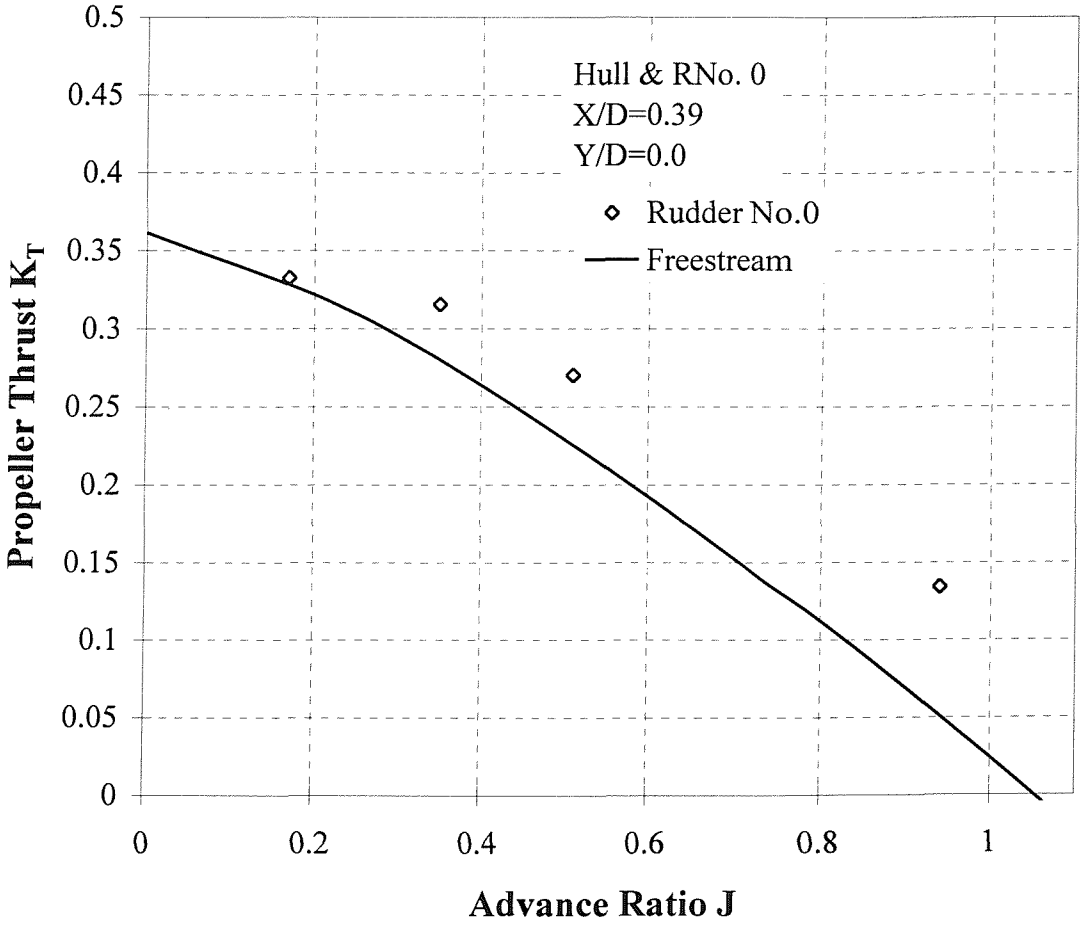

Figure A-26 Propeller Thrust and Thrust Increment Against Advance Ratio for Skeg-Rudder No. 0 and Hull.

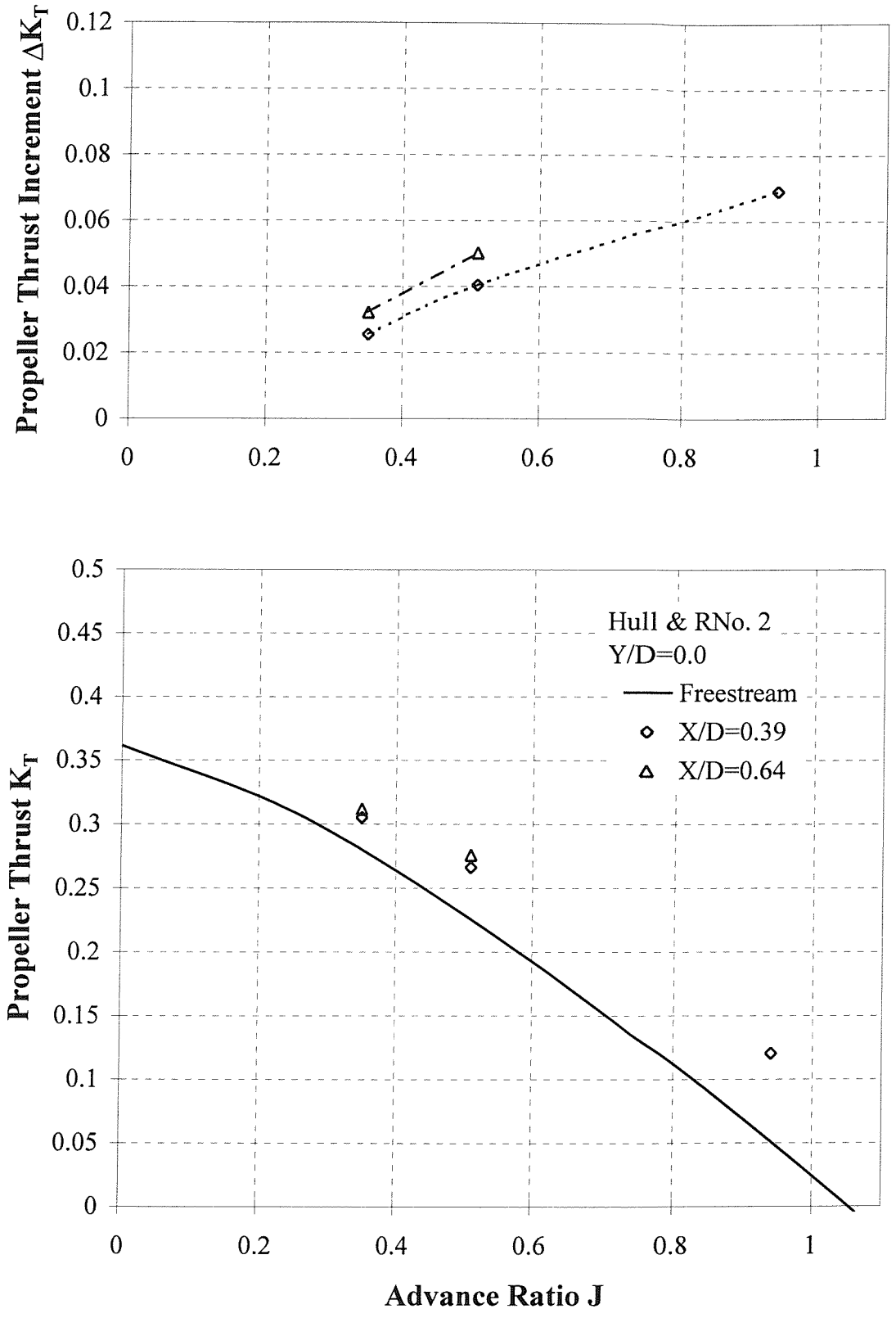

Figure A-27 Comparison of Propeller Thrust and Thrust Increment Against Advance Ratio for a Longitudinal Separation of Rudder No. 2 and Propeller of X/D=0.39 and 0.64

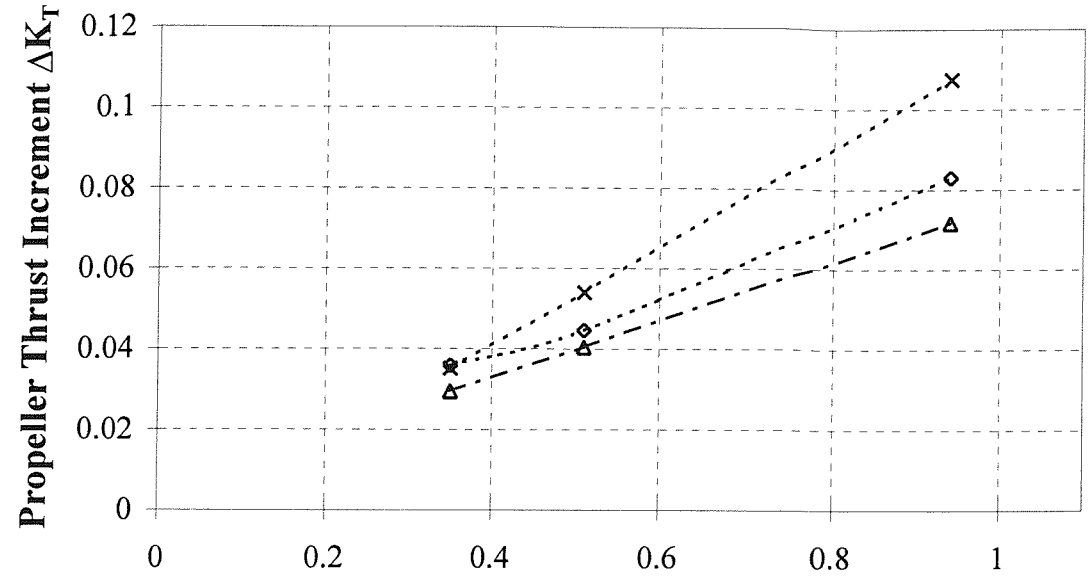

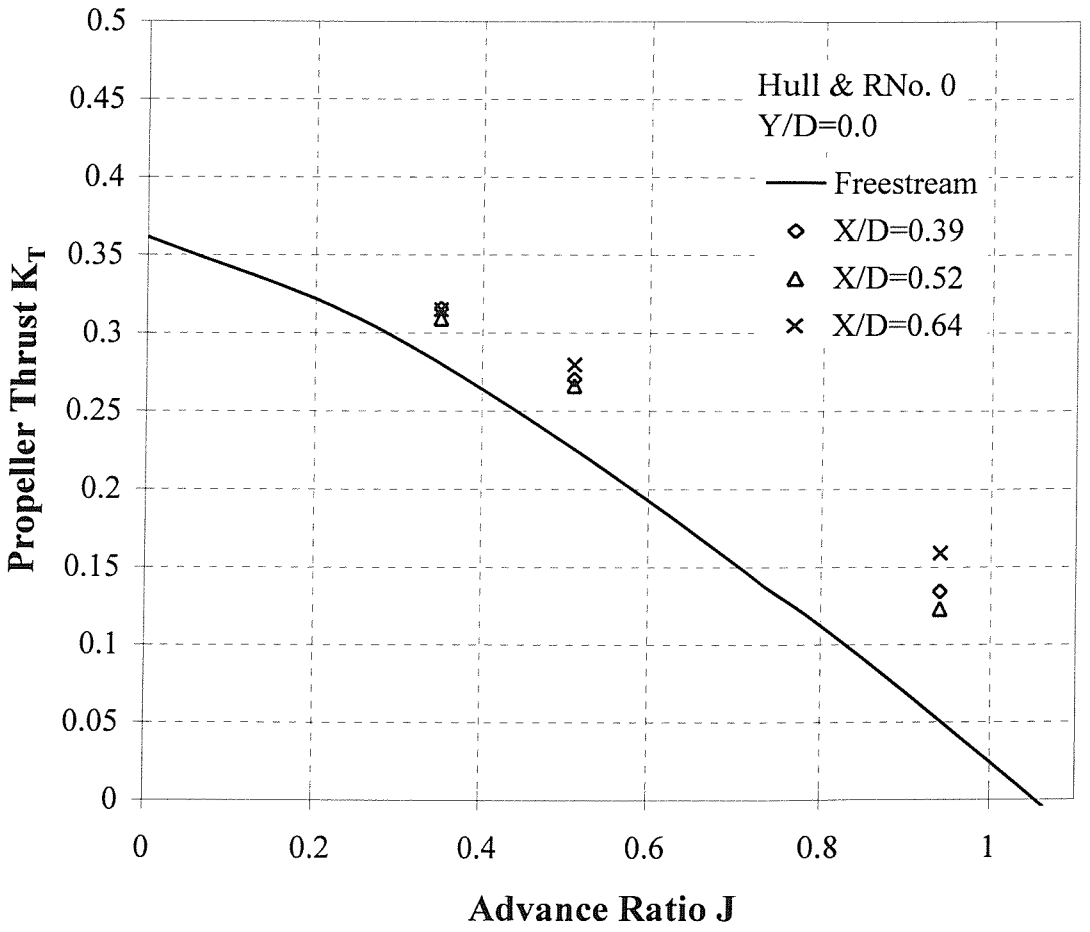

Figure A-28 Comparison of Propeller Thrust and Thrust Increment Against Advance Ratio for a Longitudinal Separation of Skeg-Rudder No. 0 and Hull of X/D=0.39, 0.52 and 0.64.

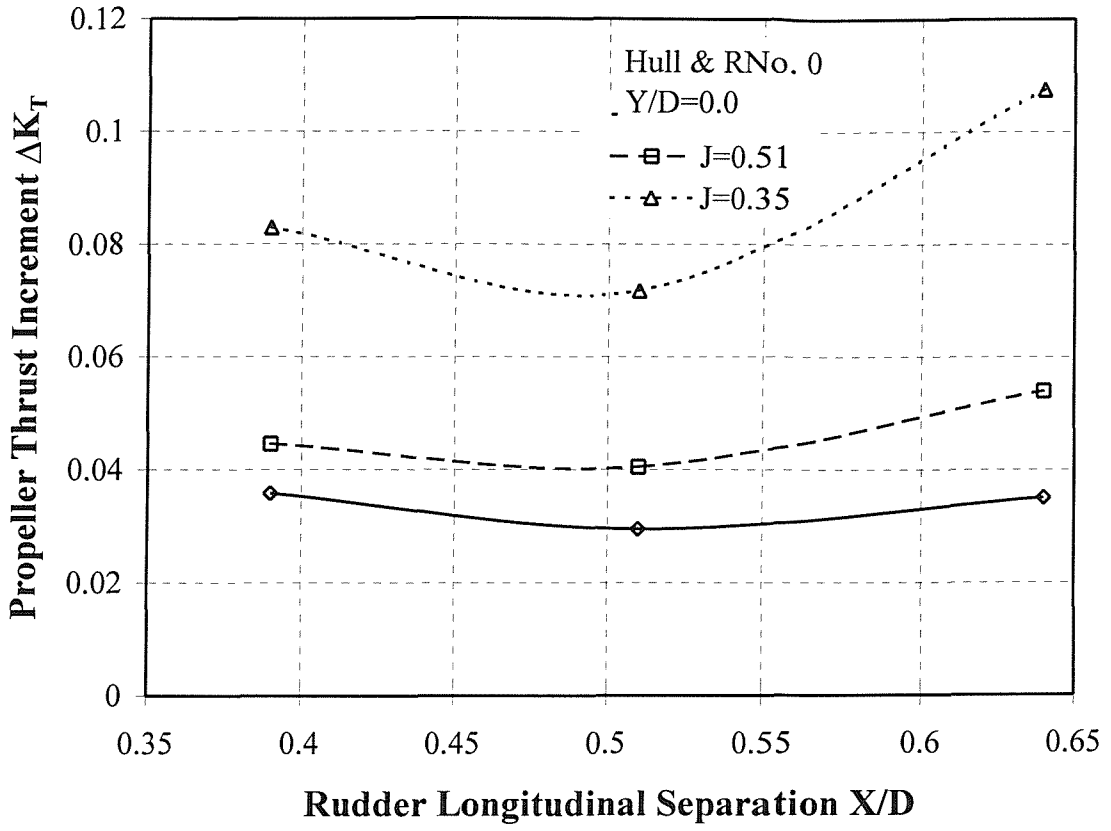

Figure A-29 **Thrust Increment Against Rudder/Propeller Longitudinal Separation X/D of Skeg-Rudder No. 0 and Hull for Three Advance Ratios of J=0.94, 0.51 and 0.35.**

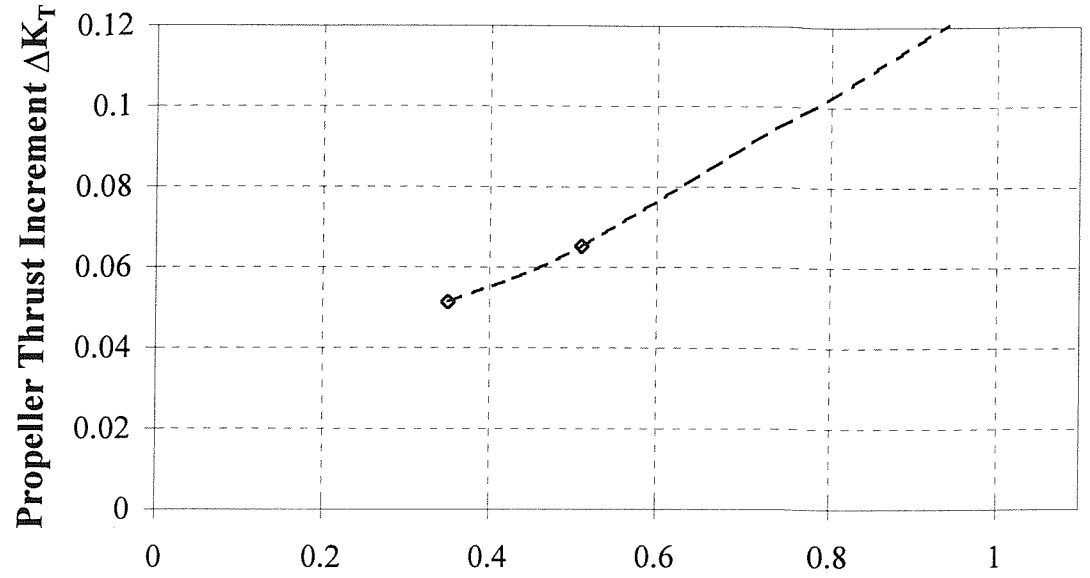

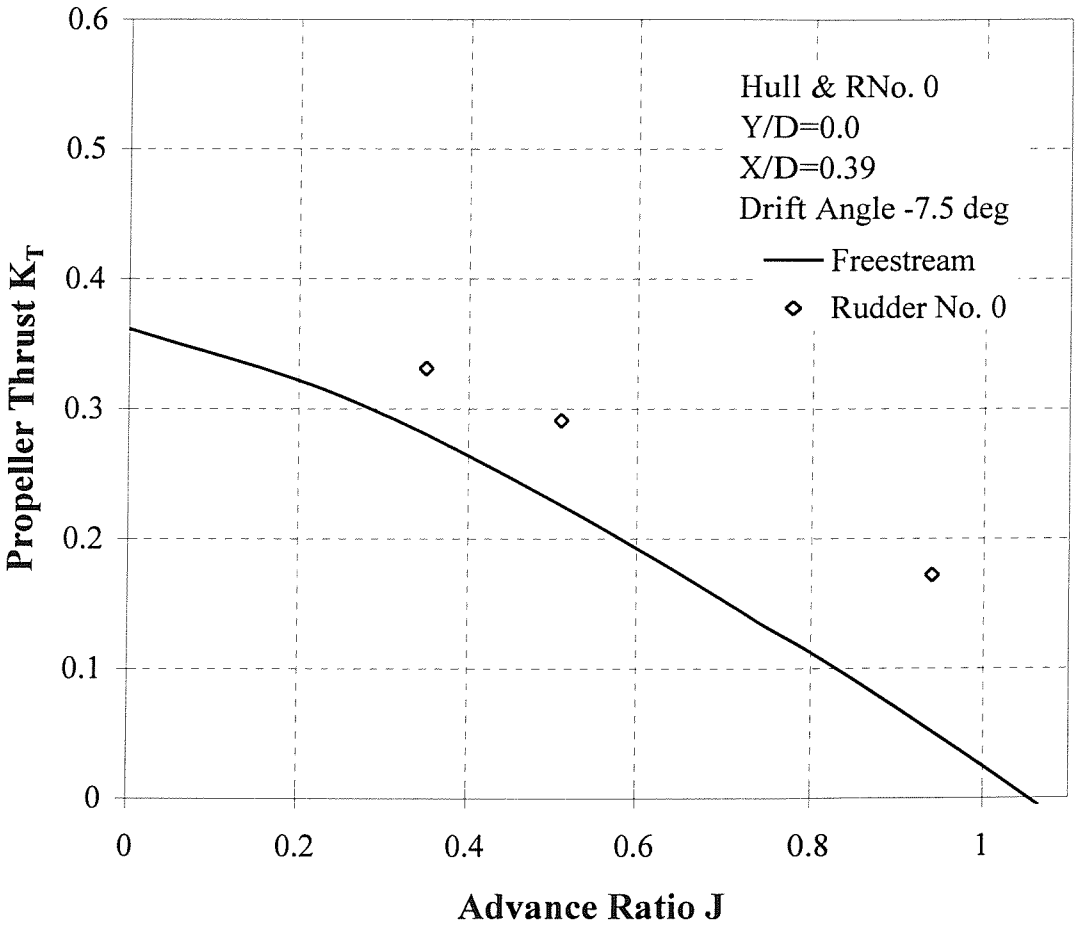

Figure A-30 Propeller Thrust and Thrust Increment Against Advance Ratio for Skeg_rudder No. 0 and Hull at a Drift Angle of -7.5 degrees.

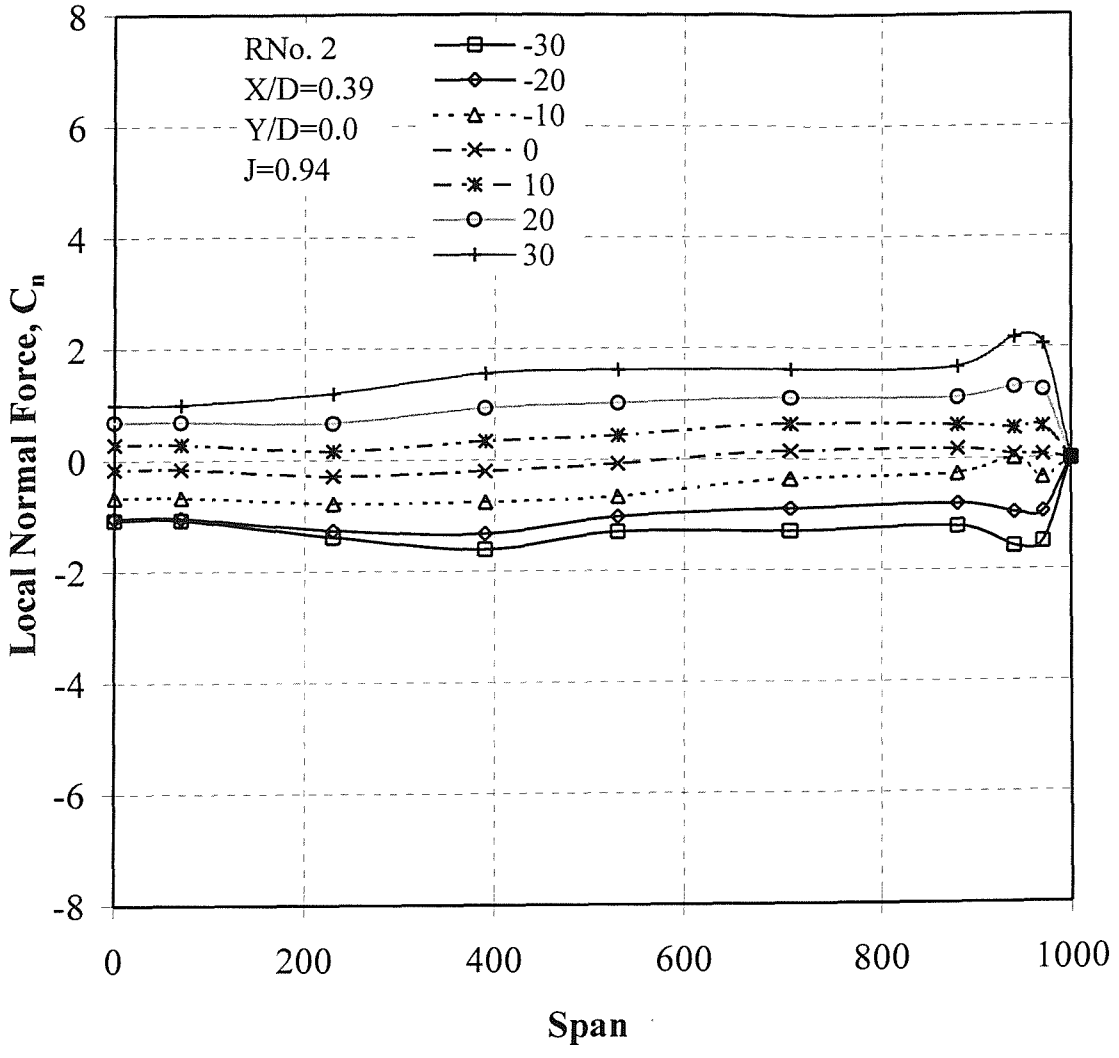

Figure A-31 Variation of Spanwise Distribution of Local Section Cn with incidence for Rudder No. 2 at a propeller advance ratio of J=0.94.

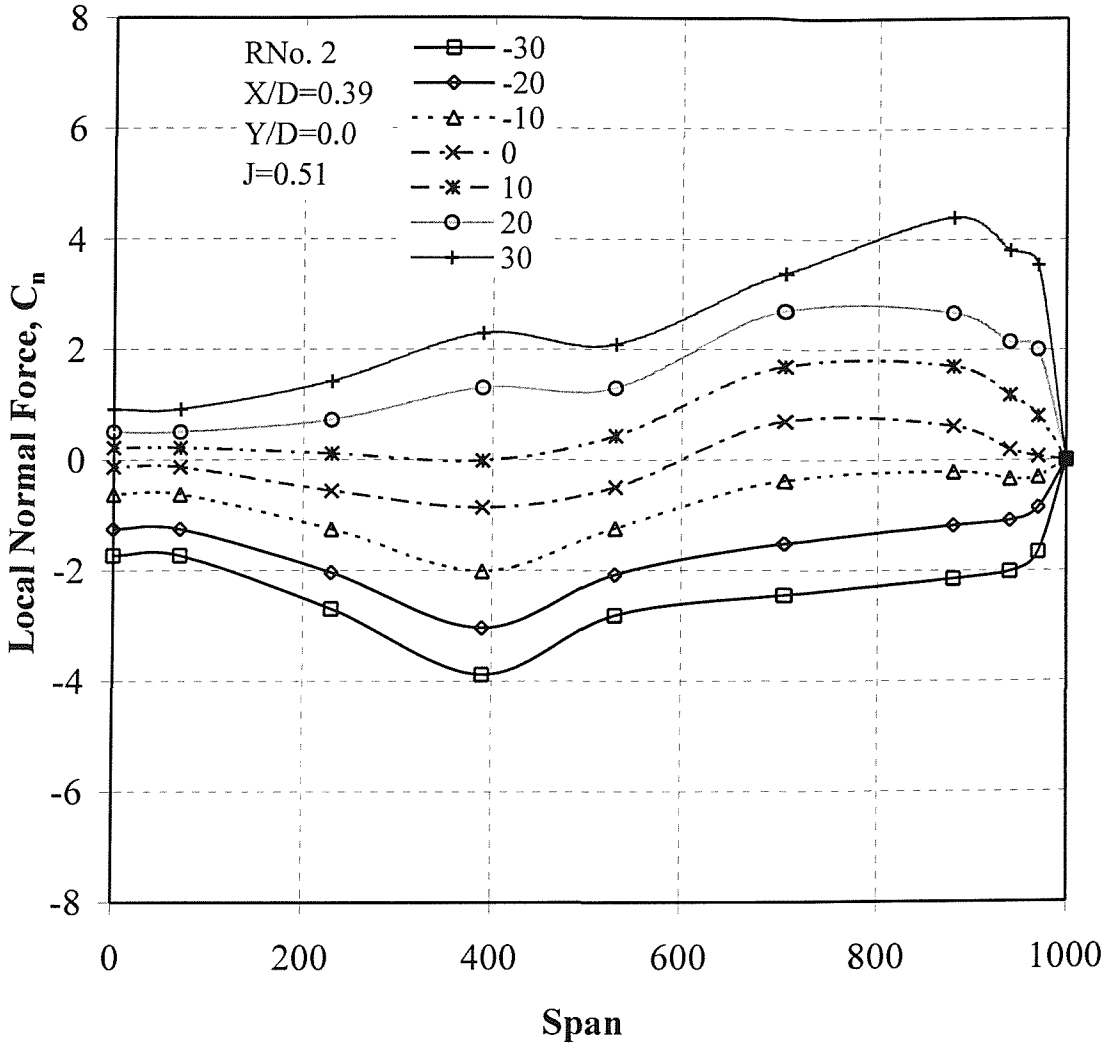

Figure A-32 Variation of Spanwise Distribution of Local Section Cn with incidence for Rudder No. 2 at a propeller advance ratio of J=0.51.

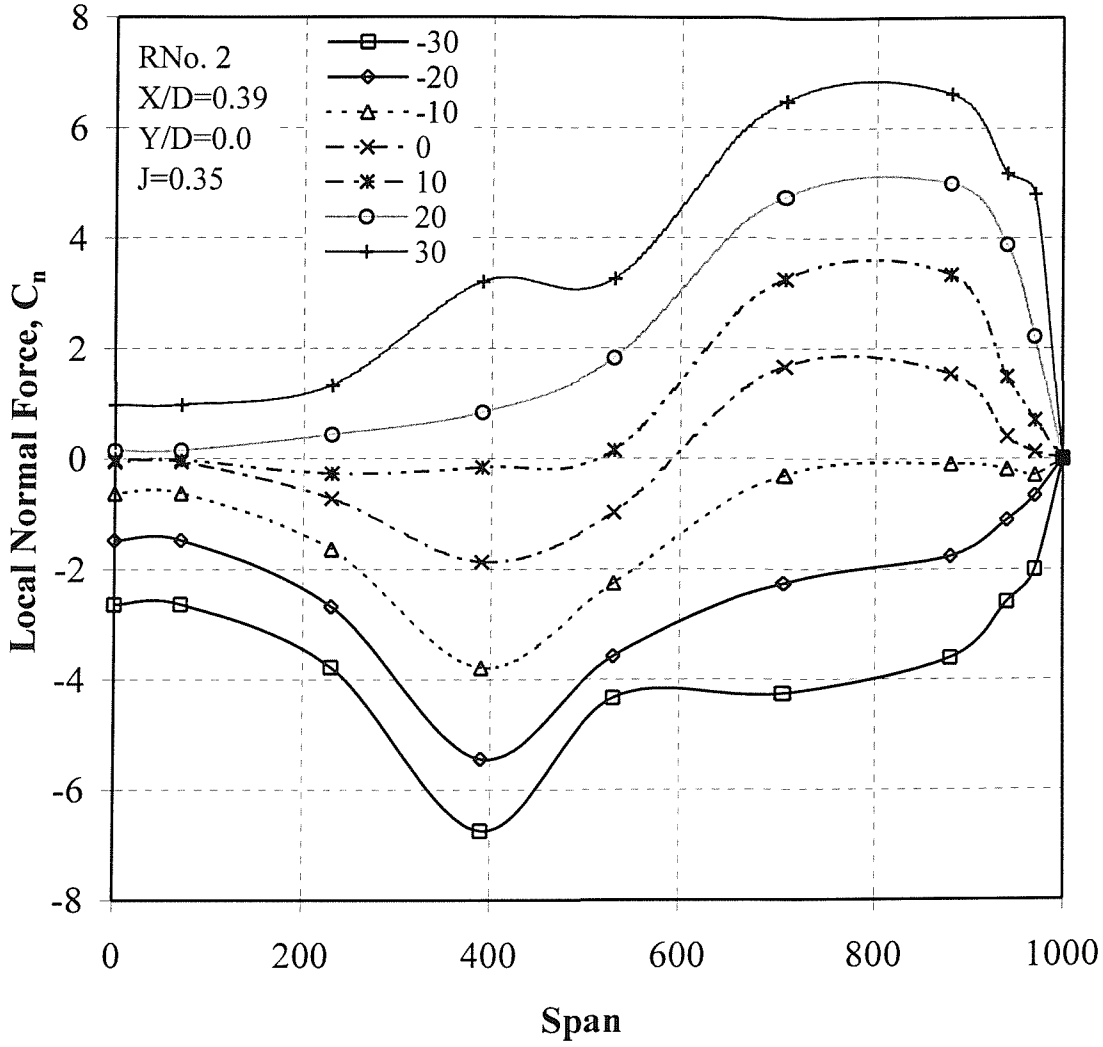

Figure A-33 Variation of Spanwise Distribution of Local Section Cn with incidence for Rudder No. 2 at a propeller advance ratio of J=0.35.

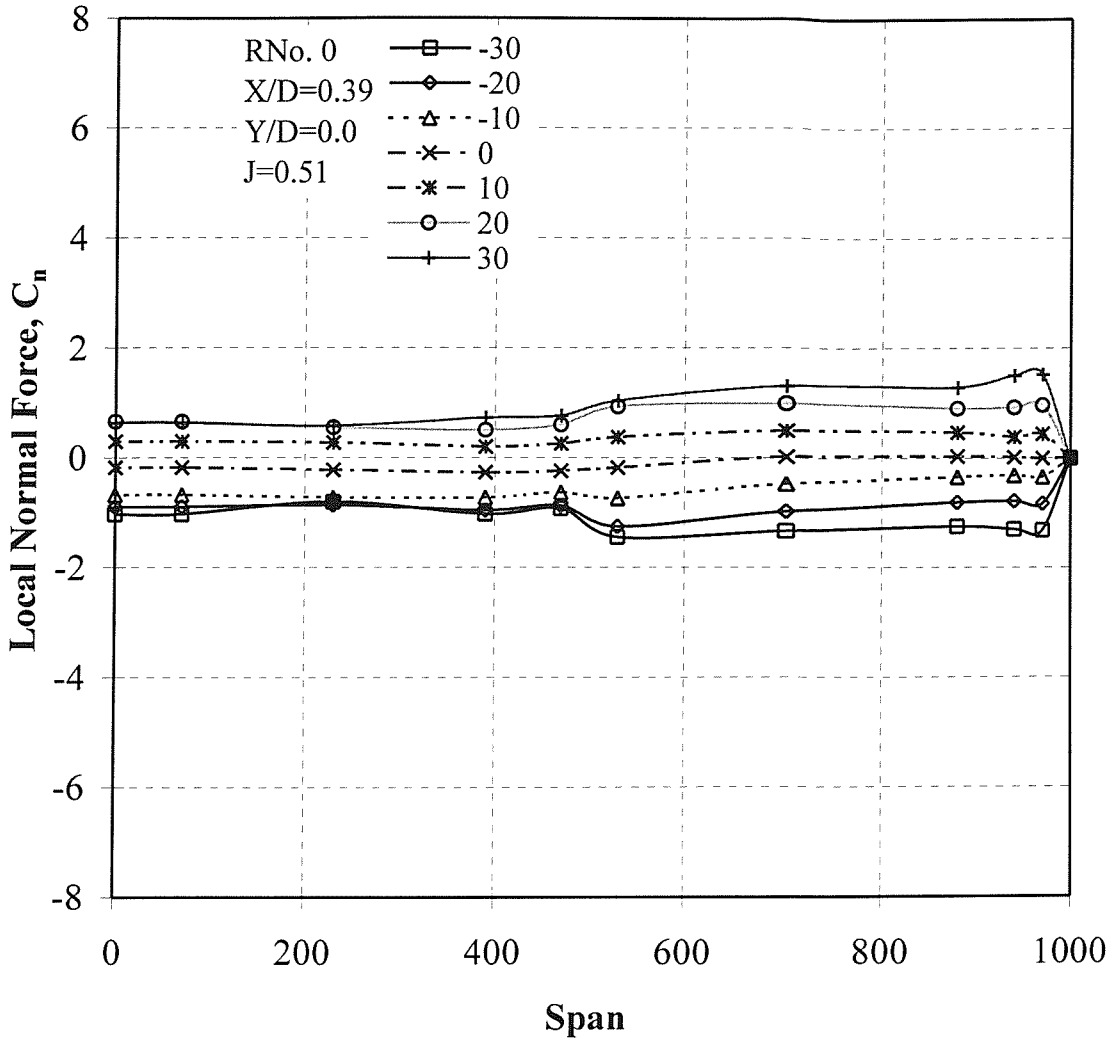

Figure A-34 Variation of Spanwise Distribution of Local Section Cn with incidence for Skeg-Rudder No. 0 at a propeller advance ratio of J=0.94.

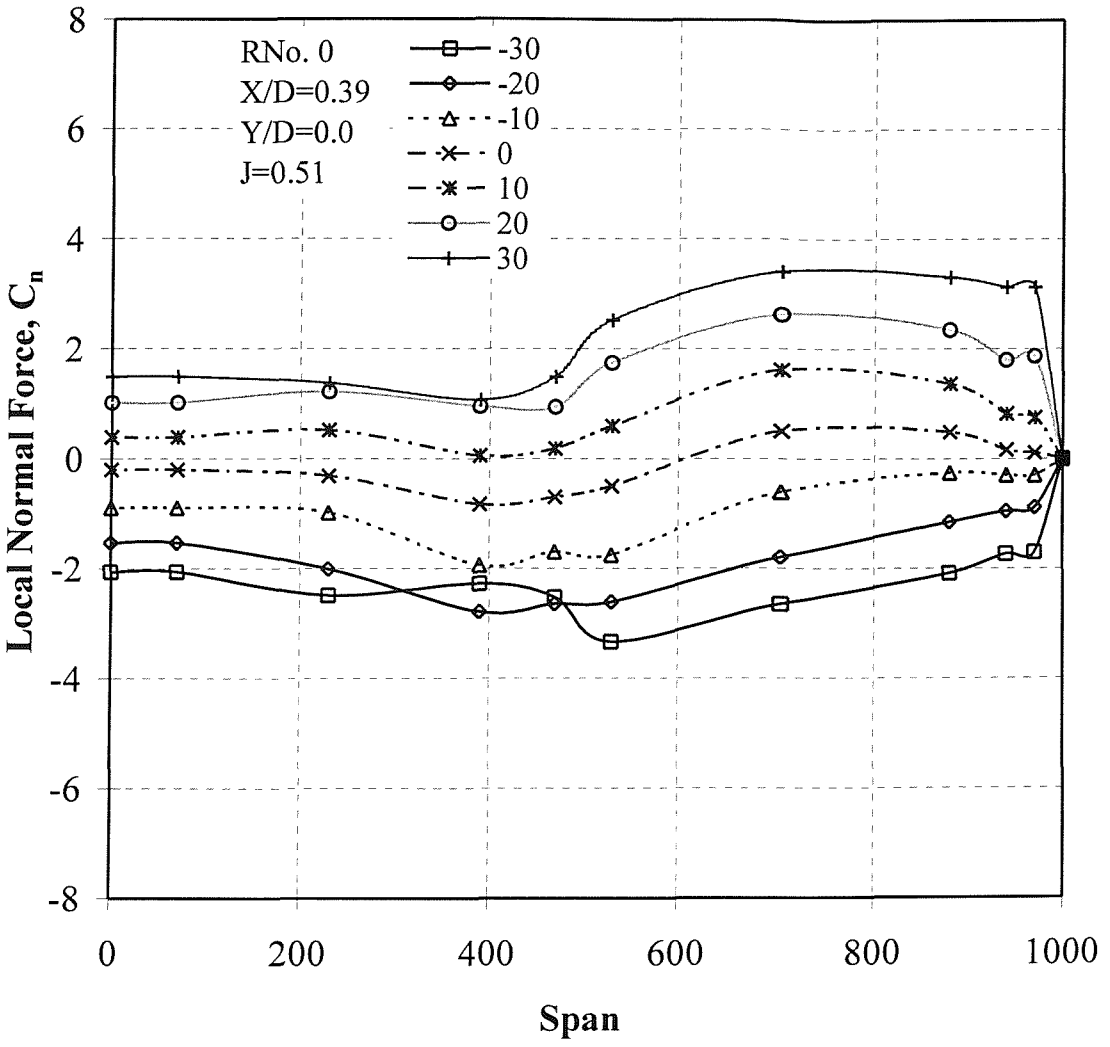

Figure A-35 Variation of Spanwise Distribution of Local Section Cn with incidence for Skeg-Rudder No. 0 at a propeller advance ratio of J=0.51.

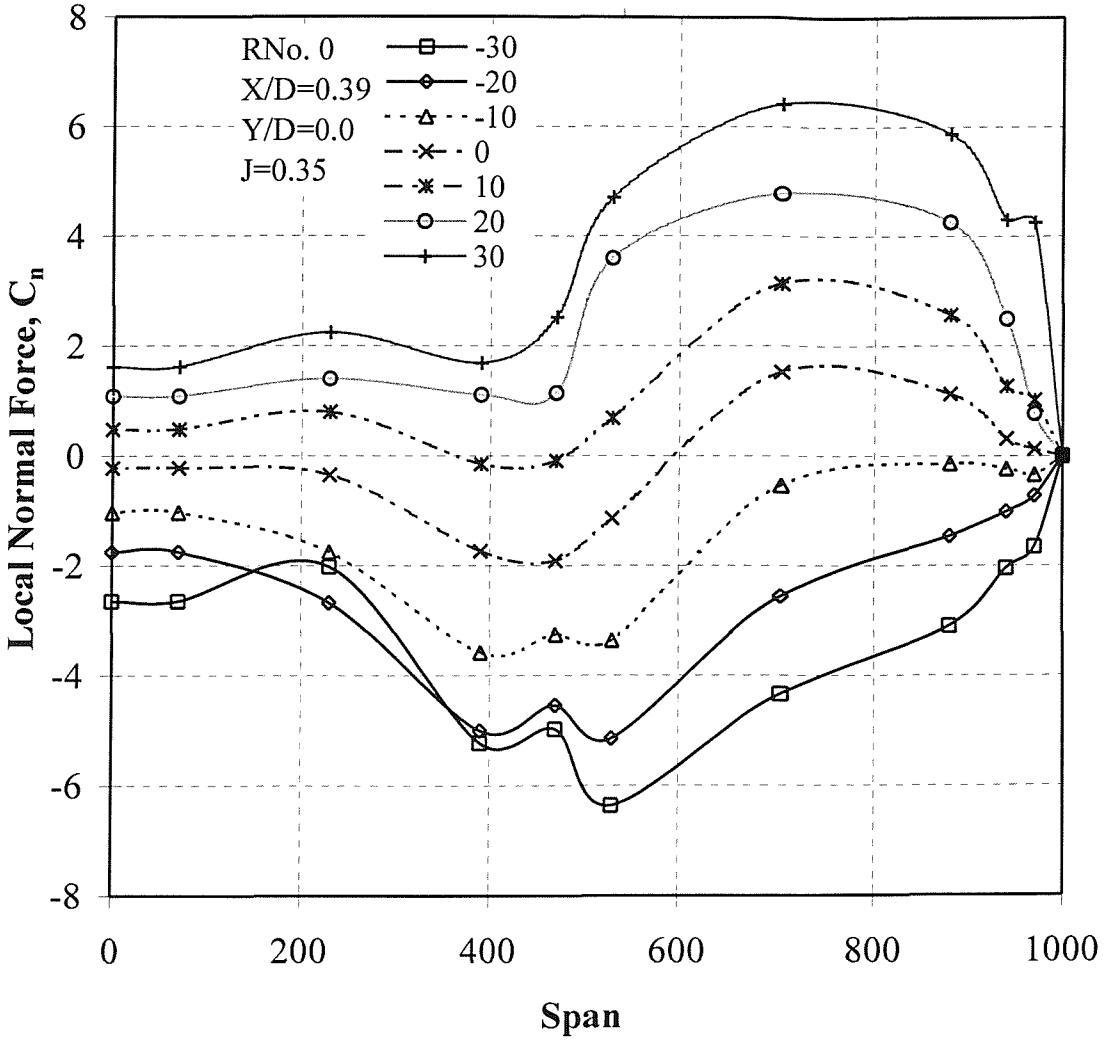

Figure A-36 Variation of Spanwise Distribution of Local Section Cn with incidence for Skeg-Rudder No. 0 at a propeller advance ratio of J=0.35.

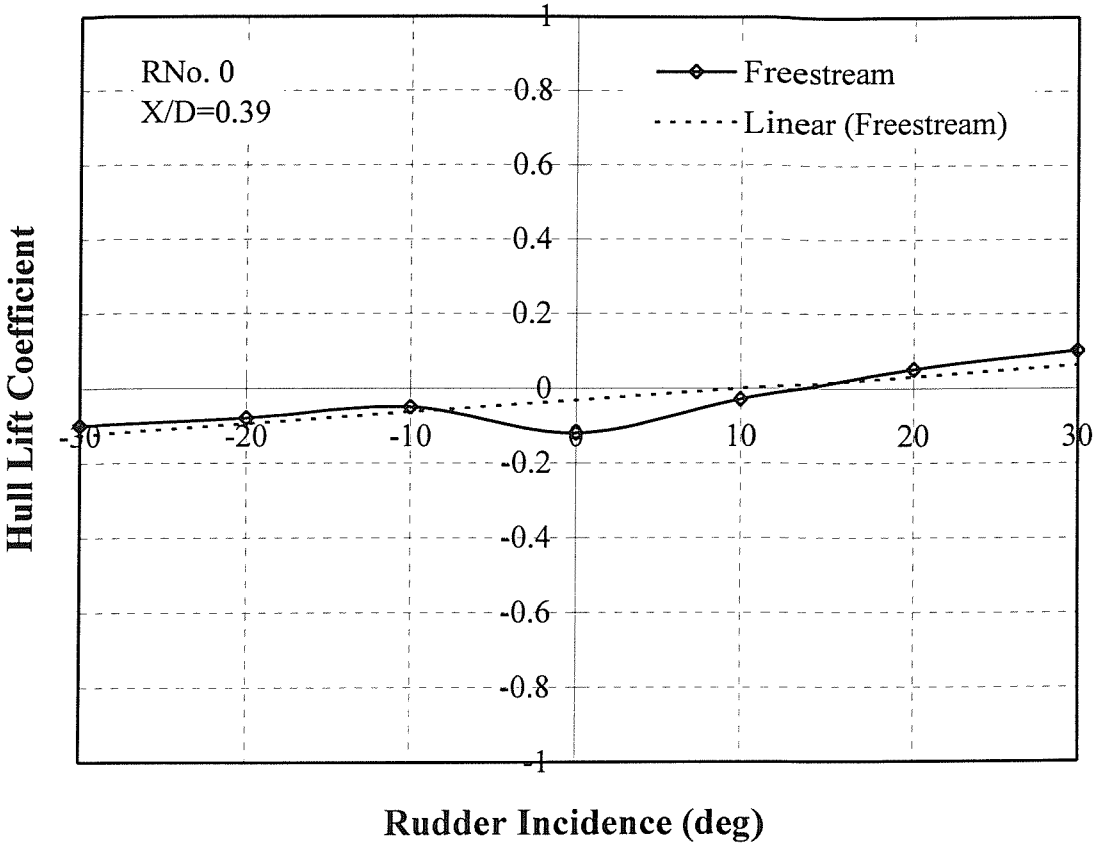

Figure A-37 Hull Lift Performance in Freestream with Skeg Rudder and Stationary Propeller

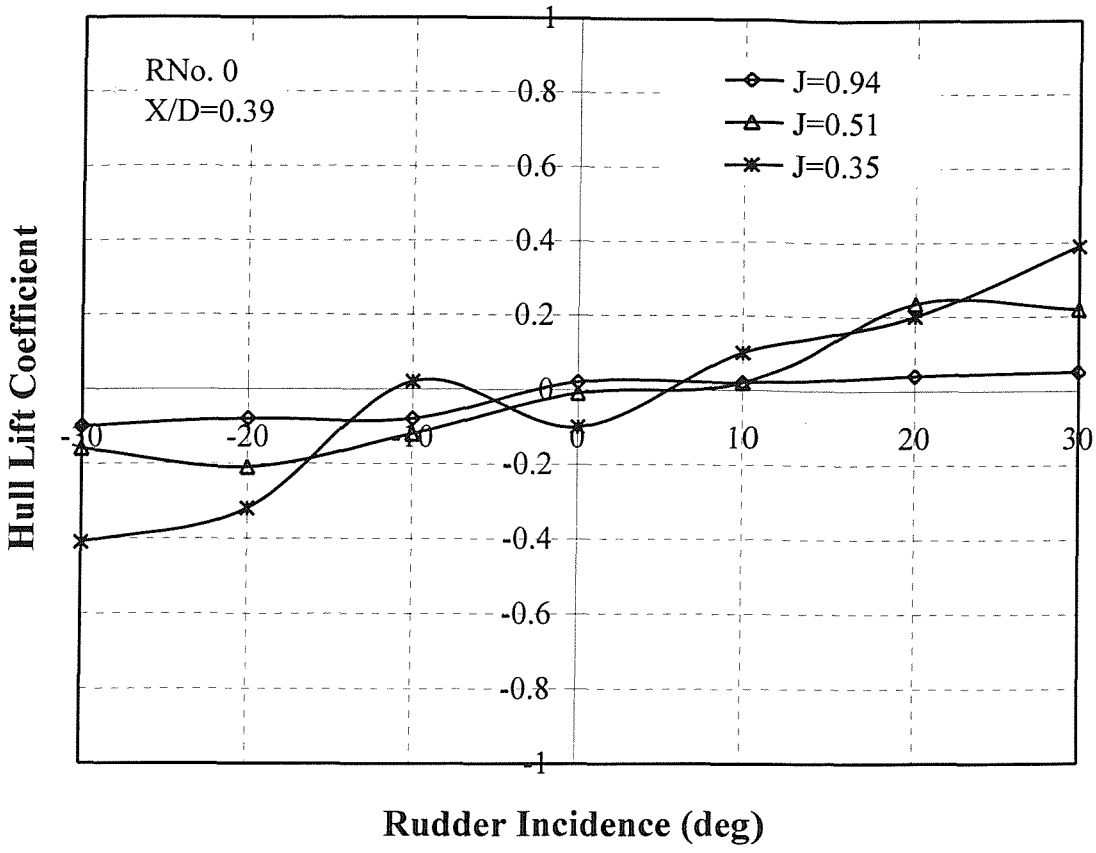

Figure A-38 Influence of Propeller Thrust Loading on the Hull Lift Performance at a Longitudinal Separation of X/D=0.39

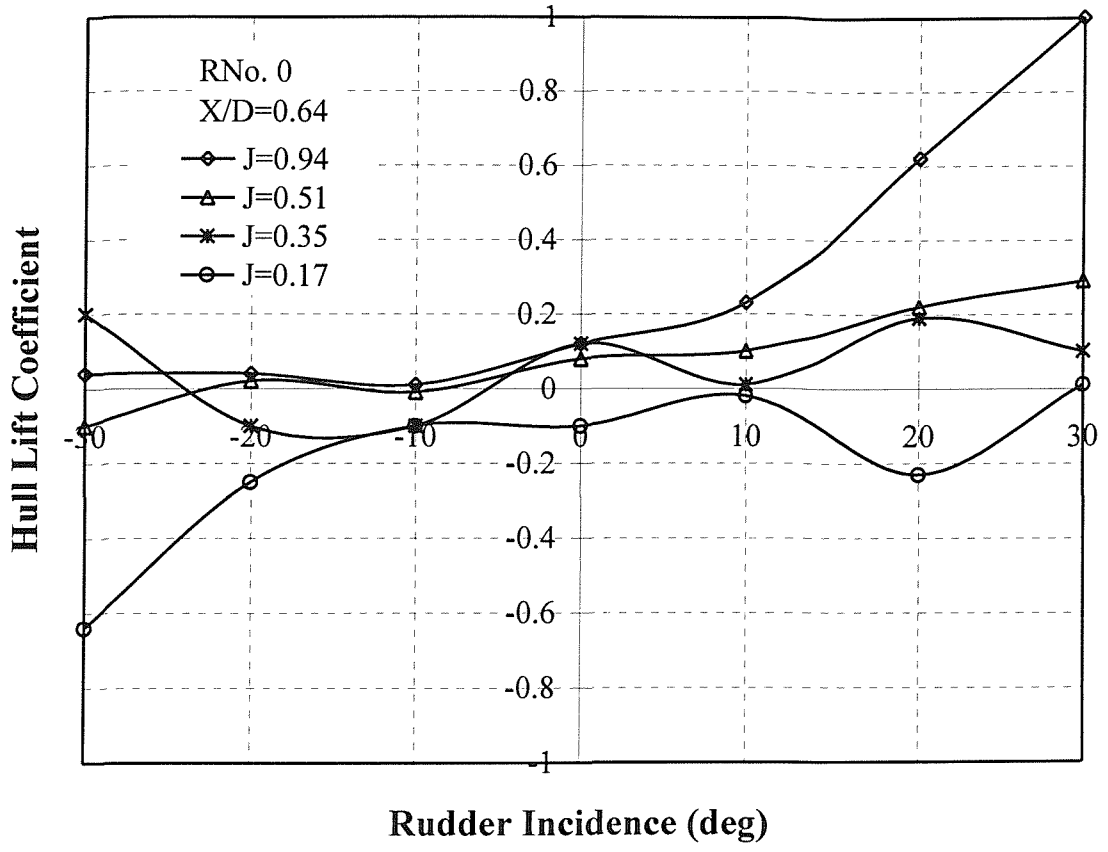

Figure A-39 Influence of Propeller Thrust Loading on the Hull Lift Performance at a Longitudinal Separation of X/D=0.64

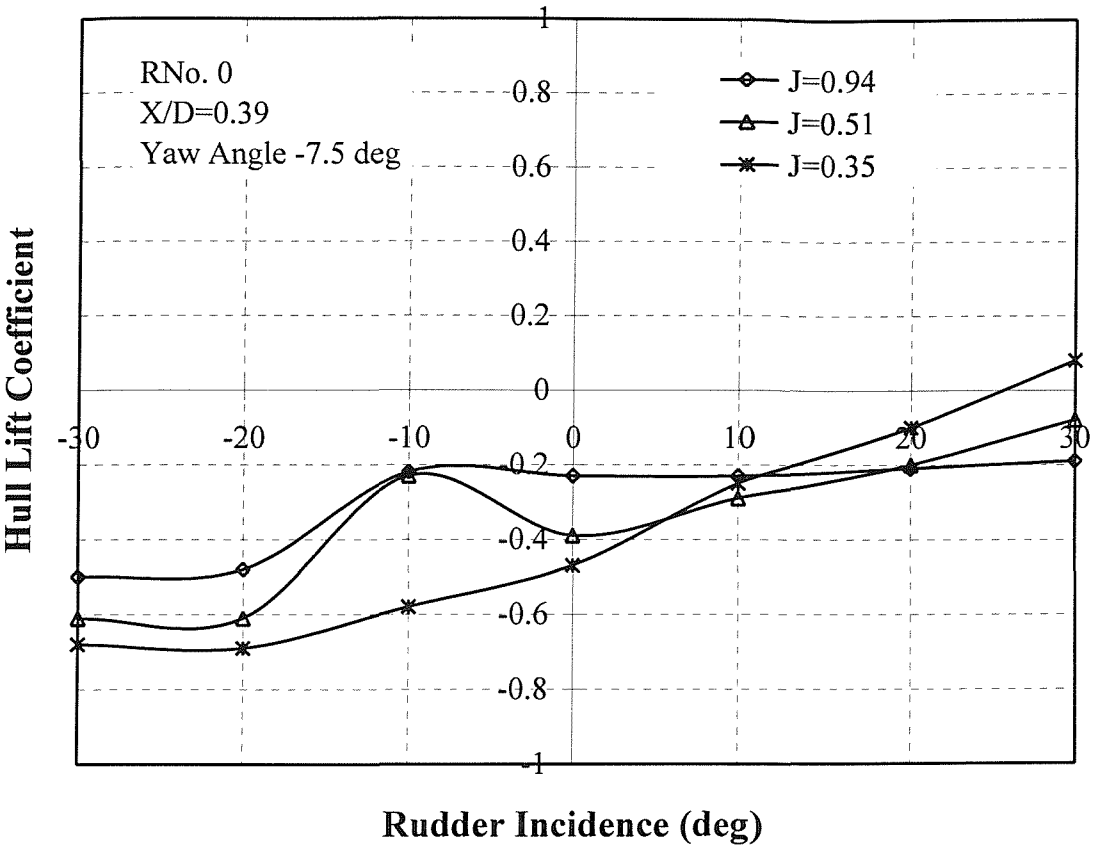

Figure A-40 Influence of Propeller Thrust Loading on the Hull Lift Performance at a Longitudinal Separation of X/D=0.39 and at a Yaw Angle of -7.5 degrees

APPENDIX B - PLOTS OF RESULTS FROM LABORATORY TESTS

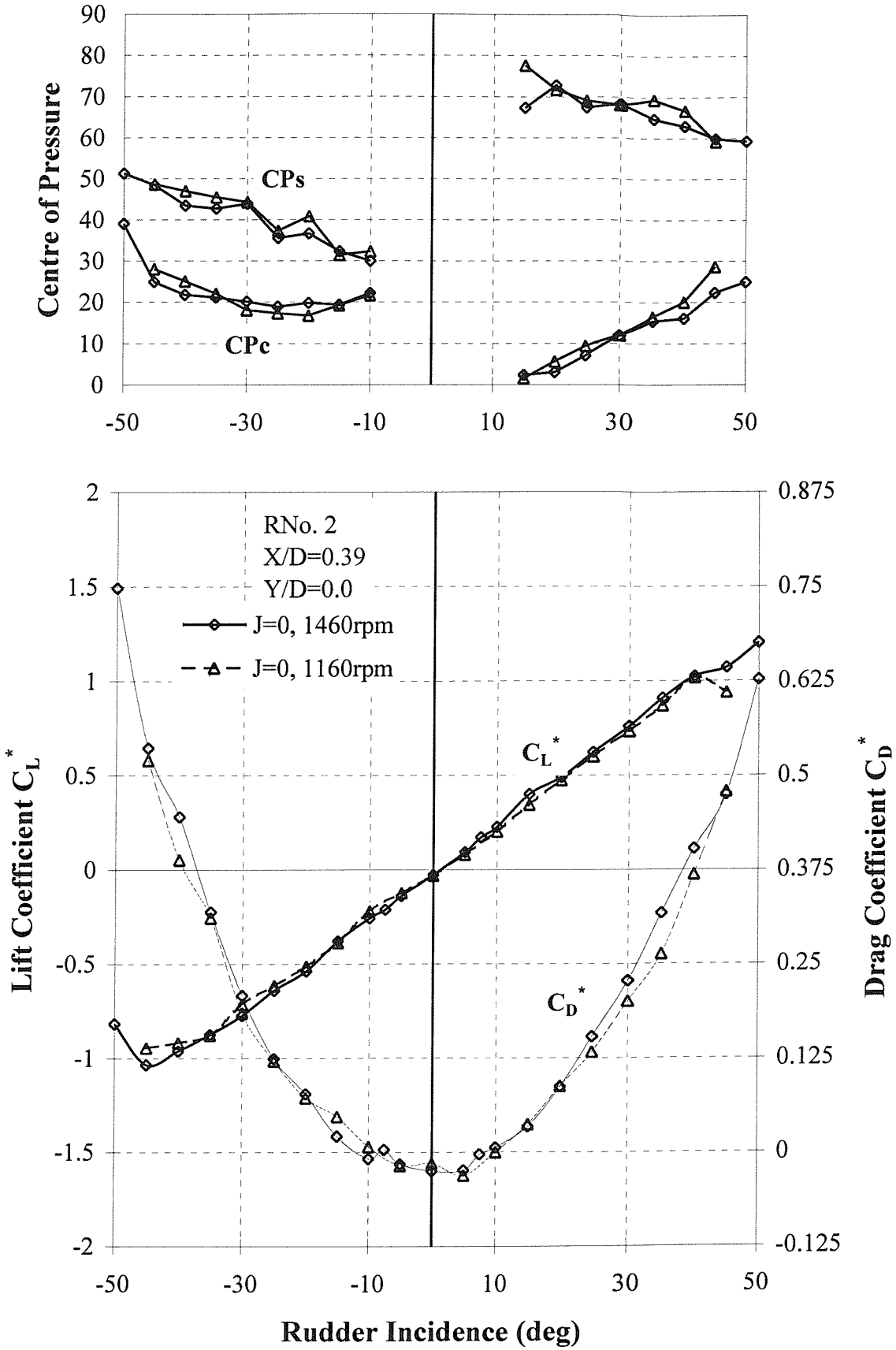

Figure B-1 **Influence of Propeller RPM at Zero Advance Ratio (J=0) on the Performance of All-Movable Rudder No. 2**

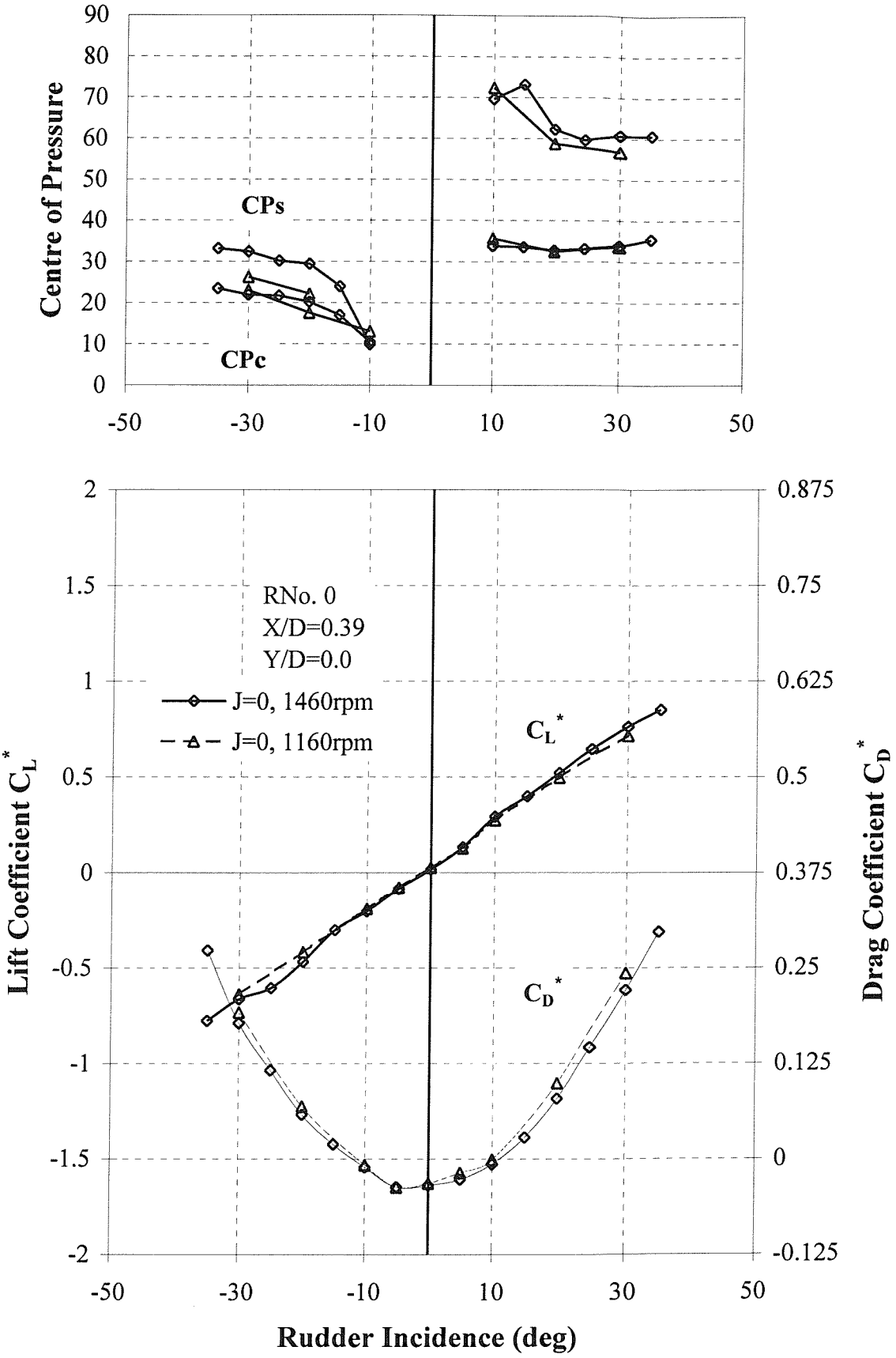

Figure B-2 **Influence of Propeller RPM at Zero Advance Ratio (J=0) on the Performance of Skeg-Rudder No. 0**

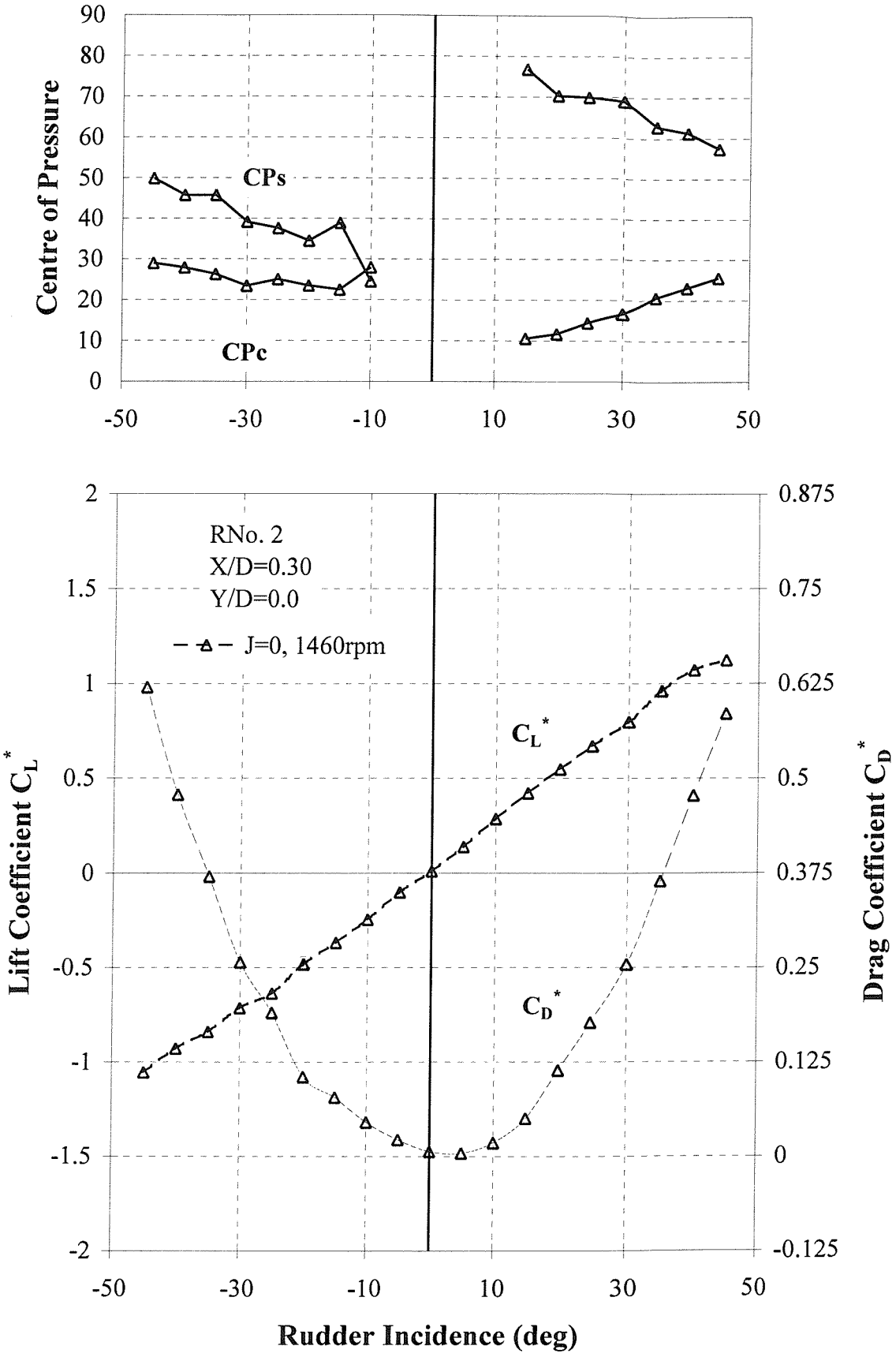

Figure B-3 **Influence of Propeller at Zero Advance Ratio (J=0) on the Performance of All-Movable Rudder No. 2 at a Longitudinal Separation of X/D=0.30.**

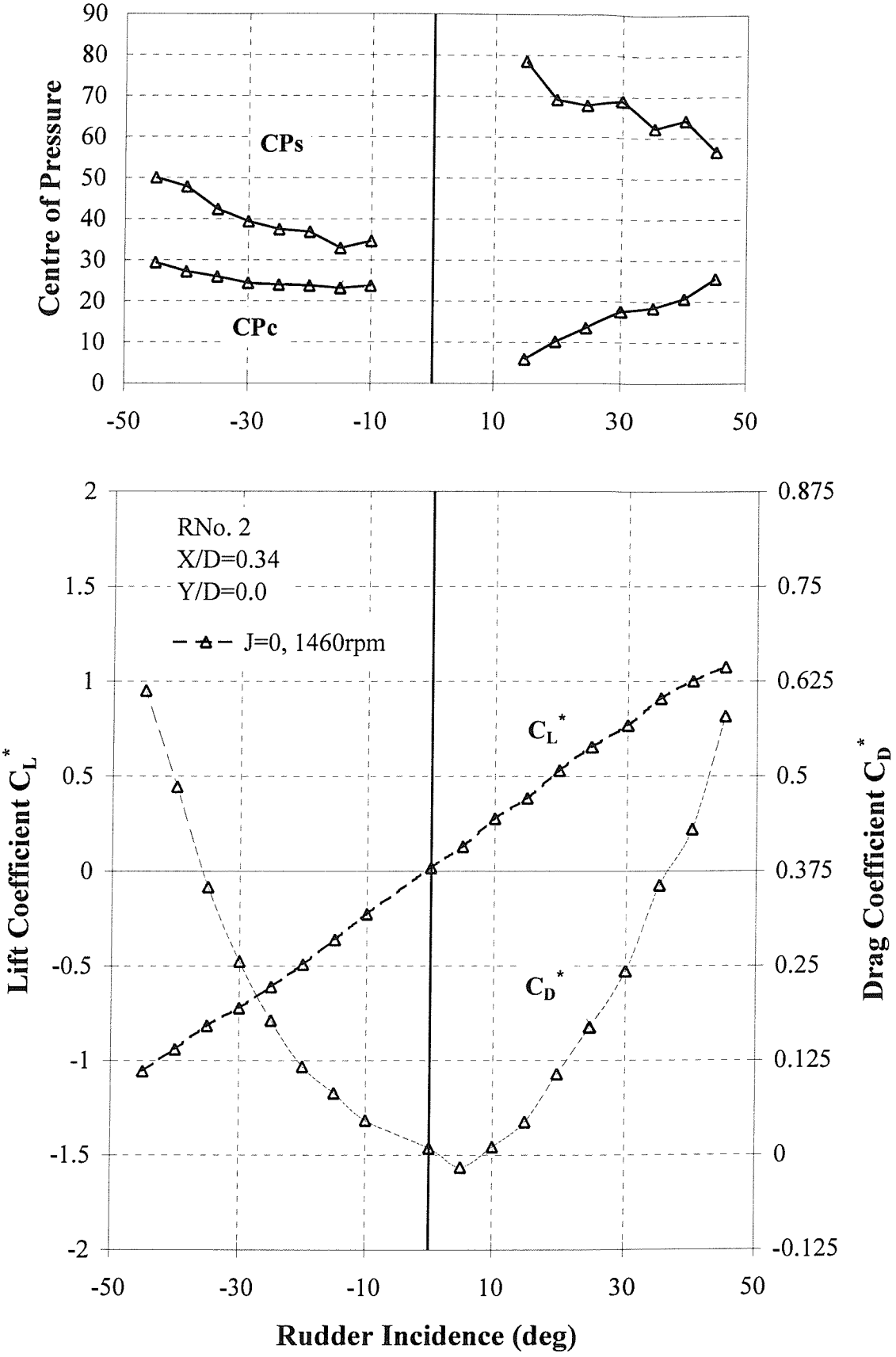

Figure B-4 **Influence of Propeller at Zero Advance Ratio (J=0) on the Performance of All-Movable Rudder No. 2 at a Longitudinal Separation of X/D=0.34.**

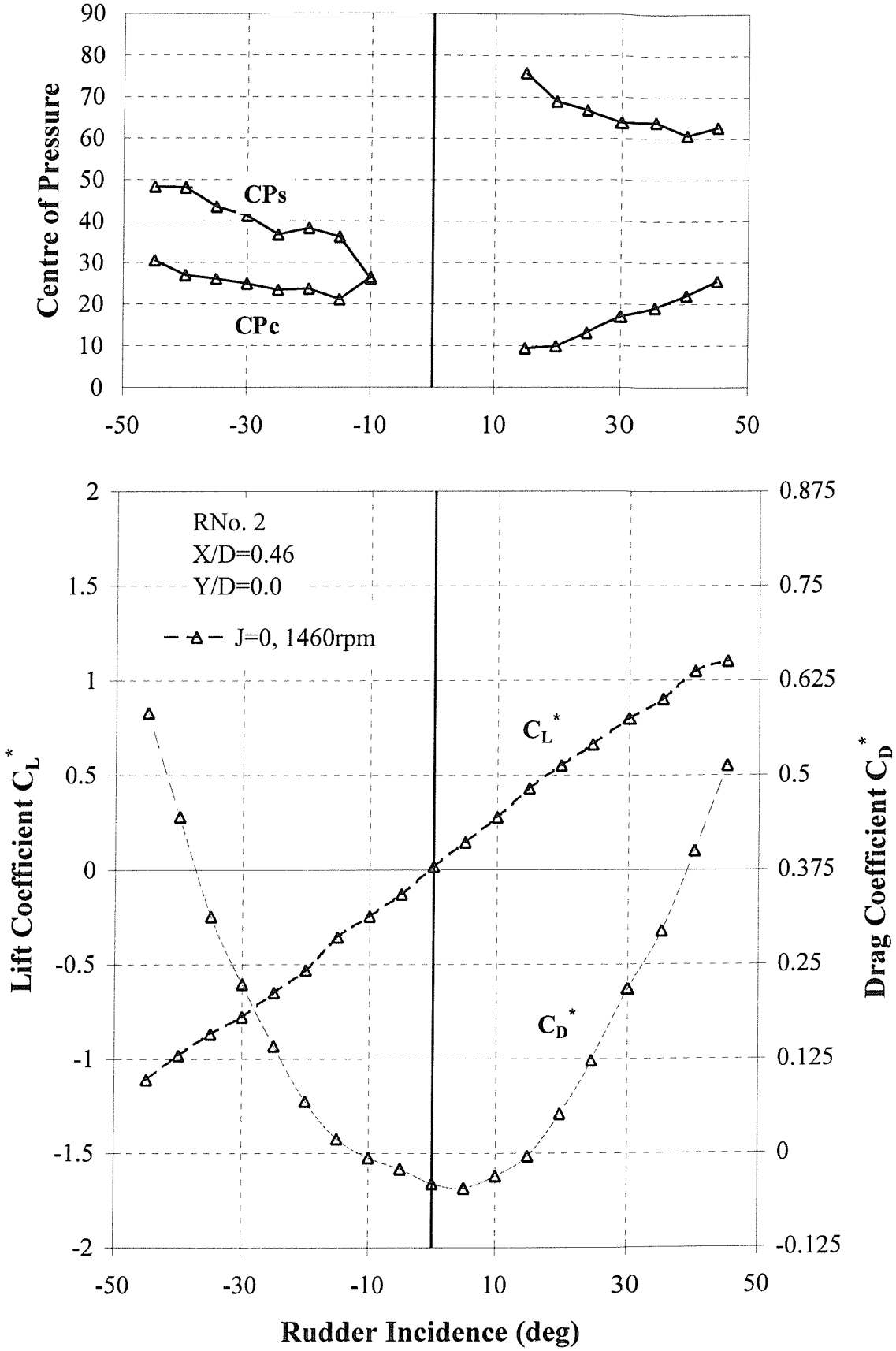

Figure B-5 **Influence of Propeller at Zero Advance Ratio (J=0) on the Performance of All-Movable Rudder No. 2 at a Longitudinal Separation of X/D=0.46.**

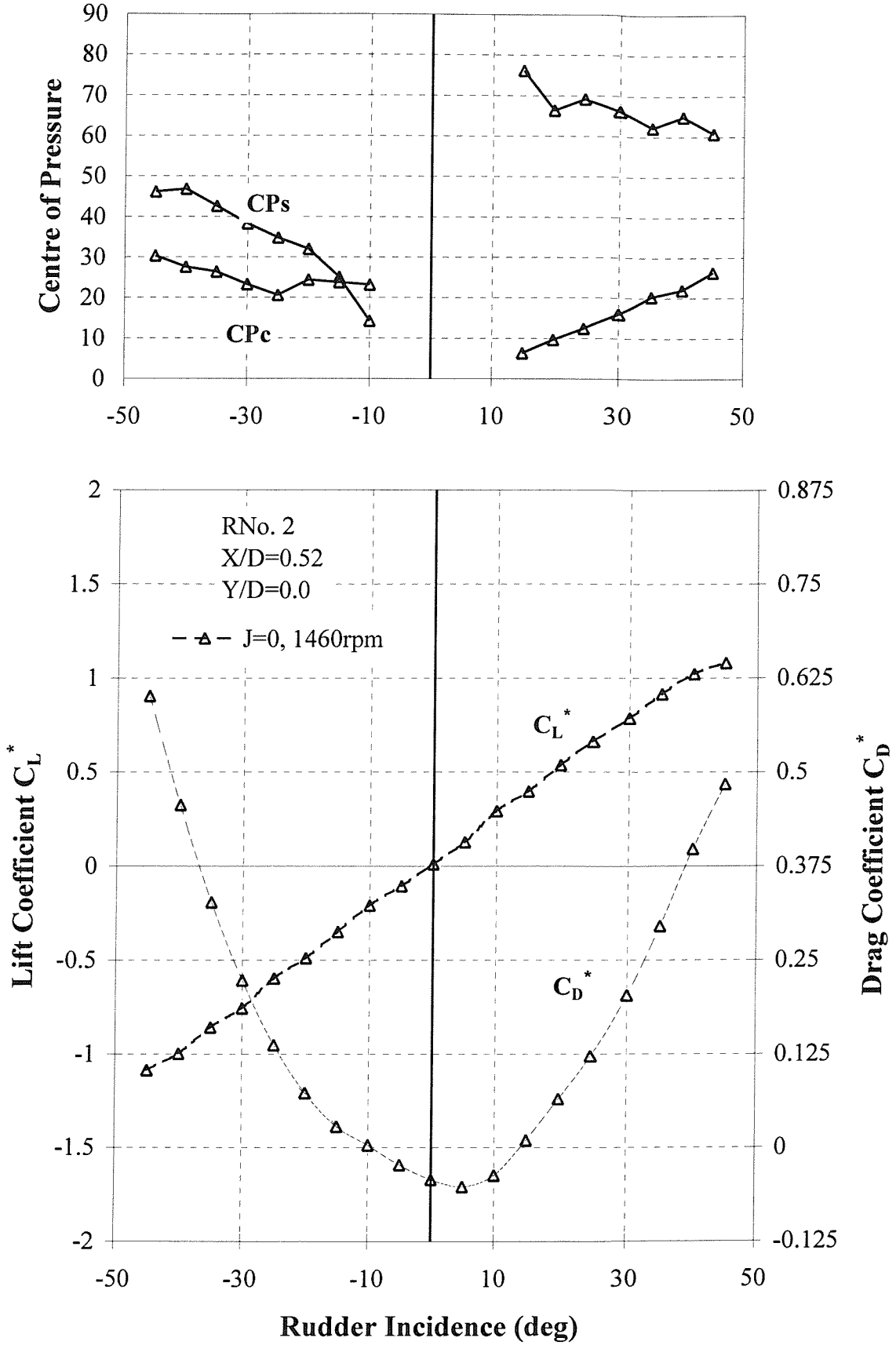

Figure B-6 **Influence of Propeller at Zero Advance Ratio (J=0) on the Performance of All-Movable Rudder No. 2 at a Longitudinal Separation of X/D=0.52.**

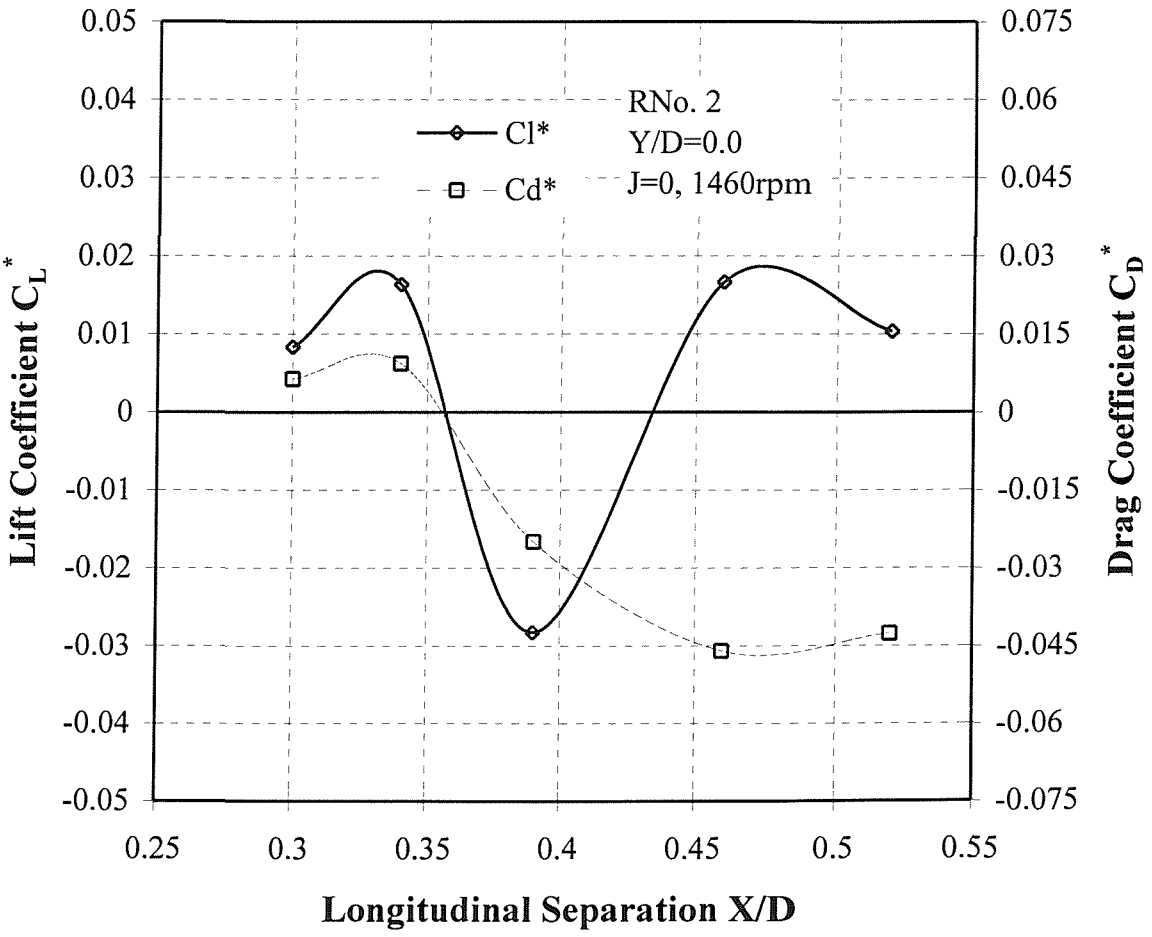

Figure B-7 **Influence of Longitudinal Separation (X/D) on Lift and Drag at Zero Incidence of All-Movable Rudder No. 2 at Zero Advance Ratio (J=0)**

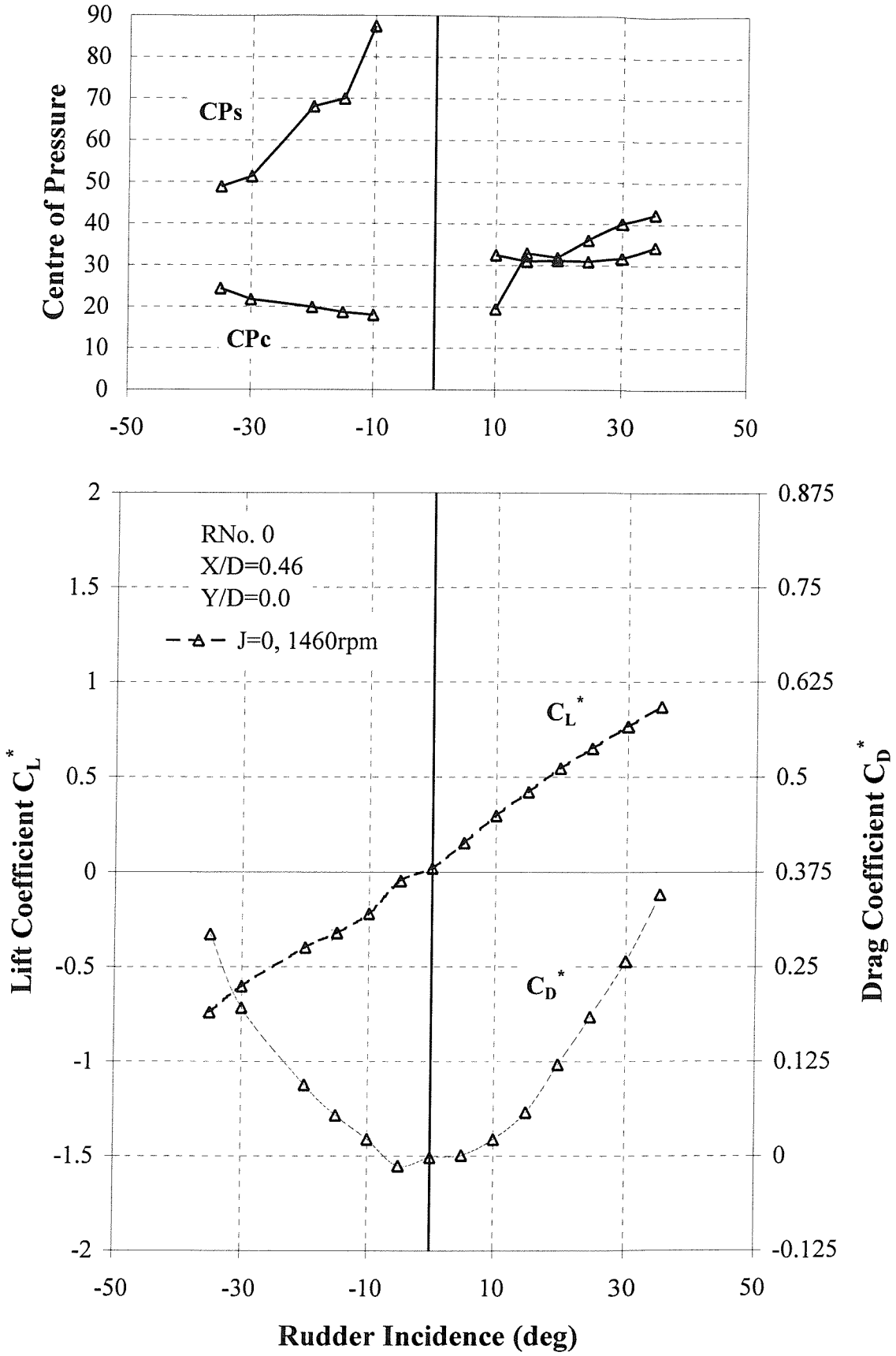

Figure B-8 **Influence of Propeller at Zero Advance Ratio (J=0) on the Performance of Skeg-Rudder No. 0 at a Longitudinal Separation of X/D=0.46.**

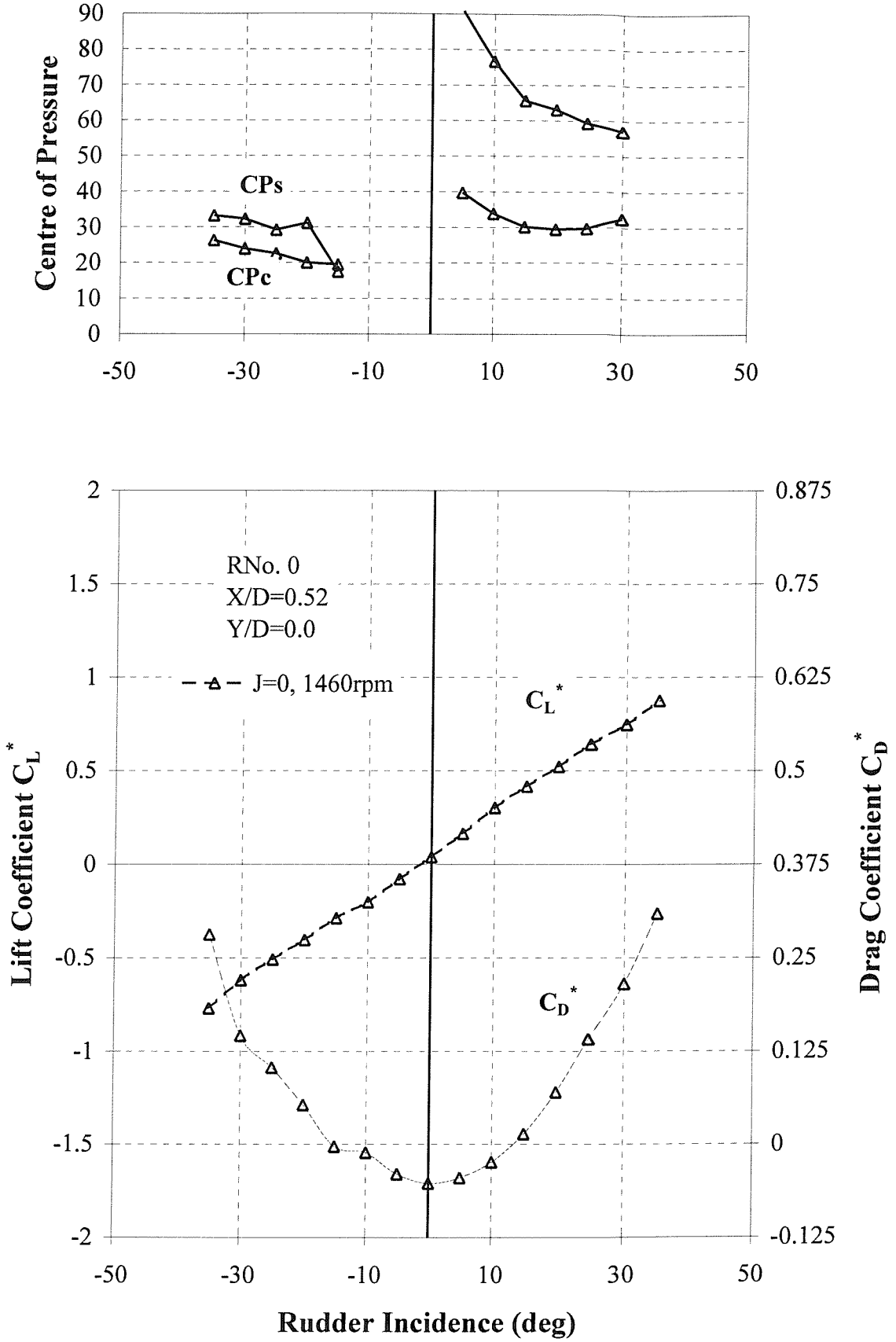

Figure B-9 **Influence of Propeller at Zero Advance Ratio (J=0) on the Performance of Skeg-Rudder No. 0 at a Longitudinal Separation of X/D=052.**

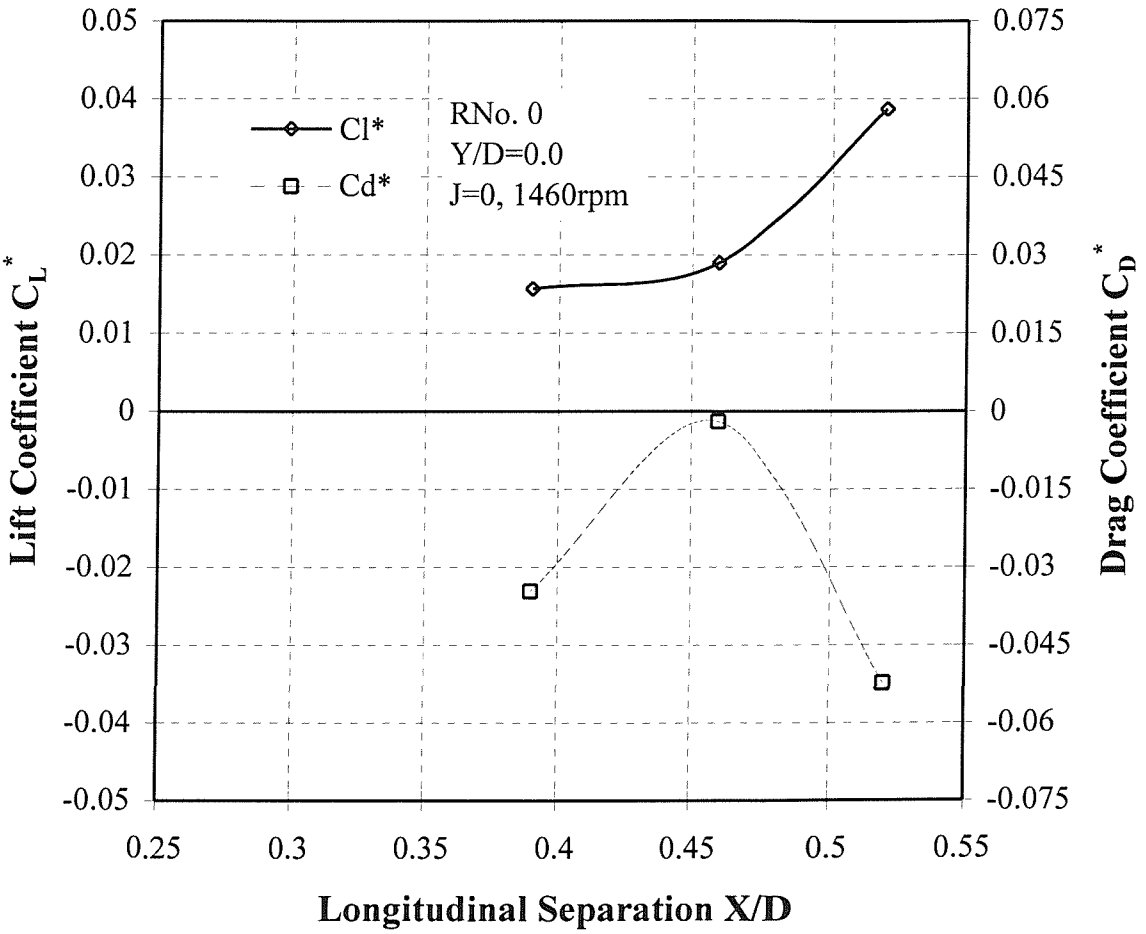

Figure B-10 **Influence of Longitudinal Separation (X/D) on Lift and Drag at Zero Incidence of Skeg-Rudder No. 0 at Zero Advance Ratio (J=0)**

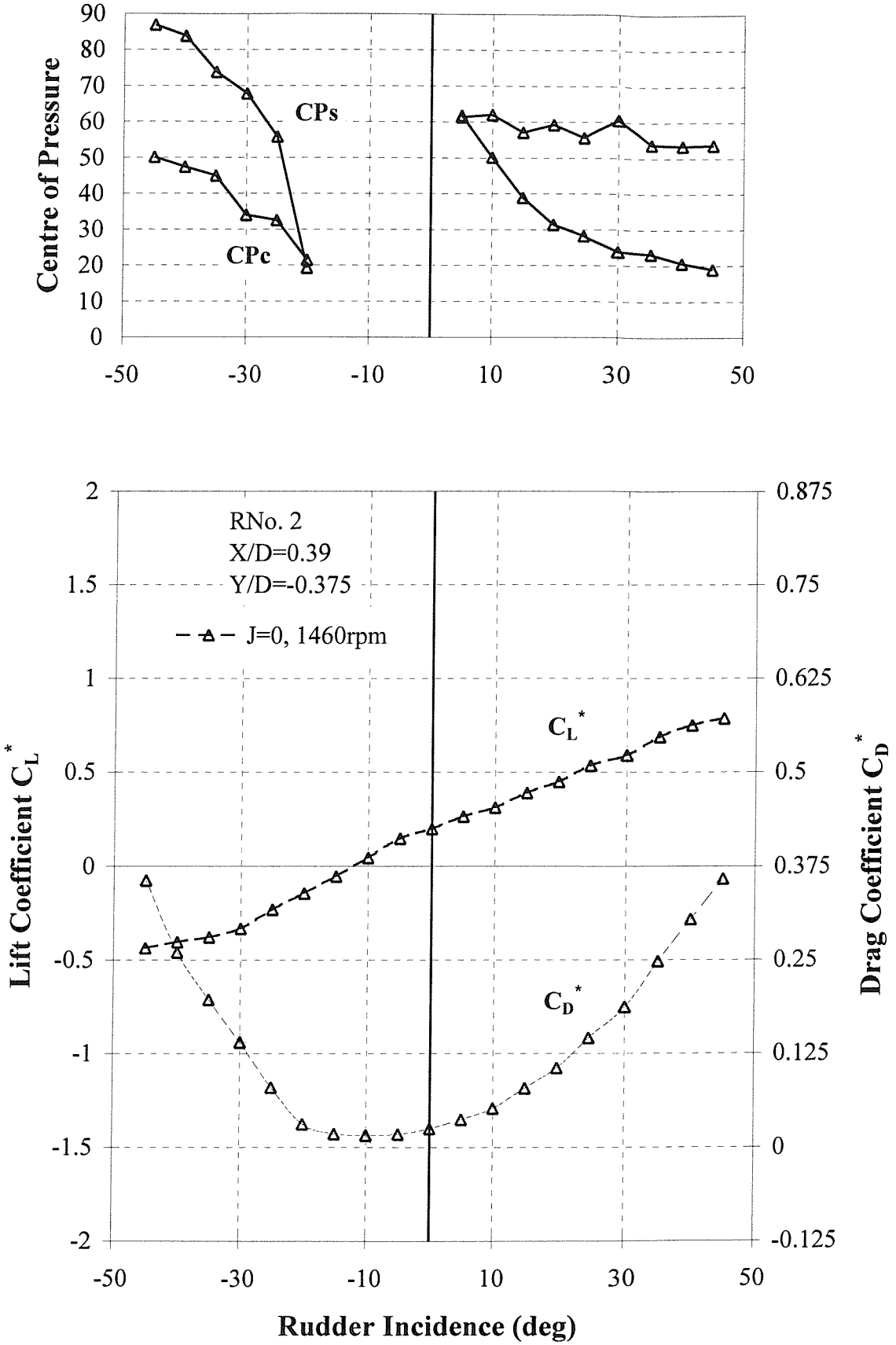

Figure B-11 **Influence of Propeller at Zero Advance Ratio (J=0) on the Performance of All-Movable Rudder No. 2 at a Lateral Separation of Y/D=-0.375**

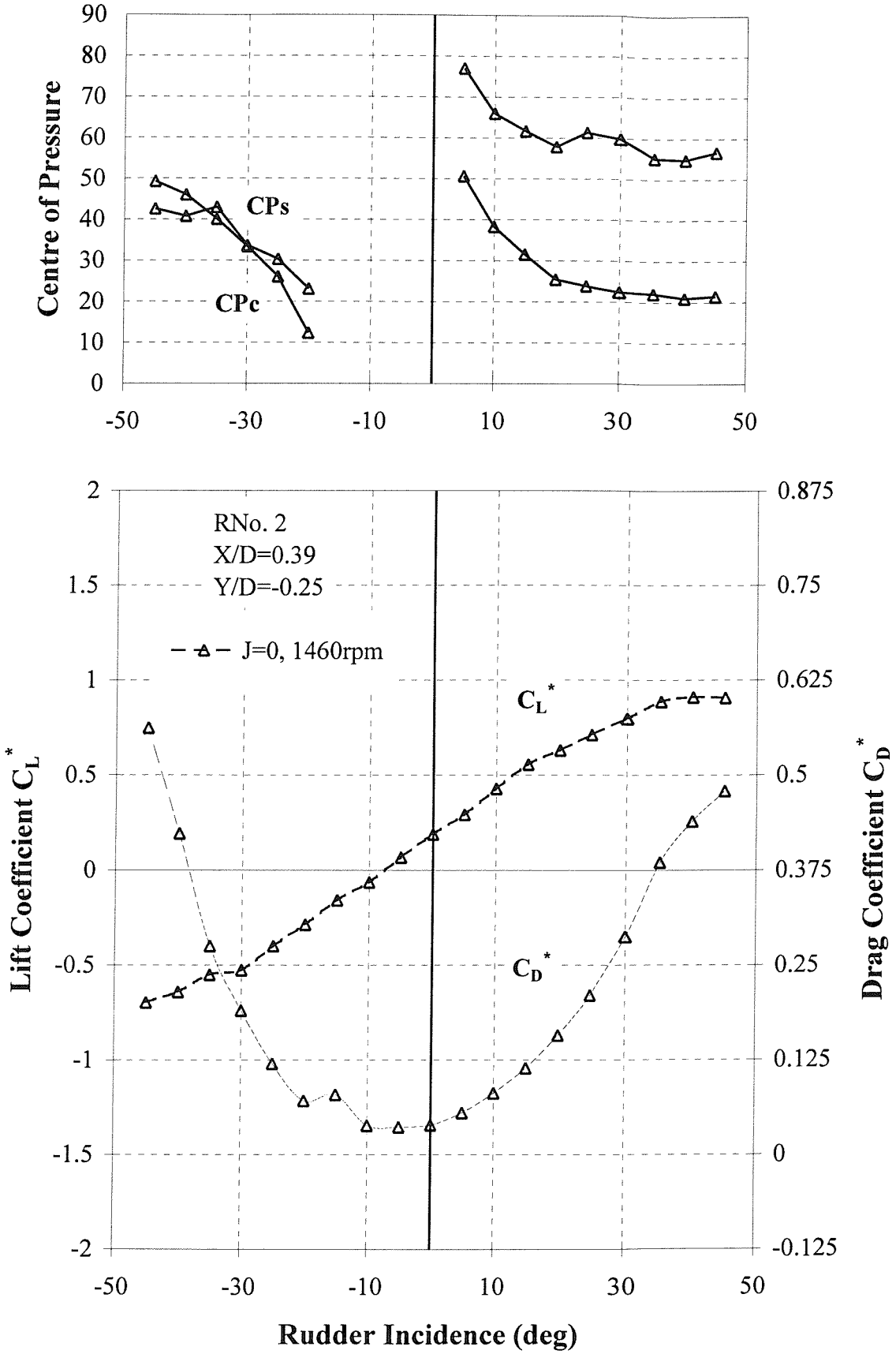

Figure B-12 Influence of Propeller at Zero Advance Ratio (J=0) on the Performance of All-Movable Rudder No. 2 at a Lateral Separation of Y/D=-0.25

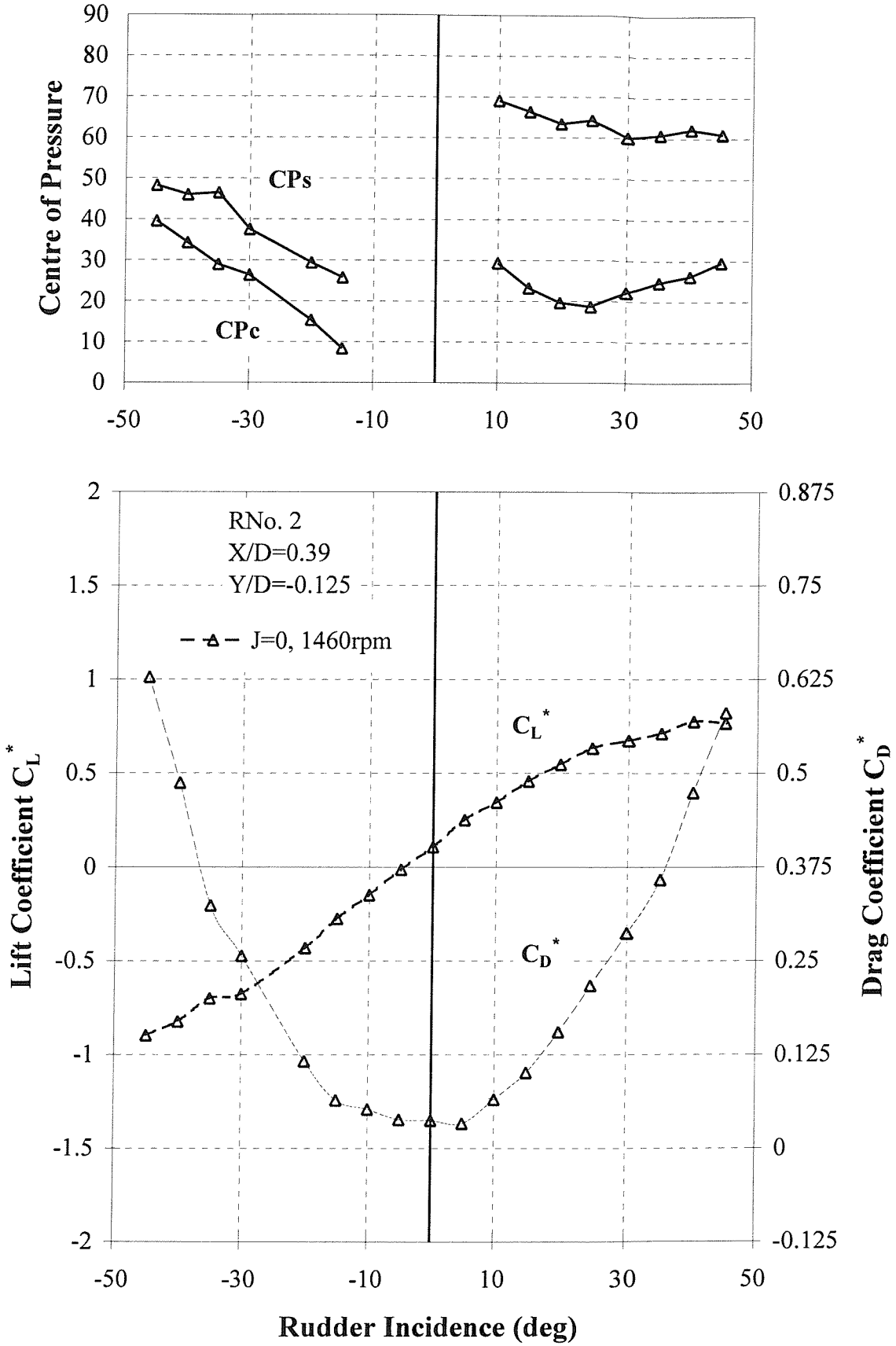

Figure B-13 **Influence of Propeller at Zero Advance Ratio (J=0) on the Performance of All-Movable Rudder No. 2 at a Lateral Separation of Y/D=-0.125**

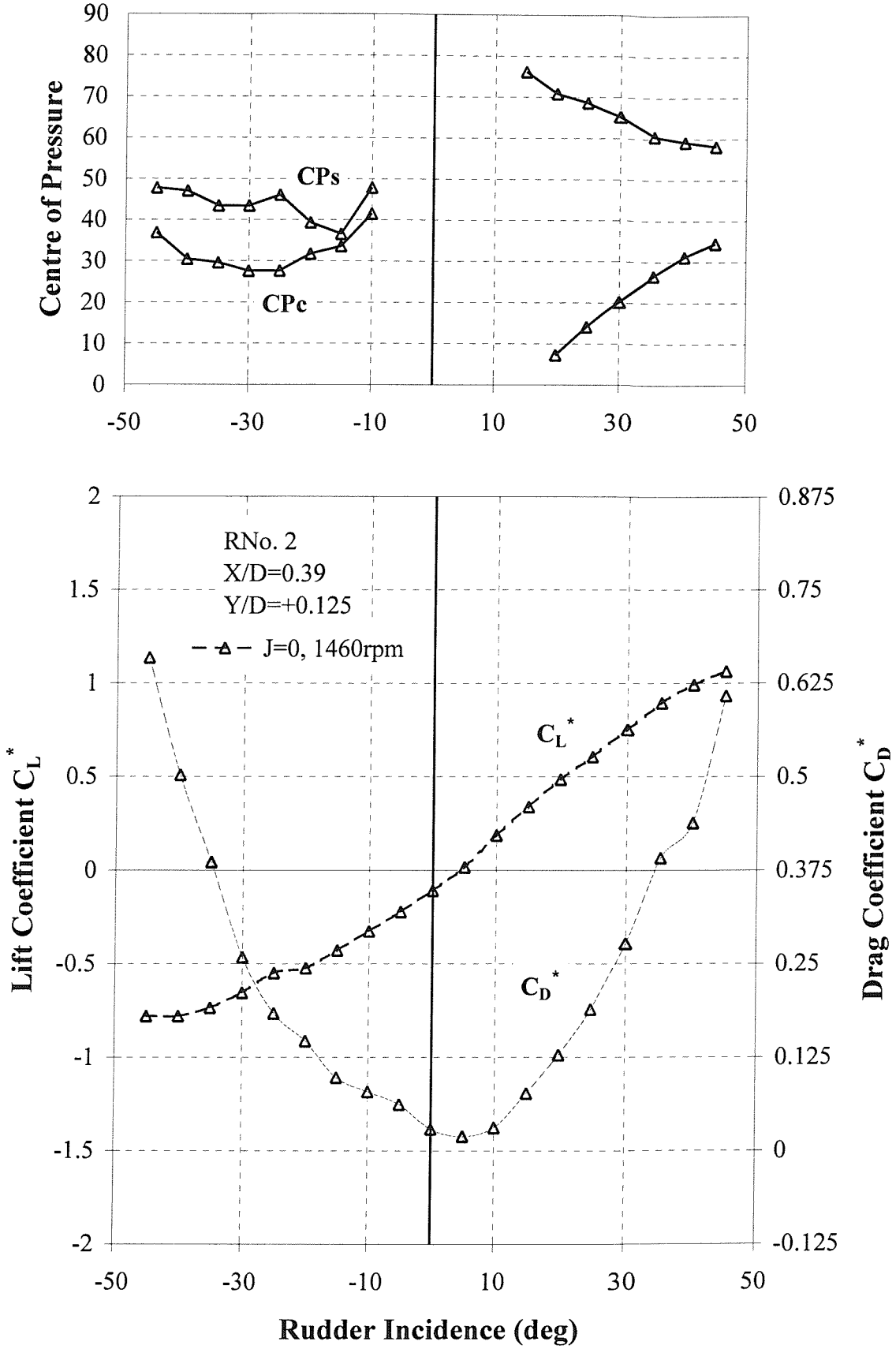

Figure B-14 **Influence of Propeller at Zero Advance Ratio (J=0) on the Performance of All-Movable Rudder No. 2 at a Lateral Separation of Y/D=+0.125**

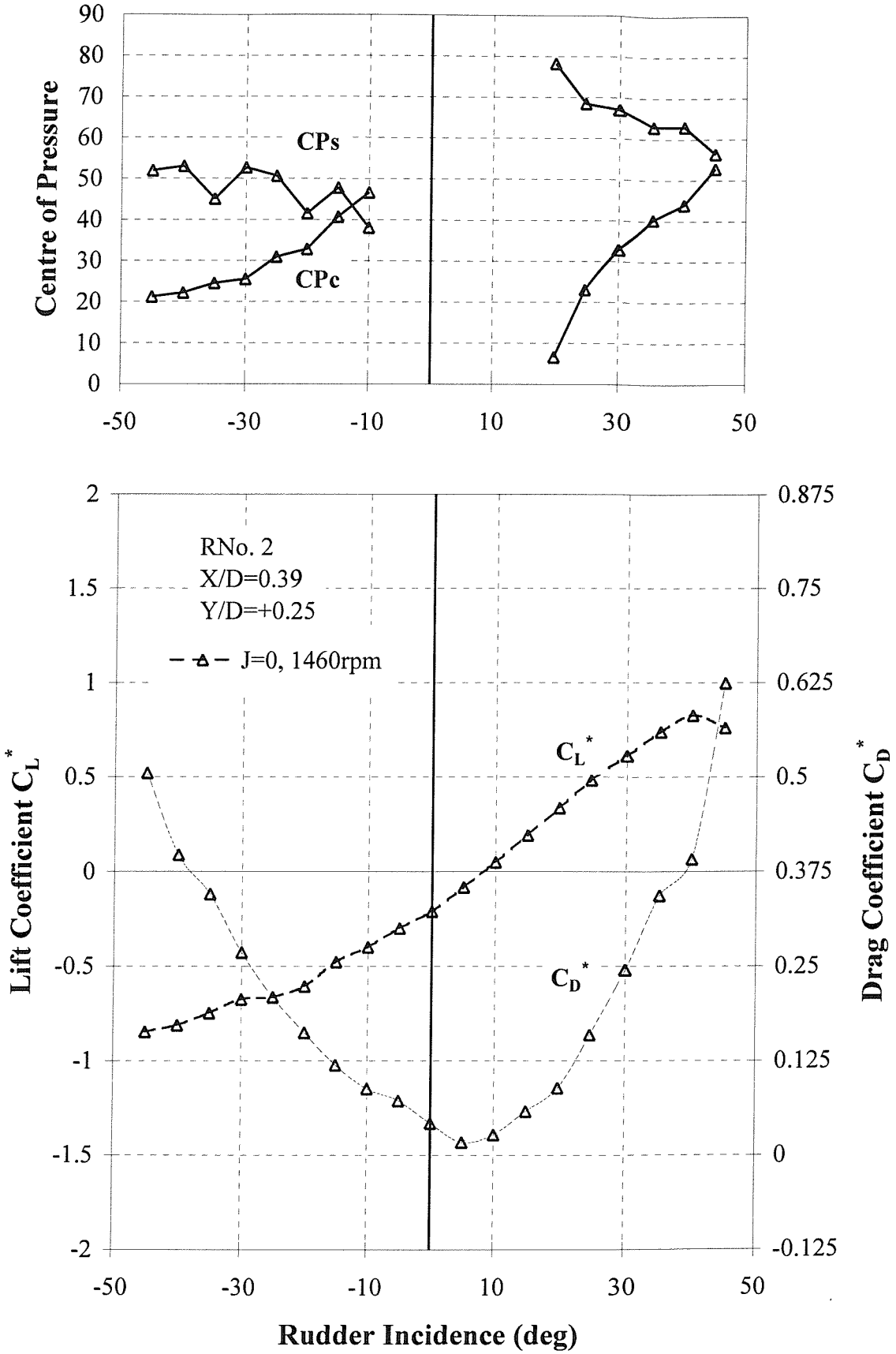

Figure B-15 **Influence of Propeller at Zero Advance Ratio (J=0) on the Performance of All-Movable Rudder No. 2 at a Lateral Separation of Y/D=+0.25**

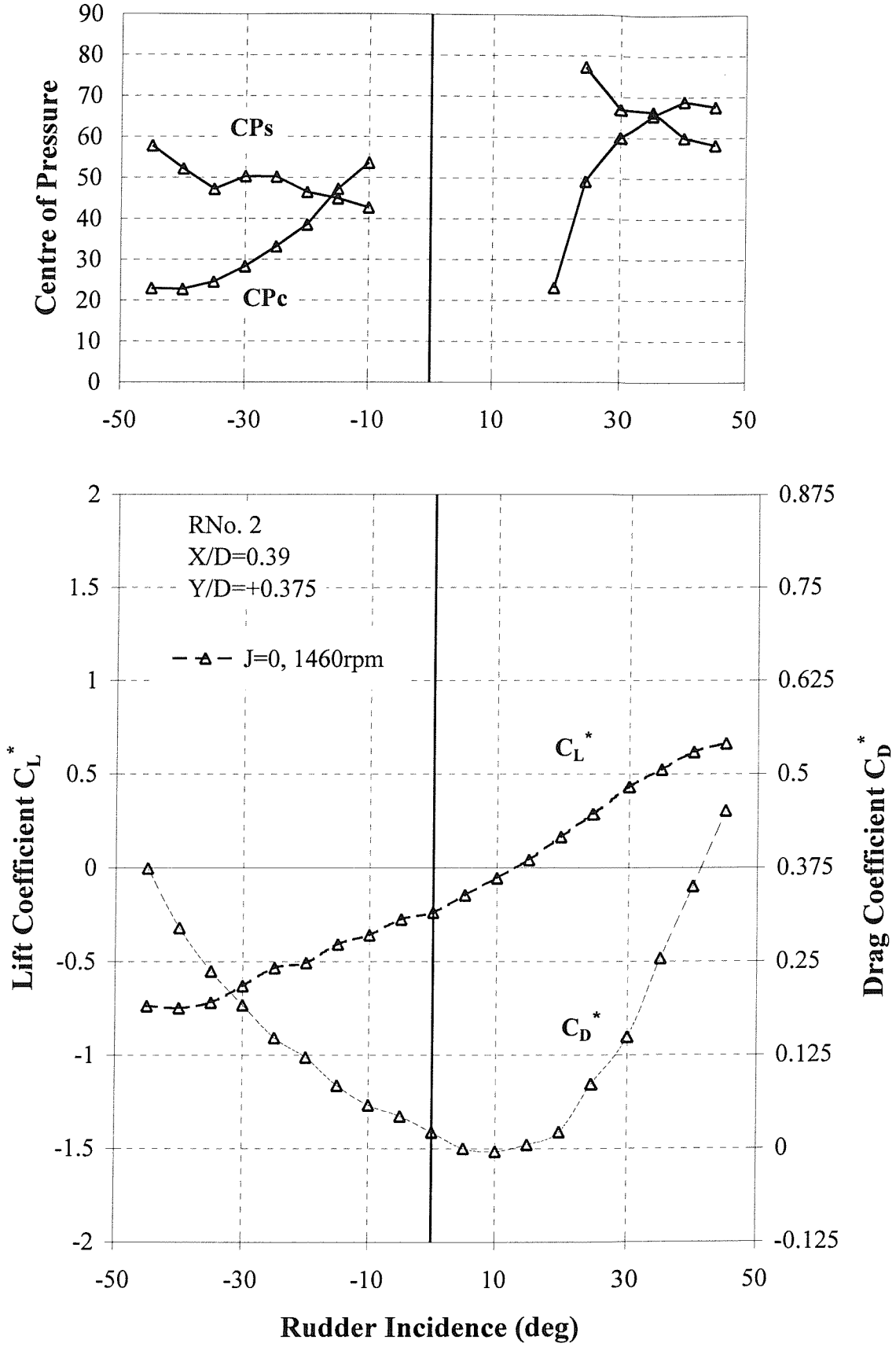

Figure B-16 **Influence of Propeller at Zero Advance Ratio (J=0) on the Performance of All-Movable Rudder No. 2 at a Lateral Separation of Y/D=+0.375**

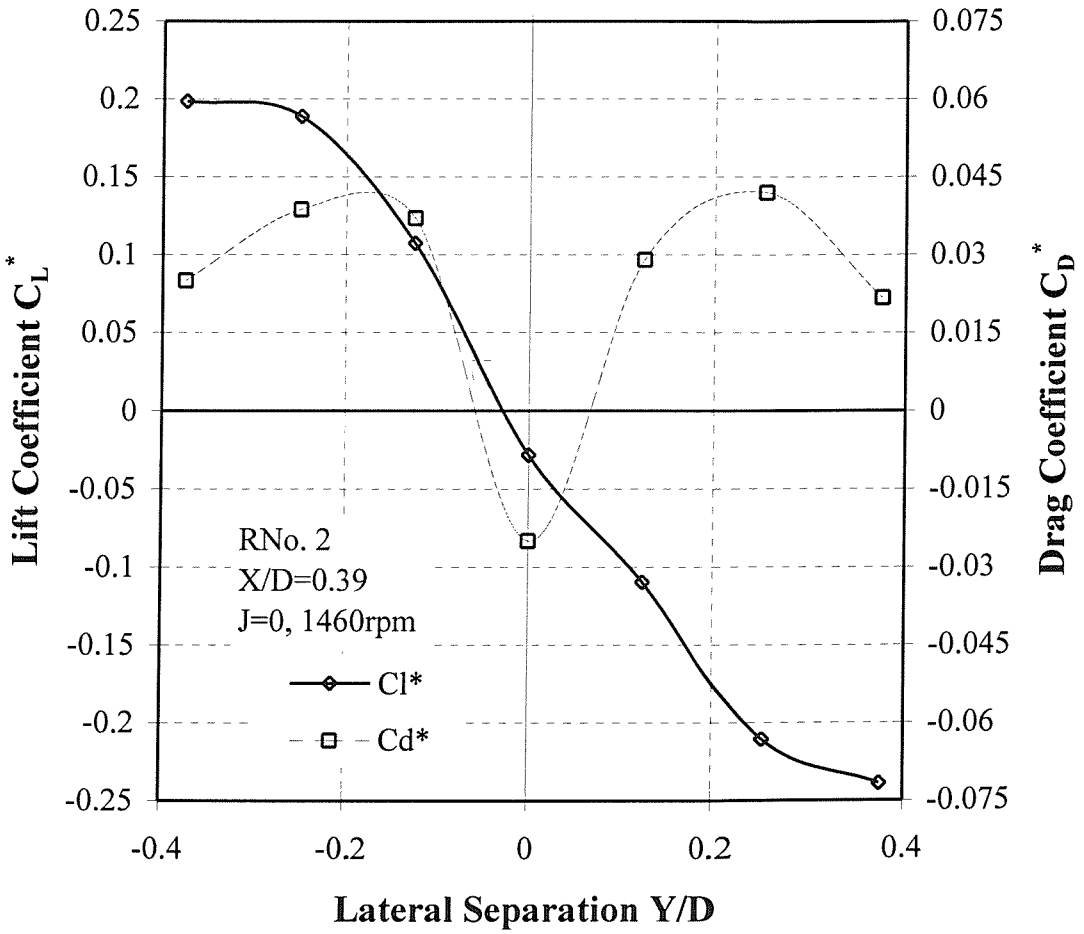

Figure B-17 Influence of Lateral Separation (Y/D) on Lift and Drag at Zero Incidence of All-Movable Rudder No. 2 at Zero Advance Ratio (J=0)

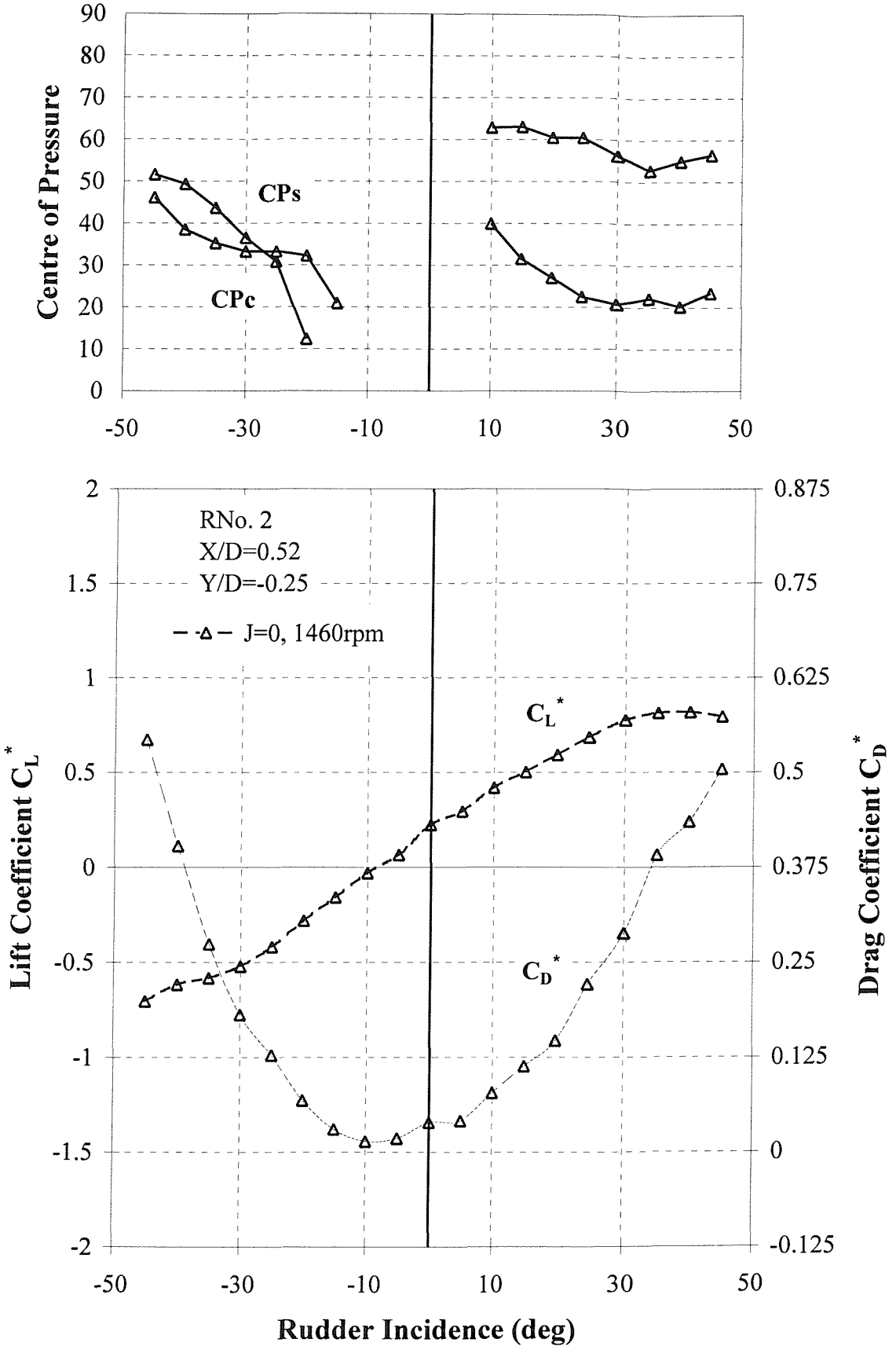

Figure B-18 **Influence of Propeller at Zero Advance Ratio (J=0) on the Performance of All-Movable Rudder No. 2 at a Lateral Separation of Y/D=-0.25 and a Longitudinal Separation of X/D=0.52.**

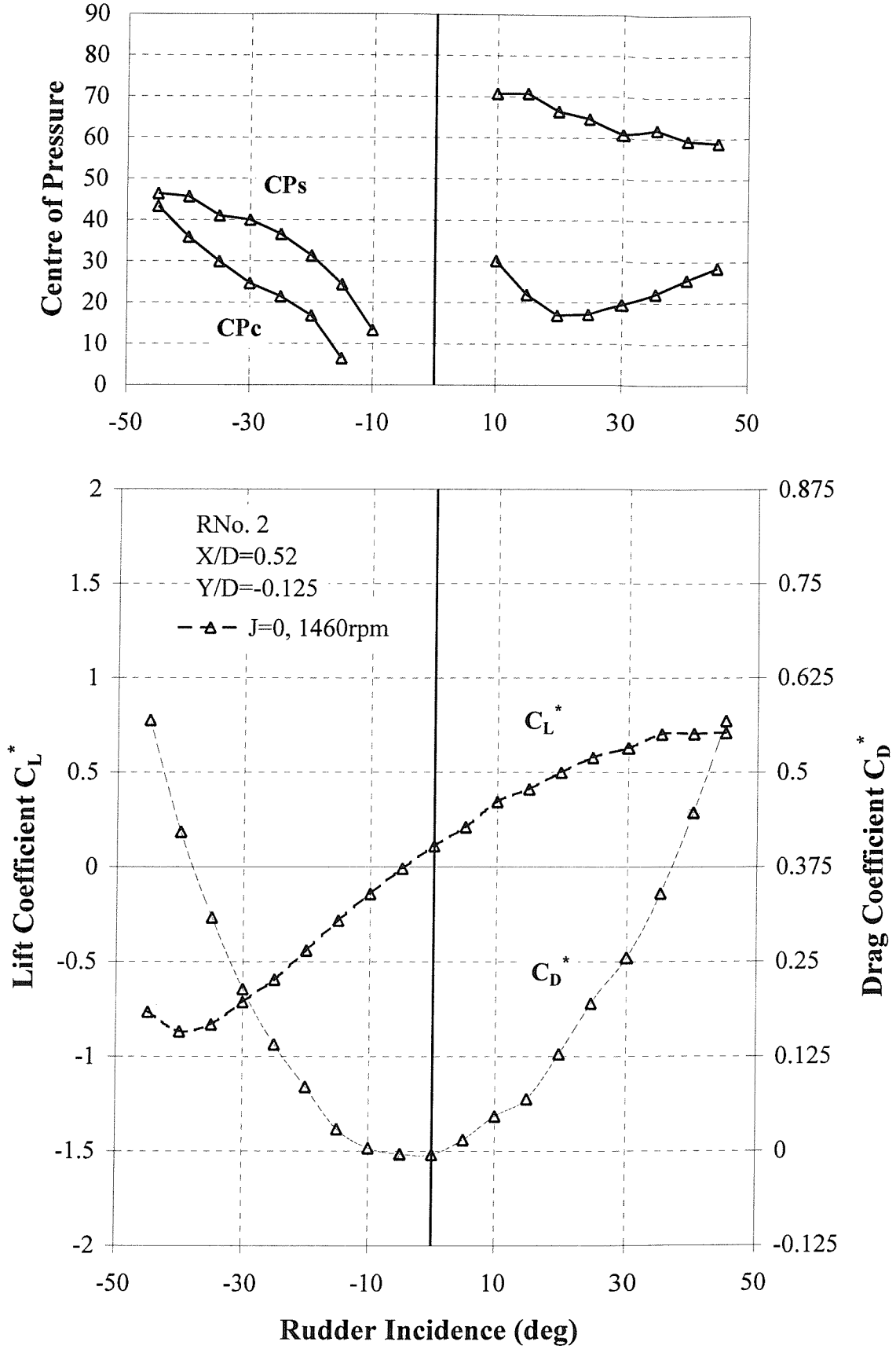

Figure B-19 **Influence of Propeller at Zero Advance Ratio (J=0) on the Performance of All-Movable Rudder No. 2 at a Lateral Separation of Y/D=-0.125 and a Longitudinal Separation of X/D=0.52.**

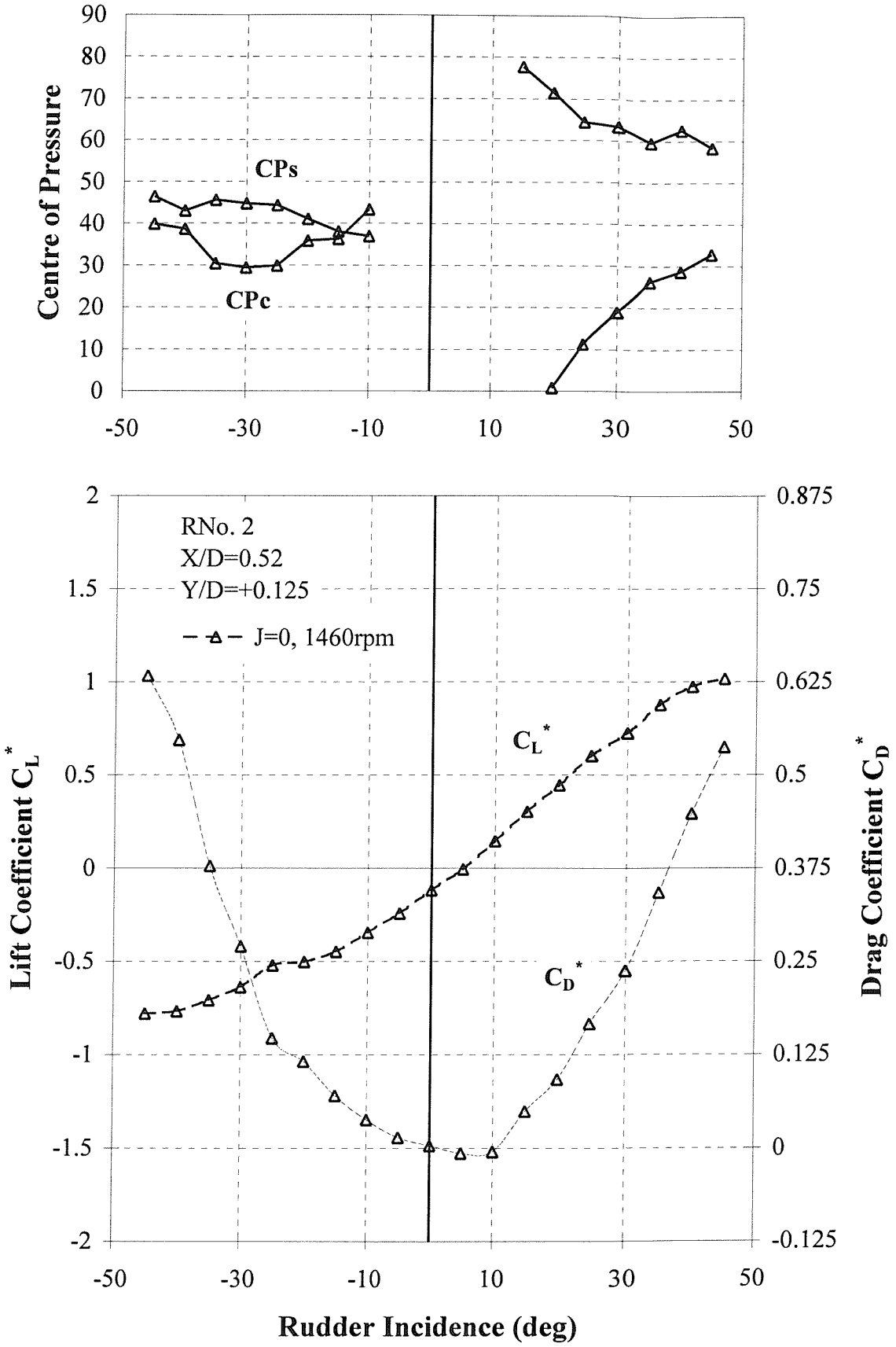

Figure B-20 **Influence of Propeller at Zero Advance Ratio (J=0) on the Performance of All-Movable Rudder No. 2 at a Lateral Separation of Y/D=+0.125 and a Longitudinal Separation of X/D=0.52.**

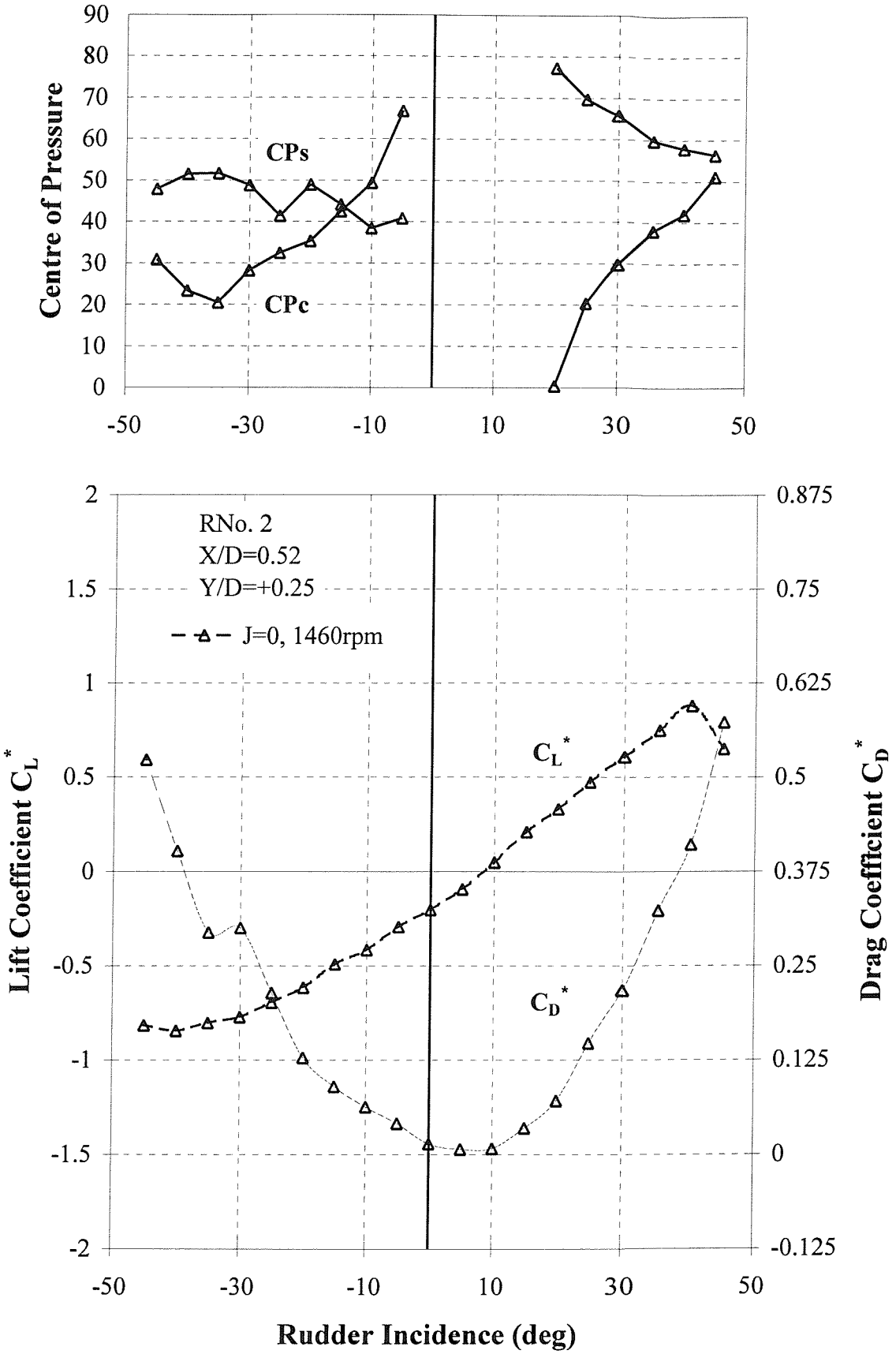

Figure B-21 **Influence of Propeller at Zero Advance Ratio (J=0) on the Performance of All-Movable Rudder No. 2 at a Lateral Separation of Y/D=+0.25 and a Longitudinal Separation of X/D=0.52.**

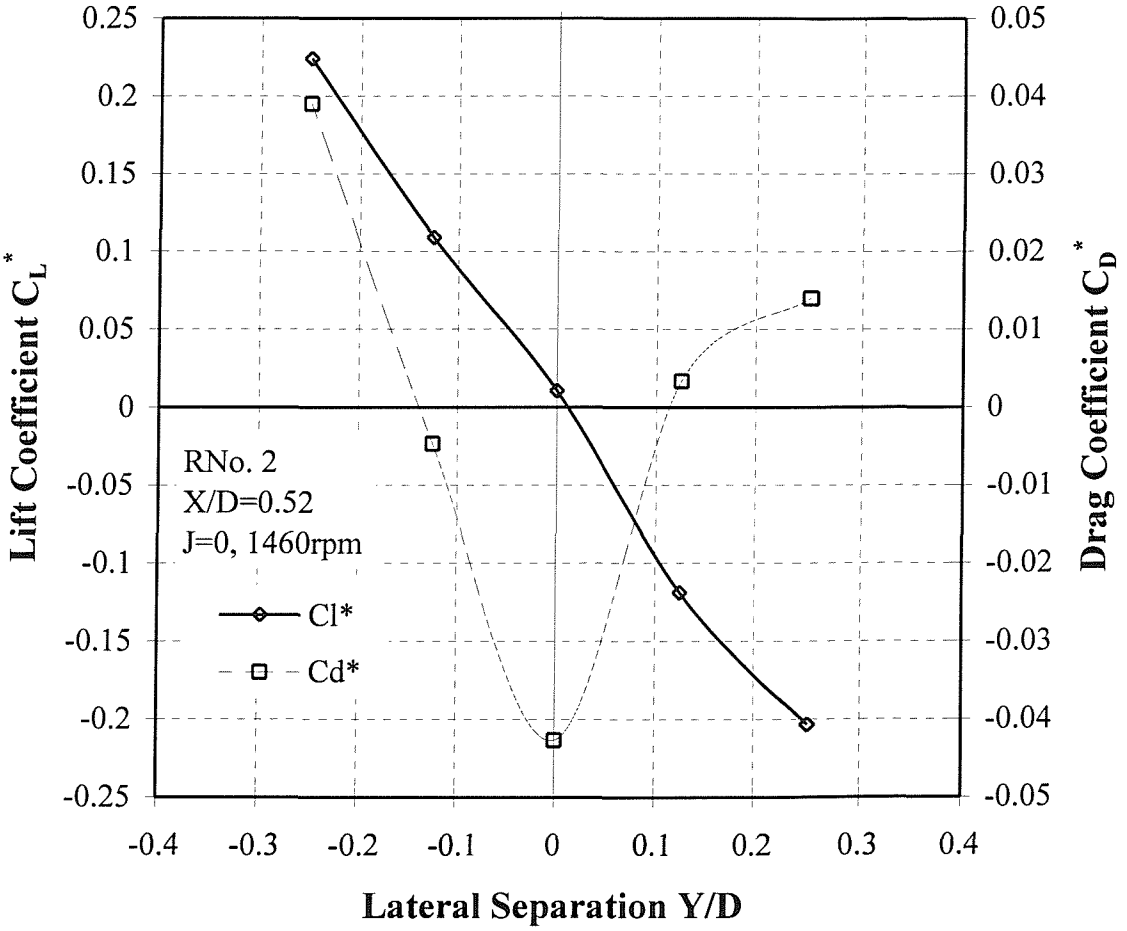

Figure B-22 Influence of Lateral Separation (Y/D) on Lift and Drag at Zero Incidence and X/D=0.52 of All-Movable Rudder No. 2 at Zero Advance Ratio (J=0)

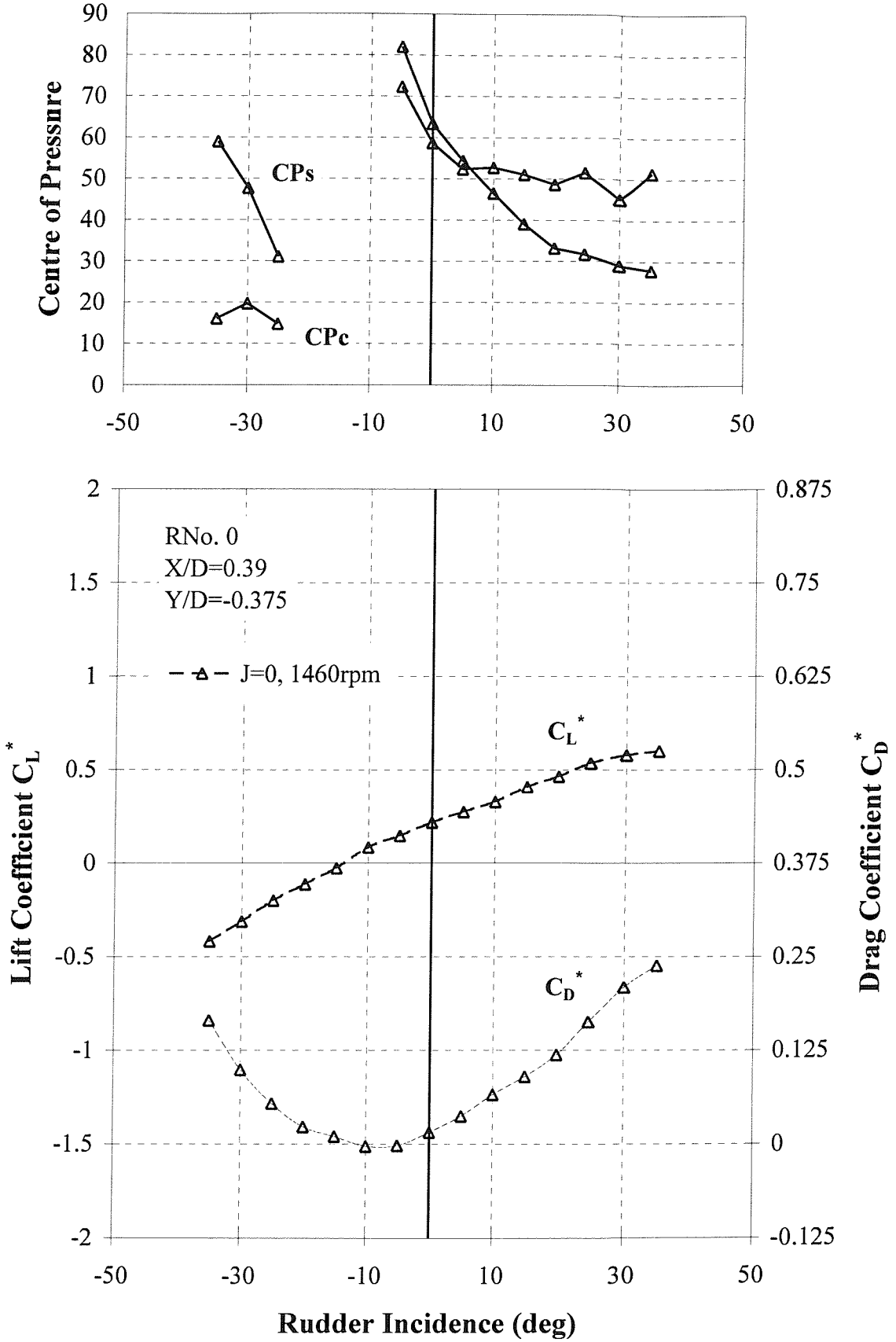

Figure B-23 **Influence of Propeller at Zero Advance Ratio (J=0) on the Performance of Skeg-Rudder No. 0 at a Lateral Separation of Y/D=-0.375.**

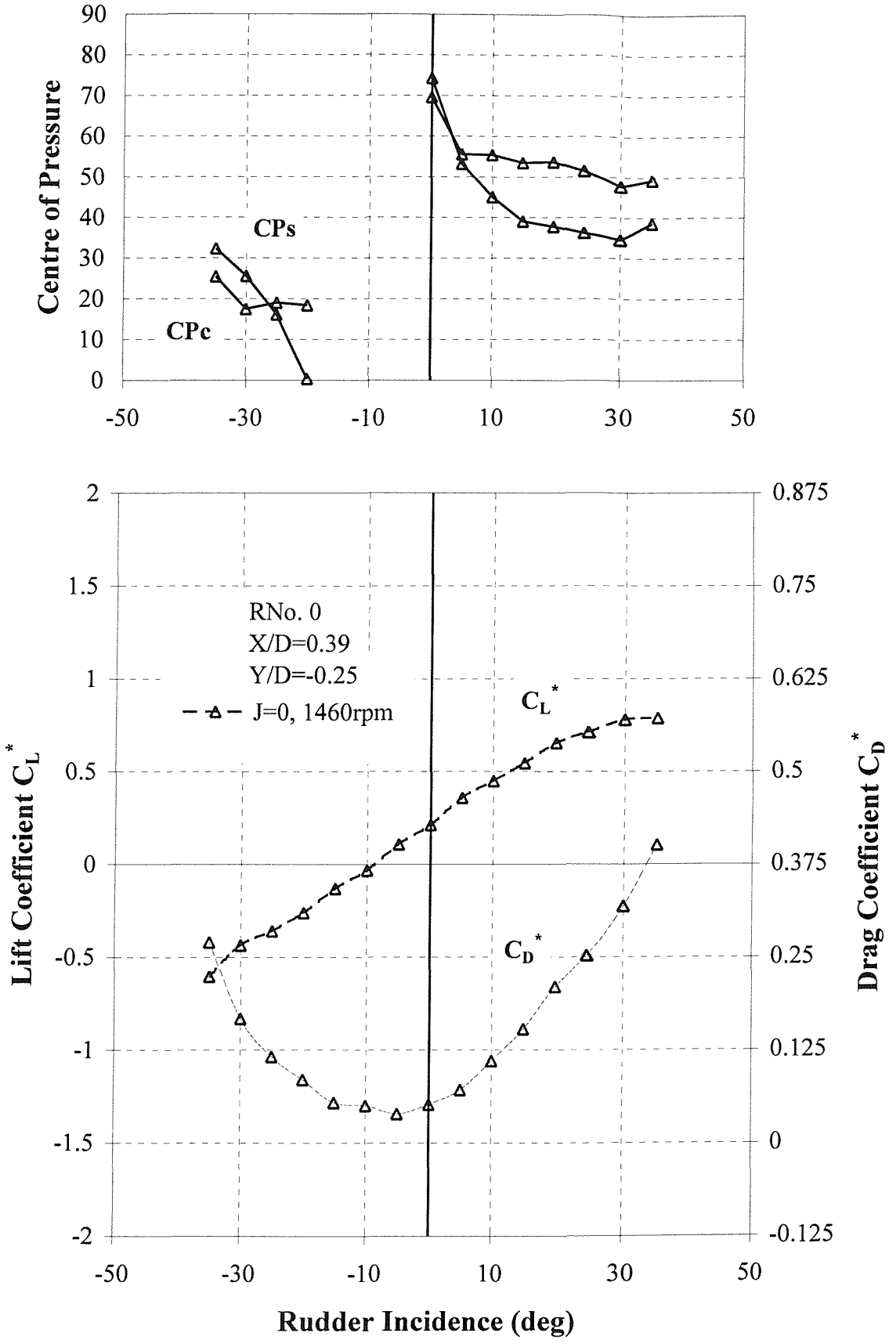

Figure B-24 **Influence of Propeller at Zero Advance Ratio (J=0) on the Performance of Skeg-Rudder No. 0 at a Lateral Separation of Y/D=-0.25.**

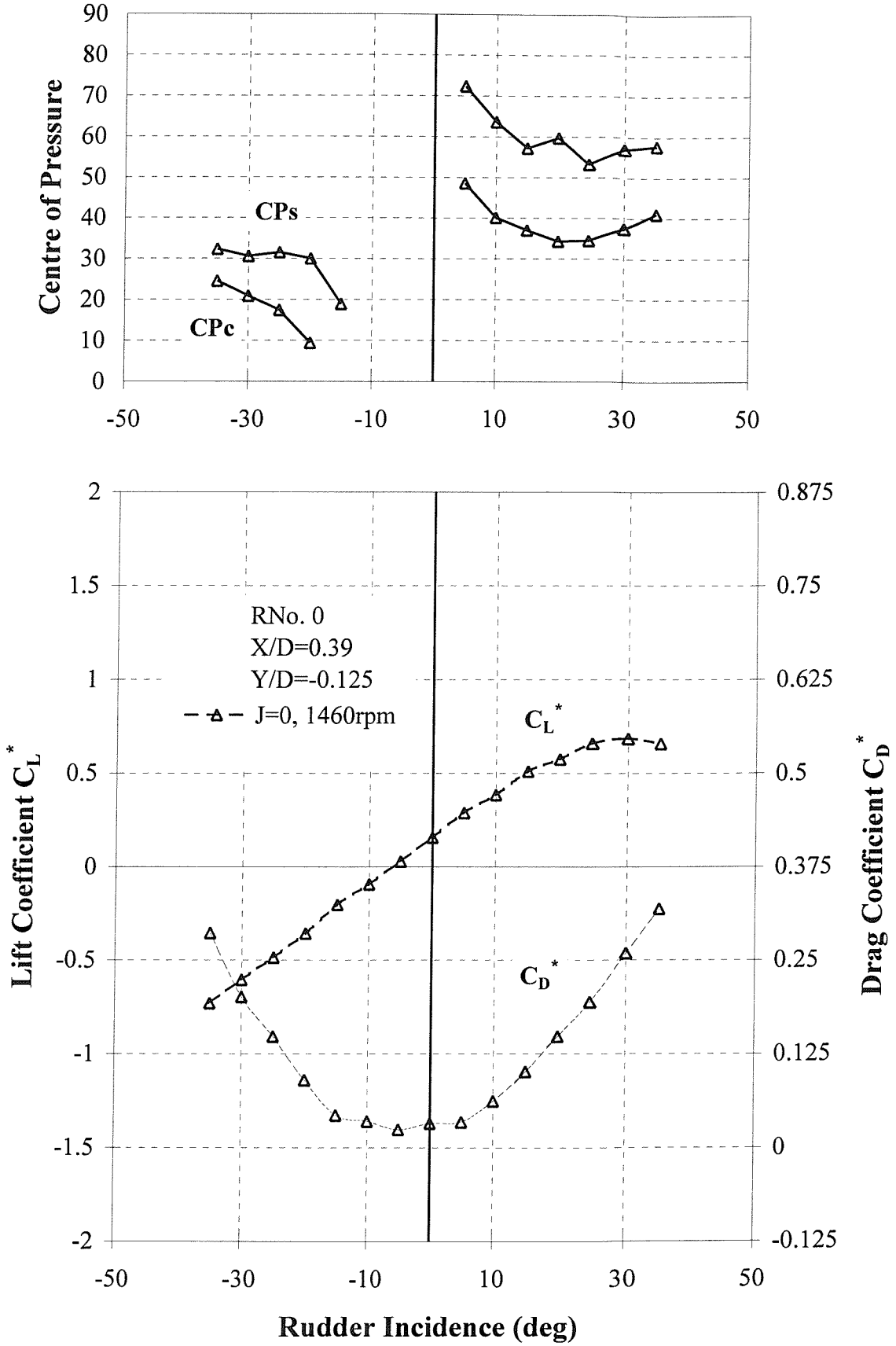

Figure B-25 **Influence of Propeller at Zero Advance Ratio (J=0) on the Performance of Skeg-Rudder No. 0 at a Lateral Separation of Y/D=-0.125.**

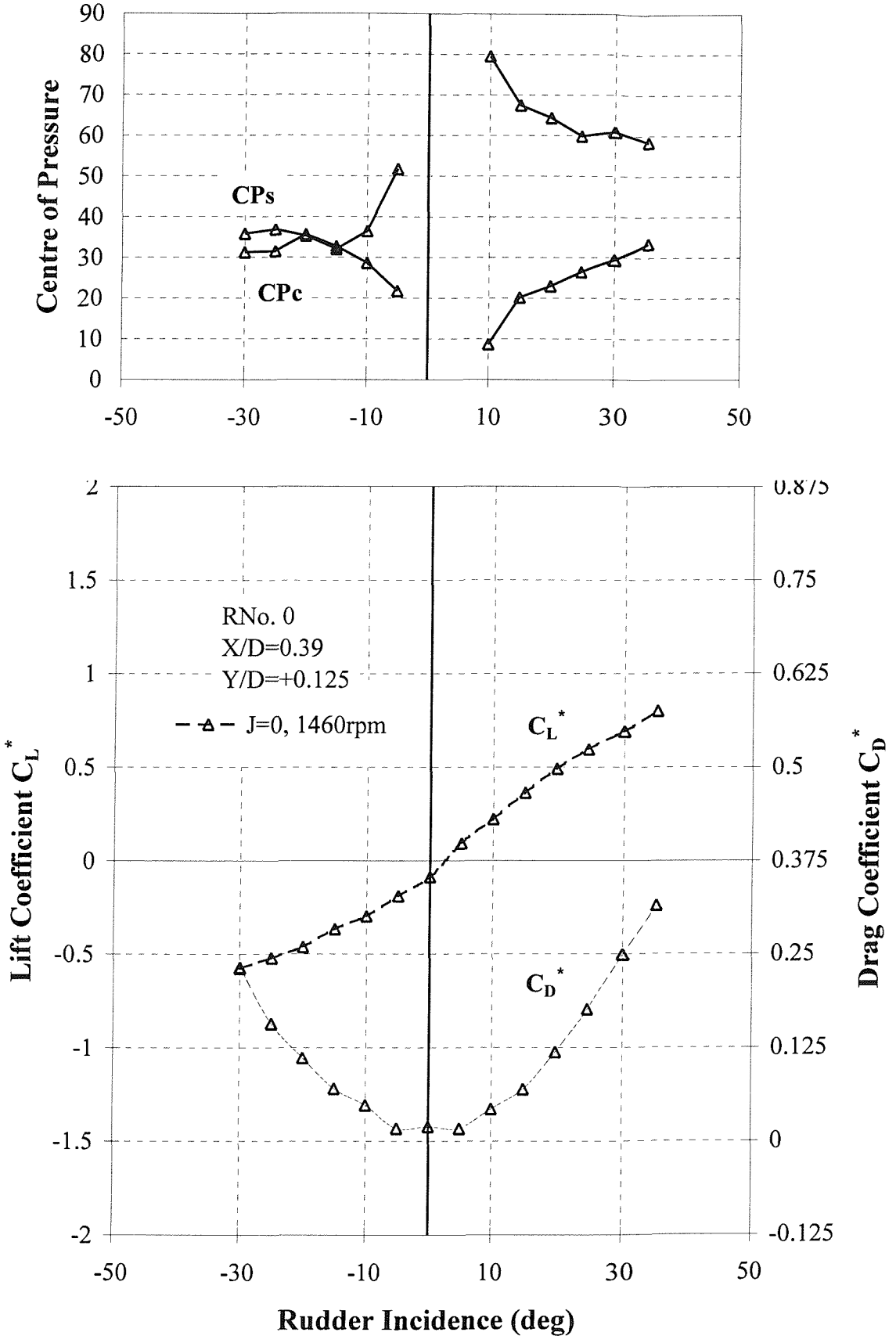

Figure B-26 **Influence of Propeller at Zero Advance Ratio (J=0) on the Performance of Skeg-Rudder No. 0 at a Lateral Separation of Y/D=+0.125.**

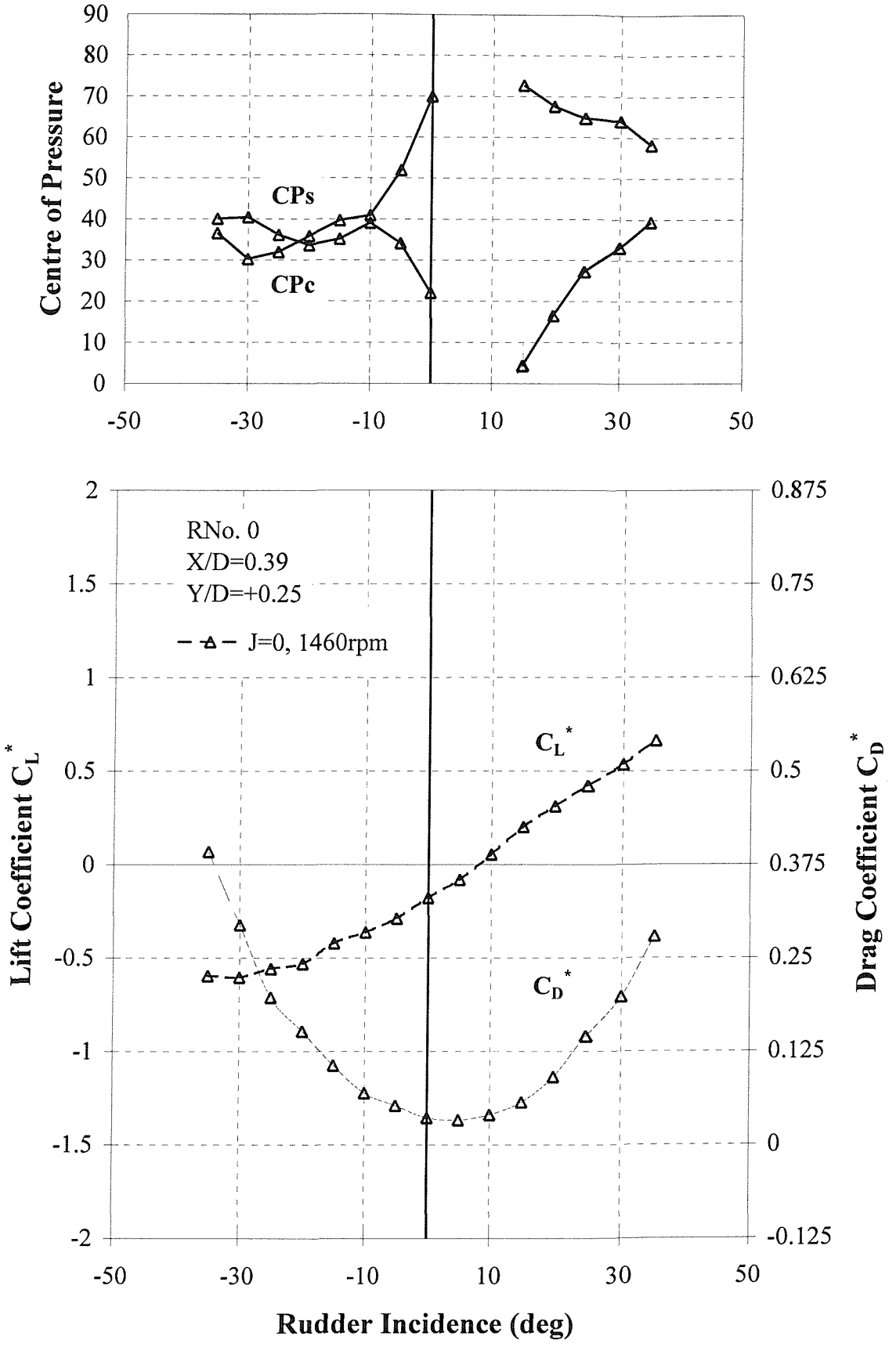

Figure B-27 **Influence of Propeller at Zero Advance Ratio (J=0) on the Performance of Skeg-Rudder No. 0 at a Lateral Separation of Y/D=+0.25.**

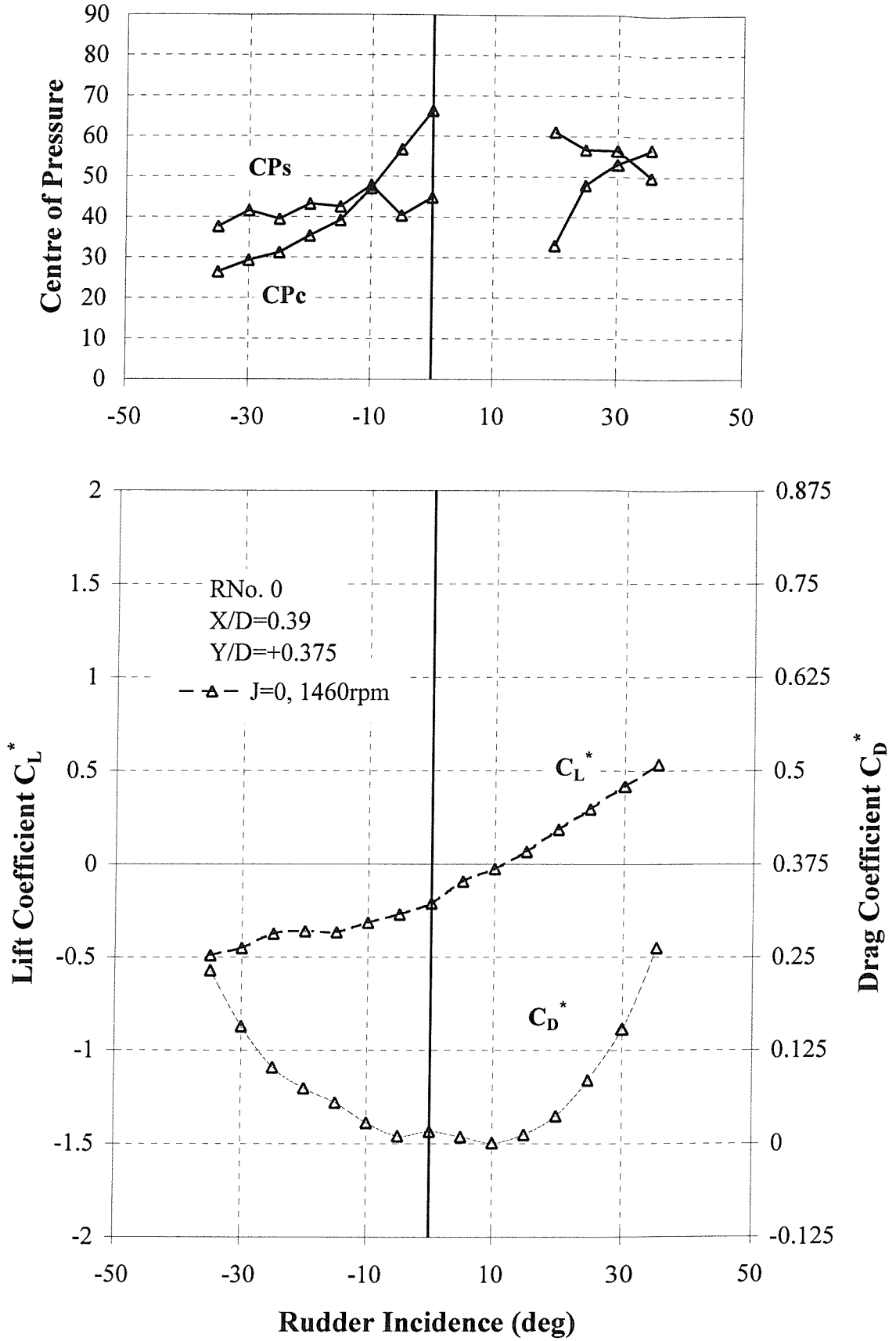

Figure B-28 **Influence of Propeller at Zero Advance Ratio (J=0) on the Performance of Skeg-Rudder No. 0 at a Lateral Separation of Y/D=+0.375.**

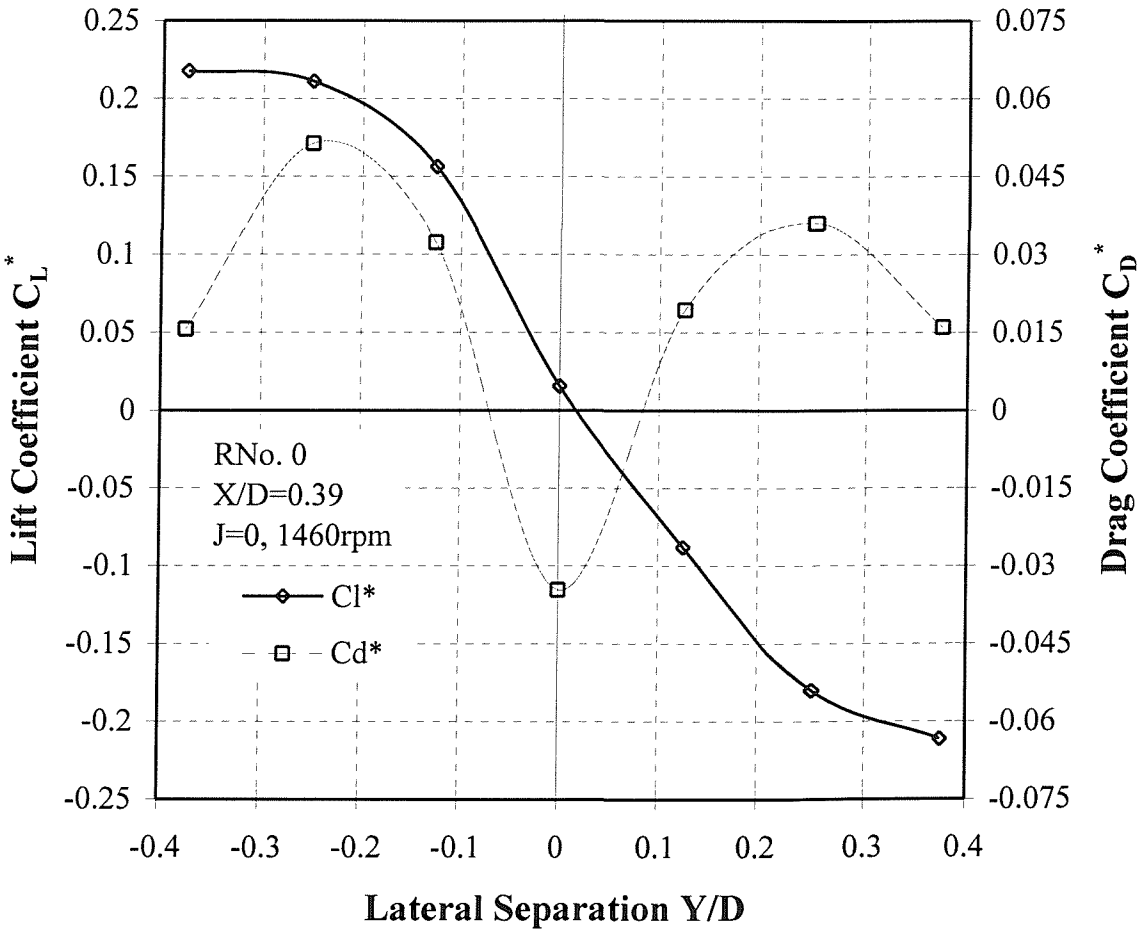

Figure B-29 Influence of Lateral Separation (Y/D) on Lift and Drag at Zero Incidence of Skeg Rudder No. 0 at Zero Advance Ratio (J=0).

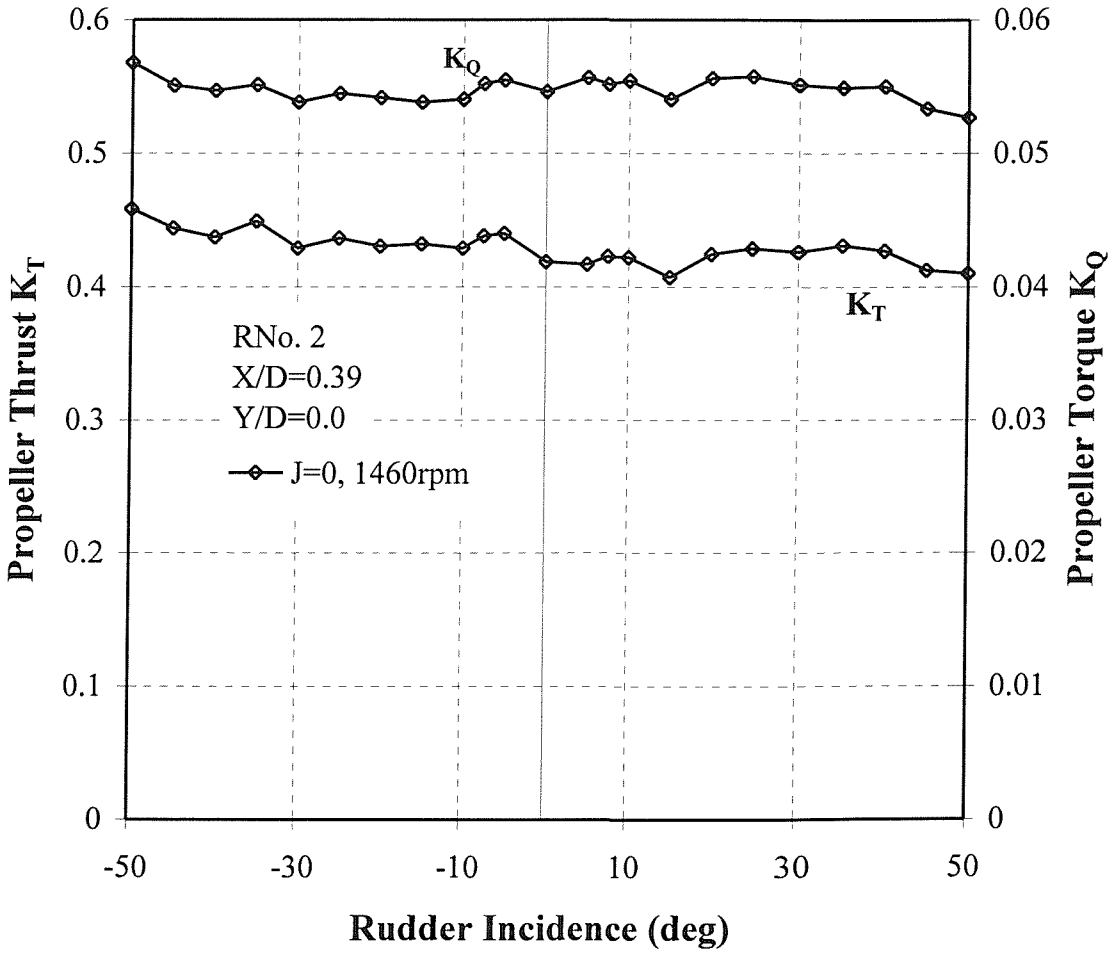

Figure B-30 Influence of All-Movable Rudder No. 2 on Propeller Thrust and Torque at Zero Advance Ratio (J=0)

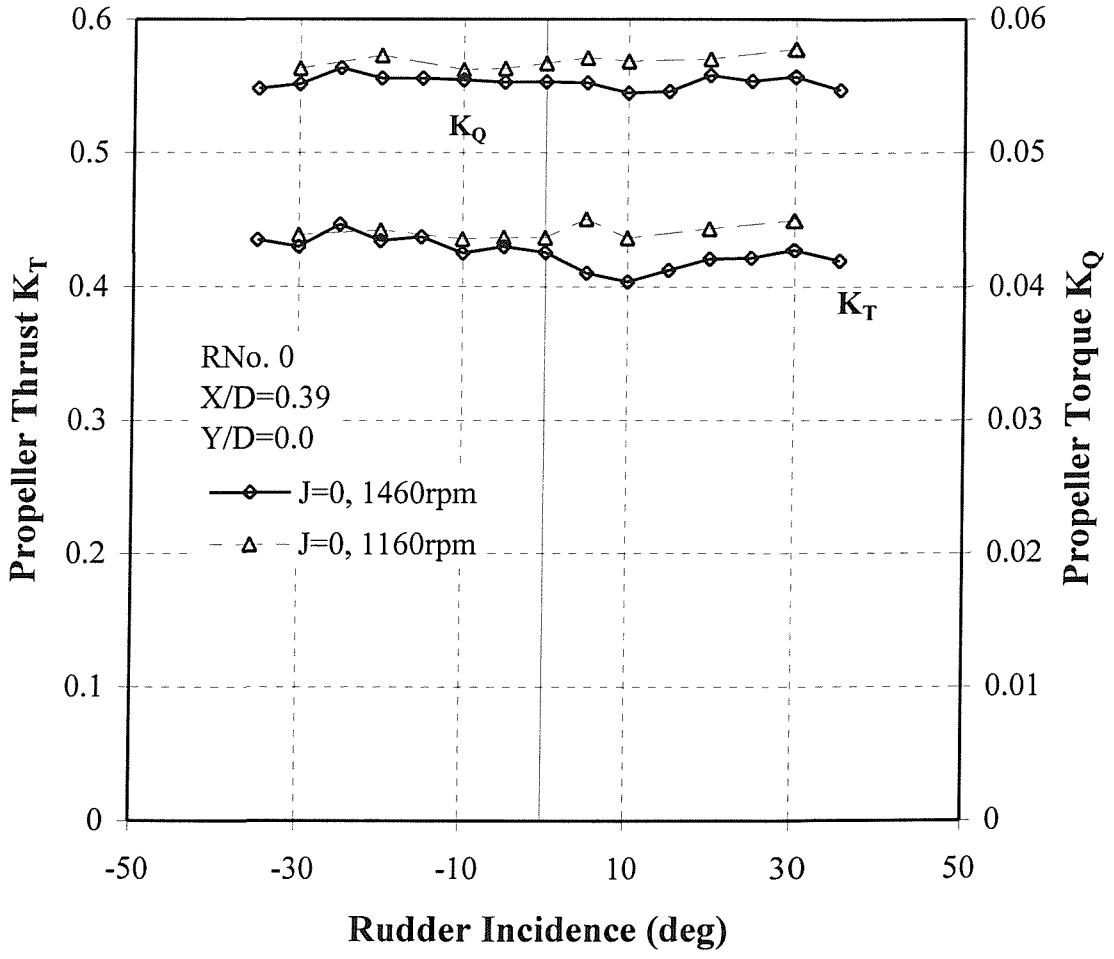

Figure B-31 Influence of Skeg Rudder No. 0 on Propeller Thrust and Torque at Zero Advance Ratio (J=0)

APPENDIX C – EXAMPLE CODE FROM RUDDER DESIGN SOFTWARE

Declaration of Rudder Variables

```
//////////////////////////////////////////////////////
// Rudder Declarations
CRudRec::CRudRec()
{
        name="";
        span=0.0;
        tipchord=0.0;
        rootchord=0.0;
        tipoff=0.0;
        stockpos=0.0;
        steerpos=0.0;
        secttype="";
        pos.x=0.0;
        pos.y=0.0;
        pos.z=0.0;
        fsdatatype=0;
        dclda=0.0;
        stalla=0.0;
        fname="";
}
```

Assigning of Rudder Object

```
CRudRec CRudRec::operator=(const CRudRec& p)
{
        name=p.name;
        span=p.span;
        tipchord=p.tipchord;
        rootchord=p.rootchord;
        tipoff=p.tipoff;
        stockpos=p.stockpos;
        steerpos=p.steerpos;
        secttype=p.secttype;
        pos=p.pos;
        angles=p.angles;
        fsdatatype=p.fsdatatype;
        fsdata=p.fsdata;
        dclda=p.dclda;
        stalla=p.stalla;
        fname=p.fname;
        return *this;
}
```

Storing and Loading of Rudder Object

```
void CRudRec::Serialize(CArchive &archive)
{
        CObject::Serialize(archive);
        if (archive.IsStoring())
        {
                archive << name << span << tipchord << rootchord << tipoff << stockpos << steerpos << secttype
                        << pos.x << pos.y << pos.z;
                archive << fsdatatype << dclda << stalla << fname;
                angles.Serialize(archive);
//              fsdata.Serialize(archive);
        }
        else
        {
                archive >> name >> span >> tipchord >> rootchord >> tipoff >> stockpos >> steerpos >> secttype
                        >> pos.x >> pos.y >> pos.z;
                archive >> fsdatatype >> dclda >> stalla >> fname;
                angles.Serialize(archive);
//              fsdata.Serialize(archive);
        }
}
```

Rudder Area Function

```
double CRudRec::Area()
{
        return(span*((rootchord+tipchord)/2));
}
```

Rudder Mean Chord Function

```
double CRudRec:: MeanChord()
{
        return((rootchord+tipchord)/2);
```

```
}

double CRudRec::SweepBack()
{
        return(atan((tipoff-0.25*rootchord+0.25*tipchord)/span));
}

double CRudRec::AspectRatio()
{
        return(span*span/Area());
}

double CRudRec::CFactor()
{
        double dem;
        dem=1.8+cos(SweepBack())*sqrt((4*AspectRatio()*AspectRatio()/pow(cos(SweepBack()),4))+4);
        return(2*AspectRatio()/dem);
}

void CRudRec::DrawRudProfile(CDC *dc, CPoint *orig)
{
        CBrush rbrush(RGB(0,0,255));
        CBrush sbrush(RGB(255,255,255));
        dc->SelectObject(&rbrush);
        CPoint pnt[5];
        pnt[0]=*orig;
        pnt[1].x=orig->x-1000*rootchord;
        pnt[1].y=orig->y;
        pnt[2].x=orig->x-1000*(tipoff+tipchord);
        pnt[2].y=orig->y+1000*span;
        pnt[3].x=orig->x-1000*tipoff;
        pnt[3].y=orig->y+1000*span;
        pnt[4]=*orig;
        CRect srect(orig->x-1000*stockpos-25*rootchord, orig->y,
                                orig->x-1000*stockpos+25*rootchord, orig->y+200*span);
        dc->Polygon(pnt,5);
        dc->SelectObject(&sbrush);
        dc->Rectangle(srect);
}

void CRudRec::DrawRudPlan(CDC *dc, CPoint *orig)
{
        int roothalfthick, tiphalfthick;
        CPoint rpnt[8];
        CPoint tpnt[8];
        CBrush rbrush(RGB(0,0,255));
        CBrush sbrush(RGB(255,255,255));
        dc->SelectObject(&rbrush);
        roothalfthick=1000*rootchord*0.1;
        tiphalfthick=1000*tipchord*0.1;
//      CRect rrect(orig->x-1000*rootchord, orig->y-roothalfthick, orig->x, orig->y+roothalfthick);
//      CRect trect(orig->x-1000*tipchord-1000*tipoff, orig->y-tiphalfthick, orig->x-1000*tipoff, orig->y+tiphalfthick);
        CRect srect(orig->x-1000*stockpos-roothalfthick/5,orig->y-roothalfthick/5,
                                orig->x-1000*stockpos+roothalfthick/5, orig->y+roothalfthick/5);
//      dc->Ellipse(rrect);
//      dc->Ellipse(trect);
        rpnt[0].x=orig->x-1000*rootchord;
        rpnt[0].y=orig->y;
        rpnt[1].x=orig->x-400*rootchord;
        rpnt[1].y=orig->y-roothalfthick;
        rpnt[2].x=orig->x-200*rootchord;
        rpnt[2].y=orig->y-roothalfthick;
        rpnt[3].x=orig->x;
        rpnt[3].y=orig->y-0.25*roothalfthick;
        rpnt[4].x=rpnt[3].x;
        rpnt[4].y=orig->y+0.25*roothalfthick;
        rpnt[5].x=rpnt[2].x;
        rpnt[5].y=orig->y+roothalfthick;
        rpnt[6].x=rpnt[1].x;
        rpnt[6].y=orig->y+roothalfthick;
        rpnt[7]=rpnt[0];

        tpnt[0].x=orig->x-1000*tipchord-1000*tipoff;
        tpnt[0].y=orig->y;
        tpnt[1].x=orig->x-400*tipchord-1000*tipoff;
```

Rudder Quarter Chord Sweepback Angle Function

Rudder Aspect Ratio Function

Rudder *f* Factor Function

Rudder Profile Drawing Method

Rudder Plan Drawing Method

```
            tpnt[1].y=orig->y-tiphalfthick;
            tpnt[2].x=orig->x-200*tipchord-1000*tipoff;
            tpnt[2].y=orig->y-tiphalfthick;
            tpnt[3].x=orig->x-1000*tipoff;
            tpnt[3].y=orig->y-0.25*tiphalfthick;
            tpnt[4].x=tpnt[3].x;
            tpnt[4].y=orig->y+0.25*tiphalfthick;
            tpnt[5].x=tpnt[2].x;
            tpnt[5].y=orig->y+tiphalfthick;
            tpnt[6].x=tpnt[1].x;
            tpnt[6].y=orig->y+tiphalfthick;
            tpnt[7]=tpnt[0];
            dc->Polygon(rpnt,8);
            dc->Polygon(tpnt,8);
            dc->SelectObject(&sbrush);
            dc->Ellipse(srect);
}
IMPLEMENT_SERIAL(CRudRec, CObject, 0)


////////////////////////////////////////////
//Propeller Declarations
```

Declaration of Propeller Variables

```
CPropRec::CPropRec()
{
            name="";
            diam=0.0;
            pond=0.0;
            pos.x=0.0;
            pos.y=0.0;
            pos.z=0.0;
            owdatatype=0;
            direction=0;
            fixedT=0.0;
            ktatj0=0.0;
            jatkt0=0.0;
            power=1.35;
            fname="";
}
```

Assigning of Propeller Object

```
CPropRec CPropRec::operator=(const CPropRec& p)
{
            name=p.name;
            diam=p.diam;
            pond=p.pond;
            pos=p.pos;
            nrpm=p.nrpm;
            name=p.name;
            diam=p.diam;
            pond=p.pond;
            pos=p.pos;
            nrpm=p.nrpm;
            owdatatype=p.owdatatype;
            owdata=p.owdata;
            direction=p.direction;
            fixedT=p.fixedT;
            ktatj0=p.ktatj0;
            jatkt0=p.jatkt0;
            power=p.power;
            fname=p.fname;
            return *this;
}
```

Storing and Loading of Propeller Object

```
void CPropRec::Serialize(CArchive &archive)
{
            CObject::Serialize(archive);
            if (archive.IsStoring())
            {
                        archive << name << diam << pond << pos.x << pos.y << pos.z
                                    << owdatatype << direction << fixedT << ktatj0 << jatkt0
                                    << power << fname;
                        nrpm.Serialize(archive);
//                      owdata.Serialize(archive);
            }
            else
            {
                        archive >> name >> diam >> pond >> pos.x >> pos.y >> pos.z
```

```
                                        >> owdatatype >> direction >> fixedT >> ktatj0 >> jatkt0
                                        >> power >> fname;
                        nrpm.Serialize(archive);
//                      owdata.Serialize(archive);
        }
}

////////////////////////////
//prop performance

double CPropRec::GetKtfromJ(double J)
{
        double B;
        double x1,x2,xreq,y1,y2;
        int i;
        //provisional curve fit
        if (owdatatype==OWCURVE)
        {
                B=ktatj0/(pow(jatkt0,power));
                return(ktatj0-B*pow(J,power));
        }
        if (owdatatype==OWTABLE) //|| (owdatatype==PRMTABLE))
        {
                for(i=1;i<owdata.J.no_in_range;i++)
                {
                        if ((J>=owdata.J.value[i-1]) && (J<=owdata.J.value[i]))
                        {
                                x2=owdata.J.value[i];
                                x1=owdata.J.value[i-1];
                                xreq=J;
                                y2=owdata.Coef[0].value[i];
                                y1=owdata.Coef[0].value[i-1];
                                return(((y2-y1)*(xreq-x1)/(x2-x1))+y1);
                        }
                }
        }
        return(NULL);
}

double CPropRec::CalcKtfromT(double nrpm, double density, double T)
{
        return(T/(density*nrpm*nrpm*pow(diam,4)/3600));
}

double CPropRec::CalcT(double nrpm, double density, double Kt)
{
        if (Kt==NULL) return(NULL);
        else return(Kt*density*nrpm*nrpm*pow(diam,4)/3600);
}

double CPropRec::CalcJ(double nrpm, double V)
{
        if (nrpm!=0.0) return(V/(nrpm*diam/60));
        else return(NULL);
}

void CPropRec::CalcHeights(CRudRec *rud, double *hr, double *ht)
{
        double a,theta;
        theta=acos(2*(rud->pos.y-pos.y)/diam);
        a=fabs(diam*sin(theta)/2);
        if((rud->pos.z+rud->span)>(pos.z+a)) *ht=fabs((pos.z-rud->pos.z)+a);
        else *ht=rud->span;
        if(rud->pos.z<(pos.z-a)) *hr=fabs((pos.z-rud->pos.z)-a);
        else *hr=0.0;
}

double CPropRec::Balance(CRudRec *rud)
{
        double ht,hr,h1,h2,yond,A1,A2,ct,cb,cm;
        CalcHeights(rud,&hr,&ht);
```

Calculation of K_T for J value from Propeller Open Water Data

Calculation of K_T from T value from Propeller Open Water Data

Calculation T from K_T

Calculation of J Function

Calculation of Relative Rudder-Propeller Heights

Calculation of Rudder-Propeller Balance

```
        TRACE("hr=%10.2f, ht=%10.2f\n",hr,ht);
        h1=ht+rud->pos.z-pos.z;
        h2=pos.z-rud->pos.z-hr;
        if (h1<0.0) h1=0.0;
        if (h2<0.0) h2=0.0;
        TRACE("h1=%10.2f, h2=%10.2f\n",h1,h2);
        yond=(rud->pos.y-pos.y)/diam;
        ct=rud->rootchord+((rud->tipchord-rud->rootchord)*ht)/rud->span;
        cb=rud->rootchord+((rud->tipchord-rud->rootchord)*hr)/rud->span;
        cm=rud->rootchord+((rud->tipchord-rud->rootchord)*(pos.z-rud->pos.z))/rud->span;
        A1=h1*(ct+cm)/2;
        A2=h2*(cb+cm)/2;
        TRACE("A1=%10.5f, A2=%10.5f\n",A1,A2);
        TRACE("\n");
        if (fabs(yond)>=0.5) return(0.0);
//      else return(yond*2*sqrt(0.25-yond*yond)+(h1/diam)-(h2/diam));
        else return(yond*2*sqrt(0.25-yond*yond)-((A1-A2)/(diam*cm)));
}

double CPropRec::Coverage(CRudRec *rud)
```

Calculation of Rudder-Propeller Coverage

```
{
        // only calculates correct coverage if rudder is within propeller diameter
        double hr,ht,cr,ct;

        CalcHeights(rud,&hr,&ht);
        ct=rud->rootchord+((rud->tipchord-rud->rootchord)*ht)/rud->span;
        cr=rud->rootchord+((rud->tipchord-rud->rootchord)*hr)/rud->span;
        return(((ht-hr)*(cr+ct)/2)/rud->Area());
}

void CPropRec::DrawPropProfile(CDC *dc, CPoint *orig)
```

Propeller Profile Drawing

```
{
        CBrush brush(RGB(255,255,0));
        dc->SelectObject(&brush);
        CPoint pnt[5];
        double width;
        width=1000*diam/20;
        pnt[0].x=orig->x;
        pnt[0].y=orig->y+1000*diam/2;
        pnt[1].x=orig->x+width;
        pnt[1].y=orig->y;
        pnt[2].x=orig->x-width;
        pnt[2].y=orig->y;
        pnt[3].x=orig->x;
        pnt[3].y=orig->y-1000*diam/2;
        pnt[4]=pnt[0];
        dc->Polygon(pnt,5);
        /*CRect topblade(orig->x-width, orig->y-1000*diam/2, orig->x+width, orig->y);
        CRect botblade(orig->x-width, orig->y, orig->x+width, orig->y+1000*diam/2);
        dc->Ellipse(topblade);
        dc->Ellipse(botblade); */
}
IMPLEMENT_SERIAL(CPropRec, CObject, 0)
```

APPENDIX D – PAPER ON THE PRACTICAL ANALYSIS OF THE HYDRODYNAMIC PERFORMANCE OF THE REFLEX 28 KEEL AND RUDDER

Presented at the International Conference on the Modern Yacht, The Royal Institution of Naval Architects, Portsmouth, 18 & 19 March 1998.

J E T Smithwick, S R Turnock,.
Wolfson Unit M.T.I.A, Department of Ship Science, University of Southampton, Southampton. SO17 1BJ, U.K.

ABSTRACT

The performance of the underwater appendages and hull of the Reflex 28 yacht have been analysed using a surface panel code. The objective of the work was to assess the ease with which such a code could be used as part of the design process using computational resources already available to the yacht designer. The flexible geometry creation process allowed the complete hull, keel-bulb and rudder configuration to be defined both for upright and heeled configurations and tested for a range of hull drift and rudder angles. The surface panel solution was obtained using an iterative process whereby each underwater component was solved independently and then in the presence of the velocity field induced by all the other components. This Interaction Velocity Field approach allows high panel density on each component and reduces the numerical difficulties associated with body-wake intersection. The results of the analysis confirmed performance features observed in the actual behaviour of the Reflex28, allowed greater insight into the mechanisms of flow interaction and allowed the relative side force contributions to be determined. It was concluded that, used with care, surface panel codes can provide the yacht designer with a detailed understanding of underwater appendage performance. The ability to rapidly change the geometric definition offers the possibility of cost-effective design optimisation even on a modest budget.

1. INTRODUCTION

The complex interaction of modern yacht underwater appendages requires a detailed understanding of the flow in order to produce an optimum design. The presence and shape of the bulb can strongly affect the side force generated by the keel. The yaw and heel of the hull in turn controls the flow field experienced by both the keel-bulb and rudder. The magnitude and influence of these interaction effects on the overall performance of the underwater appendages will often be a major factor in determining whether a particular design has a competitive edge. Good design requires a full knowledge of how individual components interact with each other and therefore what trade-offs are required to achieve optimum performance.

There are various investigation methods available to the designer which enable the performance of yacht appendages to be studied. These include theoretical, computational and experimental techniques. The results of the chosen method need to be able to be used to predict the performance of the appendages under a variety of realistic conditions at a reasonable cost.

Traditional tank testing or actual physical modelling is currently the most widely used method, see for example Reference 1 and Reference 2 . However, the detailed test programmes required to fully investigate appendage interaction are likely to be expensive especially if a large variation of geometrical parameters need to be investigated with the requirement for model making and tank hire charges. Theoretical methods based on straightforward application of fundamental understanding are useful at the preliminary design stage (Reference 3) but are limited when complex flow interaction needs to be studied and their very simplicity often limits the confidence with which they can be used for detailed design.

The potential advantage of a computationally based analysis is that it offers the designer a middle way between the expense of a full parametric experimental test programme and the simplicity of basic theory. The ability of a Computational Fluid Dynamics (CFD) flow solver to carry out detailed parametric investigations without the need for a large investment of time once the initial computational model has been developed offers the designer an effective method of reducing the scope of a subsequent test programme. However, in order to provide confidence in such a process the designer needs to have assurance that the results obtained are valid. One of the objectives of the analysis presented has been to assess the current state of technology for assessing appendage performance using computational resources already available to yacht designers. Although the analysis presented was carried out post-design it can offer a considerable insight into the actual flow behaviour between appendages.

There are a number of CFD codes applicable to the yacht designer that have been used to model whole underwater yacht geometries. The codes include DAWSON (Reference 2) a potential flow code, RAPID (Reference 4) a non-linear development of DAWSON which includes a quasi-static wave making correction, SPLASH (Reference 5) another potential flow based code with a linear free surface boundary conditions and YACHT97 (Reference 6) a higher order finite volume, viscous flow method with a non-linear free surface algorithm just to mention a few.

A reasonable compromise between computational effort and physical accuracy in modelling the flow interaction is achieved by the use of a surface panel method. Panel methods have been widely used in yacht design, DAWSON, RAPID and SPLASH all using this approach. Until recently such codes have not been accessible with the main bulk of their use being reserved for higher budget projects such as IACC yachts. These types of projects in the past have generally required large mainframe computers or workstations to commit to time consuming calculations and budget consuming prices. Now with the increased computational power and memory available on a desktop computer and the development of codes to exploit these types of machines it

is becoming increasingly feasible to analyse underwater appendages on the PC already sitting on the desk of the yacht designer.

In the Department of Ship Science a panel method developed in-house (Reference 7) has been proven to be a robust and reliable method for computational fluid dynamic modelling of yacht hulls and appendages and other complex geometries such as rudder and propellers. The surface panel code has been validated, of which Reference 8 and Reference 9 are examples. The numerical results when compared against wind tunnel and towing tank data show reliable correlation with the actual physical performance.

The aim of the work presented has been to demonstrate the ease of use of surface panel codes for practical yacht design and design validation. Such software can now be implemented on small workstations and the latest generation of PCs making it widely accessible. As a case study the analysis has been performed on a new yacht design, the Reflex 28 by Christian Stimson Yacht Design.

The Reflex 28 is a 28 foot racing yacht designed to be optimised under the Channel Handicapping System and the Sportsboat Class. The yacht was created using a combination of empiricism and conventional yacht design methods using resources lesser than that available to say an IACC yacht design team. The boat has been sailed and its performance proven, winning several races at events in the first year of it sailing. With its performance proven the designer desired a further insight into the appendages and their performance under various conditions particularly in the heeled state and also to assess the helm balance of the boat with respect to the centre of lateral resistance under these varying conditions.

The paper briefly discusses the surface panel theory used to carry out the investigation. The development of the computational geometry model is presented, detailing how the geometry was created and the necessary steps required to generate a complete working CFD model of the yacht hull and appendages. The yacht model has been used to predict side force, centre of lateral of resistance and overall performance as well as rudder performance downstream of the keel and bulb. Results and comparisons are made with more "accessible" theories such as simple lifting wing formulae. The validity and practical limitations with respect to the absence of free-surface, unsteadiness and viscous effects on the results are discussed. Future work is also discussed and finally conclusions are presented.

2. SURFACE PANEL ANALYSIS

2.1 GENERAL

The method used to predict the performance of a yacht is based on theoretical foundation of a lifting surface model. In a lifting surface panel formulation the approximation of the full Navier-Stokes equation assumes that the flow is inviscid, incompressible and irrotational and satisfies Laplace's potential equation:

$$\nabla^2\phi = 0 \qquad [1]$$

A body is described in the formulation by dividing the surface into discrete quadrilateral panels. Each panel is represented numerically as a known distribution of constant strength sources and dipoles of unknown strength. The flow is then solved by solving a matrix of source and dipole influences upon the fluid. A further condition is required in order that the difference in pressure on the trailing edge of the body is zero, (Kutta-Joukowski condition). This is carried out by defining the wake sheet downstream of the body and iterating the solution by adjusting the wake strength until the pressure difference is as near to zero as required for an accurate solution.

A detailed description of the method and a review of its historical development is given by Hess (Reference 10). Lamb (Reference 11) showed that a quantity satisfying Laplace's equation can be written as an integral over the bounding surface S of a source distribution per unit area s and a normal dipole distribution per unit area m distributed over the S. If v represents the disturbance velocity field due to the bounding surface (or body) and is defined as the difference between the local velocity at a point and that due to the free-stream velocity then.

$$\underline{v} = \nabla\phi \qquad [2]$$

where ϕ is defined as the disturbance potential. This can be expressed in terms of a surface integral as:

$$\phi = \int_{S_B}\int \left[\frac{1}{r}\sigma + \frac{\partial}{\partial n}\left(\frac{1}{r}\right)\mu\right]dS + \int_{S_W}\int \frac{\partial}{\partial n}\left(\frac{1}{r}\right)\mu dS \qquad [3]$$

where S_B is the surface of the body and S_W a trailing wake sheet. In the expression r is the distance from the point for which the potential is being determined to the integration point on the surface. $\partial/\partial n$ is a partial derivative in the direction normal to the local surface. A dipole distribution is used to represent the wake sheet. Hess (Reference 12) showed that this can be directly related to the vorticity distribution used in vortex lattice methods (VLM). For a steady-state solution the wake dipole strength distribution is uniquely determined by the application of the Kutta condition at the body trailing edge. Based on Morino's method, Reference 13, on the body surface the source strength per unit area is prescribed by satisfying the condition for zero normal velocity at the panel centroid

$$\sigma_s = U \cdot n \qquad [4]$$

where n is the unit normal outward from the panel surface and U the specified inflow velocity at the panel centroid. Numerical discretisation of [3] is achieved by representing the actual body surface as N quadrilateral panels. This gives the dipole potential at the centroid of panel i as:

$$\phi_i = \frac{1}{2\pi}\sum_{j=1}^{N}((U \cdot n_j)\, S_{ij} - \phi_j\, D_{ij}) + \sum_{k=1}^{M}\Delta\phi_k W_{ik} \quad [5]$$

where for panel j:

S_{ij} is the source influence coefficient of a unit strength panel.

D_{ij} is the dipole influence coefficient of a unit strength panel and

W_{ik} the influence of the constant strength wake strip extending to infinity.

As there are N independent equations corresponding to the N body surface panel centroids, [5] is closed and can be evaluated. Expressed in matrix form it becomes:

$$[\, D_{ij} + W_{ik} \,]\, \phi = [\, S_{ij} \,] U \cdot n_j - [\, W_{ik} \,] \left(\frac{d\Delta\phi}{d\Delta p} \Delta p \right)' \quad [6]$$

which can then be iteratively solved by progressive adjustment of the wake strength until the pressure loading at the trailing edge has been removed to any significant degree. Solution of the linear system of equations gives the vector of dipole potentials ϕ. Numerical differentiation of this potential along the body surface allows the surface velocity, hence pressures on the surface to be evaluated.

The process primarily involves calculation of the interaction matrix and then solving a dense set of linear equations in the form of the dipole matrix. Solving the dipole matrix is accomplished using a Jacobian block iterative solver. With this particular solver the memory requirement is proportional to the square of the number of panels.

2.2 CALCULATION OF LOCAL PRESSURES, FORCES AND VELOCITIES

The numerical solution determines the final dipole strength at the centre of each panel and hence potential on the surface of the body. To obtain practical information from this result a numerical differentiation is carried out. The differentiation of dipole potential is used to find the disturbance velocity tangential to the panel surface. The disturbance velocity can then be used to calculate the total surface velocity on the body and from this the velocity in the overall co-ordinate system. This velocity is used to calculate the local non-dimensional pressure coefficient Cp for each panel.

$$C_p = 1 - \frac{U_t^2}{U_\infty^2} \quad [7]$$

To obtain the total forces the distribution of pressure is integrated over the surface of the body for all panels and from the forces non-dimensional lift and drag coefficients are derived. The use of potential flow theory allows the circulation and hence lift (side force) and lift induced drag to be determined. However, as the local velocity is known for each panel the local panel skin friction coefficient can be empirically estimated and summed to give a total frictional force.

2.3 INTERACTION VELOCITY FIELD METHOD

Reference 8 and Reference 9 demonstrate the ability of the panel method to model yacht hulls and appendages in isolation. This same experience can be applied to model the complete set of appendages for the Reflex 28 knowing that each individual component of the underwater yacht can be adequately modelled using the surface panel method. With memory at a premium and also the tightly coupled interaction between the hull and appendages the method chosen to model the interaction was to separate the hull, keel/ bulb and rudder and to account for the interaction between them through the use of a modified inflow velocity field. This approach, initially developed to model rudder-propeller systems (Reference 14) is referred to as the interaction velocity field (IVF) method.

The IVF approach allows the available number of panels for a given body to be maximised to the memory available and hence allow higher quality grids to be created on the individual bodies or it can be used to lower the memory requirement for each numerical pass. In this way the numerics of the algorithm in essence create a matrix conditioner for the solution of the dipole strengths on the surface of the body. This matrix conditioner is particularly useful when there is a concentrated interaction between two bodies. In this way the matrix can be solved at a faster rate and to a better quality by the iterative solution algorithm. Without this conditioning a direct matrix solver may have to be used which greatly increases the number of operations the code has to execute and thus increasing the amount of time to obtain a converged solution to the problem.

Using the interaction method the bodies are not all modelled in one numerical pass thus creating a further iteration loop around the theory described earlier. This process is shown in Figure 1. First the hull flow model is solved to get a velocity influence upon the keel and bulb. The keel/ bulb model is then solved to get a velocity influence on the rudder. The rudder flow model is then solved with the imposed velocity field from the hull, keel and bulb. This process is repeated with the starting point on the hull being the velocity influence solved in the previous numerical pass. The procedure repeats until the difference in the results of body forces have iterated down to a minimum required value.

3. DEVELOPMENT OF COMPUTATIONAL GEOMETRY MODELS

3.1 GENERAL

The surface panel method requires a three-dimensional geometry definition of the actual body surface. Geometric definition within the code is carried out by a series of parametric cubic splines fitted around an initial set of definition points located on the body surface. By interpolating the cubic splines, varying panel distributions can be set over the body to concentrate panels in areas of intense curvature and regions of particular interest. The body is discretised into quadrilateral panels to create a grid over the surface of the body and on the wake sheet. For further information on the process of geometry definition within the panel code see Reference 7.

An effective geometric definition of the individual bodies of the yacht (i.e. hull, keel, bulb and rudder) is required to give a discretisation of suitable quality such that the numerical method will converge. Care must be taken over the number of panels in the chord-wise and span-wise directions, panel size distributions and wake definition. Each parameter can affect the solution or indeed whether the CFD model will converge to a solution at all. Several numerical tests are conducted varying the available parameters. By validation, examination of convergence histories and inspecting particular areas of interests such as high pressure gradients the geometric definition of the surface of the bodies and the wake can be adjusted such that the solution is as stable and as numerically correct as possible. By use of an automated process and experience the geometric definition was quick with a complete working CFD model of hull, keel, bulb and rudder produced within a few hours.

Wake adaptation by means of aligning the wake to the flow has not been implemented with this particular model as the computational time and effort increases quite considerably using this method. In general the wake is defined behind and parallel to the body and is rotated with the body if necessary.

Figure 2 shows the panelled geometry of the hull, keel, bulb and rudder combination and also indicates the axis system used. The geometry is input into the CFD code at full scale. The tests were run at a representative yacht speed for the purposes of calculating the frictional component of resistance.

3.2 HULL DEFINITION

Initial hull surface definition was obtained using a lines-fairing package to create a set of waterlines extending from the waterline to the bottom of the hull. The waterlines can be produced for any heel angle and at any required trim. Output from the lines program can then be modified and reformatted via a spreadsheet package for use by the CFD code.

In the yacht hull model the hull is represented with a flat reflection plane. This is an approximation to reality as the hull creates a wave system downstream of the hull and also a static wave profile on the surface of the hull. For the purpose of this study these free surface effects have not been modelled. The purpose of this analysis was the consideration of the side force production of the appendage system and as such free surface effects will not strongly affect performance.

Separate hull geometries are made for the flat and heeled case as the intersection between the reflection plane and the hull must be exact. The yacht has to be defined to the waterline and must not project through the free surface as numerically and physically this would be incorrect. The last or deepest waterline of the yacht is defined as the first keel section to ensure a neat fit between the hull and keel. The panel distribution used is an even distribution along the lengthwise and girthwise direction to maintain an even panel size over the hull.

The hull at yaw or heeled will act as a lifting surface and therefore requires a wake of shed vorticity. For the purpose of this analysis the circulation is shed from the aft most position on the hull and the hull wake sheet trails back from the after most point of the hull in a vertical plane. This is an approximation as the hull in reality will have an area of separation, particularly at leeway, which cannot be modelled using this method. The difficulties with wake definition behind the hull is the skewed nature of the wake panels coming off the trailing edge due to the shallow angle of the aft run. To align the panels to the flow the wake is adjusted so that it dips at the keel position expanding the panels in the correct direction, (see Figure 3). It is considered that this provides a reasonable approximation and predicted performance compares well with side force measurements in the towing tank (Reference 8).

3.3 APPENDAGE DEFINITION

Appendages are created using the profile and the required foil section. As with the hull the appendages are defined as a series of waterlines. Heel and trim for the appendages can be established by simply specifying centres, axes, and angles of rotation in a pre-processor to the CFD code and it will then perform the necessary translations and rotations.

The keel is defined as a series of sections with the last or deepest section being the intersection between the keel and bulb. It was not deemed necessary to have a fillet between the keel and bulb as this was inconsequential with respect to the conducted analysis. The keel/ bulb intersection can be seen in Figure 5. The keel wake extends from the trailing edge to past the rudder position ensuring the flow interaction method can superimpose the correct velocity field onto the rudder. The keel had a higher panel density at the leading edge as this is an area of high curvature.

The bulb is designed as a rotated section but in this case it is defined again as waterlines with the deepest section defined as small as numerically possible to ensure the body was closed. The bulb is not defined with a wake and therefore is not a lifting body as the principal effect with respect to flow is to stop end circulation of the keel and not act primarily as a lifting body. The bulb had an even distribution over the surface to maintain even panel size.

The rudder is defined in much the same way as the keel with the wake defined from the trailing edge approximately three chord lengths downstream. The rudder again had a higher panel distribution at the leading edge to account for the high curvature.

4. PRESENTATION OF RESULTS

The output from the surface panel analysis is in the form of total force and moments for each body, surface pressure values on the body surface, and if required total velocity at inspection points within the fluid. There have been no model tests carried out on the Reflex28. The method of validating the numerical analysis has been by comparison of the performance of the individual components with theory and for the keel-bulb and keel-hull performance it is based on the results from previous studies.

Some overall performance characteristics can be compared with actual handling of the yacht. Although this approach is not a formal validation it does ensure that the created CFD model is emulating the physical flow with a minimum of geometrical and numerical errors.

Results for foils (i.e. rudder and keel) are compared using a series of equations developed by Whicker and Fehlner (Reference 15). Whicker and Fehlner conducted a series of tests on low aspect ratio airfoils to develop a set of equations that could adequately predict their performance.

The equations used to predict lift or side force and drag are as follows:

$$\frac{\partial C_L}{\partial \alpha} = \frac{2\pi}{57.3 \cdot \left(1 + \frac{3}{AR_E}\right)} \qquad [8]$$

$$C_L = \frac{\partial C_L}{\partial \alpha} \cdot \alpha \qquad [9]$$

$$C_D = C_{D0} + X \cdot \frac{C_L^2}{AR_E} \qquad [10]$$

Where X=0.37 may be assumed as a satisfactory value for practical design purposes. C_{D0} or profile drag is assumed to be 0.015.

For the hull, slender wing theory is used to predict lift. The equation for the lift curve slope is as follows:

$$\frac{\partial C_L}{\partial \alpha} = \frac{\pi}{2} AR_{hull} \qquad [11]$$

Figure 5 shows the results for rudder lift and drag coefficients against rudder incidence. Also presented on the Figure is the data derived from [8] and [9] for the rudder. The forces are non-dimensionalised with respect to the rudder planform area.

Figure 7 shows the keel lift and drag coefficients against keel incidence or leeway angle. Again, non-dimensionalised with respect to keel planform area. Also shown is the data derived from [8] and [9] for the keel.

Figure 8 shows the dimensional Hull lift area ($L/0.5\rho V^2$) against leeway angle. Lift area is used as the surface area alters for the heeled case and to compare the lift coefficients would not give a true representation of the absolute forces produced by the hull. The data derived from [10] is also presented.

The relative magnitudes of the three appendage components are shown in Figure 6. The corresponding position of the centre of lateral resistance (CLR) as a function of rudder helm angle is shown in Figure 9. Also presented on the figure is the centre of lateral resistance predicted by using the centre of geometric area, derived by taking the moments of projected area of the hull and keel and dividing by the total area. This does not change for differing rudder helm angle.

As a measure of the likely influence of the flow asymmetry on wave making effects Figure 10 shows the port and starboard variation of pressure coefficient Cp at positions along the length of the yacht for the panel centroids closest to the reflection plane (free surface).

5. DISCUSSION

5.1 RESULTS

The lift and drag results for the rudder modelled in free stream with no upstream influence from hull, keel or bulb correlates well with that predicted by Whicker and Fehlner using [8] and [9]. The estimate is marginally over that of the CFD solution. For the same rudder angle the rudder modelled downstream of the hull and keel with no heel angle exhibits a drop in the lift and an increase in drag. This is due to the blockage effects from the hull and keel. The heeled case of 10^{o} shows an offset of lift at 0^{o} rudder incidence as expected as the heel produces a cambered shape.

The results of lift and drag for the keel modelled in isolation with no bulb correlates well with that predicted by Whicker and Fehlner. As with the rudder results, the prediction is greater than for the CFD solution. An increase in keel lift is experienced when the bulb is affixed to the end of the keel due to the end effect of the flow maintaining the pressure at the tip. Results with the hull upstream yield an increase in lift and also an increase in the frictional component of the drag at 0^{o} leeway. This is principally due to the hull increasing the keel's effective span and thus increasing the keel's lift curve slope while the surface area of the bulb contributes to the frictional drag. The hull and keel heeled at 10^{o} shows a decrease in lift compared with that experienced at no heel but the lift curve slope still remains greater than that presented for the 0^{o} heel case.

The hull modelled in isolation correlates well with that predicted by slender wing theory indicating the hull wake approximation is reasonable, but at higher leeway angles the CFD model shows a decrease in lift. This difference is likely to be due to the assumption of no separation. With the keel a marked increase in hull lift is experienced this is due to the knock-on effect from the keel maintaining the pressure on the hull and thus enhancing lift. This is also exhibited by the 10^{o} heeled case. The heeled case shows an initial offset in lift at 0^{o} of leeway due to the asymmetry of the heeled hull. The presence of the keel will more strongly influence the behaviour of flow over the hull and the wake model therefore remains a reasonable assumption.

In general, it can be seen that CLR moves aft with rudder angle due to the moment increased by applying helm. Comparing the CLR with that predicted using the geometric centre of area the CFD solution gives a result further aft. This is primarily due to the influence of the rudder. CLR moves forward with a heel of 10^{o} this is due to the asymmetry of the hull and the principle part of the lift for a slender body comes from the forward part of the body. The result also compares well with that experienced when sailing the yacht. The relative magnitudes of the forces and how heel influences them can be seen and corresponds to the change of CLR.

The pressure distribution for the no heel and no leeway case shows a high pressure at the forebody reducing to a low pressure at the centre of the yacht and then increasing at the after end of the yacht. This occurrence coincides with the wave profile produced by a yacht. Another interesting phenomenon for the heeled case at 10^{o} is the asymmetry of the pressure from the starboard side (i.e. positive side) to the port side. This effect produces the lift for the heeled form. Increasing the leeway angle increases the separation of the pressure from starboard to port side. These results indicate that although the free-surface has not been modelled qualitative effects of the spill over of lift around the hull on the free surface can be observed.

Overall, the side force prediction results are reasonable both for the appendage components in isolation and their interaction. The modelling process has reproduced the performance which has been experienced when sailing the yacht. Additionally, the detailed CFD results provide the designer with a wealth of information which could be used to quantify the effect of design changes prior to production.

5.2 COMPUTATIONAL PERFORMANCE

Timings were performed using a networked 64 bit dual processor Sun Ultra Sparc II workstation with 256 megabytes of memory and for a 32 bit 233MHz Pentium II personal computer (PC) with 64 megabytes of memory. Timings for the upright case, a leeway angle of 3 degrees and 3 degrees of helm are as follows.

Workstation:	24 mins 18 secs = 1458 secs
Personal Computer:	27 mins 20 secs = 1640 secs

The timings are quite similar for both types of computer the principal difference being optimisation of the executable code. The PC compiler is more tailored to suit the particular processor rather than the workstation with a more generalised code compiler. For a full interaction problem these run times are considered reasonable. On the PC with 64 Mbyte of RAM memory the maximum possible number of panels on a single body is 2,200 panels which is more than sufficient to ensure that the error due to numerical discretisation has been reduced to an acceptable level.

5.3 FURTHER THOUGHTS

Drag predictions using the surface panel method presented will be under-predicted. This is because in the current implementation of the code the viscous interaction of

pressure distribution and boundary layer development is neglected. The absence of a free surface and therefore lack of wave-making resistance further reduces the theoretical values obtained. However, at a leeway or incidence angle the important component of drag when considering alternative lifting surfaces is the induced drag, which is calculated to a high degree of confidence. The other assumption made in the modelling with respect to a fixed wake shape can also have an influence on the interaction force prediction although previous work has indicated that it should not be large on these particular lifting surfaces.

As discussed in the introduction, the local adaptation of the appendage and hull wake-surfaces, effects of viscous interaction on form drag and free-surface can be successfully included within a surface panel code. However, the computational requirement can be significantly increased with such additions. It is judged that at present it is more cost-effective for a designer to account for their influence through empirical corrections based on available test data or experience and use information such as the hull waterline surface pressures to infer the effect on wave making performance.

In the next five years the increased capability of work-stations will allow the designer cost-effective access to surface panel codes with viscous interaction, free-surface, wake adaptation and unsteady capabilities. How such information is used to enhance design and yacht performance will depend on the skill of the designer in interpreting the results of the calculation and being able to determine the key geometrical parameters which control performance. This has always been the case with new technological developments when made available.

6. CONCLUSION

The surface panel method has been found to be a reliable method for modelling yacht hull and appendage configurations. The results obtained are used to define the performance of the Reflex28 under various sailing conditions and correspond to effects determined for the original design and found in practice. Flexibility of the geometry definition and panelling algorithm allowed fast geometry creation times for all configurations leaving more time to complete the parametric tests. This ability allows the area balance between keel and rudder and their relative position to be investigated in a straight-forward manner and also investigate novel configurations without the need for expensive model tests.

Although a full validation exercise has not been performed a quantitative comparison of the effects of heel, leeway angle, rudder angle and other parameters has been demonstrated using the current method.

If this approach had been used at the design stage a deeper understanding of the Reflex 28 performance would have been available and would have allowed greater confidence in the design choices made or allowed investigation of other factors. The case-study on the yacht has shown that the surface panel code is a worthwhile investigation tool worthy of consideration by yacht designers. It offers the capability

to the designer at an early design stage to investigate the effects of varying quantities that most designers would leave to empiricism, received wisdom, or conventional yacht design techniques.

7. NOMENCLATURE

A	Area (m^2)
AR_E	Effective aspect ratio
AR_G	Geometric aspect ratio
c	Chord (m)
C_d	Drag coefficient $(d/\frac{1}{2}\rho AU_\infty^2)$
C_f	Coefficient of Skin Friction
C_L	Lift coefficient $(L/\frac{1}{2}\rho AU_\infty^2)$
CLR	Centre of Lateral Resistance, $(M_Z/(L\cos\alpha+D\sin\alpha))$
C_p	Pressure Coefficient
d	Drag force (N)
L	Lift force (N)
n	Unit surface normal vector
N	Number of panels
q	$\frac{1}{2}\rho U_\infty^2$
Rn	Reynolds Number $(\rho U_\infty c/\mu)$
S	Span (m)
S_E	Effective span (m)
U	Velocity vector (u,v,w), (m/s)
U_∞	Free-stream speed (m/s)
VMG	Velocity made good (m/s)
α	Angle of incidence (deg)
δ_R	Rudder helm angle (deg)
ϕ	Heel angle (deg)
λ	Leeway angle (deg)
ρ	Density (kg/m^3)
μ	Dynamic Viscosity (kg/m^3)

8. ACKNOWLEDGEMENTS

Reflex 28 designed and information kindly supplied by Christian Stimson of Christian Stimson Yacht Design, Cowes Yacht Haven, Vectis Yard, High Street Cowes, Isle of Wight.

9. REFERENCES

Reference 1 DESAIX, P - "Yacht Keels - An Experimental Study", Second Chesapeake Sailing Yacht Symposium, 18 January 1975, pp. 7-1 - 7-29.

Reference 2 KEUNIG, J A, KASPENBER, G K - "Wing - Body Interaction on a Sailing Yacht" Twelfth Chesapeake Sailing Yacht Symposium, 28 January 1995, pp. 133-144.

Reference 3 MARCHAJ, C A - "Aero Hydrodynamics of Sailing", 1979, Granada Publishing.

Reference 4 VAN DEN BERG, W, RAVEN H C, VALKHOF H H - "Free-Surface Potential Flow Calculations for Merchant Vessels", CFD and CAD in Ship Design, 25-26 September 1990, pp.165-181.

Reference 5 ROSEN, B S, LAIOSA J. P.- "SPLASH Non-Linear and Unsteady Free Surface Analysis Code for Grand Prix Yacht Design", Thirteenth Chesapeake Sailing Yacht Symposium, 25 January 1997, pp. 211-225.

Reference 6 FARMER, J, MARTINELLI, L, JAMESON, A - "YACHT97: A Fully Viscous Non-linear Free-Surface Analysis Tool for IACC Yacht Design" Twelfth Chesapeake Sailing Yacht Symposium, 28 January 1995, pp. 157-170.

Reference 7 TURNOCK, S R - "Technical Manual and User Guide for the Surface Panel Code: PALISUPAN", Ship Science Report No. 100, October 1997, University of Southampton.

Reference 8 SMITHWICK, J E T- "An Investigation into the Hydrodynamic Forces and Interaction of the Hull and Keel of a Yacht using a Parallel Lifting Surface Panel Method." 3rd Year MEng individual project thesis, May 1993, University of Southampton.

Reference 9 TESSIER, Y- "Investigation of the hydrodynamic performance of stretched yacht keel bulbs", M.Sc. Thesis, University of Southampton 1994

Reference 10 HESS, J L - "Panel Methods in Computational Fluid Dynamics", Annual Review of Fluid Mechanics, Vol 22, 1990, pp. 225-274.

Reference 11 LAMB, H - "Hydrodynamics", Cambridge University Press, sixth edition, 1932.

Reference 12 HESS, J L - "The problem of three-dimensional lifting flow and its solution by means of a surface singularity distribution", Computational Methods Applied Mechanical Engineering, 4:283-319 also 1972, Rep MDC-J5679, McDonnell Douglas Aircraft Co. Long Beach, Calif.

Reference 13 MORINO, L AND KUO, C-C - "Subsonic Potential aerodynamics for Complex Configurations: A general theory", A.I.A.A. Journal, Vol 12., No. 2 Feb 1974.

Reference 14 TURNOCK S R, WELLICOME, J F AND MOLLAND, A F - "Interaction Velocity Field Method for Predicting Ship Rudder-Propeller Interaction", S.N.A.M.E., Propellers/Shafting Symposium, No. 18, Sept 1994.

Reference 15 WHICKER, L F AND FEHLNER L F - "Free Stream Characteristics of a Family of Low Aspect Ratio Control Surfaces for Application to Ship Design", December 1958, D.T.M.B. Report 933.

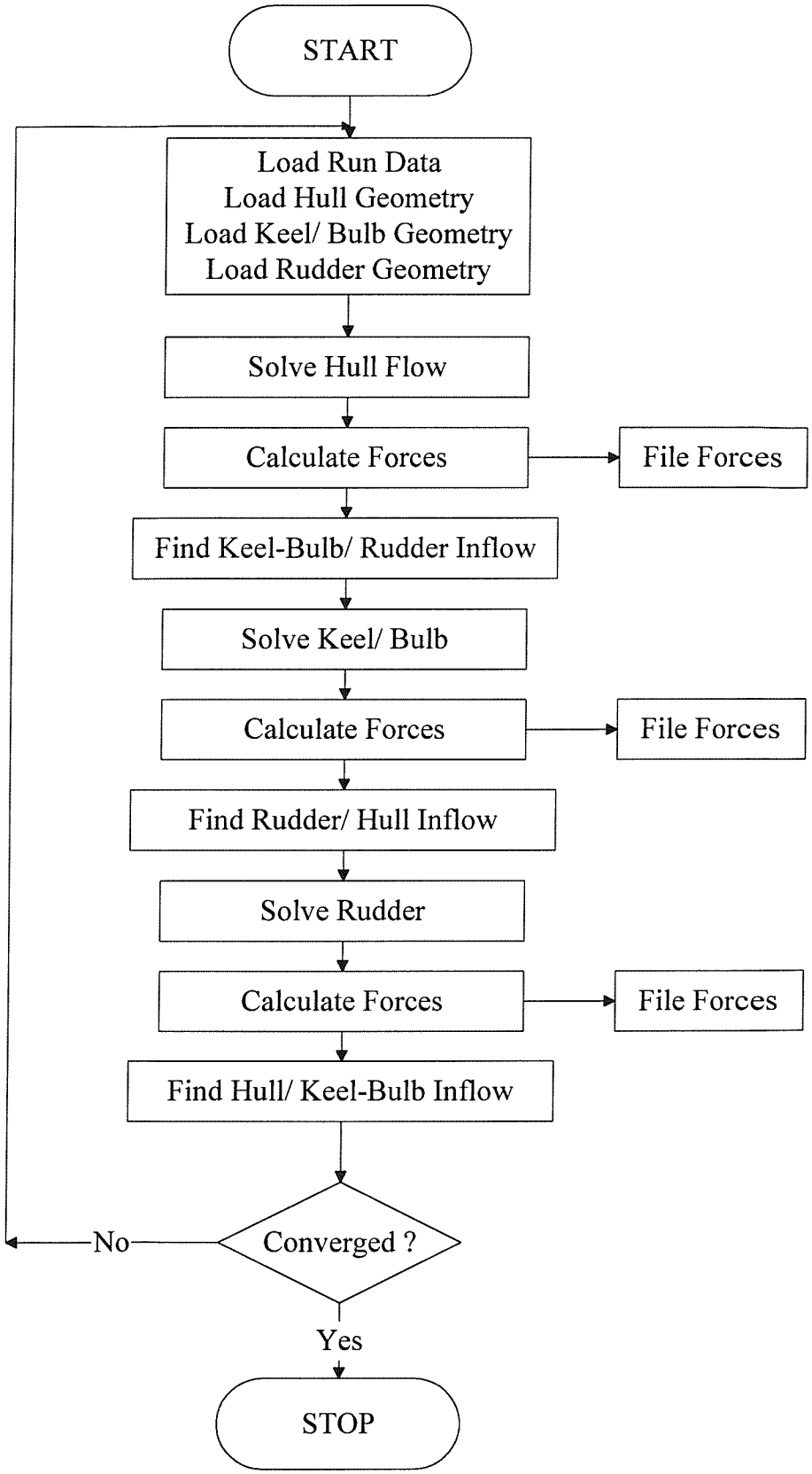

Figure 1 Velocity Interaction Method Flow Diagram

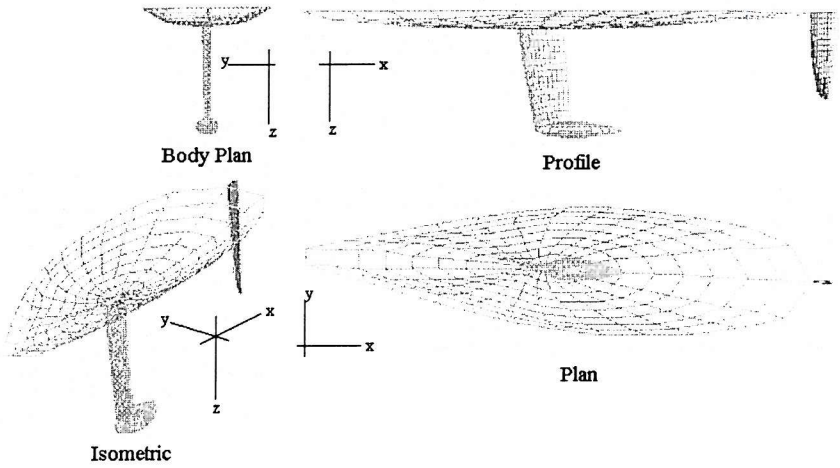

Figure 2 Panelled Geometry

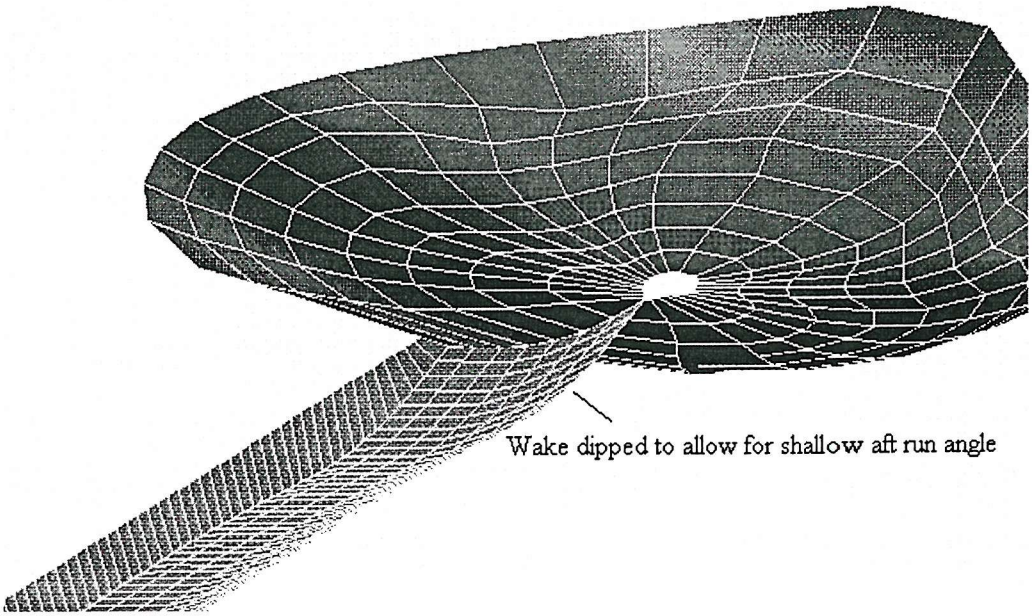

Figure 3 Adjusted Hull Wake

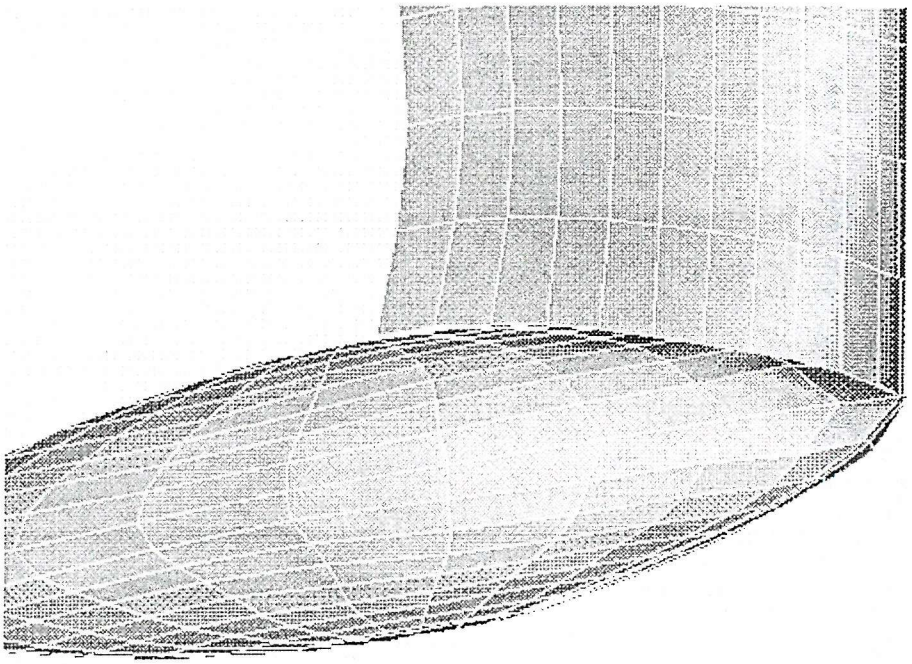

Figure 4 Keel/ Bulb Intersection

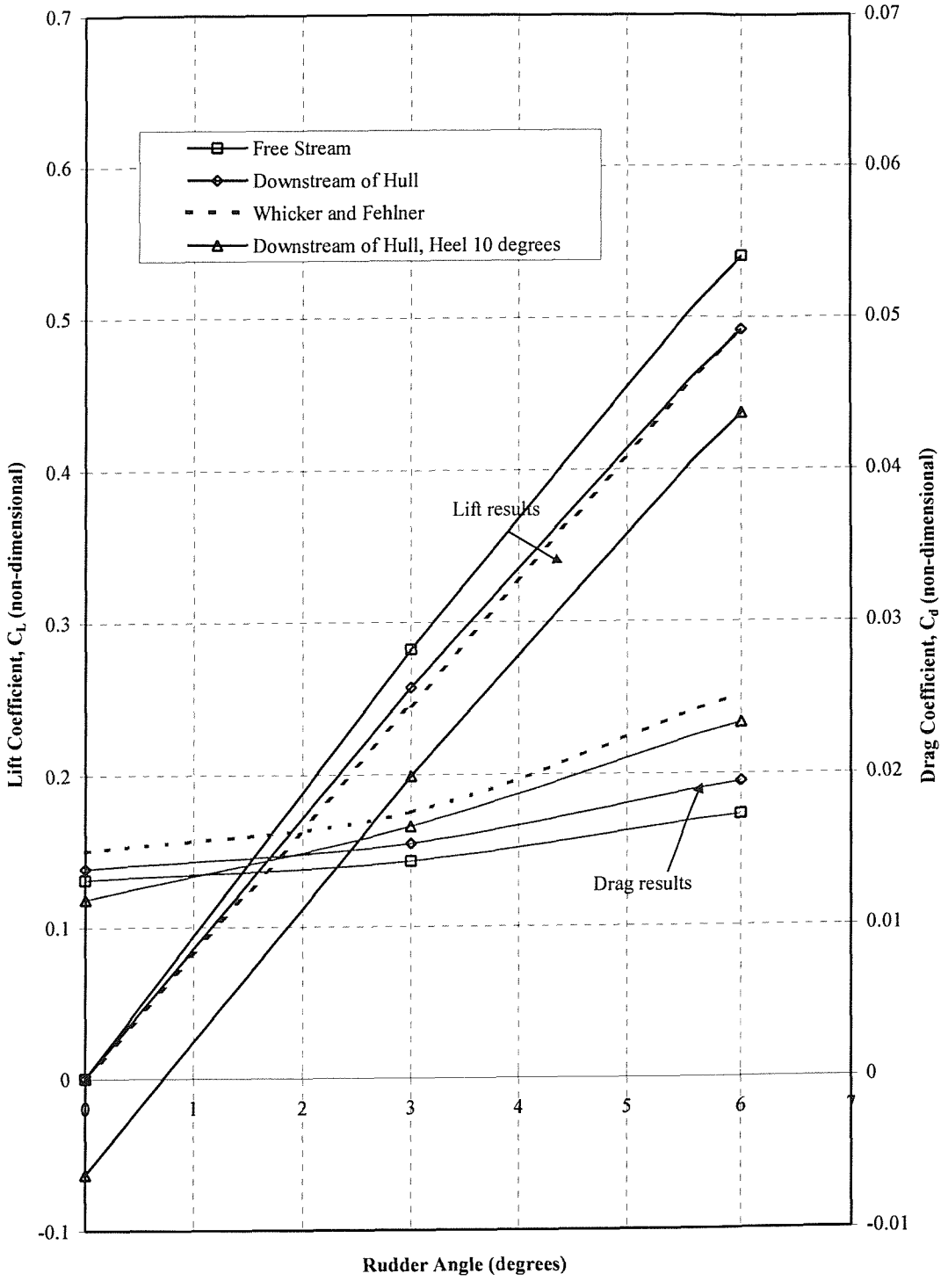

Figure 5 Rudder Performance at Zero Yaw

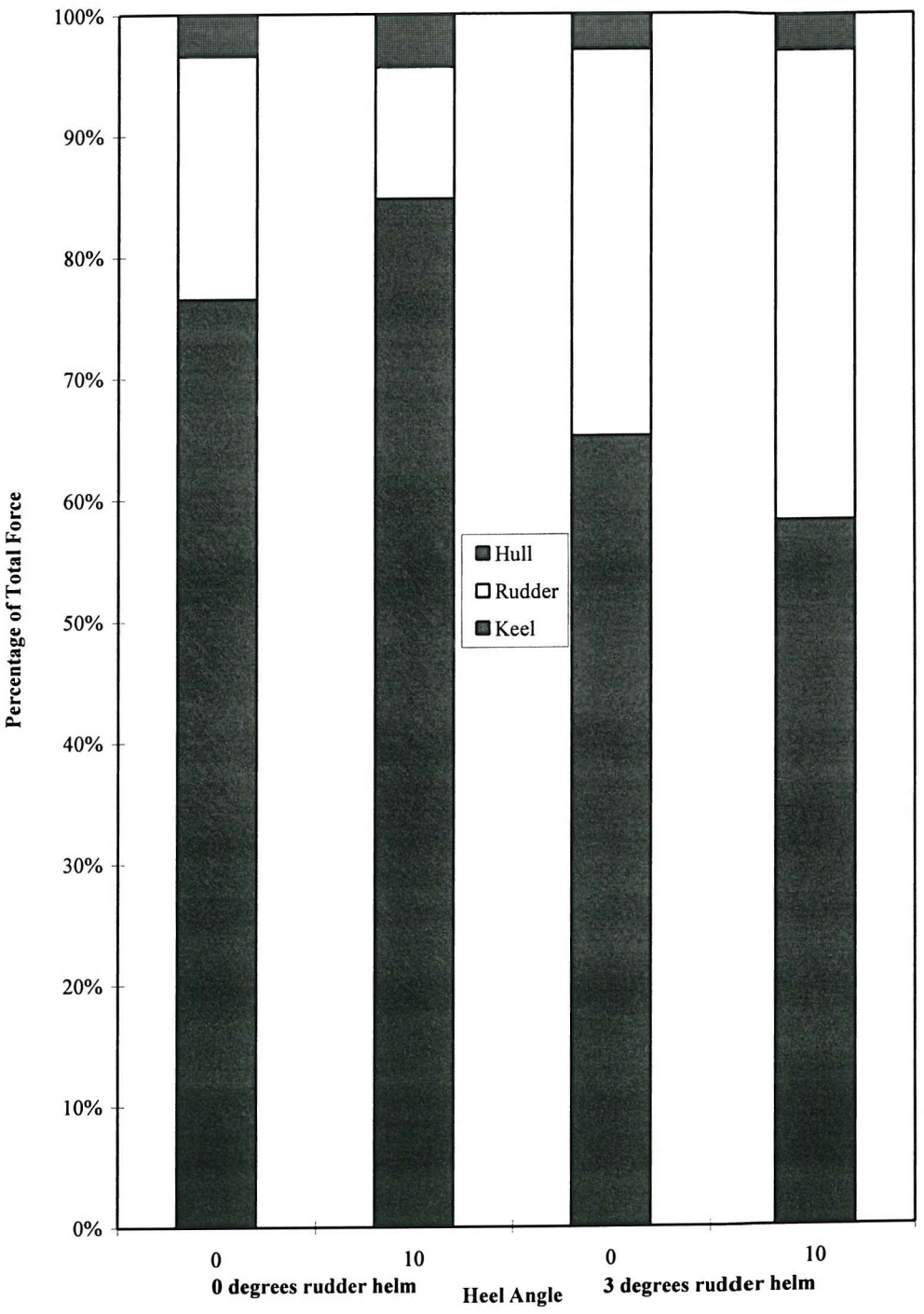

Figure 6 Relative Magnitude of the Yacht Components

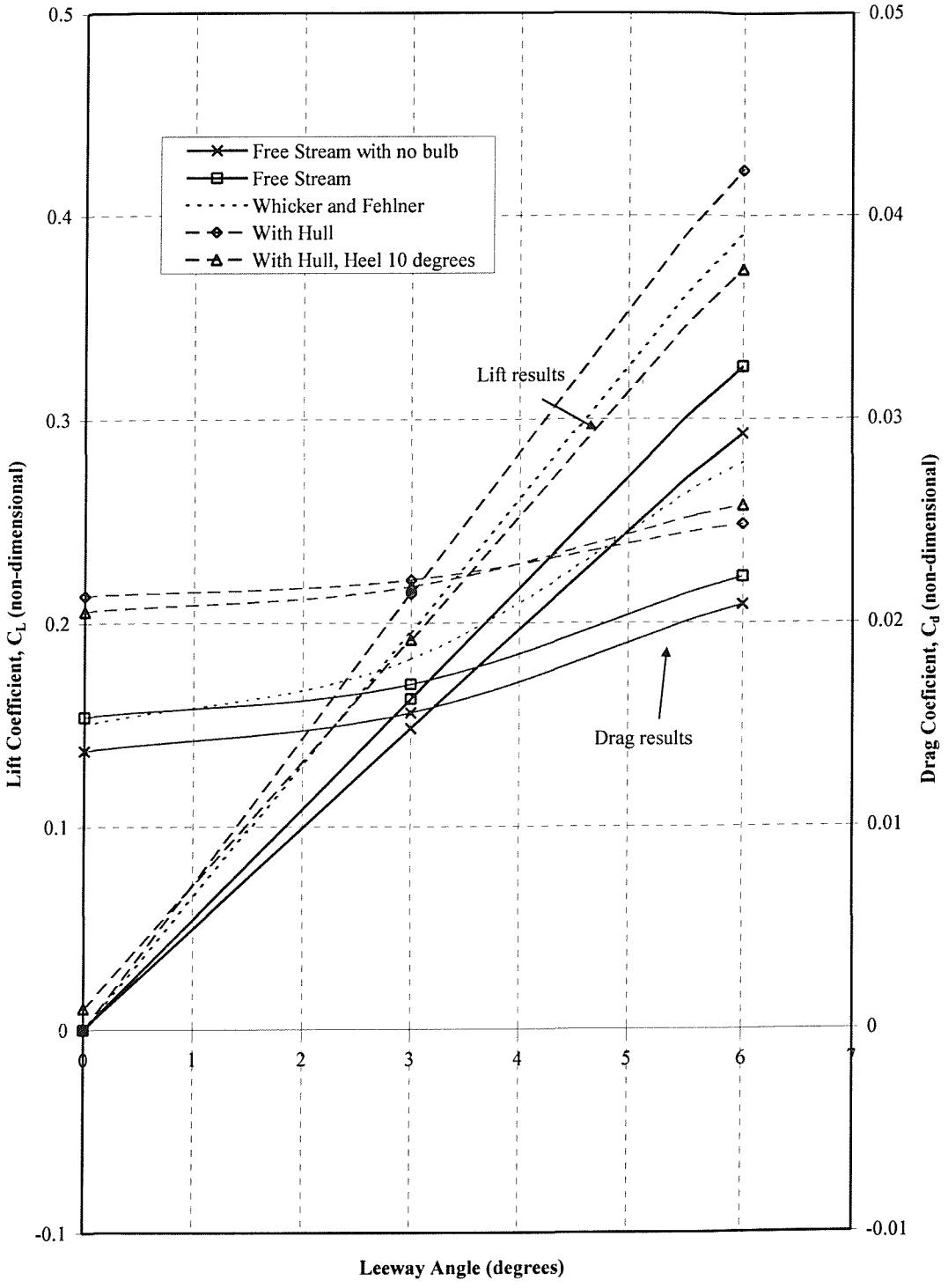

Figure 7 Keel Performance

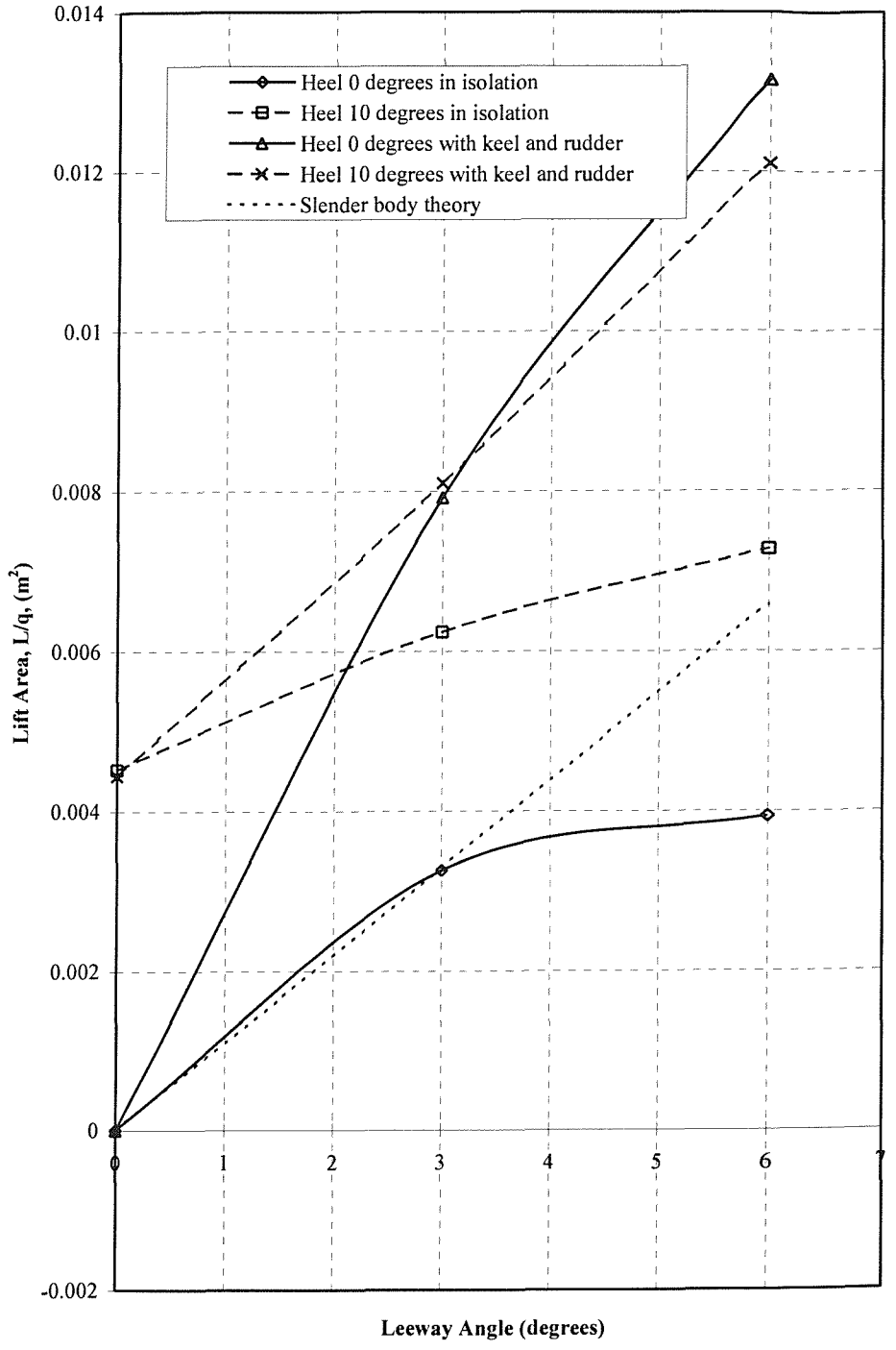

Figure 8 Hull Performance

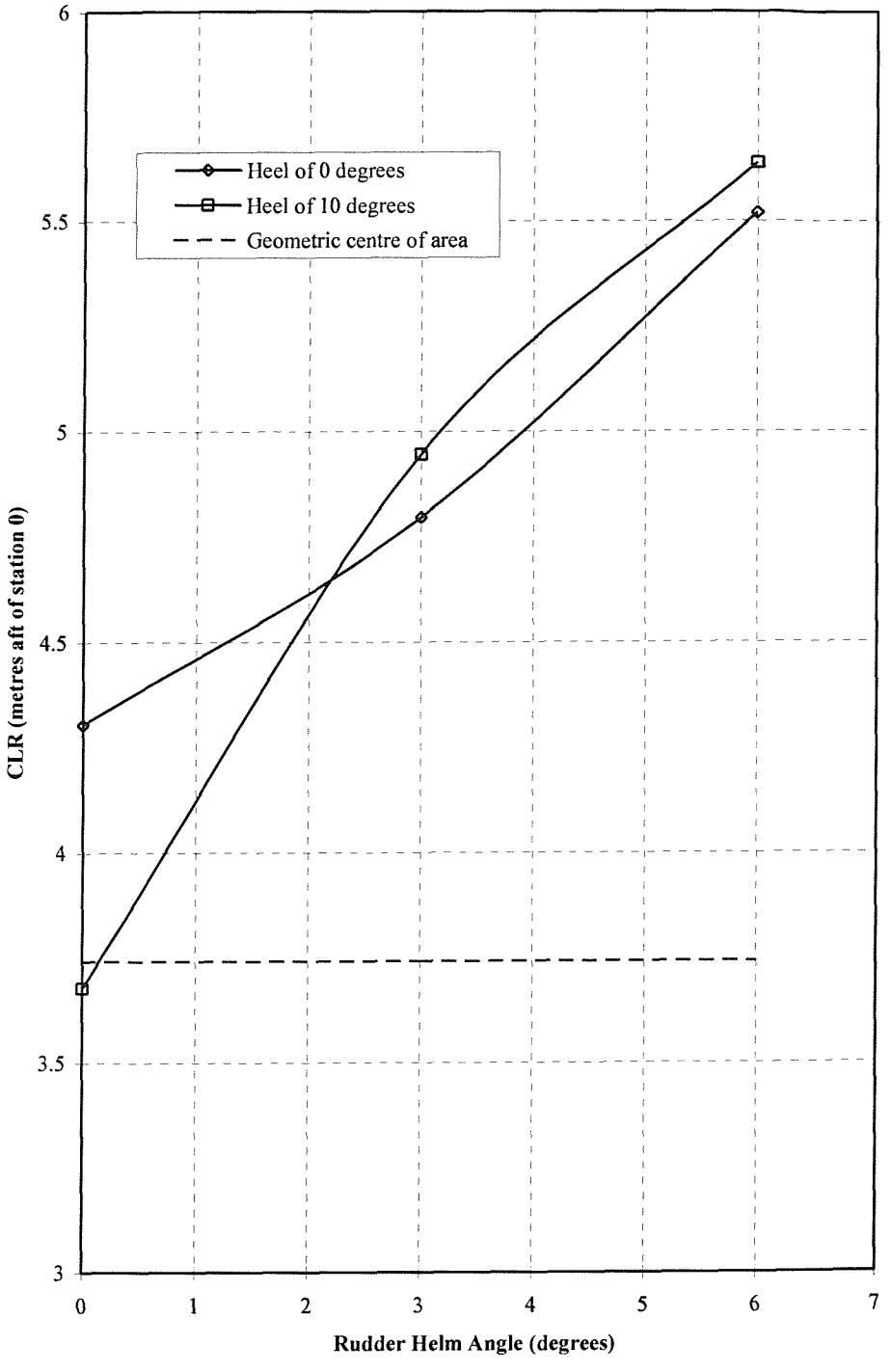

Figure 9 Centre of Lateral Resistance (CLR)

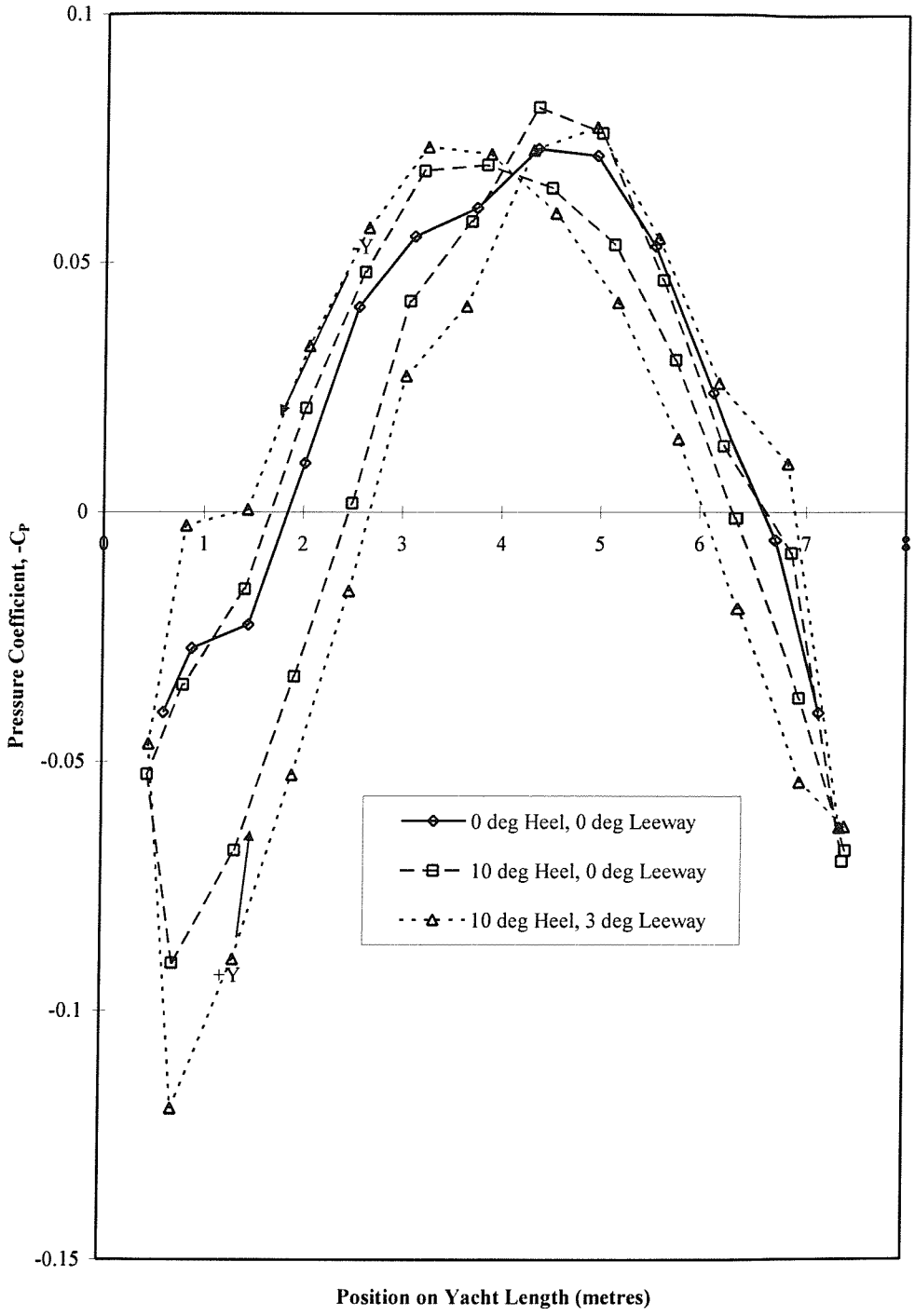

Figure 10 Pressure Distribution at Waterline

APPENDIX E – RUDDER PERFORMANCE PREDICTION METHOD DATABASE

(* indicates the set of tests presented in Chapter 3)

Rudder 0

Modified Wageningen B.4.40

Z/D	Y/D	X/D	V(m/s)	Rpm	
0.75	-0.25	0.39	10.0	2100	*
0.75	-0.25	0.39	10.0	1460	*
0.75	-0.25	0.39	10.0	800	*
0.75	-0.125	0.39	10.0	2100	*
0.75	-0.125	0.39	10.0	1460	*
0.75	0.00	0.39	3.3	1460	*
0.75	0.00	0.39	10.0	2100	*
0.75	0.00	0.39	10.0	1460	*
0.75	0.00	0.39	10.0	800	*
0.75	0.125	0.39	10.0	2100	*
0.75	0.125	0.39	10.0	1460	*
0.75	0.25	0.39	10.0	2100	*
0.75	0.25	0.39	10.0	1460	*
0.75	0.375	0.39	0.0	1460	*
0.75	0.000	0.46	0.0	1460	*
0.75	0.000	0.52	0.0	1460	*
0.75	-0.375	0.39	0.0	1460	*
0.75	-0.25	0.39	0.0	1460	*
0.75	-0.125	0.39	0.0	1460	*
0.75	0.00	0.39	0.0	1460	*
0.75	0.125	0.39	0.0	1460	*
0.75	0.25	0.39	0.0	1460	*

Rudder 1

Modified Wageningen B.4.40

Z/D	Y/D	X/D	V(m/s)	Rpm
0.75	0.00	0.34	10.0	2750
0.75	0.00	0.34	10.0	2130
0.75	0.00	0.34	10.0	1420
0.75	0.00	0.34	10.0	779

Rudder 2

Modified Wageningen B.4.40

Z/D	Y/D	X/D	V(m/s)	Rpm
0.75	0.00	0.30	10.0	2078
0.75	0.00	0.30	10.0	1433
0.75	0.00	0.30	10.0	792
0.75	-0.25	0.39	10.0	2158
0.75	-0.25	0.39	10.0	1479
0.75	-0.25	0.39	10.0	781
0.75	0.00	0.39	10.0	2103
0.75	0.00	0.39	10.0	1460
0.75	0.00	0.39	10.0	792

Z/D	Y/D	X/D	V(m/s)	Rpm	
0.75	0.25	0.39	10.0	2159	
0.75	0.25	0.39	10.0	1489	
0.75	0.25	0.39	10.0	782	
0.75	0.00	0.52	10.0	2079	
0.75	0.00	0.52	10.0	1433	
0.75	0.00	0.52	10.0	791	
1.125	0.00	0.39	10.0	2165	
1.125	0.00	0.39	10.0	1460	
1.125	0.00	0.39	10.0	784	
0.75	0.00	0.30	0.0	1460	*
0.75	0.00	0.36	0.0	1460	*
0.75	-0.375	0.39	0.0	1460	*
0.75	-0.25	0.39	0.0	1460	*
0.75	-0.125	0.39	0.0	1460	*
0.75	0.00	0.39	0.0	1460	*
0.75	0.125	0.39	0.0	1460	*
0.75	0.25	0.39	0.0	1460	*
0.75	0.375	0.39	0.0	1460	*
0.75	0.00	0.46	0.0	1460	*
0.75	-0.25	0.52	0.0	1460	*
0.75	-0.125	0.52	0.0	1460	*
0.75	0.00	0.52	0.0	1460	*
0.75	0.125	0.52	0.0	1460	*
0.75	0.25	0.52	0.0	1460	*

Rudder 3
Modified Wageningen B.4.40

Z/D	Y/D	X/D	V(m/s)	Rpm
0.75	0.00	0.30	10.0	790
0.75	0.00	0.39	10.0	2079
0.75	0.00	0.39	10.0	1434
0.75	0.00	0.39	10.0	791
0.75	0.00	0.52	10.0	2076
0.75	0.00	0.52	10.0	1432
0.75	0.00	0.52	10.0	792

Rudder 4
Modified Wageningen B.4.40

Z/D	Y/D	X/D	V(m/s)	rpm
1.125	0.00	0.39	10.0	779
1.125	0.00	0.39	10.0	1460
1.125	0.00	0.39	10.0	2163

Rudder 5
Modified Wageningen B.4.40

Z/D	Y/D	X/D	V(m/s)	rpm
0.75	0.00	0.39	10.0	785
0.75	0.00	0.39	10.0	1460
0.75	0.00	0.39	10.0	2160

Rudder 6
Modified Wageningen B.4.40

Z/D	Y/D	X/D	V(m/s)	rpm
0.75	0.00	0.39	10.0	784
0.75	0.00	0.39	10.0	1462
0.75	0.00	0.39	10.0	2163